

REAL-TIME CONTROL AND POWER MANAGEMENT  
FOR INTERCONNECTED MICROGRIDS WITH  
SELF-HEALING CAPABILITY

SHAMEEM AHMAD

FACULTY OF ENGINEERING  
UNIVERSITY OF MALAYA  
KUALA LUMPUR

2022

**REAL-TIME CONTROL AND POWER MANAGEMENT  
FOR INTERCONNECTED MICROGRIDS WITH  
SELF-HEALING CAPABILITY**

**SHAMEEM AHMAD**

**THESIS SUBMITTED IN FULFILMENT OF THE  
REQUIREMENTS FOR THE DEGREE OF DOCTOR OF  
PHILOSOPHY**

**FACULTY OF ENGINEERING  
UNIVERSITY OF MALAYA  
KUALA LUMPUR**

**2022**

**UNIVERSITY OF MALAYA**  
**ORIGINAL LITERARY WORK DECLARATION**

Name of Candidate: Shameem Ahmad

Matric No: 17057543/1

Name of Degree: Doctor of Philosophy

Title of Project Paper/Research Report/Dissertation/Thesis ("this Work"):

REAL-TIME CONTROL AND POWER MANAGEMENT FOR  
INTERCONNECTED MICROGRIDS WITH SELF-HEALING CAPABILITY

Field of Study: Power Systems (Electricity and Energy)

I do solemnly and sincerely declare that:

- (1) I am the sole author/writer of this Work;
- (2) This Work is original;
- (3) Any use of any work in which copyright exists was done by way of fair dealing and for permitted purposes and any excerpt or extract from, or reference to or reproduction of any copyright work has been disclosed expressly and sufficiently and the title of the Work and its authorship have been acknowledged in this Work;
- (4) I do not have any actual knowledge nor do I ought reasonably to know that the making of this work constitutes an infringement of any copyright work;
- (5) I hereby assign all and every rights in the copyright to this Work to the University of Malaya ("UM"), who henceforth shall be owner of the copyright in this Work and that any reproduction or use in any form or by any means whatsoever is prohibited without the written consent of UM having been first had and obtained;
- (6) I am fully aware that if in the course of making this Work I have infringed any copyright whether intentionally or otherwise, I may be subject to legal action or any other action as may be determined by UM.

Candidate's Signature

Date:

Subscribed and solemnly declared before,

Witness's Signature

Date:

Name:

Designation:

**REAL-TIME CONTROL AND POWER MANAGEMENT FOR  
INTERCONNECTED MICROGRIDS WITH SELF-HEALING CAPABILITY**

**ABSTRACT**

Compelled by economic and environmental factors, microgrid (MG) has emerged as pioneer small-scale power generation system. However, it is necessary to ensure reliable and resilient operation of the MGs to avoid power failure incidents, which is a challenging task. Connecting multiple MGs to form interconnected MGs can improve power distribution systems resiliency and reliability. However, there are challenges while interconnecting multiple MGs, like possibility of power imbalance between distributed generators (DGs) capacity and load demand, complexity in modeling MGs controllers, and uncertainty of balanced power sharing among multiple MGs. To address all these issues, in this thesis, real-time control and power management systems (PMSs) for two interconnected MGs are developed. Voltage source inverters (VSIs) are important elements of grid-connected single MG to integrate photovoltaic system with utility grid which require fast response, stable and robust controllers for efficient operation. In this thesis, three power control methods are modeled for PV VSI among which the first two are fuzzy logic controller (FLC) and proportional integral (PI) controller based direct power control (DPC) methods, while, the remainder is dq current control theory (CCT) based power control method without using phase-locked-loop (PLL) and Park transformation. In addition, to ensure balanced power flow from different sources to the loads for acquiring better power quality and stable operation of MG, real-time PMSs are developed for both grid-connected and islanded modes of MG's operation by taking into account the maximum utilization of renewable energy sources, energy storage systems and prioritization of critical loads together. Further, to improve the reliability of power distribution system, intelligent interconnection methods (IIM) for interconnecting two MGs with self-healing and interconnection capability are proposed by considering the

power imbalance between DGs generation capacity and load demands of all the MGs. Moreover, to ensure balanced power sharing among multiple MGs during self-healing and interconnected modes of operation, PMSs for individual MGs are developed. Finally, to ensure flexible and smooth transition of multiple MGs among various operation modes like grid-connected, islanded, interconnected and self-healing, a multi-layer control strategy (MLCS) is formed. The real-time simulations are carried out using real-time digital simulator (RTDS) to validate the performance of the proposed power controllers, PMS, IIMs, and MLCS. From the simulation results, it has been observed that the proposed power controllers have better reference power tracking time ranging from (0.03 s – 0.11 s) along with reduction in output power ripples and current total harmonic distortion (THD) which are ranged from 1.6 % to 2.492 %. Further, the results show that through the implementation of the proposed PMS, maximum use of renewable energy sources and energy storage systems are ensured in MG by maintaining balance between supply-demand. The results also demonstrate that the developed IIMs can interconnect two MGs successfully to operate in self-healing and interconnected modes while the PMSs ensure balanced power sharing among the MGs. The final simulation results confirmed that the two MGs can operate flexibly and transit from one operating mode to another smoothly by employing the proposed MLCS.

**Keywords:** Microgrid, Interconnected Micorgrid, Power Management System, Self-healing, Voltage Source Inverter, Real-Time Control.

**PENGURUSAN KUASA DAN KAWALAN SECARA LANGSUNG UNTUK  
SISTEM GRID MIKRO BERSEPADU DENGAN KEUPAYAAN  
PENYEMBUHAN SENDIRI**

**ABSTRAK**

Faktor ekonomi dan persekitaran telah mendorong Grid Mikro (MG) untuk muncul sebagai perintis sistem penjanaan kuasa berskala kecil. Namun begitu, cabaran utama adalah untuk memastikan kebolehpercayaan dan daya tahan dalam pengendalian MG bagi mengelakkan kejadian kegagalan kuasa. Kebolehpercayaan dan daya tahan sistem pengagihan kuasa boleh ditingkatkan melalui pengabungan jenis MG yang berbeza untuk membentuk MG yang bersepadu. Walau bagaimanapun, terdapat cabaran apabila menghubungkan beberapa MG, seperti ketidakseimbangan kuasa di antara kapasiti penjana teragih (DG) dengan kehendak beban, kerumitan dalam memodelkan pengawal MG dan ketidakpastian keseimbangan kuasa diantara pelbagai MG. Untuk menangani semua isu ini, kajian berkenaan sistem kawalan dan pengurusan kuasa (PMS) secara langsung untuk MG bersepadu telah dibangunkan. Penyongsang sumber voltan (VSI) ialah elemen yang penting bagi MG tunggal yang disambungkan ke grid untuk menyepadukan sistem fotovoltan dengan grid utiliti yang memerlukan tindak balas pantas, pengawalan yang stabil dan teguh untuk menghasilkan operasi yang cekap. Di dalam tesis ini, tiga kaedah kawalan kuasa telah dimodelkan untuk PV VSI iaitu kaedah pengawal logik kabur (FLC) dan kaedah kamiran berkadar (PI) yang berasaskan kawalan kuasa langsung (DPC), kaedah kawalan kuasa berasaskan dq CCT tanpa menggunakan gelung berkunci fasa (PLL) dan transformasi Park. Di samping itu, untuk memastikan keseimbangan aliran kuasa dari sumber yang berbeza kepada beban sekaligus menghasilkan kuasa yang berkualiti dan operasi MG yang lebih stabil, sistem kawalan PMS secara langsung telah dibangunkan untuk kedua-dua jenis mod operasi MG iaitu mod yang disambungkan dan tidak disambungkan kepada grid dengan mengambil kira

penggunaan sumber tenaga boleh diperbaharui secara maksima, sistem penyimpanan dan keutamaan kepada beban kritikal. Ini adalah untuk memastikan keseimbangan aliran kuasa daripada pelbagai sumber kepada beban dan pengimbangan permintaan bekalan serta-merta. Selanjutnya, untuk meningkatkan kebolehpercayaan sistem pengagihan kuasa, kaedah integrasi pintar (IIM) untuk menyambung dua MG dengan keupayaan penyembuhan diri dan bersepadu telah dicadangkan dengan mempertimbangkan ketidakseimbangan kuasa antara kapasiti penjanaan DG dan permintaan beban untuk semua MG. Selain itu, PMS untuk MG individu telah dibangunkan untuk memastikan perkongsian kuasa yang seimbang di antara beberapa MG semasa penyembuhan diri dan mod operasi yang saling berkaitan. Akhir sekali, strategi kawalan berbilang lapisan (MLCS) telah dibangunkan untuk memastikan kelancaran dan penyesuaian peralihan berbilang MG di antara mod operasi yang berbeza seperti mod bersambung kepada grid, tidak bersambung kepada grid, bersepadu dan penyembuhan sendiri. Simulasi secara langsung telah dijalankan menggunakan simulasi digital masa nyata (RTDS) untuk mengesahkan prestasi pengawal kuasa yang dicadangkan iaitu PMS, IIM dan MLCS. Keputusan simulasi telah menunjukkan bahawa pengawal kuasa yang dicadangkan mempunyai masa pengesanan kuasa rujukan yang lebih baik iaitu di antara 0.03s hingga 0.11s serta pengurangan dalam hasil kuasa riak dan jumlah semasa herotan harmonik (THD) yang berjulat dari 1.6 % hingga 2.492 %. Selanjutnya, keputusan menunjukkan bahawa melalui pelaksanaan PMS yang dicadangkan, penggunaan sumber tenaga boleh diperbaharui dan sistem penyimpanan tenaga di dalam MG adalah pada tahap maksima dengan mengekalkan keseimbangan di antara permintaan dan bekalan. Hasil juga menunjukkan bahawa IIM yang dibangunkan telah berjaya menghubungkan dua MG untuk beroperasi dalam mod penyembuhan sendiri dan bersepadu manakala PMS pula memastikan keseimbangan perkongsian kuasa di antara MG yang berbeza. Keputusan simulasi akhir mengesahkan bahawa dengan menggunakan MLCS yang dicadangkan,

kedua-dua MG boleh beroperasi secara fleksibel dan beralih dari satu mod operasi ke mod operasi yang lain dengan lancar.

**Kata kunci:** Microgrid, Micorgrid Bersambung, Sistem Pengurusan Kuasa, Penyembuhan sendiri, Penyongsang Sumber Voltan, Kawalan Masa Nyata.

Universiti Malaya

## ACKNOWLEDGEMENTS

All praise to Allah Almighty for His countless blessing. With the blessing of Allah, prayers of my parents, siblings, wife and guidance of my respected supervisors, I become able to complete this thesis.

I would like to acknowledge special thanks to my respected supervisors, Prof. Dr. Saad Mekhilef and Prof. Ir. Dr. Hazlie Mokhlis for their professional guidance, expertise and assistance throughout my PhD tenure.

I want to render my special thanks to my Dearest Wife and Counterpart for her help, sacrifice and support throughout my PhD journey and for sharing my griefs and sorrows in each and every step of my life with her. I am also thankful to her for being patient for such a long period by tolerating and accepting all my mistakes.

I wish to express my deepest gratitude to my parents for their support and sacrifice of living without me for long period. I would like to thank my siblings, and friends for their encouragement and support.

## TABLE OF CONTENTS

Abstract .....	iii
Abstrak .....	v
Acknowledgements .....	viii
Table of Contents .....	ix
List of Figures .....	xiv
List of Tables.....	xix
List of Abbreviations.....	xxi
<b>CHAPTER 1: INTRODUCTION.....</b>	<b>1</b>
1.1 Background.....	1
1.2 Problem Statement.....	3
1.3 Research Objectives.....	8
1.4 Methodology.....	9
1.5 Outline of the Thesis.....	10
<b>CHAPTER 2: LITERATURE REVIEW.....</b>	<b>12</b>
2.1 Introduction.....	12
2.2 MG Definition and Benefits .....	12
2.3 Different Configurations of Microgrid .....	14
2.3.1 AC Microgrid .....	14
2.3.2 DC Microgrid .....	15
2.3.3 Hybrid Microgrid .....	16
2.4 Microgrid Operating Modes .....	18
2.4.1 Grid Connected Mode .....	18
2.4.2 Islanded Mode .....	19

2.5	Control Architectures in Microgrids.....	19
2.5.1	Centralized Control .....	19
2.5.2	De-centralized Control .....	21
2.5.2.1	MAS Theory.....	23
2.5.3	Hierarchical Control .....	24
2.5.4	Distributed Control.....	24
2.6	Control Schemes Adopted by Local Controllers in Microgrid.....	25
2.6.1	Non-classical Control Schemes.....	26
2.6.2	Classical Control Schemes .....	26
2.6.2.1	Hysteresis Current Control.....	26
2.6.2.2	Linear Control with Pulse Width Modulation (PWM).....	28
2.7	Microgrid Inverter Control Methods .....	29
2.7.1	PQ Control.....	30
2.7.2	V-f Control .....	36
2.7.3	Droop Control.....	37
2.8	Microgrid Power Management.....	38
2.8.1	Power Management Systems.....	39
2.8.1.1	Power Management Systems based on Optimisation Methods	39
2.8.1.2	Power Management Systems based on Artificial Intelligence (AI) Methods .....	43
2.9	Interconnected Microgrid System .....	47
2.9.1	Advantages of Interconnected Microgrid System.....	47
2.9.2	Control Modes of Microgrids in the Interconnected MG System.....	49
2.9.2.1	Master-Slave Mode .....	49
2.9.2.2	Peer-to-Peer Mode.....	51
2.9.2.3	Combined Control Mode.....	52

2.9.3	Control, Management and Methods of Interconnection of Multiple Interconnected Microgrids .....	53
2.10	Gap of the Research.....	55
2.11	Summary.....	55
<b>CHAPTER 3: METHODOLOGY .....</b>		<b>57</b>
3.1	Introduction.....	57
3.2	Proposed Microgrid Configuration.....	57
3.2.1	AC Microgrid .....	57
3.2.2	Hybrid Microgrid .....	58
3.2.3	Interconnected Microgrid .....	60
3.3	Modeling of Microgrid Components.....	63
3.3.1	PV Generation System .....	63
3.3.2	Battery Storage System .....	64
3.3.3	Diesel Generator.....	65
3.3.4	Grid.....	66
3.3.5	Load.....	66
3.4	Voltage Source Inverter Modelling and Control .....	66
3.4.1	Current Control Theory (CCT) based PV Inverter Modelling.....	66
3.4.2	PCC Voltage Modulated Theory (PVMT) based PV Inverter Modelling	71
3.4.3	Voltage Source Inverter Control during AC Microgrid's Grid-connected mode .....	75
3.4.3.1	PLL less CCT based Power Control Method.....	75
3.4.3.2	Direct Power Control (DPC) method for PV Inverter.....	79
3.4.3.3	Fuzzy Logic Controller (FLC) for proposed FLDPC method...	82
3.4.3.4	DC link Voltage Control .....	85
3.4.3.5	Robust Control Design.....	86

3.4.4	Voltage Source Inverter Control during AC Microgrid’s Islanded Mode	90
3.4.5	Bidirectional Voltage Source Inverter Control for Hybrid Microgrid	94
3.4.5.1	Droop Characteristics of DC and AC MG	94
3.4.5.2	Bidirectional Voltage Source Inverter Control Strategy during Hybrid MG Islanding Operation	95
3.4.5.3	Power Sharing Strategy of Hybrid MG	96
3.5	Proposed Real-time Power Management System for Single Microgrid	97
3.5.1	Real-time PMS for Single Microgrid’s Grid-connected Operation	97
3.5.2	Real-time PMS for Single Microgrid’s Islanded Operation	98
3.6	Proposed Intelligent Interconnection Method for Multiple Islanded Microgrids (Self-healing Mode)	102
3.6.1	Power Management System for MG1 during Self-healing Mode	104
3.6.2	Power Management System for MG2 during Self-healing Mode	105
3.7	Proposed Intelligent Interconnection Method for Multiple Grid-connected Microgrids (Interconnected Mode)	108
3.7.1	Power Management System for MG1 during Interconnected Mode	109
3.7.2	Power Management System for MG2 during Interconnected Mode	110
3.8	Proposed Multi-layer Control Strategy for Multiple Interconnected Microgrids	113
3.9	Summary	115
<b>CHAPTER 4: RESULTS AND DISCUSSIONS</b>		<b>116</b>
4.1	Introduction	116
4.2	Performance Analysis of the Proposed PV VSI Control Methods	116
4.2.1	Reference Power Tracking Performance Analysis	117
4.2.1.1	Steady-state Performance Analysis	121
4.3	Performance Analysis of the Proposed Real-time Power Management System	127
4.3.1	AC Microgrid	127

4.3.2	Hybrid Microgrid .....	135
4.4	Performance Analysis of the Proposed Intelligent Interconnection Method and Power Management Strategy for two MGs in Self-healing mode.....	142
4.5	Performance Analysis of the Proposed Intelligent Interconnection Method and Power Management Strategy for two MGs in Interconnected mode .....	150
4.6	Performance Analysis of the Proposed Multi-Layer Control Strategy for Two Interconnected MGs.....	157
4.7	Comparative Study of Proposed PV VSI Controllers with Conventional PV VSI Controllers used in AC Microgrid .....	164
4.8	Comparative Study of Proposed Interconnected Microgrids Performance with previously Developed Interconnected Microgrids.....	166
4.9	Summary.....	168
 <b>CHAPTER 5: CONCLUSIONS AND FUTURE WORKS .....</b>		<b>169</b>
5.1	Conclusions .....	169
5.2	Limitations and Challenges of the Study.....	173
5.3	Future Works .....	174
	References .....	175
	List of Publications and Papers Presented .....	185

## LIST OF FIGURES

Figure 1.1:	Microgrid operation strategy (Nikam & Kalkhambkar, 2021).....	3
Figure 1.2:	Overall methodology of the proposed research work.....	9
Figure 2.1:	Typical structure of a microgrid (Hatziaargyriou, 2014).....	13
Figure 2.2:	General configuration of AC microgrid .....	15
Figure 2.3:	General configuration of DC microgrid .....	16
Figure 2.4:	General configuration of hybrid AC-DC microgrid .....	17
Figure 2.5:	Hysteresis current control for a VSI (a) control scheme, (b) load current (Mohan & Undeland, 2003).....	27
Figure 2.6:	Pulse width modulation for a VSI (a) control scheme, (b) waveforms (Mohan & Undeland, 2003) .....	29
Figure 2.7:	Microgrid droop control characteristics .....	38
Figure 2.8:	Architecture of microgrid under master-slave control mode (Fusheng, Ruisheng, & Fengquan, 2016).....	50
Figure 2.9:	Architecture of microgrid under peer-to-peer control mode (Fusheng et al., 2016).....	51
Figure 3.1:	Schematic of AC microgrid.....	58
Figure 3.2:	Schematic of hybrid microgrid .....	60
Figure 3.3:	Schematic of interconnected microgrids.....	62
Figure 3.4:	Schematic of grid-connected MG's VSI (a) conventional CCT based power controller with PLL system, and (b) proposed CCT based power controller without PLL system .....	67
Figure 3.5:	Schematic of grid-connected MG's VSI (a) proposed PVMT based PIDPC, and (b) proposed PVMT based FLDPC without PLL system .....	72

Figure 3.6:	SPWM technique for VSI .....	77
Figure 3.7:	Membership functions of (a) P-error ( $e_P$ ), (b) Error_rate of P ( $de_P/dt$ ) and (c) Output of FLC ( $F_P$ ).....	84
Figure 3.8:	Membership functions of (a) Q-error ( $e_Q$ ), (b) Error_rate of Q ( $de_Q/dt$ ) and (c) Output of FLC ( $F_Q$ ).....	84
Figure 3.9:	Schematic of DC link voltage controller .....	85
Figure 3.10:	Schematic of V-f control strategy for VSI of islanded microgrid .....	91
Figure 3.11:	Power transfer control strategy between AC and DC MGs of hybrid MG .....	96
Figure 3.12:	Real-time power management systems for single MG during (a) grid-connected and (b) islanded operations.....	101
Figure 3.13:	Flowchart of the proposed intelligent interconnection algorithm for MGs self-healing mode.....	103
Figure 3.14:	Power management systems for (a) MG1 and (b) MG2 during self-healing mode.....	107
Figure 3.15:	Flowchart of the proposed intelligent interconnection algorithm for MGs interconnected mode.....	108
Figure 3.16:	Power management systems for (a) MG1 and (b) MG2 during interconnected mode.....	112
Figure 3.17:	Multi-layer control strategy for multiple interconnected microgrids.....	114
Figure 4.1:	Laboratory setup of the proposed controller for MGs with RTDS .....	117

Figure 4.2:	Real power tracking performance of (a) FLDPC method, (b) PIDPC method, (c) PLL less dq CCT and (d) dq CCT based power controller with PLL .....	119
Figure 4.3:	Reactive power tracking performance of (a) FLDPC method, (b) PIDPC method, (c) PLL less dq CCT and (d) dq CCT based power controller with PLL.....	121
Figure 4.4:	Real power steady-state performance of (a) FLDPC method, (b) PIDPC method, (c) PLL less dq CCT and (d) dq CCT based power controller with PLL.....	122
Figure 4.5:	Reactive power steady-state performance of (a) FLDPC method, (b) PIDPC method, (c) PLL less dq CCT and (d) dq CCT based power controller with PLL .....	123
Figure 4.6:	VSI output voltage for (a) FLDPC method, (b) PIDPC method, (c) PLL less dq CCT and (d) dq CCT based power controller with PLL .....	125
Figure 4.7:	VSI output current for (a) FLDPC method, (b) PIDPC method, (c) PLL less dq CCT and (d) dq CCT based power controller with PLL .....	126
Figure 4.8:	THD of VSI output current for PLL less proposed power controllers along with conventional PLL based dq CCT power controller .....	127
Figure 4.9:	Active power flow between different sources and loads in AC microgrid.....	128
Figure 4.10:	Power supply to critical and non-critical loads in AC MG .....	130

Figure 4.11:	During both load and solar irradiation changes PV inverter output (a) power, (b) current and (c) voltage .....	132
Figure 4.12:	During both load and solar irradiation changes battery inverter output (a) power, (b) current and (c) voltage .....	133
Figure 4.13:	THD of (a) PV VSI output current, (b) Battery VSI output current and (c) PV & battery VSIs output voltage .....	134
Figure 4.14:	During both load and solar irradiation changes grid (a) power, (b) current and (c) voltage .....	135
Figure 4.15:	Active power flow from different power sources to loads in hybrid MG.....	136
Figure 4.16:	Power supply to critical DC load and variable AC load in hybrid MG .....	138
Figure 4.17:	During both load and solar irradiation changes BVSI output (a) power, (b) current and (c) voltage .....	140
Figure 4.18:	During both load and solar irradiation change grid (a) power, (b) current and (c) voltage .....	141
Figure 4.19:	THD of BVSI output (a) current and (b) voltage .....	142
Figure 4.20:	Power flow between the DERs and load for (a) MG1 and (b) MG2.....	143
Figure 4.21:	Power flow between MG1 and MG2 at POI.....	148
Figure 4.22:	During self-healing mode at POI (a) voltage, (b) MG1 current and (c) MG2 current .....	149
Figure 4.23:	Power flow between the DERs and load for (a) MG1 and (b) MG2.....	150
Figure 4.24:	Power flow between MG1 and MG2 at POI.....	155

Figure 4.25:	During interconnected mode at POI (a) voltage, (b) MG1 current and (c) MG2 current.....	156
Figure 4.26:	Power flow between the DERs and load for (a) MG1 and (b) MG2..	157
Figure 4.27:	Power flow between MG1 and MG2 at POI.....	162
Figure 4.28:	During MGs different operating modes at POI (a) voltage, (b) MG1 current and (c) MG2 current .....	163

Universiti Malaya

## LIST OF TABLES

Table 2.1:	Comparison among different MGs .....	17
Table 2.2:	Comparison among different MGs control methods .....	25
Table 2.3:	Comparison among different PQ control methods of grid-connected AC MGs .....	35
Table 2.4:	Summary of different PMS methods of MG .....	46
Table 3.1:	Parameters of AC MG components.....	59
Table 3.2:	Parameters of hybrid MG components.....	61
Table 3.3:	Parameters of Interconnected MGs components .....	62
Table 3.4:	Values of PI controllers' coefficients for conventional and proposed CCT base power control methods.....	79
Table 3.5:	Values of PI controllers' coefficients proposed PIDPC .....	82
Table 3.6:	Rule table for FLCs of real and reactive power .....	84
Table 3.7:	Values of PI controllers' coefficients for V-f control strategy .....	93
Table 4.1:	Active power flow during both load and solar irradiation changes in AC microgrid.....	128
Table 4.2:	Active power flow during both AC load and solar irradiation change in hybrid microgrid.....	136
Table 4.3:	Summary of power flow between the DERs and load for both MG1 and MG2 in self-healing mode.....	144
Table 4.4:	Summary of power flow between the DERs and load for both MG1 and MG2 in interconnected mode .....	151
Table 4.5:	Summary of power flow between the DERs and load for both MG1 and MG2 after implementing MLCS.....	158

Table 4.6: Results of comparison between proposed and conventional grid-tied MGs power controllers .....	165
Table 4.7: Results of comparison between proposed and existing controllers for interconnected MGs .....	167

Universiti Malaya

## LIST OF ABBREVIATIONS

AI	:	Artificial intelligence
ANN	:	Artificial neural network
ARMA	:	Auto regressive moving average
BPSO	:	Binary particle swarm optimization
BSS	:	Battery storage system
BVSI	:	Bidirectional voltage source inverter
CCT	:	Current control theory
CCM	:	Current control mode
CHP	:	Combined heat power
DER	:	Distributed energy resources
DES	:	Distributed energy storage
DG	:	Distributed generators
DiG	:	Diesel generator
DPC	:	Direct power control
ESS	:	Energy storage systems
FLC	:	Fuzzy logic controller
FLDPC	:	Fuzzy logic direct power control
IIM	:	Intelligent Interconnection Method
MAS	:	Multi-agent system
MG	:	Microgrid
MGCC	:	Microgrid central controller
MI	:	Modulation index
MILP	:	Mixed integer linear programming
MIMO	:	Multiple-Input Multiple-Output

MINLP	:	Mixed integer nonlinear programming
MLCS	:	Multi-layer control strategy
MPC	:	Model predictive control
MPPT	:	Maximum power point tracking
PCC	:	Point of common coupling
PI	:	Proportional integral
PIDPC	:	Proportional integral direct power control
PLL	:	Phase-locked-loop
PMS	:	Power management system
POI	:	Point of interconnection
PV	:	Photovoltaic
PVM	:	PCC voltage modulation
PVMT	:	PCC voltage modulated theory
QoS	:	Quality of service
RE	:	Renewable energy
RES	:	Renewable energy sources
RTDS	:	Real time digital simulator
SDP	:	Stochastic dynamic programming
SOC	:	State of Charge
SPSA	:	Simultaneous perturbation stochastic approximation
SPWM	:	Sinusoidal pulse width modulation
THD	:	Total harmonic distortion
VCM	:	Voltage control mode
V-f	:	Voltage-frequency
VSI	:	Voltage source inverter
WT	:	Wind turbine

## CHAPTER 1: INTRODUCTION

### 1.1 Background

According to the International Energy Agency, around 1.2 billion people (16% of the global population) do not have access to electricity. More than 95% of those living without electricity are residents of sub-Saharan African and developing Asian countries, while around 80% of them reside in rural areas (Outlook, 2018). Electrification of these remote areas via national grid is unviable due to large up-front cost requirements.

In addition, centralized power grid bears a heavy burden in a time when consumers expect an uninterrupted reliable power supply, a reduction in carbon emissions, increased efficiency within the national grid and power supplied to remote communities. This has led to alternatives being sought for centralized power generation, which is prone to outages (due to long distance transmission), is a substantial contributor to global carbon emissions, has large transmission losses and is often not a practical solution when supplying remote communities (Burmester, Rayudu, Seah, & Akinyele, 2017).

Distributed generator (DG) looks to remedy these inadequacies by producing power close to its point of consumption, often utilizing carbon neutral, renewable energy (RE) sources (sun, wind). To maximize the efficient use of DG, control structures are used to balance the intermittent RE power production with consumer power consumption (Burmester et al., 2017). However, distributed generation based on DGs, particularly RE, has two major disadvantages preventing its widespread integration into residential/commercial properties (Nasir et al., 2018). The first is the intermittent nature of its power output and the second one is the financial capital required to install RE sources (RES) and the lengthy payback time before seeing a financial return (Nasir et al., 2018). These inadequacies can be addressed from a control system point of view, to optimize supply and demand. One such control system currently popular in this field of

research is the microgrid (MG) (Nikam & Kalkhambkar, 2021). MGs have great potential to deliver economic, environmental, and other benefits, but have been hampered by being a relatively small market, too small to have industry-wide technology standards that enable large price reductions and high degrees of interoperability (Nikam & Kalkhambkar, 2021).

MG is an important and necessary part of the development of smart grid. The MG is characterized as the “building block of smart grid” (Nikam & Kalkhambkar, 2021). It comprises low voltage (LV) system with distributed energy resources (DERs) together with storage devices and flexible loads. The DERs such as micro-turbines, fuel cells, wind generator, photovoltaic (PV) and storage devices such as flywheels, energy capacitor and batteries are used in a MG. The MG can benefit both the grid and the customer (Nikam & Kalkhambkar, 2021).

From the customer’s view: MGs answer to both thermal and electricity needs and enhance local reliability, reduce emission, improve power quality by supporting the voltage and frequency and potentially lower costs of energy supply.

From the utility’s view: A MG can be seen as a controlled entity within the power system as a single dispatchable unit (load or generator) or ancillary services provider.

Normally, a MG has two modes of operation: the island mode and the grid-connected mode. In the island mode, the production is required to meet the load demand. On the other hand, when the MG is connected to grid, it can either receive or inject power into the main grid. Furthermore, the grid connected MG can provide power supporting to its local loads demand. When a disturbance occurs, the MG is disconnected from the distribution network as soon as possible to avoid any further damage. In that case, the MG will operate in an island mode. Furthermore, the operation mode is related to the

elasticity supply, local loads demand and the electricity market. Thus, the objectives of the optimal operation scheduling in MGs are concerned with the economical, technical and environmental aspects.

A MG can provide a large variety of economic, technical, environmental, and social benefits to both internal and external stakeholders depending on its operation strategy (Nikam & Kalkhambkar, 2021). The MG operation strategy is presented in Figure 1.1. In this thesis, emphasis has been given to enhance the technical benefits of the MG to ensure efficient, reliable and resilient MG.

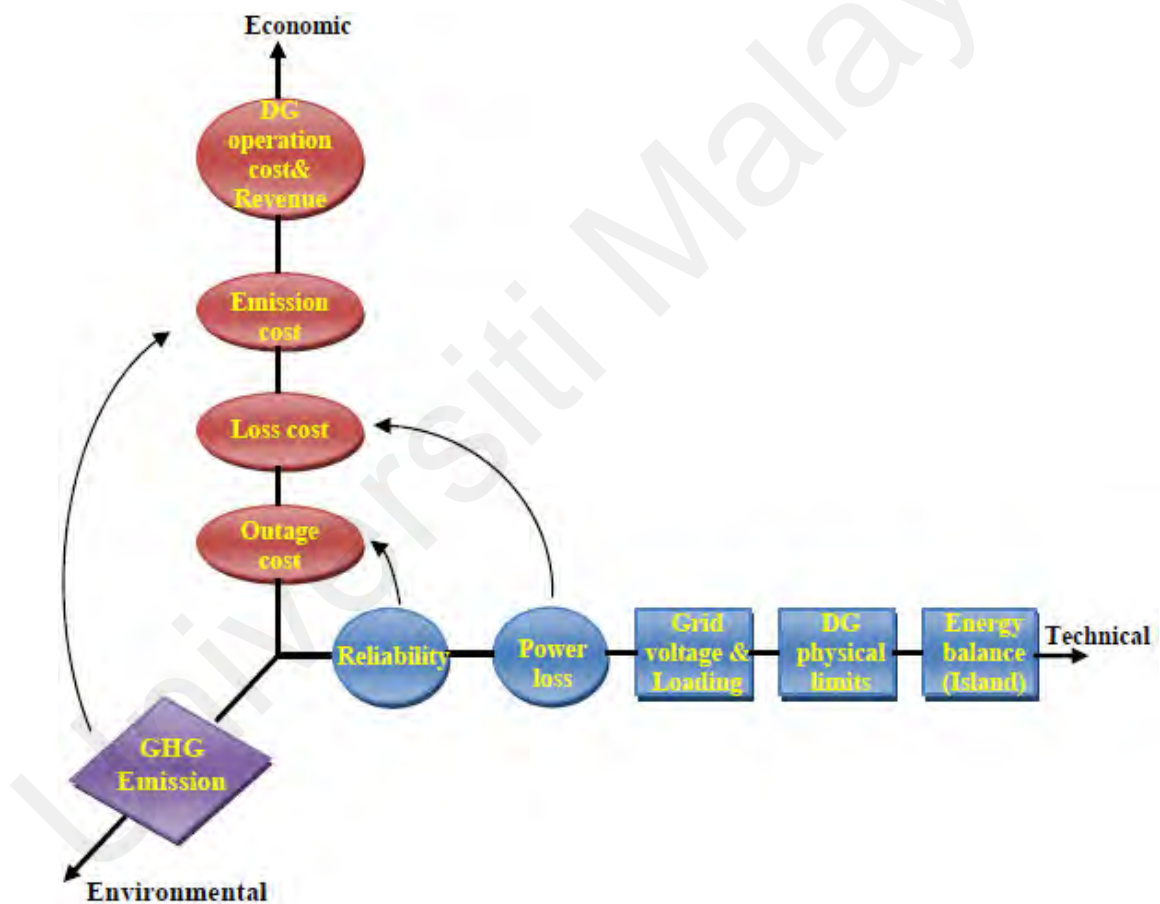


**Figure 1.1: Microgrid operation strategy (Nikam & Kalkhambkar, 2021)**

## 1.2 Problem Statement

A MG consists of an interconnected network of several energy sources (including both conventional and RE generators) and serves the local electrical loads from residential, commercial, and industrial consumers. In comparison with centralized and conventional

models of power system, MG brings several benefits: reducing power transmission loss, enhancing the system resilience, and integrating DG especially from renewable sources (Nikam & Kalkhambkar, 2021). Wide deployment and proper management of MGs can have significant positive impact on the overall power grid system. However, regarding MG operation, there are numerous technical difficulties are existed, which includes power flow control strategies between MG and the main grid (Nikam & Kalkhambkar, 2021); voltage-control methods within a MG (Trivedi & Saroha, 2020); and frequency control during isolated operation (Choudhury, 2020). Grid-connected voltage source inverters (VSI) are one of the key devices of MG, which interconnect DG units of MG with main grid and regulate power flow between MG and grid by adopting an appropriate power control mode. Even though efficient power control strategies are required for the VSI to ensure flexible power transfer between the MG and utility grid however, lack of focus is observed to cover this area in MG research specially the grid synchronization technique.

Recently for grid-connected MGs, many power control schemes have been proposed by researchers (Go & Choi, 2020; Guichi, Mekhilef, Berkouk, & Talha, 2021; Islam et al., 2019; Kaushal & Basak, 2020; Lou, Gu, Zhu, Li, & Zhang, 2020; Safa, Berkouk, Messlem, & Gouichiche, 2018; Tahri, Foitih, & Tahri, 2021; Tang, Zhang, Xiao, & Li, 2021; Teekaraman et al., 2020; Worku, Hassan, & Abido, 2019) to enhance the efficiency, safety and reliability of the VSIs. All these methods are based on dq current control theory (CCT) where phase angle from the grid voltages need to be extracted accurately for Park transformation to ensure grid voltage and dq axes currents are in phase (Lee et al., 2020). Most commonly used system nowadays for phase angle extraction of the grid voltage is phase-locked-loop (PLL) (Ahmadzadeh, Mortazavi, & Saniei, 2018; Ali et al., 2018). By filtering grid voltages and using the arctangent function, the phase angle can be extracted (Lee, Kim, Sul, & Blaabjerg, 2004). However, a slow transient response will be the result of the PLL system. High power ripples in the real and reactive powers are also caused by

PLL system (Davari & Mohamed, 2016; Wang & Blaabjerg, 2018; Wang, Harnefors, & Blaabjerg, 2017). Furthermore, the stability of VSIs may be deteriorated by PLL via initiating negative resistance at low frequencies (Harnefors, Wang, Yepes, & Blaabjerg, 2015; Selakov, Bekut, & Sarić, 2016; Wen et al., 2015). In addition, in the existing power controllers of VSI, two control loops namely the outer power control loop and inner current control loop have been considered while designing the power control scheme. Due to the presence of two control loops the computation burden has been increase (Gui, Wang, & Blaabjerg, 2018). Therefore, in this study prominence has been given to develop a power control strategy for grid-connected PV VSI without using PLL to ensure appropriate power control between the MG and utility grid with better power quality.

Another important aspect of MG system is the development of efficient power management system (PMS) for improving the dynamic response of the MGs under different load conditions. A PMS helps in solving various issues such as maintaining transient stability while connecting and disconnecting a particular device to the MG system, allowing a smooth transition of MG from grid-connected to islanded mode and vice versa, as well as optimal utilization of RESs (Jamal, Tan, & Pasupuleti, 2021). However, in literature (Hannan et al., 2019; Helal et al., 2019; Iris & Lam, 2021; Mosa & Ali, 2021; Salazar, Berzoy, Song, & Velni, 2020; Tabar, Ghassemzadeh, & Tohidi, 2019; Yang, Zhang, He, Ren, & Weng, 2018), most of the proposed MG PMSs are developed and tested for MG economic operation in offline mode which require prior historical data to obtain optimum result. As a result, real-time implementations of these methods are not possible. Further, these methods focus more on market-based or cost function-based optimization problems rather than instantaneous supply-demand balance for MG stability and better power quality. Apart from that there are also PMSs available which have been developed for MG operation and control (Belmokhtar & Cano, 2021; Ciupageanu, Barelli, Ottaviano, Pelosi, & Lazaroiu, 2019; Faria, Pombo, Calado, &

Mariano, 2019; Gao & Ai, 2018; Singh & Lather, 2020; Wang, He, & Deng, 2019). These PMSs objectives were either to ensure maximum utilization of RES or life span enhancement of storage systems. However, in MG, power management towards load is also an important factor, especially during MG's islanded mode operation to ensure uninterrupted power supply to critical loads. From the state-of-art of PMS, it is found that none of the existing PMS has taken into account the maximum utilization of RES, storage systems as well as prioritization of critical loads together. Therefore, there is a need for development of PMS for MG system which can be implemented in real-time by addressing all the issues for both grid-connected and islanded modes of MG operation.

A single MG system can only generate and distribute power within a localized area. In addition, the intermittent power generated by solar PV units and wind turbines (WT) often causes variations in the output power, voltage and frequency (Arefifar, Mohamed, & El-Fouly, 2013). Furthermore, in the event of unavailability/failure of one or more DG units in the single MG system during the islanded mode of operation, the single MG system itself will not be secured enough to meet its own load demand due to restricted energy generation capability (Marvasti, Fu, DorMohammadi, & Rais-Rohani, 2014). In such cases, the single MG system usually employs load shedding technique to ensure supply-demand balance which is usually inconvenient and economically undesirable as it poses the risk of causing disruption to customers' business operations (Marvasti et al., 2014). On the other hand, during grid-connected mode also MG consumers and businesses encounter difficulty in managing electricity cost in both regulated and deregulated electricity markets. In regulated market, in most of the countries the tariff is not fixed throughout the day. In peak hours, normally the electricity price is higher than off-peak hours. In this case, consumers and businesses can purchase electricity from adjacent MG rather than utility companies. Similarly, in de-regulated electricity market, consumers and businesses are dependent on different Retail Electricity Providers (REPs) to buy

electricity at convenient cost rather than their local utility. Therefore, it can be said that the interconnection of MGs can play an important role to resolve the issues of a single MG in both islanded and grid-connected modes. Multiple MGs in adjacent locations can be interconnected or coupled to form interconnected MGs to ensure the cost effective and improved security of power supply.

Though the interconnected MGs have exhibited advantages, however, there is issue in forming the interconnection among multiple MGs due to variations in generation capacity, type, number, locations of DERs, and energy storage systems (ESSs). After the interconnection of multiple MGs, if diverse operating uncertainties like power imbalance between power generated by DERs and load demand will occur, then this phenomenon will lead to blackout in the interconnected MGs. All the existing frameworks (Bazmohammadi, Tahsiri, Anvari-Moghaddam, & Guerrero, 2019; Hans, Braun, Raisch, Grüne, & Reincke-Collon, 2018; Liu, Fang, & Li, 2017; Nikmehr, Najafi-Ravadanegh, & Khodaei, 2017; Ren et al., 2018; Samadi Gazijahani & Salehi, 2017) proposed for interconnecting MGs do not consider the instantaneous supply-demand power imbalance while developing the framework. Further, these frameworks are not tested in real-time platform, only offline simulations are conducted. Therefore, further research on development of frameworks is needed for the interconnection of multiple MGs in both grid-connected and islanded modes of operations of multiple MGs by considering the power imbalance constraints of individual MGs which can be implemented in real-time to ensure maximum power supply security. Further, during the interconnecting mode, it is necessary to control the power flow in real-time from different DERs of MGs to the individual MGs own loads as well as to the other MGs by prioritizing RES and storage systems maximum utilization. This feature has also been not considered in the existing interconnected MGs. Therefore, in this research different PMSs are developed to ensure that multiple MGs can operate effectively both in self-healing mode (islanded MGs) and

interconnected modes (grid-connected MGs) to ensure better stability and power quality of all the MGs.

Another challenge associated with multiple MGs while modeling the multi-layer control and PMSs. Since the MGs involved in the interconnected MGs system can operate in different possible configurations including islanded, grid-connected, interconnected and self-healing. These possible configurations and specific characteristics of RE offer challenges in designing control and management algorithms for power, voltage, and frequency in all operating scenarios. There is no multi-layer control strategy (MLCS) proposed in any of the available literature on interconnected MGs to allow several MGs to run in distinct operating modes. In order to ensure flexible and reliable operation of interconnected MGs, a controller with multiple layers is required which will help MGs to smoothly transit among grid-connected, islanded, interconnected and self-healing modes of operations.

### **1.3 Research Objectives**

The main objective of the research is to develop real-time control and PMSs for two interconnected MGs with self-healing feature to improve the power quality, reliability and ensure flexible & smooth operation under different operating modes. This aim can be achieved through the accomplishment of the following sub-objectives.

1. To model power control methods for grid-connected microgrid's PV voltage source inverter without using PLL and Park transformation.
2. To design power management systems for grid-connected and islanded single microgrid prioritizing maximum utilization of renewable energy sources, energy storage and critical load.
3. To propose an intelligent interconnection method (IIM) for interconnecting two microgrids based on microgrids' generation capacity and load demands.

4. To develop power management strategies for enhancing reliability of two interconnected microgrids during self-healing and interconnected modes of operation.
5. To form a multi-layer control strategy for two interconnected microgrids to ensure smooth transition among grid-connected, islanded, interconnected and self-healing modes of operation.

#### 1.4 Methodology

This overall methodology to accomplish the aims of the study is presented in Figure 1.2.

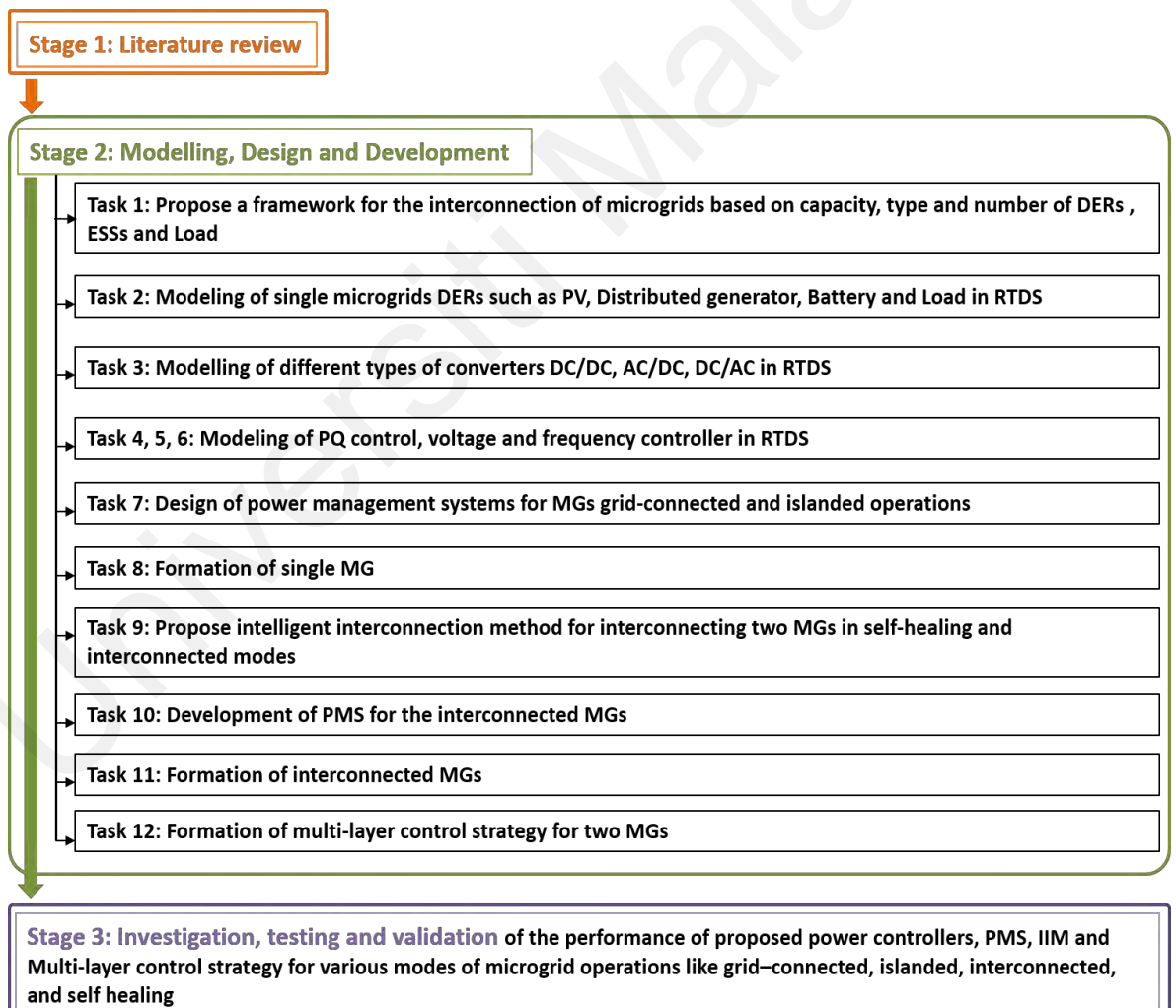


**Figure 1.2: Overall methodology of the proposed research work**

## **1.5 Outline of the Thesis**

### **Chapter 1: Introduction**

This chapter introduces the basic concept of MG system along with its benefits and related issues. Later, the problems associated with the single and multiple interconnected MGs operation, control and management are briefly discussed. Finally, it outlines the research objectives, brief methodology and organization of the thesis.

### **Chapter 2: Literature Review**

In this chapter, a comprehensive literature review on the single MG different control schemes and advantages of the centralized scheme used in this thesis are explained in detail. In addition, the advantage & disadvantage, methods of MGs interconnection formation, control and management of interconnected MGs are presented extensively. Finally, a discussion is presented by summarizing the gaps of the existing MG research.

### **Chapter 3: Methodology**

Chapter 3 presents different architectures of single MG and interconnected MG used in this study. In this chapter, two power control methods for grid-connected PV VSI of MG are proposed without using PLL system. Further, an algorithm to interconnect multiple MGs along with the power management strategies adopted for resilient operation during self-healing and interconnected mode is presented. Finally, a multi-layer control strategy is proposed for the interconnect multiple MGs system to ensure smooth transition among different operating modes.

### **Chapter 4: Results and Discussions**

In this chapter, the results obtained to validate the performance of the proposed power control method for PV VSI of single grid-connected MG, real-time energy management

system proposed for grid-connected and islanded modes of operation of single MG are presented at the beginning. Later on, the performance of the proposed IIMs, power management strategies during self-healing and interconnected modes of multiple interconnected MGs are presented. Finally, the performance of the multi-layer control strategy proposed for smooth transition of multiple interconnected MGs in various operating modes is presented.

## **Chapter 5: Conclusions and Future Works**

In Chapter 5, by highlighting the important points of the research, extensive conclusions are drawn related to the accomplishment of each objective which is followed by citing the future works of the study to extend the research further.

## CHAPTER 2: LITERATURE REVIEW

### 2.1 Introduction

In this chapter, in the beginning, a detailed literature review on MG's benefits, control schemes, and energy management system is presented. Later on, the advantage & disadvantage, methods of MGs interconnection formation, control and management of interconnected MGs are presented extensively. Finally, a discussion is presented by summarizing the gaps of the existing MG research.

### 2.2 MG Definition and Benefits

Power generation in the traditional power grid is highly centralized, with power and energy flowing unidirectionally from large synchronous generators through a transmission/distribution network to end users. However, the technological issues associated with traditional electric utilities, as well as the environmental problems caused by the combustion of fossil fuels, have stimulated research and development into new power system technologies. With the emergence of DER units, e.g., wind, PV, battery, biomass, micro-turbine, fuel cell, etc., MG technologies have attracted increasing attention as an effective means of integrating such DER units into power systems. However, there is no clear definition of a MG, and the concept varies in different countries and regions. Based on the European Technology Platform of Smart Grids (Hatziargyriou, 2014), a MG is a platform that facilitates the integration of DGs, ESSs and loads to ensure that the power grid can supply sustainable, price-competitive and reliable electricity. Figure 2.1 shows a typical MG structure, comprising DGs, such as combined heat and power unit (CHP), microturbines, PV systems, wind power systems, fuel cells; a distributed energy storage (DES) facility such as battery banks, super-capacitors, flywheels, electric vehicles; flexible loads and control devices.

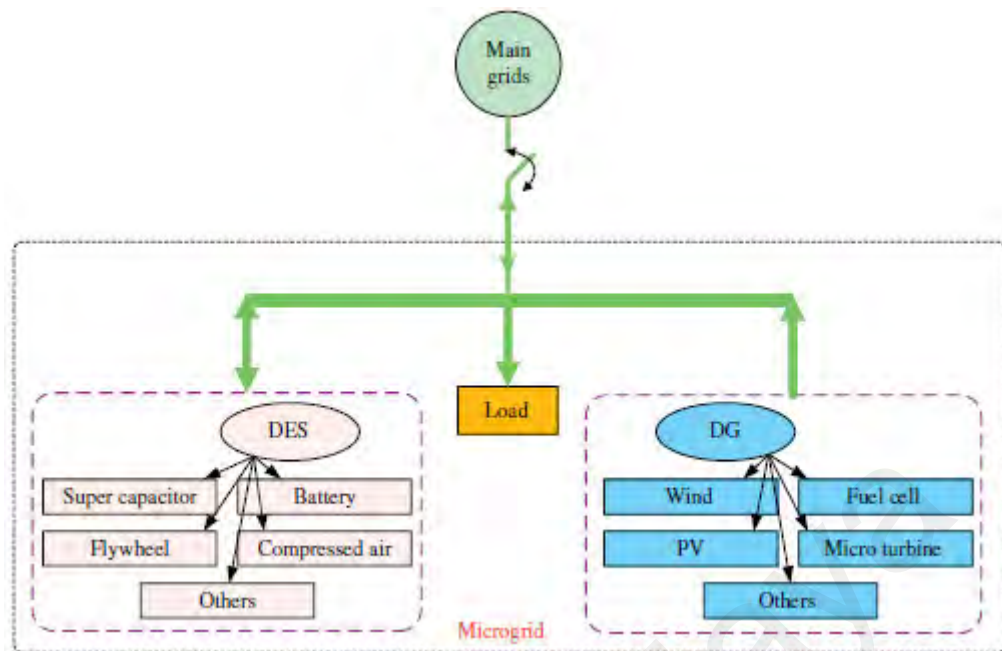


**Figure 2.1: Typical structure of a microgrid (Hatziaargyriou, 2014)**

As mentioned, MGs provide an effective way for integrating small-scale DERs in proximity of load into low-voltage distribution network. MGs can supply highly reliable power to a wide range of customers, both residential and commercial, such as schools, hospitals, warehouses, shopping centers, university campuses, military installations, data centers, etc. Various research stations (Arctic-based or space-based) can also utilize this technology to enhance their operation since it will provide an uninterrupted power supply. It is also useful for remote places having no or limited access to the utility grid. Further, it is beneficial for customers facing large power outages (for example, hurricane-prone areas). MG technology can also be used in areas facing high stress and congestion in their transmission and distribution systems.

There are many benefits of implementing MGs. They help facilitate the integration of DG, most notably, RE resources such as wind and solar. This helps curb the dependency on fossil fuels as a source of electricity, significantly reducing carbon emissions and pollution, and thus promoting energy sustainability. They also facilitate the use of highly efficient generators which utilize combined heat and power technology. They can

increase the quality of power at the consumer side. With proper control, MGs increase electrical reliability by decreasing outage occurrences as well as their duration. Utilities see MGs as controllable loads, which can contribute to peak shaving during times of peak demand by reducing their consumption via shedding of non-critical loads and delivering more power to the main grid utility. MGs can lower overall distribution system losses by implementing DG located at the demand site eliminating the need for transmission lines and deferring the construction of new transmission lines to a later time. This also results in higher energy efficiency. By using RE resources like wind and solar fuel costs can be reduced.

### **2.3 Different Configurations of Microgrid**

In practice, three different configurations of MG are used namely, AC MG, DC MG and Hybrid AC-DC MG based on load types. In this section, the detailed constructions of these MGs are presented. At the end of this section, a comparison among the MGs is presented in Table 2.1.

#### **2.3.1 AC Microgrid**

The utility grid is connected to the AC MG via AC bus, and it controls the connection and disconnection using a circuit breaker depending on the system condition. Figure 2.2 shows AC MG structure in which PV, wind, other renewable sources, and the battery storage system (BSS) is connected with the suitable converter to the AC bus and load is directly connected without any power electronics interface. The AC MG is preferable considering the fact that almost all the electrical load works on AC supply system and is most dominant in the research and development. The advantage of AC MG is that it directly connects with the utility grid without any bi-directional converter. The disadvantage is that it requires a sophisticated control system and its operation and management are difficult.

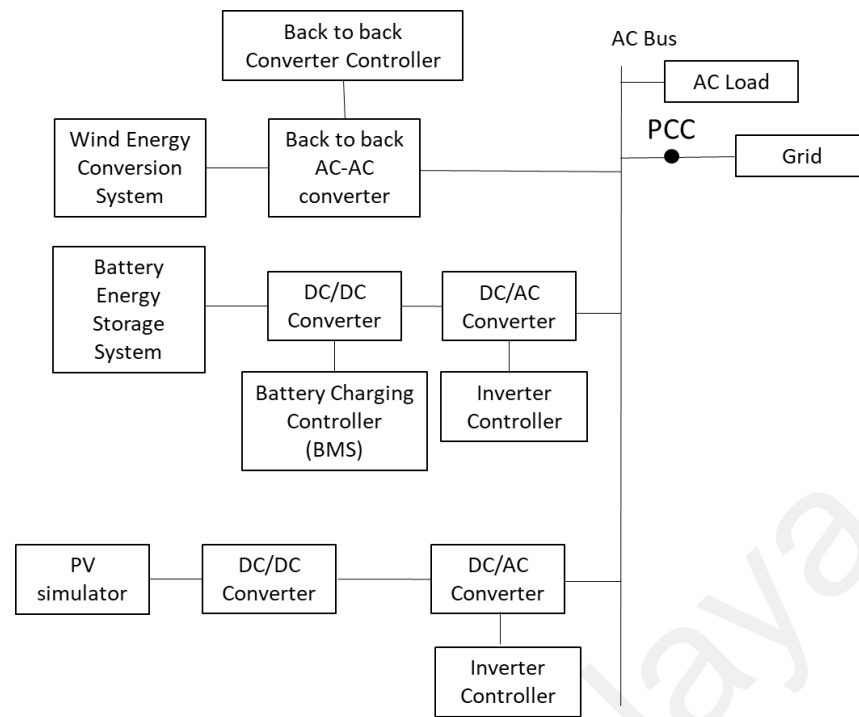


**Figure 2.2: General configuration of AC microgrid**

### 2.3.2 DC Microgrid

As shown in Figure 2.3, the PV, wind, other renewable sources, battery, and the load is connected to DC bus with appropriate individual converter system. The DC bus is connected with the utility grid with bi-direction DC-AC converter for power exchange for maintaining the power balance. The advantages of DC MG are as follows:

- Higher energy efficiency and reduced energy conversion losses with the reduction in the used-on converters.
- Easier RES integration, control, and coordination as control solely based on DC voltage.
- More efficient supply to the load.
- RES generation and load fluctuations are easily managed using a battery to supply deficient power.
- Optimal operation of rotating renewable generators with the elimination of the need for synchronization.
- Easier to damp circulating current between RES.

- Grid integration is easier.

Most of the load work on AC and requirement of inverters to convert the DC supply to AC is its only disadvantage. Also, in DC MG distribution system, the voltage drops in a subsequent part of the network, and at the far end of the network the voltage level is low, hence requires intermediate voltage boost in case of medium to vast DC MG distribution network.

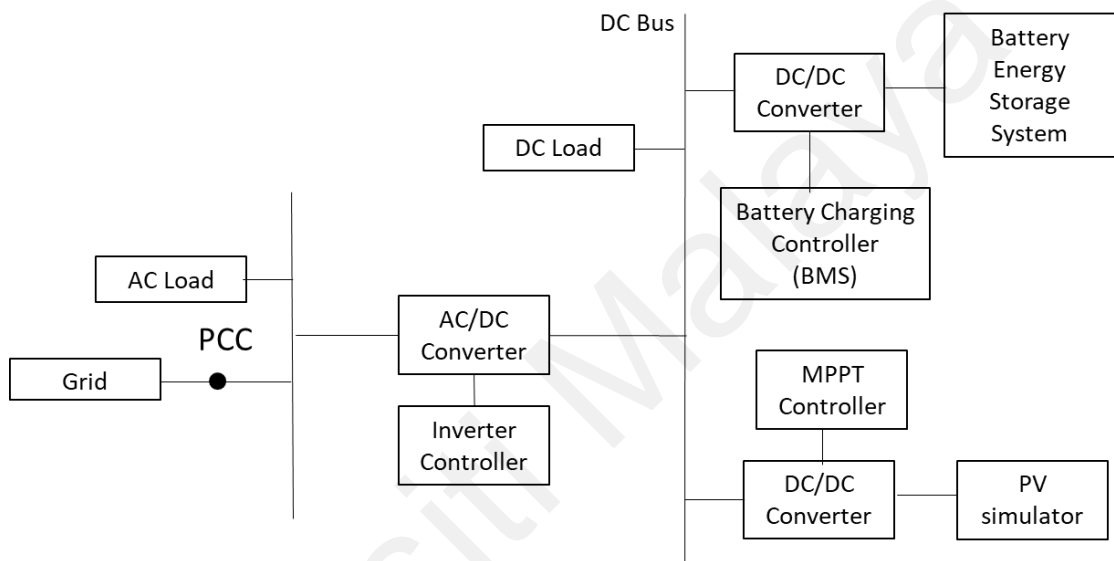


**Figure 2.3: General configuration of DC microgrid**

### 2.3.3 Hybrid Microgrid

The hybrid MG consists of AC as well as DC bus in MG structure, as shown in Figure 2.4. The AC bus directly connects to the utility grid without any converter and supplies power to loads. The DC bus connects PV, wind, other renewable sources, and battery directly and can supply power to DC loads if any. The power exchange between AC bus and DC bus occurs using a bi-directional converter to provide power to AC loads, store cheap utility power in batteries and perform various grid support functions like ancillary support, grid voltage support, etc. The hybrid MG has advantages of DC as well as AC MG, which overcomes the disadvantage of both structures. A comparison among AC, DC and hybrid MGs are presented in Table 2.1.

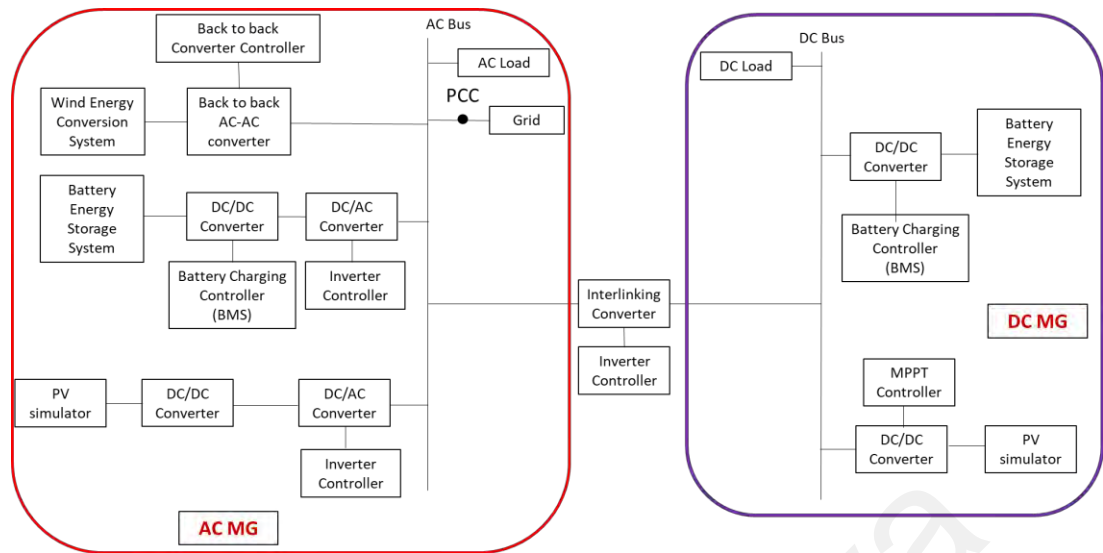


**Figure 2.4: General configuration of hybrid AC-DC microgrid**

**Table 2.1: Comparison among different MGs**

Factors	AC Microgrid	DC Microgrid	AC/DC Hybrid Microgrid
<b>Conversion efficiency</b>	Multiple energy conversion reduce efficiency	Less conversion processes increase efficiency	Multiple energy conversion in AC MG reduce efficiency
<b>Transmission efficiency</b>	Continuous reactive current loss reduces efficiency	Absence of reactive components increases efficiency	Continuous reactive current loss in AC MG reduces efficiency
<b>Stability</b>	Affected by external disturbances	Free from external effects	AC MG is affected by external disturbances
<b>Synchronisation</b>	Synchronisation required	No synchronisation required	Synchronisation required in AC MG
<b>Power supply reliability</b>	Supply can be affected during seamless transfer	Power supply generally reliable	Supply can be affected during seamless transfer in AC MG
<b>Microgrid controls</b>	Control process complex due to frequency	Simple control approach	Control process complex due to frequency in AC MG
<b>Protection system</b>	Simple, cheap and mature protection system	Complex, costly and immature protection system	Complex, costly and immature protection system
<b>Suitability</b>	AC loads	DC loads	AC and DC loads
<b>Calculation methods</b>	Complex numbers involved	Only real number used	Complex numbers involved

## 2.4 Microgrid Operating Modes

MG operates in two modes, which are grid-connected mode and Islanded mode. The grid-connected mode is divided into two operating modes as power-mismatched operation and power-matched operation as per power exchange between MG and utility grid. In the power-mismatched mode of operation active power ( $\Delta P \neq 0$ ) and reactive power ( $\Delta Q \neq 0$ ) are not equal to zero and current flows between MG and utility grid. If  $\Delta P > 0$ , the power flows from network to MG to cater the load demand as power generation from RES is insufficient and if  $\Delta P < 0$ , the energy flows from MG to the system after meeting load demand as power generation from RES is surplus. In the power-matched operation mode, active ( $\Delta P=0$ ) and reactive ( $\Delta Q=0$ ) are balanced which means that generated power from RES meets the load demand and no power exchange between MG and grid occurs. Hence this mode is the most economical MG operation mode. Similarly, reactive power is excessive if  $\Delta Q < 0$  and deficient if  $\Delta Q > 0$ , this variation in reactive power is categorized under power mismatch.

### 2.4.1 Grid Connected Mode

In this mode of operation, MG is connected with the utility at Point of Common Coupling (PCC) to exchange power with the distribution network. The MG can transfer its mode using connection/disconnection controls as:

- When MG is operational and connected with utility via PCC, it can be disconnected from utility by grid disconnection control; when not connected with utility, it can be connected by grid connection control.
- In grid disconnection control, MG stop working in grid-connected mode and switch to Islanded mode while in grid connection control, MG stop working in Islanded mode and switch to the grid-connected mode of operation.

- When MG is operating in grid-connected or Islanded mode, it can stop working using shut control.

#### **2.4.2 Islanded Mode**

In this mode of operation, the MG is disconnected from the utility due to grid faults or scheduled disconnection operation. The RESs, BSS, other renewable sources and load work independently with individual control functions. The electricity generated in this mode might not be sufficient all the time to cater to the load demand, and hence, it is necessary to prioritize the critical loads. An Islanded mode of operation is carried by shedding unimportant load during inadequate availability of electrical energy in MG using load-shedding control to ensure the uninterrupted electricity supply.

### **2.5 Control Architectures in Microgrids**

Depending on the functions performed by different control levels, the MG system can be operated based on centralized or decentralized scheme (Hatziargyriou, 2014). At the end of this section, a comparison among different MG control methods is presented in Table 2.2.

#### **2.5.1 Centralized Control**

In a single MG, MG central controller (MGCC) is the central controller (Hatziargyriou, 2014). MGCC collects information such as load demand, generation capacity of DG units, state-of-charge (SOC) of storage battery units, solar irradiation, wind speed, etc. (Liu, McArthur, & Lee, 2016). Using this information, MGCC runs an optimization algorithm to determine the optimal operation based on chosen objectives (Madureira, 2010). MGCC has the function of sending the required power set-points to DG and storage battery units according to the load demand in MGs (Korres, Hatziargyriou, & Katsikas, 2011). Thus, the fundamental objective of MGCC is the optimal operation of the MG system

(Madureira, 2010). Generally, two market services are identified for the MG system as follows (Hatziargyriou, 2014):

- The MG system can cater to its own needs or load demands and try to minimize power drawn from the grid.
- MG participates in the energy market through an aggregator and tries to achieve profit maximization by the optimal usage of generation and load.

In normal grid-connected mode of the MG system, the consumers can participate in energy market by providing interruptible loads (Hatziargyriou, 2014). In this way, consumers can shift the operation of their loads by shifting their load consumption from peak periods to off-peak periods (Liu et al., 2016). The centralized controllers such as MGCC help the consumers to shed the desired loads and achieve energy savings and reasonable profit margins (Madureira et al., 2011). These centralized controllers should not have their primary motivation as profit maximization in market participation, but their primary goal should be to serve load and heat demand and to achieve improved power quality and better efficiency in the MG system (Hatziargyriou, 2014). Different research works on centralized control of MG systems are available in the literature (Olivares, Cañizares, & Kazerani, 2014; Tan, Peng, So, Chu, & Chen, 2012).

Centralized control scheme is suitable for a MG system which has a common goal or operational aim, e.g., centralized control scheme is suitable for an industrial MG system in which the complete ownership of the MG system lies in the hand of a single owner (Liu et al., 2016). Dedicated personnel can also be employed to manage the centralized operation of the whole MG system (Liu et al., 2016). In addition, optimization problems for a MG system in centralized control scheme will have limited objectives such as minimization of fuel cost and limited constraints such as minimum and maximum operating costs (Madureira, 2010). Also, centralized controller is more preferable to

enable the interconnection of several MG systems and for setting up a large-scale energy market for energy trading among MG systems and the distribution grid in the future.

If centralized controller fails, the local controllers will take over the function of controlling the MG. Even though high communication needs are required for a centralized control scheme, reliable and high speed communication between centralized and local controllers will ensure the effective operation of the MG system (Liu et al., 2016). In addition, the centralized control scheme is more suitable for a large interconnected power system like the interconnected MG system, where high level of coordination is required among centralized and different local controllers. Moreover, standardized procedures and easy implementations are among the other advantages of centralized control scheme (Parhizi, Lotfi, Khodaei, & Bahramirad, 2015). The main disadvantages of centralized control scheme are the increased requirements for communication and the risk of single point failure (Liu et al., 2016). Because of its specific advantages, the centralized approach is used in this thesis for the operation and control of MG systems.

### **2.5.2 De-centralized Control**

Decentralized control scheme is also being used nowadays in MG and interconnected MG systems. In this scheme, the DGs, inverters and loads are controlled individually by local controllers and these controllers interact and communicate with each other to achieve optimal operation of the MG system (Liu et al., 2016).

Decentralized control scheme for MG control provides many distinct advantages in several practical cases, for example, when DG units have different owners and different objectives (Hatziargyriou, 2014). For example, DG owners might have different objectives such as heat production for DG units, providing backup system for local critical loads, maintaining voltage locally at a certain level, and so on, and these diverse objectives cannot be easily scheduled centrally (Hatziargyriou, 2014). Moreover, DG

owners in a MG operating in a market environment would most probably prefer that several decisions are taken locally by their intelligent controllers, rather than accepting set-points dictated by a centralized controller (Hatziargyriou, 2014). Such characteristics favor the application of decentralized control.

In a decentralized control scheme, the main disadvantage is that there is less coordination between centralized and local controllers (Hatziargyriou, 2014). Thus, the connection of the whole MG system directly as single entity to the distribution grid will be difficult (Liu et al., 2016). This results in reduced participation of DG and storage battery units of the MG system in the wholesale energy market (Hatziargyriou, 2014). For this scheme, high capital investment is required to install local controllers for all the individual MGs of the interconnected MG system and to satisfy the high communication requirements between these MGs (Liu et al., 2016). In order to manage high-voltage and medium-voltage distribution grids, high levels of peer-to-peer communication are needed which might be higher than the centralized communication requirements (Hatziargyriou, 2014). Also, in case of decentralized scheme, multiple owners, one for each MG system in the MG system will create uncertainty over what each owner wants at any particular moment (Liu et al., 2016).

Operation and control of decentralized systems are based on multi-agent system (MAS) theory (Liu et al., 2016). Many studies on decentralized control of interconnected MG systems are conducted in (Gu, Xiang, Li, & He, 2013; Liang, Choi, Zhuang, & Shen, 2013) and also MAS theory is explained and implemented in several MG systems in (Dou & Liu, 2013; Logenthiran, Srinivasan, Khambadkone, & Aung, 2012; Yue, Zhang, & Dou, 2021).

### 2.5.2.1 MAS Theory

From literature, the basic features of MAS theory are given as follows (Hatzargyriou, 2014):

- An agent is defined as a physical or virtual device that directly controls a DG unit or a battery unit, e.g., it can be a piece of software that controls a DG unit.
- An agent can modify the environment in which it operates, e.g., a battery unit, by modifying its power output, can alter the power outputs of other adjacent DG or battery units.
- Agents need to maintain a good level of communication capability to achieve a reliable operation of the MG or MG system, e.g., consider a system that includes a DG unit and a battery unit. The battery unit charges itself by taking energy from the DG unit and it discharges when the power output of DG unit is less. To achieve this coordinated operation, the two agents of battery and DG units should communicate effectively.
- Agents can divide the level of autonomy of their operation, e.g., a battery unit can decide when to get charged or discharged. It can decide to get charged when the cost of power supplied by grid is low and it can also decide to discharge when the cost of power supplied by grid is high.
- Agent needs to have knowledge of its local environment but is not necessarily required to know the details of the entire system which is one of the main ideas of MAS theory.
- An agent has special skills or services, which are unique, e.g., an agent whose primary aim is to provide uninterruptible power supply to a load has a different behavior from an agent whose goal is to mainly achieve profits in the energy market.

### **2.5.3 Hierarchical Control**

Next, the researchers made the system controller a bit more complicated and came up with a hierarchical control system. In this control system, the whole control is divided into different levels. At the primary control level, each source has its primary control, and it is in charge of keeping the active power balance. Above this control level is the secondary control or the MGCC. At this level, the system tries to coordinate those primary controllers of the MG, and it does not interfere too much with the primary control operation, but it does give some settings and setpoints for them to follow. The next level of control is the tertiary level distribution network controller. If the system is composed of multiple MGs then this stage of control is going to coordinate all the central controllers of the MGs with respect to each other.

It can be said that Hierarchical is a much higher-level control system, Centralized is the middle-level control system, and decentralized is a very primary level control system. The main difficulty of the Hierarchical and Decentralized system is that there is a need for a strong communication system because, in these systems, almost every element communicates with one other. One of the main intentions to go towards building MGs in remote areas is to cut down on electricity costs but adding communications infrastructure is going to make the system more expensive. Then the idea of a distributed control system came into existence.

### **2.5.4 Distributed Control**

Distributed control scheme, a non-centralized control scheme similar to decentralized control scheme, has several advantages such as it does not require a dedicated communication network and a centralized controller to coordinate the DG units in a MG (Hatziargyriou, 2014). In this control method, the DG units have autonomous local controllers and there is effective communication among these local controllers over a

sparse communication network (Hatziargyriou, 2014). In addition, this method allows for the plug and play of new DG units and loads. Thus, the distributed control provides better flexibility and extensibility over the centralized control method (Hatziargyriou, 2014). In Table 2.2, a comparison among different MGs control methods is presented.

**Table 2.2: Comparison among different MGs control methods**

<b>Type</b>	<b>Advantage</b>	<b>Disadvantage</b>
<b>Centralized control</b>	<ul style="list-style-type: none"> <li>• Easy to implement</li> <li>• Easy to maintenance in the case of single point failure</li> </ul>	<ul style="list-style-type: none"> <li>• Computational burden</li> <li>• Not easy to expand (so it is not suitable for smart grids)</li> <li>• Single point of failure (highly unstable)</li> <li>• Requires a high level of connectivity</li> </ul>
<b>Decentralized control</b>	<ul style="list-style-type: none"> <li>• Local in formation only</li> <li>• No need for a comprehensive two-way high-speed communication</li> <li>• Without leaders, system still includes some control island-area</li> <li>• Parallel computation</li> </ul>	<ul style="list-style-type: none"> <li>• Absence of communication links between agents restricts performance</li> <li>• Moderate scalability</li> </ul>
<b>Distributed control</b>	<ul style="list-style-type: none"> <li>• Easy to expand (high scalability)</li> <li>• Low computational cost (parallel computation)</li> <li>• Avoids single point of failure</li> <li>• Suitable for large-scale systems</li> <li>• Not affected by changes in system topology.</li> <li>• Practical solution for plug- and-play characteristic of smart grid</li> </ul>	<ul style="list-style-type: none"> <li>• Needs synchronization</li> <li>• Maybe time-consuming for local agents to reach consensus</li> <li>• Convergence rates may be affected by the communication network topology</li> <li>• Needs a two-way communication infrastructure</li> <li>• Cost to upgrade on the existing control and communication infrastructure</li> </ul>

## 2.6 Control Schemes Adopted by Local Controllers in Microgrid

Local controllers are used to control the DG and storage battery units in the MG system (Hatziargyriou, 2014). With appropriate instructions from the centralized controller, the local controllers help in efficient power sharing among DG and storage battery units, and effective voltage and frequency regulation in the MG system (Liu et al., 2016). Different DG units such as PV, wind, and microturbine are connected to the load bus of the MG system through several converters such as AC/DC, DC/AC and DC/DC converters. Several control schemes are available to control the output currents of these converters

during grid-connected and islanded modes of the MG system (Liu et al., 2016). These control schemes are generally classified into classical and non-classical control schemes, which are explained as follows:

### **2.6.1 Non-classical Control Schemes**

With the advent of powerful fast microprocessors and workstations, new non-classical control schemes such as sliding mode, fuzzy logic and predictive control have come into existence (Holtz, 1994; Mohan & Undeland, 2003). In sliding mode control, the switching nature of the power converters is considered and in fuzzy logic control, the parameters of the controlled system are not known (Mohan & Undeland, 2003). Predictive control is an interesting control algorithm that has become popular for converter control in recent years (Blaabjerg, Teodorescu, Liserre, & Timbus, 2006). Various advantages of predictive control are that it is easy to understand its concepts; it can easily include constraints and non-linearities and it can consider different multi-variable cases (Mohan & Undeland, 2003). One disadvantage of predictive control is that it involves a lot of mathematical calculations (Blaabjerg et al., 2006). Therefore, predictive control is not the preferred control method used for various power converters in this thesis.

### **2.6.2 Classical Control Schemes**

Over the last few decades, current control has been used extensively for power converters. Among the classical control schemes, the most popular are hysteresis control and linear control using pulse width modulation (PWM) (Blaabjerg et al., 2006; Kazmierkowski, Krishnan, & Blaabjerg, 2002; Mohan & Undeland, 2003).

#### **2.6.2.1 Hysteresis Current Control**

Basic principle of hysteresis current control is to keep current error within a desired upper and lower limit or band (Kazmierkowski et al., 2002). In Figure 2.5 (a), hysteresis control scheme for a single-phase inverter is shown. Here if the current error is greater

than the upper limit  $\delta/2$ , then the switches  $T_1$  and  $T_4$  are turned on (Mohan & Undeland, 2003). If the current error is less than the lower limit  $-\delta/2$ , then the switches  $T_2$  and  $T_3$  are turned on (Mohan & Undeland, 2003). From Figure 2.5 (b), it can be seen that the load current  $i_L$  follows its reference  $i_L^*$  very closely. This method is simple to implement and has a good dynamic response (Mohan & Undeland, 2003). The disadvantage of this method is that switching frequency varies with the variation in the hysteresis band and a variable switching frequency causes resonance problem and switching losses (Kazmierkowski et al., 2002). These disadvantages restrict hysteresis control to lower power levels (Kazmierkowski et al., 2002). Also, a very high sampling frequency is needed to implement hysteresis controller in a digital control platform (Mohan & Undeland, 2003). Due to these disadvantages, hysteresis control is not suitable for inverter control in the proposed MG systems in this thesis.

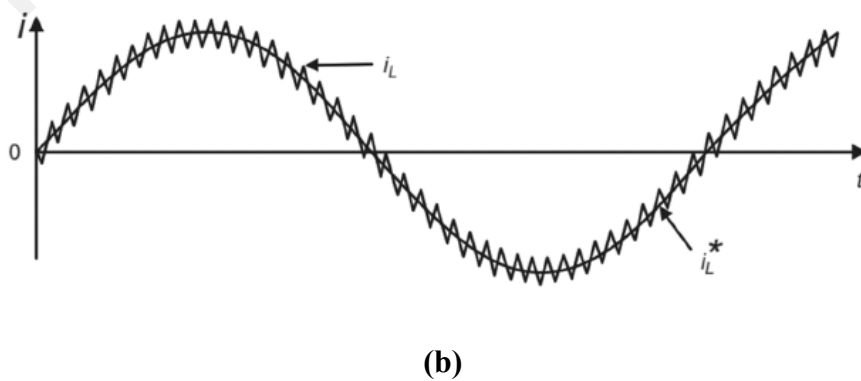
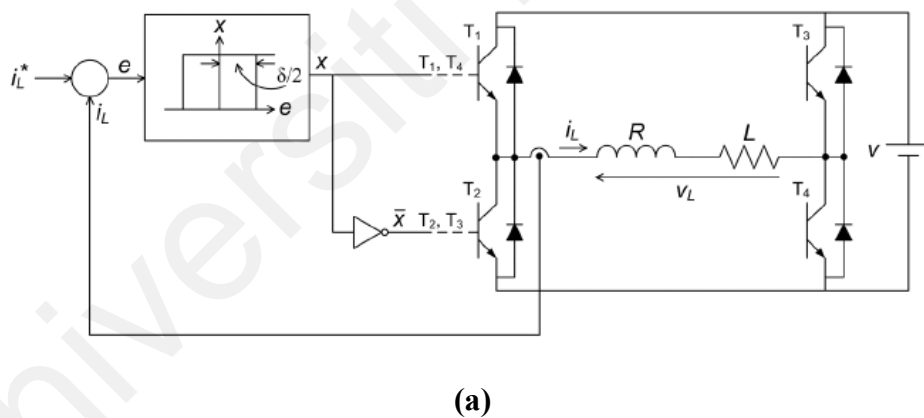


**Figure 2.5: Hysteresis current control for a VSI (a) control scheme, (b) load current (Mohan & Undeland, 2003)**

### 2.6.2.2 Linear Control with Pulse Width Modulation (PWM)

PWM of a single-phase inverter is shown in Figure 2.6 (a). In this method, a triangular carrier wave signal is compared with reference voltage and the voltage error signal is then fed into a comparator (Kazmierkowski et al., 2002). The output of this comparator is then used to drive the inverter switches (Mohan & Undeland, 2003). Generally, a proportional-integral (PI) controller is used as a comparator (Holtz, 1994).

Figure 2.6 (b) shows the waveforms for PWM. The amplitude of the carrier wave is same as that of the reference voltage (Mohan & Undeland, 2003). A pulsed voltage waveform is generated by comparing a triangular carrier wave with a reference sinusoidal voltage. The reference voltage is proportional to the fundamental component of this pulsed voltage (Mohan & Undeland, 2003).

The performance of PI controller depends mainly on the proportional and integral gains, and the frequency of the reference current (Mohan & Undeland, 2003). An advantage of PI controller is that it gives a zero steady-state error in case of continuous fixed reference, but its main disadvantage is that it gives a noticeable error in case of sinusoidal references (Blaabjerg et al., 2006). To overcome this issue, in case of sinusoidal references, the different variables involved are converted from the original coordinate transformation into a rotating reference frame, where the reference currents are constant values (Mohan & Undeland, 2003). This linear control is adopted for the control of multiple inverters in this thesis.

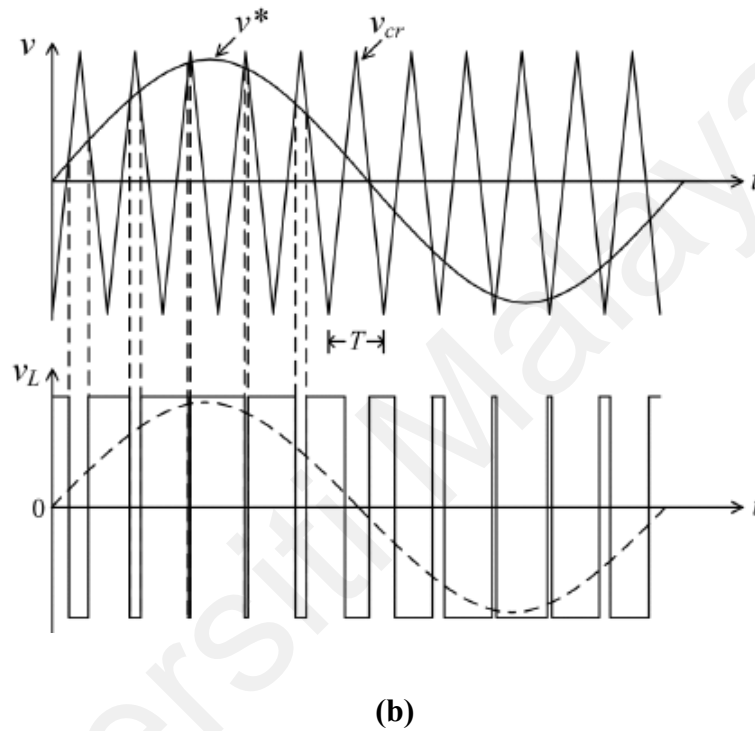
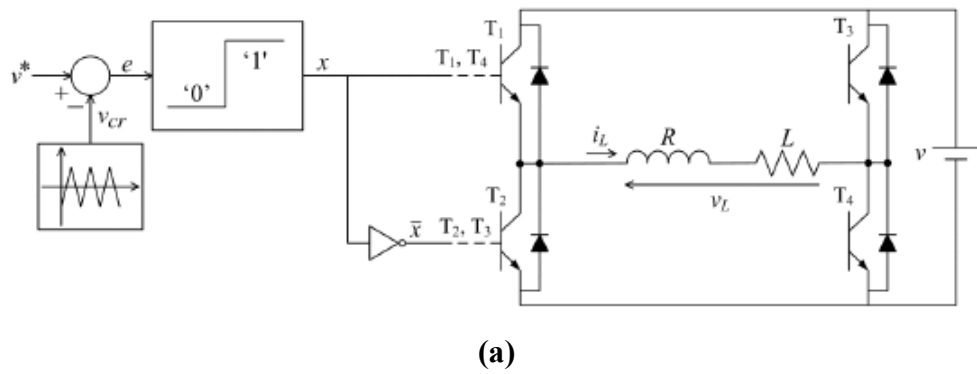


**Figure 2.6: Pulse width modulation for a VSI (a) control scheme, (b) waveforms (Mohan & Undeland, 2003)**

## 2.7 Microgrid Inverter Control Methods

In a MG, different kinds of control methods are applied to ensure reliable operation, in both grid-connected mode and islanded mode. Depending on the DG and operating conditions, there are three main types of control methods: PQ control, V/f control and droop control.

### 2.7.1 PQ Control

The main objective of PQ control is to keep the DERs' active power and reactive power constant when the frequency and voltage deviation stay within prescribed limits. In PQ control, the active and reactive power are firstly decoupled in order to achieve independent control. The active power controller aims to maintain the active power output constant at a given reference value within the permissible frequency range. The reactive power controller aims to maintain the reactive power output constant at the given reference value within the permissible voltage range. However, this PQ control method cannot maintain the frequency and voltage constant, so an extra DG is needed to regulate the voltage and frequency of the MG within the acceptable range. If MG operates in the grid-connected mode, the main power grid is responsible for maintaining the voltage and frequency of the MG.

For grid-tied MG, many power control schemes have been proposed based on dq CCT in past studies to enhance the efficacy, safety and reliability of the VSIs. For instance, for grid integration of PV and BSS in AC MG, a decoupled dq current control based power control strategy is designed and validated in (Worku et al., 2019). A rigid power controller is proposed in (Safa et al., 2018) for a grid-connected VSI to improve AC MG power quality. For grid-tied AC MG, real power, reactive power and voltage of PCC are used in (Adhikari, Li, & Li, 2015) to develop power control strategy for VSI. By cascading voltage and current controller, a new power control scheme is proposed in (Lou et al., 2020) for an AC MG VSI. For a hybrid grid-tied PV/hydrogen system, a siding mode based power control strategy is presented in (Abadlia, Adjabi, & Bouzeria, 2017). In (Al-Saedi, Lachowicz, Habibi, & Bass, 2013), an optimal power flow control method based on real-time self-tuning approach is proposed for a grid-tied MG. A power control strategy is proposed for a PV/Battery hybrid system integrated with utility grid in (Adhikari & Li, 2014). A coupled voltage support and harmonic compensation method is

presented in (Mousavi, Jalilian, Savaghebi, & Guerrero, 2018), for DG interfaced VSIs in grid-tied AC MG. In (Feng, Sun, Guan, Guerrero, & Xiao, 2016), for enhancing the quality of power, a control strategy is developed where the MG is connected to distorted grid. In (Sedaghati & Shakarami, 2019), for a grid-connected MG, new control and power management strategy were presented. A new power control method based on ANN (ANN) to control the power quality of PV incorporated AC MG is presented in (Kaushal & Basak, 2020). By cascading voltage and current controller, a new power control scheme is proposed in (Lou et al., 2020) for an AC MG VSI. A CCT based dq axes synchronous reference frame based power control method is proposed in (Ahmad, Mekhilef, & Mokhlis, 2020) for grid-connected AC MG's VSI. A rigid power controller is proposed in (Safa et al., 2018) for a grid-connected VSI to improve AC MG power quality. For a grid-connected MG PV system, optimal power control is proposed in (Guichi et al., 2021) under partially shaded conditions. For controlling the VSI of a grid-tied AC MG, Smadi et. al. proposed a compact control strategy based on dq CCT (Smadi, Albatran, & Alsyouf, 2018). To regulate the power flow between grid and PV/battery hybrid system, Go et. al. proposed a power control strategy for VSI (Go & Choi, 2020). For controlling the output power of grid-tied PV VSI in AC MG, a voltage-oriented power coordination strategy was proposed by Tang et. al. (Tang et al., 2021). A summary of different power control methods implemented in grid-tied VSIs in AC MG system are presented in Table 2.3.

All these methods are based on dq CCT where phase angle used in Park transformation during abc to dq transformation has to be extracted from the grid voltages correctly to ensure dq axes currents and grid voltages are in phase with each other (Lee et al., 2020). The most commonly used technique nowadays for phase angle extraction of the grid voltage for grid synchronization is PLL (Ali et al., 2018). By filtering grid voltages and using arctangent function, the phase angle can be extracted (Lee et al., 2004). However, a slow transient response will be the result of the PLL system. In (Davari & Mohamed,

2016), on the small-signal stability of VSIs, the adverse impact of the PLL has been reported. High power ripples in the real and reactive powers are also caused by PLL system (Wang et al., 2017). Furthermore, the stability of VSIs may be deteriorated by PLL via initiating negative resistance at low frequencies (Wang & Blaabjerg, 2018). In (Harnefors et al., 2015; Wen et al., 2015), the frequency coupling dynamics of VSIs introduced by the PLL have also been explicitly revealed. By using the bandwidth of PLL, the frequency range of the negative resistance is determined. Therefore, in order to improve the stability robustness of VSIs, the low bandwidth PLL is usually adopted, which jeopardizes the dynamic performance of the system significantly.

In some studies, fuzzy logic controller (FLC) based control methods have been proposed for VSIs while operating in grid-tied or autonomous modes for DG applications. Hasanien et. al. proposed a FLC based control method to maintain the output voltage of VSI for the islanded DG system during load variability and weather uncertainties (Hasanien & Matar, 2014). A type-2 FLC based control method was developed by Heydari et. al. for VSIs of autonomous Naval Shipboard MGs to damp the steady-state deviations of voltage and frequency (Heydari, Gheisarnejad, Khooban, Dragicevic, & Blaabjerg, 2019). However, in Hasanien & Matar, (2014) and Heydari et al., (2019), FLC controllers are used to control the output voltage and frequency of VSI during islanded operation. Thao et al. developed a power control method by combining feedback linearization and FLC to reduce the fluctuations in the VSI's output active and reactive powers at the steady-state for a grid-tied PV system (Thao & Uchida, 2013). FLC based power control method was proposed by Omar et. al. to control the output power of grid-connected PV VSI (Omar, El-Deib, El Shafei, & Abdallah, 2016). Jamma et al. proposed a FLC and ANN combined DPC for controlling the VSI output power of a grid-tied PV system (Jamma, Bennassar, Barara, & Akherraz, 2017). For a grid-tied PV system VSI, a control method based on FLC and Levenberg–Marquardt optimization method was

proposed by Islam et.al. (Islam et al., 2019). Shadoul et al. proposed an adaptive FLC based control method for grid-tied PV VSIs (Shadoul, Yousef, Abri, & Al-Hinai, 2021). FLC based active and reactive power control was proposed by Tahri et al. for a grid-tied PV system's neutral-point-clamped VSI (Tahri et al., 2021). Teekaraman et al. developed a FLC based current control method for a grid-tied Z-source VSI (Teekaraman et al., 2020). In all these studies, even though FLC is considered while designing the feedback controller, however, all the control methods are based on dq CCT where Park Transformation has also been used for abc to dq transformation and PLL was implemented to extract the voltage angle. As mentioned earlier, due to the use of PLL system, the control methods performance deteriorated and most of the control methods consist of two control loops. As a result, undesirable ripples are observed in the VSI output powers, and controllers took longer time to track the reference powers. Further, the performances of all these controllers are validated only for grid-tied PV systems which are not connected to MGs.

To resolve the problem of PLL system, some of the studies (Kewat & Singh, 2020; Rodríguez et al., 2010; Šimek, Škramlík, & Valouch, 2019) have proposed frequency locked loop (FLL) based synchronization technique for MG's VSI. Though for these control methods power tracking performance has improved slightly, but there are still undesirable ripples in both real and reactive power are found.

In the aforementioned controllers, two control loops namely outer and inner control loops for power and current control, respectively have been considered while designing the power control scheme. Due to the presence of two control loops the computation burden increases (Gui, Wang, et al., 2018). Therefore, direct power control (DPC) method is proposed for VSI without using any inner-loop current regulator. For example, based on only power control loop in (Gui, Kim, et al., 2018; Gui, Wang, et al., 2018) a control mechanism has been proposed to control real and reactive power. However, these

methods have variable switching frequency; therefore, the designing of line filter is difficult as the variable switching frequency causes an unexpected harmonic spectrum. In order to enhance robustness and fast tracking of the real and reactive power references in (Gui, Lee, Kim, & Chung, 2017), a sliding mode control based DPC method has been introduced. Though power tracking performance has been improved, but there are still undesirable ripples in both real and reactive power are found. By considering the system limitations, nonlinearities and multivariable sample, DPC strategy based on model predictive control (MPC) is proposed in (Choi & Lee, 2014; Vazquez et al., 2014). However, this method possessed extra computational burden. Furthermore, the performances of the above-mentioned control methods are greatly influenced by the accurate tuning of PI controller gains, conditions of grid voltage and comprehensiveness of the current decoupling (Gui, Kim, & Chung, 2017). In addition, these controllers perform poorer during varying dynamic load conditions due to the existence of multivariable parameters.

**Table 2.3: Comparison among different PQ control methods of grid-connected AC MGs**

#	Control Method	Synchronization method	No of control loops	Filter types and Values	Power Ripple	Settling Time	Controller	% THD of VSI Output Current
1	(Worku et al., 2019)	PLL based	2	Low pass LC, large	Large	Long	PI	$\leq 4.5$
2	(Safa et al., 2018)	PLL based	2	Low pass LC, large	Large	Long	PI	$\leq 4.5$
3	(Kaushal & Basak, 2020)	PLL based	2	Band pass, large	Large	Long	PI	$\leq 4.5$
4	(Adhikari et al., 2015)	PLL based	2	LCL, large	Medium	Medium	PI	$3.5 \leq \text{THD} \leq 4.5$
5	(Lou et al., 2020)	PLL based	2	L, large	Medium	Medium	PI	$3.5 \leq \text{THD} \leq 4.5$
6	(Abadlia et al., 2017)	PLL based	2	Low pass LC, large	Large	Long	PI	$\leq 4.5$
7	(Al-Saedi et al., 2013)	PLL based	2	Low pass LC, large	Large	Long	PI	$\leq 4.5$
8	(Adhikari & Li, 2014)	PLL based	2	Low pass LC, large	Large	Long	PI	$\leq 4.5$
9	(Mousavi et al., 2018)	PLL based	2	Low pass LC, large	Large	Long	PI	$\leq 4.5$
10	(Feng et al., 2016)	PLL based	2	Low pass LC, large	Large	Long	PI	$\leq 4.5$
11	(Sedaghati & Shakarami, 2019)	PLL based	2	Low pass LC, large	Large	Long	PI	$\leq 4.5$
12	(Lou et al., 2020)	PLL based	2	L, large	Medium	Medium	PI	$3.5 \leq \text{THD} \leq 4.5$
13	(Ahmad et al., 2020)	PLL based	2	Band pass, large	Large	Long	PI	$\leq 4.5$
14	(Safa et al., 2018)	PLL based	2	LCL, large	Medium	Medium	PI	$3.5 \leq \text{THD} \leq 4.5$
15	(Guichi et al., 2021)	PLL based	2	Band pass, large	Large	Long	PI	$\leq 4.5$
16	(Smadi et al., 2018)	PLL based	2	L, large	Medium	Medium	PI	$3.5 \leq \text{THD} \leq 4.5$
17	(Go & Choi, 2020)	PLL based	2	Low pass LC, large	Large	Long	PI	$\leq 4.5$
18	(Tang et al., 2021)	PLL based	2	Low pass LC, large	Large	Long	PI	$\leq 4.5$
19	(Thao & Uchida, 2013)	PLL based	2	Low pass LC, large	Medium	Medium	FLC	$3.5 \leq \text{THD} \leq 4.5$
20	(Omar et al., 2016)	PLL based	2	Low pass LC, large	Medium	Medium	FLC	$3.5 \leq \text{THD} \leq 4.5$
21	(Jamma et al., 2017)	PLL based	2	L, large	Medium	Medium	FLC	$3.5 \leq \text{THD} \leq 4.5$
22	(Islam et al., 2019)	PLL based	2	Low pass LC, large	Medium	Medium	FLC	$3.5 \leq \text{THD} \leq 4.5$
23	(Shadoul et al., 2021)	PLL based	2	Low pass LC, large	Medium	Medium	FLC	$3.5 \leq \text{THD} \leq 4.5$
24	(Tahri et al., 2021)	PLL based	2	Low pass LC, large	Medium	Medium	FLC	$3.5 \leq \text{THD} \leq 4.5$
25	(Teekaraman et al., 2020)	PLL based	2	L, large	Medium	Medium	FLC	$3.5 \leq \text{THD} \leq 4.5$

26	(Kewat & Singh, 2020)	FLL based	2	Low pass LC, large	Medium	Medium	PI	$3 \leq \text{THD} \leq 4$
27	(Šimek, Škramlík, & Valouch, 2019)	FLL based	2	Low pass LC, large	Medium	Medium	PI	$3 \leq \text{THD} \leq 4$
28	(Gui, Wang, et al., 2018)	Direct Power calculation	1	Low pass LC, large	Medium	Medium	PI	$3 \leq \text{THD} \leq 4$
29	(Gui, Wang, et al., 2018)	Direct Power calculation	1	L, large	Medium	Medium	PI	$3 \leq \text{THD} \leq 4$
30	(Gui, Lee, et al., 2017)	Direct Power calculation	1	L, large	Medium	Medium	Sliding mode control	$3 \leq \text{THD} \leq 4$
31	(Choi & Lee, 2014)	Direct Power calculation	1	L, large	Medium	Medium	PI	$3 \leq \text{THD} \leq 4$

### 2.7.2 V-f Control

In V-f control, the output voltage and frequency of VSI are needed to be constant to enable RES operation in slave mode and critical loads when the MG is disconnected from the utility. It is necessary to curtail load in Islanded mode of operation considering the low generation capacity of the MG to maintain the continuity of power supply to critical loads. Hence, this control must be able to respond and detect load switching. To keep the constant output, based on feedback from the VSI, the AC side voltage is regulated and the dual-control scheme is adopted with voltage control in outer-loop and current control in inner-loop (Guo, Li, & Zheng, 2020). The function of voltage control in outer-loop is to maintain output voltage constant and current control in inner-loop to accelerate the fast response against load fluctuations or disturbances. In V-f control mechanism, the current control in the inner loop has wide bandwidth in the inverter control which increases the speed of dynamic response of inverter dynamic response ability and adaptability for non-linear load disturbances with reduced harmonic distortion in output voltage. In terms of decoupling and control functions, the V-f control is like P-Q control. In this study, to control voltage and frequency of MG in islanded mode, this control method is used because it has high dynamic response & steady-state accuracy and it makes the best usage of system status information.

### 2.7.3 Droop Control

The droop control method is based on power converter's parallel-connection technology. This control algorithm is implemented by mimicking the droop characteristics of traditional generational connected to the utility. The voltage and frequency output of VSI is controlled according to the variation of the power output. The MG operating in Islanded mode with multiple RES inverters connected in parallel, individual inverters active and reactive power equation is expressed as:

$$P_n = \frac{VV_n}{X_n} \delta_n \quad (2.1)$$

$$Q_n = \frac{VV_n - V^2}{X_n} \quad (2.2)$$

Where  $V$  is the voltage at inverter point of connection,  $V_n$  is the output voltage of the inverter,  $\delta_n$  is an angle between  $V$  and  $V_n$  and  $X_n$  is output impedance (reactance) inverter. From Equations (2.1) and (2.2), it is evident that active inverter power mainly depends on the angular difference ( $\delta_n$ ) between the voltage at the point of connection (or PCC) and inverter output voltage while reactive power primarily on voltage magnitude. By controlling the output frequency, the inverter phase can be controlled, and the voltage can be directly controlled with appropriate triggering strategy. The frequency of the inverter is given as:

$$f_n = \frac{\omega_n}{2\pi} = \frac{d\delta_n}{dt} \quad (2.3)$$

From Equations (2.1) - (2.3), it is evident that inverter output voltage regulates its reactive power output and frequency regulates its active power. The inverse droop control strategy is to control its active and reactive power outputs based on measured grid voltage magnitude and frequency by calculating the predefined droop control characteristics (Li, Li, & Zhou, 2015). The inverter output voltage is regulated by measured active power;

hence, this control mode is inverse droop control. Figure 2.7 shows the MG droop control characteristics for active and reactive power. The DERs inverters can use any of these discussed control methods, and output can be controlled using local measurement data to achieve smooth and reliable operation of the MG.

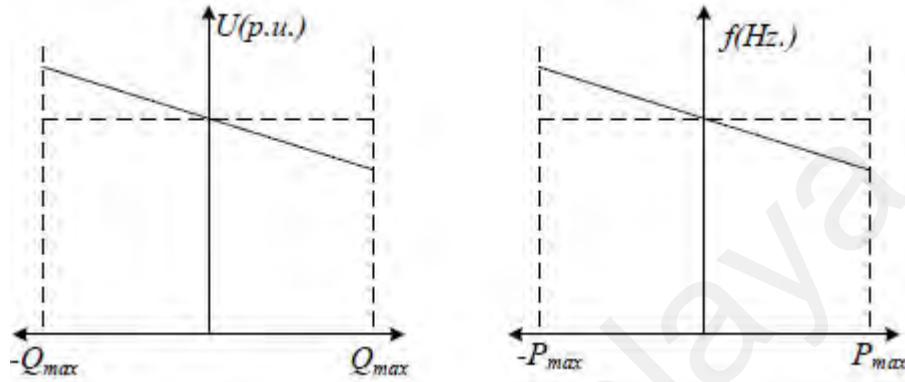


**Figure 2.7: Microgrid droop control characteristics**

## 2.8 Microgrid Power Management

In a MG, it is essential to maintain the power supply-demand balance for stability because the intermittent DERs such as PVs and WTs are hard to predict and their generation may fluctuate significantly depending on the availability of the primary sources (e.g., solar and wind). The supply-demand balancing problem becomes even more challenging when the MG is operating in islanded mode where only limited supply is available to balance the demand. To solve this problem, power management is needed to manage the operations of the DERs and loads in order to maintain the supply-demand balance in a MG. In the following section, different types of PMSs are presented.

### **2.8.1 Power Management Systems**

Sound operation of a MG requires an PMS which controls the power flows in the MG by adjusting the power imported/exported from/to the main grid, the dispatchable DERs, and the controllable loads based on the instantaneous generations, and loads information in order to meet certain operational (Fang, Misra, Xue, & Yang, 2011).

PMS techniques are classified into two types, i.e., optimization techniques and artificial intelligence (AI) techniques. The PMS based on optimization techniques generally involve a multi-objective function for maximizing the efficiency of the MG, minimizing fossil fuel consumption, and fulfilling the conditions of a successful operation (Olatomiwa, Mekhilef, Ismail, & Moghavvemi, 2016). On the other hand, the PMS based on AI techniques are used for real-time MG power flow control.

Different algorithms based on the PMS optimization and AI techniques were discussed to determine the optimal operation for assessing the reliability of the MG supply system and offering stability and resilience to it (Ciupageanu, Barelli, & Lazaroiu, 2020). The following subsections categorize and describe the various solutions and planning methodologies that are used for strategic and tactical purposes in the PMS.

#### **2.8.1.1 Power Management Systems based on Optimisation Methods**

In Yang et al., (2018), the researchers proposed a two-stage real-time demand-side management solution for the MG system that consisted of a combined WT and PV potential (1.2 MW) with a load  $\leq 1$  MW. A novel MPC optimization scheme was proposed for reducing the operational costs and ensuring the power balance under some unpredictable scenarios. For a short-time resolution that was based on the complicated optimization process, the researchers calculated the real-time power allocation in line with the real-time errors associated with some unknown factors. The role played by the grid support was based on the stationary and mobile (Electric Vehicle) ESS, which could

result in a storage space of up to 3 MWh. This could be managed using an internal pricing scheme for a permanent power balance and simultaneous cost minimization. The researchers tested the adequacy of their proposed technique using detailed simulations in various MG case studies.

A real-time MPC-based PMS technique was also proposed for the grid-connected MG system that included WTs, solar PVs, and BSS (Hooshmand, Asghari, & Sharma, 2013). In this study, the researchers aimed to minimize the energy costs and maximize the life span of the batteries. The results of the study indicated that the proposed PMS scheme helped in decreasing the energy system costs and maximizing the battery life span by 1.5 years.

In Helal et al., (2019), researchers presented the PMS for hybrid islanded AC/DC MG systems. Their proposed algorithm helped in controlling the system and ensuring the stable operation of the MG, while also providing clean water to customers. This optimization algorithm was based on the mixed integer nonlinear programming (MINLP) system, wherein the objective functions decreased the daily operational costs.

A different MINLP and global optimization technique-based PMS was proposed in (Mosa & Ali, 2021) for an MG system that consisted of solar PVs, DiG, wind, fuel cells, microturbines, and BSS. This proposed algorithm helped in minimizing the cost of the DG and the amount of greenhouse emissions. Furthermore, it also considered the no-load costs of the DGs, non-linear losses within the DG, non-linear losses in a distribution system, and the start-up/shutdown costs of a DG. The researchers noted that the BSS played a vital role in minimizing the generation costs and number of emissions, while also compensating for generation shortage.

Another optimal MPC-based PMS technique was proposed in (Valverde, Bordons, & Rosa, 2012) for the grid-connected MG systems that included PVs, fuel cells, an electrolyzer, and batteries. The objective function of this technique was minimizing the use of traditional energy sources, saving energy after using RESs, and quality and economic factors using HESSs. The results indicated that the algorithm allowed the smooth operation of the MG system, however, the life span of the ESSs was increased.

In Tabar et al., (2019), the researchers developed a real-time stochastic linear programming-based PMS technique for the hybrid MG system that included combined heat power (CHP) generation, WTs, microturbines, boilers, and solar PV generators. The algorithm proposed in this study helped in minimizing the emissions, overall costs, and demand payments. The total MG costs were highlighted as the function of maintenance, operating, and constant costs on the generation side, while on the demand side, they were the function of critical, thermal, and normal load costs. For maintaining the load balance and discouraging any curtailment, the researchers followed the load-related restrictions for every time interval. They could achieve an 11% cost saving when they implemented a deterministic strategy, whereas the emissions were decreased by 1.5%; however, no variations were noted in the demand prices.

In Iris & Lam, (2021), Mixed integer linear programming (MILP) model was proposed to address challenges concerning power management and planning integrated operations for a smart seaport grid (such as a port MG) comprising PV and BSS infrastructure. The objective is to minimize the overall operational costs due to delays and optimize energy costs considering hourly tariffs and the choice to sell energy under PV uncertainties.

In Huang, Mao, & Nelms, (2014), the researchers proposed a Lyapunov optimization-based PMS technique for the grid-connected MG system that included RESs and an ESS. This algorithm enabled the minimization of operational costs of the MG and maintained

the outage possibility for quality usage. Furthermore, quality of service (QoS) and energy storage were regarded as prime factors for resolving the optimization issue. The results of the study indicated that this algorithm could minimize the energy storage costs by 60% and further improve the QoS.

Another simultaneous perturbation stochastic approximation (SPSA)-based PMS technique was presented in (Ciupageanu et al., 2019) for the residential MG system that included solar PVs and an hybrid ESS (mechanical flywheel and BSS). The algorithm proposed in this study aimed to acquire a smooth battery power profile and decrease the grid energy exchange. The researchers used actual power records that were related to the demand and PV output to verify the proposed SPSA algorithm. They compared this algorithm to the deterministic power management scheme and noted that their SPSA approach showed a higher success rate (99% of the time) and could preserve the instantaneous current variance that was allocated to the battery at values below 1 A. It also improved the independence of the MG resources by enhancing the utilization of the hybrid ESS.

In Salazar et al., (2020), the researchers proposed a new PMS for the islanded MG. It consisted of solar PVs, fuel cell generation, and BSS. This PMS algorithm was proposed to achieve better scheduling of the battery charging and discharging processes and minimize the operational costs of generation. Furthermore, the researchers used stochastic dynamic programming (SDP) for optimizing the PMS. They also used the Markov model for predicting the solar PV irradiation cycle.

In Hannan et al., (2019), the researchers proposed a new optimal scheduling control technique for an PMS that was based on the binary particle swarm optimization (BPSO) for MGs with wind energy, solar PV, fuel cells, a diesel generator (DiG), and batteries in a virtual power plant. This proposed algorithm helped in minimizing the overall system

costs. The results indicated that the technique could efficiently minimize the grid energy consumption to 47%, while the CO<sub>2</sub> emission was reduced by 8.46%.

In Sharma & Mishra, (2017), the researchers developed a dynamic PMS technique for the independent hybrid AC/DC MG system that consisted of fuel cells, battery banks, PVs, and an ultracapacitor. It was seen that this PMS generated a real-time reference to the converter current controller that was associated with battery banks, fuel cells, and an ultracapacitor with the help of the moving average filter. The efficiency of the moving average filter was noted in the experimental results and simulations. The mean current reference was divided into the fuel cells and battery banks when it efficiently transmitted the oscillatory and transient demand devices to an ultracapacitor.

#### **2.8.1.2 Power Management Systems based on Artificial Intelligence (AI) Methods**

A novel fuzzy logic-based PMS technique was presented for the remote MG system that included wind, PV, and DiGs in (Belmokhtar & Cano, 2021). The main objective of this technique was to improve the reliability of the system, increase the RES integration, and enhance the reactive and active power performance of the MG system with the help of AI algorithms. The researchers assessed the performance of their proposed PMS technique with regard to the regulation of the active and reactive powers. For sharing a DiG based on the fuzzy logic for the active and reactive powers, the researchers proposed two simulation scenarios. The first scenario was based on the stepped solar irradiation and wind speed profiles, while scenario 2 was based on the solar irradiation and wind speed continuous profile. Results showed that this algorithm achieved better stability and reliability of the MG system. Furthermore, the active and reactive power control algorithm showed a faster response to various activities related to the remote MG, such as frequency and rapid voltage fluctuations related to the AC link system.

An optimal PMS based on fuzzy logic control (FLC) was proposed in (Saveen, Raju, Manikanta, & Praveen, 2018) for the independent DC MG in the ZigBee-based communication network. This algorithm ensured a better utilization of the RES and improved the life cycle of battery storage. All experiments validated the effectiveness of the proposed technique.

Another PMS based on the NN technique was designed and proposed in (Wang et al., 2019) for a grid-connected MG that included solar PVs, WTs, batteries, and electric cars. This model aimed to maximize the power supplied by PVs and WTs and minimize the power import from the utility grid.

A novel multi-agent-based PMS was presented in (Gao & Ai, 2018) for the AC-MG system that included PV, wind, fuel cells, microturbines, and BSS for ensuring a safe, efficient, economical, and reliable operation of the MG system. For stabilizing the distributed devices, the researchers obtained the system information regarding the average frequency and voltage using an iterative consensus algorithm. They could acquire an optimal controller using a three-level control, where level one was responsible for tracking the associated reference components. Level two helped in optimizing the voltage and frequency references of droop control and further shared the reactive and active power based on the demand. Level three aimed for optimal scheduling. In this study, the researchers considered all factors such as emission pollution, fuel consumption, and operational maintenance.

A new multi-agent-based PMS was proposed for a standalone MG system that consisted of fuel cells, RESs (wind and PV), and an ESS in (Raju, Morais, Rathnakumar, Ponnivalavan, & Thavam, 2017). The control objectives of the algorithm included the maintenance of the balance between the energy demand and supply. Additionally, the researchers used auto regressive moving average (ARMA) models to forecast the PV

irradiation, wind speed, atmospheric temperature, and the load that is connected to the system.

In Singh & Lather, (2020), the researchers proposed and implemented an ANN-based PMS technique for the standalone DC MG system that included a battery, supercapacitors, and PVs. The researchers aimed to control the DC bus voltage and manage the amount of power shared between the load and MG. They noted that this algorithm showed a better DC bus voltage regulation (2.83 V, it satisfied the general 5% allowed range), and improved power-sharing. Furthermore, all results have been experimentally verified using the hardware-in-loop (HIL) on the real-time simulator from OPAL-RT Technologies.

Another ANN-based PMS was proposed in (Faria et al., 2019) for the standalone MG that included batteries, PVs, and supercapacitors. The objective function of the study was to minimize stress on the BSS and maximize its lifespan. A PV model can be used for validating and assessing the performance of the algorithm. The researchers noted that this technique improved the life span of the battery as it could decrease the dynamic stress and peak current. Additionally, it maximized the supercapacitor utilization.

Another ANN-based PMS was proposed in (Yumurtaci, 2013) for an on-grid/off-grid MG that included wind, PV, fuel cells, an electrolyzer, and battery storage. It was developed to manage the output of the fuel cell and an electrolyzer was used for maintaining the charge of a battery within a constant range. The simulation results indicated that this algorithm displayed a fast response ability compared to the traditional techniques.

A summary of all the aforementioned PMS methods in sections 2.8.1.1 and 2.8.1.2 are presented in Table 2.4.

**Table 2.4: Summary of different PMS methods of MG**

<b>Methods</b>	<b>MG configuration</b>	<b>Aims</b>	<b>Focus Area</b>
MPC (Yang et al., 2018)	PV and Wind	To reduce the operational costs and ensure the power balance	Energy Market
MPC (Hooshmand et al., 2013)	PV, Wind and Battery	To minimize the energy costs and maximize the life span of the battery	Energy Market
MINLP (Helal et al., 2019)	PV and DiG	To decrease the daily operational costs	Energy Market
MINLP (Mosa & Ali, 2021)	PV, DiGs, wind, fuel cells, microturbines, and battery	To minimize the generation costs and amount of emission	Energy Market
MPC (Valverde et al., 2012)	PV, fuel cells, electrolyser	To minimize the use of traditional energy sources, saving energy after using RES, quality and economic factors using HESS	MG operation
Linear Programming (Tabar et al., 2019)	PV, Wind, CHP, microturbines and boilers	To minimize the emissions, overall costs, and demand payments	Energy Market
MILP (Iris & Lam, 2021)	PV and battery	To maximize the life span of the battery and minimize the operational costs	Energy Market
Lyapunov Optimization (Huang et al., 2014)	PV, Wind and Battery	To minimize the operational costs of the MG and maintain the outage possibility for quality usage	Energy Market
Simultaneous Perturbation Stochastic Approximation (Ciupageanu et al., 2019)	PV, Flywheel and battery	To acquire a smooth battery profile and decrease the grid energy exchange	MG operation
Dynamic Programming (Salazar et al., 2020)	PV, fuel cell, and battery	To minimize the overall operational cost	Energy Market
BPSO (Hannan et al., 2019)	PV, wind, fuel cell, battery, and diesel generation	To minimize the grid energy consumption, minimize CO <sub>2</sub> , emission amount, and minimize the overall operational cost	Energy Market
Dynamic Programming (Sharma & Mishra, 2017)	PV, fuel cells, battery banks and ultra capacitor	To control the DC bus voltage and manage the amount of power shared between the load and MG	MG operation
Fuzzy logic (Belmokhtar & Cano, 2021)	PV, wind and diesel genrator	To improve the reliability of the system and enhance the reactive and active power performance of the MG	MG operation
Fuzzy logic (Saveen et al., 2018)	PV, wind, fuel cell, and battery	To maximize the utilization of RE generation and maximize the lifespan of the battery	MG operation
Neural Network (T. Wang et al., 2019)	PV, wind, batteries, and electrical vehicles	To maximize the power supplied by PV and wind and minimize the power import from the utility grid	MG operation
Multi-agent (Gao & Ai, 2018)	PV, Wind, fuel cells, microturbines and battery	To ensure a safe, efficient, economical, and reliable operation of the MG system	MG operation
Multi-agent (Raju et al., 2017)	PV, wind, fuel cell, and battery	To maintain the balance between the energy demand and supply	MG operation
Neural Network (Singh & Lather, 2020)	PV, battery and supercapacitor	To control the DC bus voltage and manage the amount of power shared between the load and MG	MG operation

Neural Network (Faria et al., 2019)	PV, battery and supercapacitor	To minimize stress on the BSS and maximize its lifespan	MG operation
Neural Network (Yumurtaci, 2013)	PV, Wind, fuel cells, electrolyzer and battery	To manage the output of the fuel cell and electrolyzer to maintain the charge of a battery within a constant range	MG operation

## 2.9 Interconnected Microgrid System

To reduce the frequency and necessity of load-shedding in a remote area MG during autonomous operation, islanded neighboring MGs can be interconnected temporarily to support each other if a proper overload management technique is in place and an extra generation capacity is available in the distributed energy resources in the neighboring MGs. Otherwise, due to the unavailability of a utility feeder in remote areas, load shedding is the only alternative to managing an overloaded MG. This way, the total demand of the system of coupled MGs will be shared by all the DERs within these MGs.

### 2.9.1 Advantages of Interconnected Microgrid System

There are several advantages associated with interconnection of MG systems in the MG system which are briefly described as follows (DESA, 2006):

- **Improving reliability and sharing power reserves:** The amount of reserve capacity that must be built by an individual MG system to ensure reliable operation when power shortage occurs can be reduced by sharing reserves within an interconnected MG system.
- **Reduced investment cost in generating capacity:** Individual MG systems can reduce their generating capacity requirement, or need not add new capacity, if they are able to share the generating resources of an interconnected MG system.
- **Increasing load diversity and improving load factor:** MG systems operate most economically when the level of power demand is steady over time. There is also a need to maintain an economical operation of MG systems during peak and off-peak hours of the distribution grid. Poor load factors (the ratio of average to peak

power demand) mean that MG systems must construct generation capacity to meet peak requirements, but that this capacity sits idle much of the time. MG systems can meet the peak power requirements and improve the load factors by interconnecting to other MG systems with different types of loads with different daily or seasonal patterns that complement their own.

- **Economies of scale in new construction:** The unit costs of new generation, transmission and distribution capacity in the interconnected MGs generally decrease with increasing scale of the MG system. Sharing resources in the interconnected MG system can allow the construction of larger generation sources with lower unit costs.
- **Supply security and diversity of generation mix:** Interconnection between MG systems that use different technologies to generate electricity provides greater security in the event that one kind of generation becomes limited (e.g., solar energy during night). This complementarity can be a strong incentive for interconnection between PV dominated systems and fuel cell dominated systems, thus improving reliability and security of power supply.
- **Improving microgrid resilience:** Due to major disturbance at the utility side, MGs may encounter emergencies such as unintentional islanding and load shedding. Interconnection of MGs mitigates the impact of such emergencies and thus improves the resilience of MGs.
- **Economic exchange:** Interconnection of MGs allows the dispatch of the least costly distributed generating units within the interconnected area, providing overall cost savings that can be divided among the individual MG systems. Alternatively, it allows inexpensive power from one MG system to be sold to MG systems with more expensive power.

## 2.9.2 Control Modes of Microgrids in the Interconnected MG System

The commonly used control modes of MGs in the MG system are master-slave mode, peer-to-peer mode and combined mode (Fusheng et al., 2016).

### 2.9.2.1 Master-Slave Mode

In master-slave mode, one of the DG units in the MG acts as the master unit controlling the load bus voltage and the other DG units act as slave units by following the voltage reference fixed by the master unit (Fusheng et al., 2016). Master-slave mode of a MG is shown in Figure 2.8. In grid-connected operation of a MG in the MG system, all the DG units operate in current control mode (CCM) or real-reactive power (P-Q) control (Fusheng et al., 2016). During islanding of a MG in the MG system, one DG unit, which can give reliable and stable power supply, becomes the master unit and operates in voltage-frequency (V-f) control mode to regulate the load bus voltage. Other DG units serve as the slave units, i.e., these DG units operate in CCM and follow the load voltage reference fixed by the master unit (Fusheng et al., 2016). Different DG units with variable outputs such as PV or stable controllable DG units such as fuel cell, battery and microturbine can be used as master unit (Fusheng et al., 2016). Master-slave control mode is widely used in literature (Guerrero, Hang, & Uceda, 2008; Zhao, Zhang, & Chen, 2012).

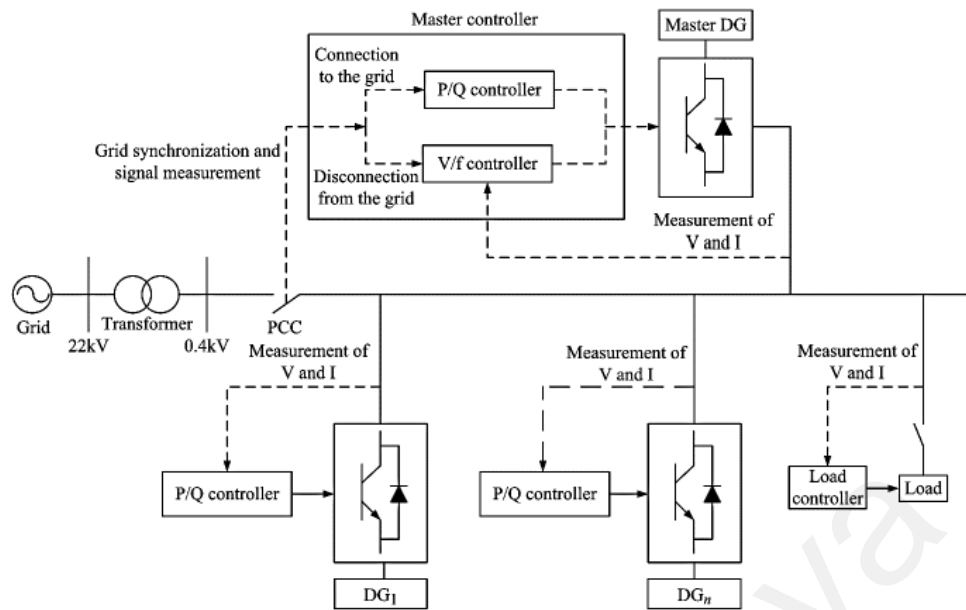


**Figure 2.8: Architecture of microgrid under master-slave control mode (Fusheng et al., 2016)**

This control mode has several advantages as follows (Fusheng et al., 2016):

- Only a simple control algorithm is required at each component level.
- Master-slave control unlike other peer-to-peer control modes does not depend on impedances of the lines interconnecting the MG systems in the MG system.

Disadvantages of master-slave control are as follows (Fusheng et al., 2016):

- Once the master DG unit fails, there is a chance of collapse of the whole MG system but if another DG unit takes the role of the master unit, this collapse can be averted.
- A high expenditure on communication and cabling system is needed but a reliable and high speed communication and cabling system will improve the efficiency and reliability of master-slave mode.

Thus, based on the aforementioned advantages of master-slave control mode, this control mode is used to control the inverters and converters in the proposed MG systems in this thesis. During islanding of a MG in the MG system, the battery and DG inverters

in the islanded MG act as the master and slave inverters, respectively (Guerrero et al., 2008). In this islanded MG, the storage battery VSI operating in voltage control mode (VCM) or V-f control mode regulates the load bus voltage while the DG inverter operates in CCM or P-Q control mode (Zhao et al., 2012).

### 2.9.2.2 Peer-to-Peer Mode

Peer-to-peer mode is based on “plug-and-play” and decentralized control scheme (Fusheng et al., 2016). It depends on the interaction between the DG units in a MG for achieving the goal of voltage and frequency control (Fusheng et al., 2016). Here all DG units are equal and there are no master and slave units (Fusheng et al., 2016). Droop control is a commonly used peer-to-peer control mode with the architecture shown in Figure 2.9.

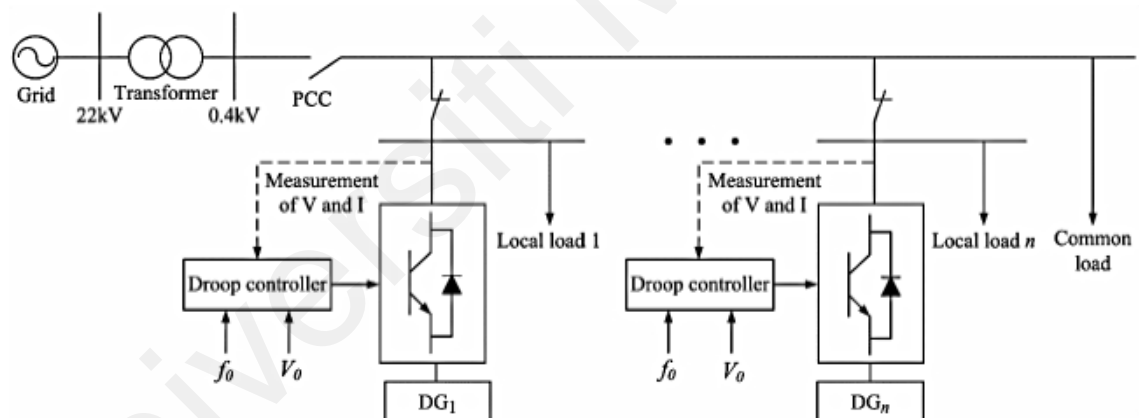


**Figure 2.9: Architecture of microgrid under peer-to-peer control mode (Fusheng et al., 2016)**

Different types of droop control can be found in literature (Guerrero, Vasquez, Matas, De Vicuña, & Castilla, 2010; Yu, Khambadkone, Wang, & Terence, 2010). In this control mode, if load changes, then that load change will be distributed among the DG units according to their droop factors (Fusheng et al., 2016). This allows for the autonomous control of the DG units especially during MG islanding. Droop control is actually a type of proportional control (Fusheng et al., 2016). When the MG is islanded, the droop control will enable the DG units to share the real power proportionally to regulate the MG system

frequency  $f$  to its nominal value  $f_0$  (Fusheng et al., 2016). Also, droop control will facilitate proportional sharing of reactive power demand by the DG units in the islanded MG to regulate the load voltage  $V$  to its nominal value  $V_0$  (Fusheng et al., 2016).

The main advantages of droop control are as follows (Fusheng et al., 2016):

- It does not require communication between centralized and local controllers.
- The control action is based only on local measurements of voltage and frequency in the MG.

Droop control will bring about new steady-state voltage and frequency values in the islanded MG and these new voltage and frequency values may differ from their nominal values in grid-connected mode. The disadvantages of droop control are as follows (Fusheng et al., 2016):

- The performance of droop control degrades with variations in system parameters and line impedances in MG systems.
- It cannot be used with non-linear loads because it is unable to compensate for the harmonic currents.

Thus, due to these disadvantages, droop control is not used in this thesis for the control of converters and inverters in the interconnected MG systems.

### **2.9.2.3 Combined Control Mode**

As the name suggests, the combined control mode is a combination of advantages peer-to-peer control mode and master-slave overcoming disadvantages of both modes. The MG may have multiple RESs or groups of RESs (for example, PV farm, wind farm, etc.) with the randomness of power generation profile or easily controllable other renewable sources. Control functions of RESs vary for different types of RESs, and the single control mode is not sufficient to meet the operational requirements of MG (Fusheng et al., 2016).

Considering dispersive aspects of RESs and loads in the MG needs different types of control modes. Hence, both the control modes can work in combination to achieve the stable, reliable and smooth operation of the MG. However, to implement this controller, 4 PB5 cards consisted Real-time digital simulator (RTDS) is required. As the RTDS used in this study has only two PB5 cards, hence this controller is not considered in this thesis.

### **2.9.3 Control, Management and Methods of Interconnection of Multiple Interconnected Microgrids**

There are few literatures found, which have been emphasized on interconnected MGs formation, control, and energy management system design. In (Samadi Gazijahani & Salehi, 2017), a new stochastic multi-objective framework was presented for dynamic planning of interconnected MGs under uncertainty from technical, reliability and environmental viewpoints. A novel and flexible interconnecting framework for MGs and corresponding energy management strategies were presented, in response to the situation of increasing renewable-energy penetration in (Liu et al., 2017). In (Wang, Chen, & Wang, 2015), a decentralized energy management system for interconnected MGs in grid-connected and islanded mode was proposed. Interactive energy management of interconnected MGs-based active distribution system considering large-scale integration of RE resources was proposed in (Lv & Ai, 2016). A resilient and privacy-preserving energy management strategy for interconnected MGs was proposed in (Hussain, Bui, & Kim, 2016). In (Nikmehr et al., 2017), probabilistic optimal scheduling of interconnected MGs considering time-based demand response programs under uncertainty was proposed. Distributed energy management for interconnected MGs using online alternating direction method of multipliers with regret was proposed in (Ma, Wang, Gupta, & Chen, 2016). In Li, Shahidehpour, Aminifar, Alabdulwahab, & Al-Turki, (2017), interconnected MGs for enhancing the power system resilience were presented. A method to enable resilient distributed power sharing in interconnected MGs through software defined

networking was proposed in (Ren et al., 2018). Stochastic multi-objective model for optimal energy exchange optimization of interconnected MGs was proposed in (Gazijahani, Ravadanegh, & Salehi, 2018). In (Parisio et al., 2017), cooperative MPC based energy management for interconnected MGs was proposed. Droop-free control for interconnected MGs was introduced in (Toro & Mojica-Nava, 2016). A hierarchical distributed MPC strategy to operate interconnected MGs is proposed in (Hans et al., 2018) with the goal of increasing the overall infeed of RES. In (Dabbaghjamanesh, Mehraeen, Kavousi-Fard, & Ferdowsi, 2018), an efficient stochastic energy management technique for interconnected MGs highly penetrated by RE resources has been investigated. An integrated operation management of cooperative MGs is formulated in (Bazmohammadi et al., 2019) using stochastic predictive control. In the proposed scheme, a joint probabilistic constraint on the MGs power exchange with the main grid couples operation of individual MGs.

One of the most evolving area in MG research is the self-healing feature of interconnected MG system to provide resilient power system network. Though the area of MG self-healing capability is emerging, however, only few research have been identified. For example, in (Arefifar, Mohamed, et al., 2013), a planning model has been proposed to divide a distribution system into networked MG for its optimal self-healing. A strategy to sectionalize the on-outage portion of a distribution system into multiple MG to increase the grid resilience has been proposed in (Wang & Wang, 2015). Arefifar et al. presented an optimal model to increase the reliability of a distribution system by dividing it into multiple MG in (Arefifar, Yasser, & El-Fouly, 2013). A self-healing strategy to enhance the overloading resilience of islanded MGs has been discussed in (Wang, Chen, Wang, & Chen, 2015). However, it can be seen that the concept of using local MG generation capacities to support other MGs for the self-healing of an interconnected MG system has not been considered in the above literature.

## 2.10 Gap of the Research

From the above literature review, the following research gaps have been identified related to single MG and interconnected MGs' control and power management systems:

- For controlling the VSI output of grid-connected single MG, none of the literature considered a PLL less grid synchronization techniques along with PCC voltage modulated DPC method to enhance power quality.
- None of the literature developed real-time PMS by considering the maximum utilization of RES, ESS and critical load together.
- None of the literature proposed intelligent interconnection methods for interconnecting multiple MGs based on instantaneous power imbalance between MGs' generation capacity and load demands.
- There is no evidence of PMS methods for enhancing reliability of multiple interconnected MGs during both self-healing and interconnected modes of operation have been found.
- None of the existing control mechanisms of interconnected MGs can adopt with all possible operational scenarios: islanded, grid-connected, interconnected and self-healing modes.

## 2.11 Summary

In this chapter, an extensive critical literature review of single MG and multiple interconnected MG systems has been conducted based on their architecture, control and management. It is found that centralized control scheme is best fitted for the single MG and interconnected MG, which will be used as testbed in this study. For generating control signals for the power switches of grid-connected MG's VSI, linear control with PWM is found the best option with PI controller. For grid-connected mode of MG operation it is observed that the existing PQ control method due to the existence of PLL system exhibit

power quality issues. The existing optimization based decentralized energy management systems proposed for MG efficient operation cannot be implemented in real-time, as they required prior statistical data of MG parameters. There is no efficient IIM for interconnecting multiple MGs, which fitted the real-time operation of interconnected MG based on MGs' generation capacity, and load demands are available. Finally, it is observed that for interconnected MGs, there is no multi-layer control mechanism is existing which will ensure reliable operation of interconnected MGs through smooth transition among various operating modes such as islanded, grid-connected, interconnected and self-healing.

Universiti Malaysia

## CHAPTER 3: METHODOLOGY

### 3.1 Introduction

This chapter presents different architectures of single MGs and interconnected MG used in this study. In this chapter, three power control methods for grid-connected PV VSI of MG are proposed without using PLL system. Further, IIMs to interconnect two MGs along with the power management strategies adopted for reliable operation during self-healing and interconnected mode are presented. Finally, a multi-layer control strategy is formed for the interconnected multiple MGs system to ensure smooth transition among different operating modes.

### 3.2 Proposed Microgrid Configuration

In this section, the configurations of three MGs used to validate the performance of the proposed control methods and PMSs are presented in brief.

#### 3.2.1 AC Microgrid

The grid-tied AC MG testbed is formed in this study by combining a PV system, a BSS and a DiG which is represented in Figure 3.1. The modeling of the MG is conducted in RSCAD platform by using modules of different components available in RSCAD library. In Table 3.1, the parameters and specifications of the PV system, battery storage, DiG, grid, loads, DC/DC converters and VSIs are given. From Figure 3.1, it can be seen that PV system and BSS are connected to AC bus through two 3-ph conventional 2 level DC/AC VSIs. The MG is connected to the grid through a 3-ph, 2 winding transformer. The AC MG is also consisted of a DiG to provide backup supply while grid fails, and constant critical and variable non-critical AC loads are considered as load demand.

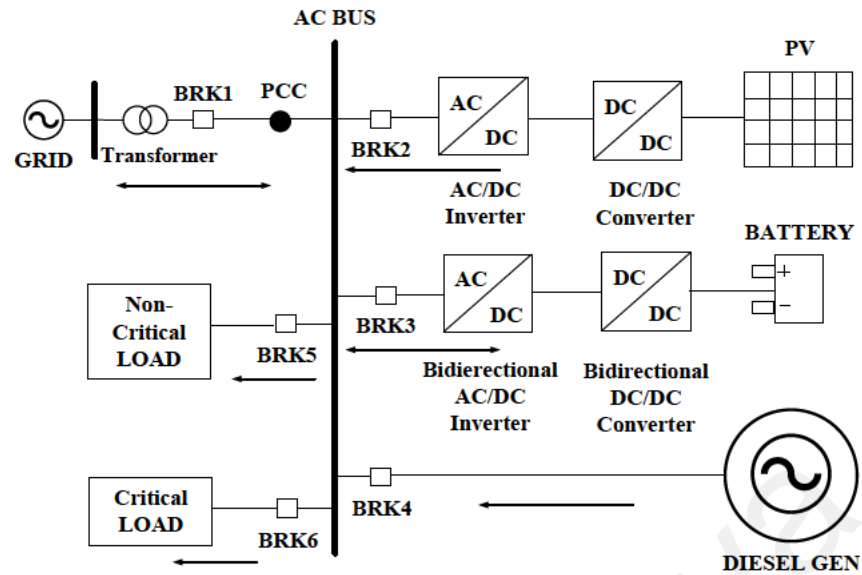


**Figure 3.1: Schematic of AC microgrid**

### 3.2.2 Hybrid Microgrid

The testbed of grid-connected hybrid MG used in this study is depicted in Figure 3.2 which, is comprised of PV generator, DiG and battery storage. All the components used in this study are obtained from the RTDS library, which are briefly illustrated in the subsequent sections. In Table 3.2, the parameters and specifications of the PV system, battery storage, DiG, grid, loads converters and VSI are given. From Figure 3.2, it can be seen that PV system and BSS are connected to a DC bus through DC-DC converters where a fixed DC load is connected to form a DC MG. The output of the DC MG is connected to the PCC via a 3-ph VSI to form AC MG. The AC MG also consisted of a DiG to provide backup while grid fails and two types of loads namely variable Critical DC load and non-critical AC load to validate the performance of the PMSs in hybrid MG.

**Table 3.1: Parameters of AC MG components**

Parameters	Values
<b>PV System (0.1 MW)</b>	
PV module Temperature	25 °C
PV modules connected in series	28
PV modules connected in parallel	68
Solar irradiation reference value	1000 W/m <sup>2</sup>
Maximum power voltage ( $V_{mpp}$ )	17.3 V
Maximum power current ( $I_{mpp}$ )	3.05 A
Voltage at open circuit ( $V_{oc}$ )	21.5 V
Current during short circuit ( $I_{sc}$ )	3.33 A
<b>Battery Storage (25 kWh)</b>	
Single cell capacity	0.85 AH
Single cell nominal voltage	3.6 V
Initial state of charge (SOC) in a single cell	90%
SOC of battery	Greater than 60%
Cells connected in parallel	290
Cells connected in series	135
<b>Diesel Generator (0.15 MVA)</b>	
Machine power rating	0.20 MVA
Line to line voltage	0.48 kV
<b>Grid</b>	
Transformer primary/secondary voltage	0.48 kV/13.2 kV
Grid Voltage	13.2 kV
Frequency	60 Hz
<b>Load</b>	
Non-critical load	0.05-0.14 MW
Critical Load	0.005-0.015 MW
<b>PV VSI</b>	
DC-link voltage	975 V
Switching frequency PV Inverter	2 kHz
DC link capacitor	500 uF
$R_{a, b, c}$	0.1 $\Omega$
$L_{a, b, c}$	5 mH
<b>Battery Inverter</b>	
DC-link voltage	975 V
Switching frequency PV Inverter	2 kHz
DC link capacitor	450 uF
$R_{a, b, c}$	0.01 $\Omega$
$L_{a, b, c}$	5.5 mH
<b>PV system DC-DC Boost Converter</b>	
DC-DC converters switching frequency	20 kHz
Inductance	8 mH
Capacitance	85 uF
<b>Battery storage bidirectional DC-DC Buck-Boost Converter</b>	
DC-DC converters switching frequency	20 kHz
Inductance	6 mH
Capacitance	74 uF

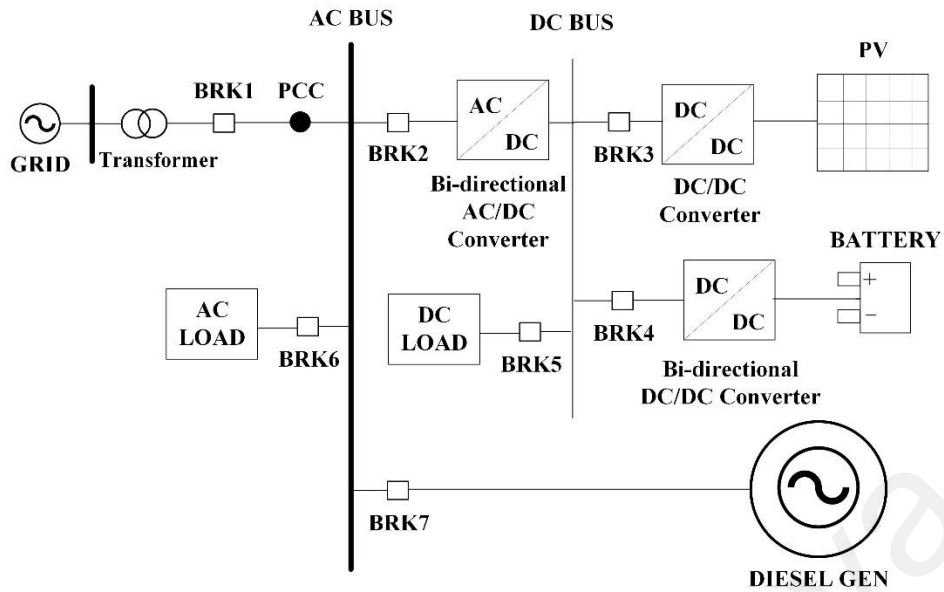


Figure 3.2: Schematic of hybrid microgrid

### 3.2.3 Interconnected Microgrid

Two MG testbeds are considered in this study to form the interconnected MG which are depicted in Figure 3.3. MG1 consists of PV system, DiG, battery and load. On the other hand, MG2 consists of the same components as MG1 except for the DiG. Both the MGs are AC and connected to the grid through a 3ph transformer. A smart switch BRK2 is used to interconnect the MGs which receives control signals from the proposed IIM. During grid-connected mode of operation this switch remains closed. All the components of both the MGs are modeled by using the components from RSCAD library. The DC/AC inverters and DC/DC converters are modeled by IGBT and MOSFET switches, respectively. The parameters of the two MGs are presented in Table 3.3.

**Table 3.2: Parameters of hybrid MG components**

Parameters	Values
<b>PV System (0.1 MW)</b>	
Reference Temperature	25 °C
Reference solar intensity	1000 W/m <sup>2</sup>
Series connected modules	28
Parallel connected Modules	68
Open circuit voltage	21.5 V
Voltage at maximum power (VMP)	17.4 V
Short Circuit current	3.33 A
Current at maximum power (IMP)	3.05 A
<b>Battery Storage (15 kWh)</b>	
Capacity a single cell	0.85 AH
Single cell nominal voltage	3.6
Initial SOC in a single cell	90%
Number of cells in series in a stack	135
Number of stacks in parallel	290
SOC of battery	Greater than 60%
<b>Diesel Generator (0.20 MVA)</b>	
Rated RMS line to line voltage	0.48 kV
Rated MVA of the machine	0.20 MVA
<b>Grid</b>	
Transformer primary/secondary voltage	0.48 kV/13.2 kV
Grid Voltage	13.2 kV
Frequency	60 Hz
<b>Load</b>	
Critical DC load	0.01 MW
Non-critical AC load	0.05-0.2 MW
<b>Bidirectional DC/AC Voltage Source Converter</b>	
Inverter DC-link voltage	975 V
Inverter switching frequency	2 kHz
$R_{a, b, c}$	0.1 $\Omega$
$L_{a, b, c}$	5 mH
<b>PV system DC-DC Boost Converter</b>	
DC-DC converters switching frequency	20 kHz
Inductance	8 mH
Capacitance	85 uF
<b>Battery storage bidirectional DC-DC Buck-Boost Converter</b>	
DC-DC converters switching frequency	20 kHz
Inductance	6 mH
Capacitance	74 uF

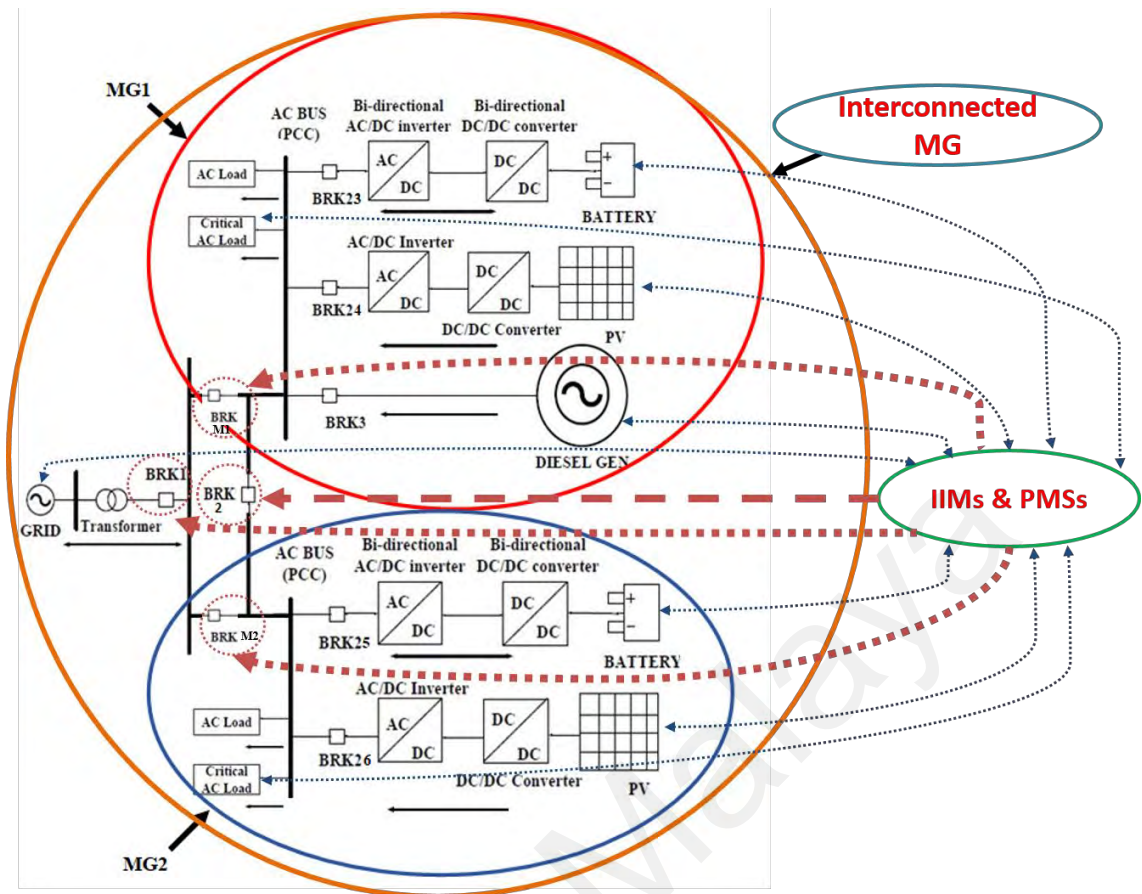


Figure 3.3: Schematic of interconnected microgrids

Table 3.3: Parameters of interconnected MGs components

Parameters	Values
<b>Microgrid 1</b>	
PV Array	0.1 MW
Variable Load	0.05 – 0.14 MW
Capacity of Battery	0.015 MWh
Diesel Generator	0.05 MVA
<b>Microgrid 2</b>	
PV Array	0.05 MW
Variable Load	0.04 – 0.075 MW
Capacity of Battery	0.015 MWh
<b>Grid</b>	
Grid Voltage	13.2 kV
Transformer voltage rating	480 kV/10.8 kV
Frequency	60 Hz

### 3.3 Modeling of Microgrid Components

In this section, the modeling of different MG components is presented briefly.

#### 3.3.1 PV Generation System

By converting photon energy into electrical energy PV systems generate electric power using solar cells in the form of direct current. PV array is formed by connected solar cells series-parallel combination. The PV system used in this study consisted of PV array rated 0.1 MW, a DC-DC boost converter and a DC-AC VSI. A PCC voltage modulation (PVM) theory (PVMT) based DPC strategy is developed in this study to control the output of the PV VSI which is described in sections 3.3 and 3.4.

The ideal relationship between voltage and current of PV system is given by (3.1):

$$I_{PV} = I_{ph} - I_D - I_{sh} = I_{ph} - I_0 \left[ \exp \frac{q}{AKT(V_{PV} + I_{PV}R_s)} - 1 \right] - \frac{V_{PV} + I_{PV}R_s}{R_{sh}} \quad (3.1)$$

Where  $I_{PV}$  is the PV cell output current (A),  $I_{ph}$  the photocurrent,  $I_D$  the diode current,  $I_{sh}$  the current through the shunt resistance,  $I_0$  the reverse saturation current, K the Boltzmann constant= $1.38 \times 10^{-23} (J/K)$ , q the charge of electron= $1.6 \times 10^{-19} (C)$ , T the cell temperature (K),  $V_{PV}$  the output terminal voltage of the PV cell (V), A the quality factor (lies between 1.2-1.6 for crystalline silicon),  $R_{sh}$  the shunt resistance ( $\Omega$ ) and  $R_s$  the series resistance ( $\Omega$ ).

A modified incremental conductance algorithm based Maximum power point tracking (MPPT) controller (Ahmad, Rashid, Ferdowsy, Islam, & Mahmood, 2015) is implemented to extract the maximum power from the PV generation system. The maximum power output is calculated using (3.2):

$$P_{pv}(t) = \eta_{pv} AI(t)(1 - 0.005(T_0(t) - 25)) \quad (3.2)$$

where,  $\eta_{pv}$  is the PV system efficiency,  $A$  is the PV cell array area,  $T_0$  is the ambient temperature and  $I$  is the solar irradiation.

### 3.3.2 Battery Storage System

The BSS used in this study is comprised of a battery storage, bidirectional DC-DC buck-boost converter and a bidirectional DC-AC VSI. A control technique proposed in (Worku et al., 2019) is employed in this study to control the battery VSI. The size of the battery is chosen based on the critical load demand so that in case of any contingency battery is able to provide backup since the aim of the paper is to design an efficient power control method for the MG. In this study, strings of lithium-ion batteries are used. The battery operates in charging mode when battery requires charging and PV has excessive power generation than demand or MG is in grid-tied mode. In contrast, battery operates in discharging mode when MG operates in islanding mode or PV output power is less than its generation capacity.

The crucial parameters of battery are terminal voltage and SOC which can be calculated based on (3.3) and (3.4) (Akram, Khalid, & Shafiq, 2017):

$$V_{bat} = i_{bat}R_{bat} + V_{oc} + V_e e^{B \int i_{bat} dt} - k \frac{Ah}{Ah + \int i_{bat} dt} \quad (3.3)$$

$$SOC = \left( 1 + \frac{\int i_{bat} dt}{Ah} \right) * 100 \quad (3.4)$$

where,  $V_{bat}$  is battery terminal voltage, open circuit voltage is  $V_{oc}$ , battery current is  $i_{bat}$ ,  $R_{bat}$  is the battery internal resistance,  $k$  is the polarization voltage,  $V_e$  is the exponential voltage, and  $B$  is the exponential capacity.

### 3.3.3 Diesel Generator

In this study, a DiG is used to provide backup supply to MG when grid fails. It is comprised of a diesel engine, a synchronous machine and for regulating the machine's speed & frequency, an excitation system driven speed governor. The modeling of three different parts of DiG is adopted from (Sen & Kumar, 2018). The dynamics of each DiG component can be given by (3.5) and (3.8).

Governor control system transfer function:

$$H_c = \frac{K_l(T_3s+1)}{(T_1T_2s^2 + T_1s+1)} \quad (3.5)$$

where,  $H_c$  is the transfer functions of governor control system,  $K_l$  is the transfer function constants and  $T_1$  to  $T_3$  are the time constants.

Actuator Transfer function:

$$H_a = \frac{(T_4s+1)}{s(T_5s+1)(T_6s+1)} \quad (3.6)$$

where,  $H_a$  is the transfer functions actuator, and  $T_4$  to  $T_6$  are the time constants.

Diesel engine transfer function

$$H_{eng} = e^{-T_Ds} \quad (3.7)$$

where,  $H_{eng}$  is the transfer function of governor control system and  $T_D$  is the time constant. Excitation system transfer function:

$$H_e = \frac{1}{(T_e s + K_e)} \quad (3.8)$$

where,  $H_e$  is the excitation system transfer function,  $K_e$  is the transfer function constant and  $T_e$  time constant.

### 3.3.4 Grid

In this study, a 3ph AC source is considered as a grid model. The grid will deliver power to the MG when there will be shortage of generation and if there is excessive power generation in MG, grid will absorb the power. The power supplied or absorbed by the grid is given by (3.9) (Akram et al., 2017).

$$P_g(t) = P_l(t) + \sum (P_{pv}(t), P_b(t)) \quad (3.9)$$

where, grid supplied/absorbed power is represented by  $P_g$ , power demand of load is depicted by  $P_l$ ,  $P_{pv}$  is the PV power and  $P_b$  is the power from BSS.

### 3.3.5 Load

In this study, for AC MG and interconnected MGs two types of load are considered namely non-critical AC load and critical load. On the other hand, for hybrid MG variable AC load and critical constant DC loads are considered. For all types of MG, load demand is chosen based on the MGs' and grid's generation capacity to verify the performance of the proposed PLL less CCT based power control method and PVMT based DPC methods.

## 3.4 Voltage Source Inverter Modelling and Control

In this section, detailed mathematical modeling of VSIs using both CCT and PVMT without PLL system are presented.

### 3.4.1 Current Control Theory (CCT) based PV Inverter Modelling

In this section, modeling of the dq CCT based VSI is briefly explained without using PLL system and Park transformation. In this study, the PV system is connected to the DC-link of the CCT based VSI through DC–DC boost converter where the output of the battery bidirectional DC-DC buck boost converter is connected to the DC link of PLL integrated conventional dq CCT based VSI. Both the inverters are connected to the grid through L-filters. The schematics of the proposed CCT based power controller along with

the conventional PLL integrated dq CCT based power control method are depicted in Figure 3.4 (b) and (a), respectively.

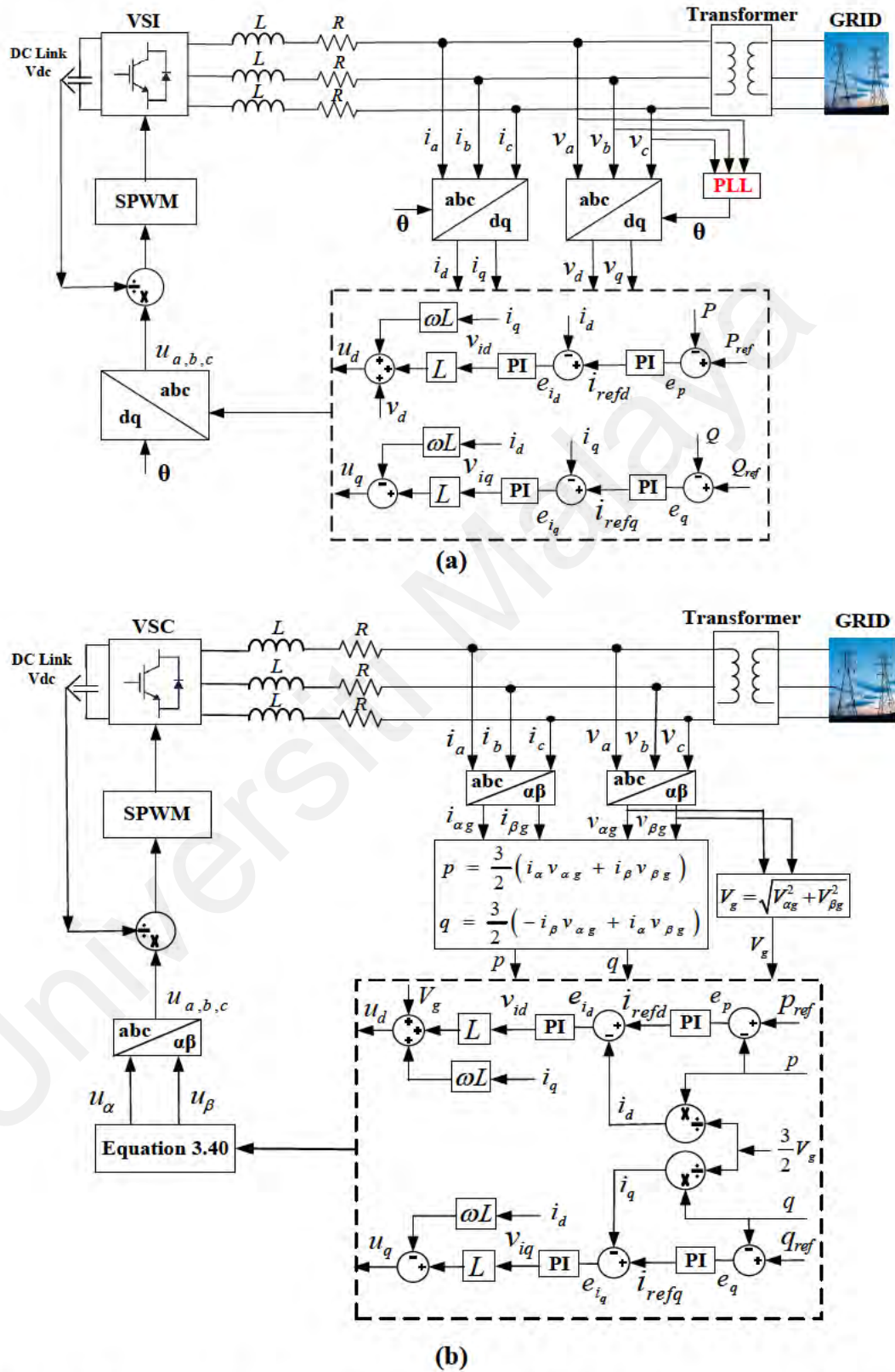


Figure 3.4: Schematic of grid-connected MG's VSI (a) conventional CCT based power controller with PLL system, and (b) proposed CCT based power controller without PLL system

The equations for grid voltages, VSI output voltages, and currents can be expressed in dynamic form as (3.10):

$$\begin{aligned} L \frac{di_a}{dt} &= -v_{ag} + u_a - Ri_a \\ L \frac{di_b}{dt} &= -v_{bg} + u_b - Ri_b \\ L \frac{di_c}{dt} &= -v_{cg} + u_c - Ri_c \end{aligned} \quad (3.10)$$

where,  $v_{abc}$ ,  $i_{abc}$ , and  $u_{abc}$  are grid voltages, VSI output voltages and currents, respectively. Filter resistance and inductance are denoted by R and L, respectively.

By using Clark transformation, the stationary reference frame of the dynamic equations expressed in (3.10) can be converted as follows:

$$\begin{aligned} L \frac{di_\alpha}{dt} &= -v_{\alpha g} + u_\alpha - Ri_\alpha \\ L \frac{di_\beta}{dt} &= -v_{\beta g} + u_\beta - Ri_\beta \end{aligned} \quad (3.11)$$

where,  $v_{\alpha\beta g}$ ,  $u_{\alpha\beta}$  and  $i_{\alpha\beta}$  represent grid voltages, VSI voltages and currents in  $\alpha$ - $\beta$  frame.

The instantaneous reactive and real power flow in the stationary reference frame between VSI to utility grid can be expressed as (3.12).

$$\begin{aligned} p &= \frac{3}{2} (i_\alpha v_{\alpha g} + i_\beta v_{\beta g}) \\ q &= \frac{3}{2} (-i_\beta v_{\alpha g} + i_\alpha v_{\beta g}) \end{aligned} \quad (3.12)$$

where,  $p$  and  $q$  are the injected/supplied grid instantaneous real and reactive powers, respectively.

By differentiating (3.12), the dynamic equations of the powers have been obtained which are expressed as (3.13).

$$\begin{aligned} \frac{dp}{dt} &= \frac{3}{2} \left( v_{\alpha g} \frac{di_\alpha}{dt} + i_\alpha \frac{dv_{\alpha g}}{dt} + v_{\beta g} \frac{di_\beta}{dt} + i_\beta \frac{dv_{\beta g}}{dt} \right) \\ \frac{dq}{dt} &= \frac{3}{2} \left( -v_{\alpha g} \frac{di_\beta}{dt} - i_\beta \frac{dv_{\alpha g}}{dt} + v_{\beta g} \frac{di_\alpha}{dt} + i_\alpha \frac{dv_{\beta g}}{dt} \right) \end{aligned} \quad (3.13)$$

Since the grid is in balanced state, simplifying the power dynamics following voltage relationship in (3.14) can be obtained.

$$\begin{aligned} v_{\alpha g} &= V_g \cos(\omega t) \\ v_{\beta g} &= V_g \sin(\omega t) \end{aligned} \quad (3.14)$$

where,

$$V_g = \sqrt{v_{\alpha g}^2 + v_{\beta g}^2} \quad (3.15)$$

where,  $V_g$  is the grid voltage amplitude,  $\omega$  is the angular frequency which can be expressed by  $\omega = 2\pi f$ , and  $f$  is the frequency of grid voltage.

By differentiating (3.14), the dynamic equations of grid voltages have been obtained which are expressed as (3.16).

$$\begin{aligned} \frac{dv_{\alpha g}}{dt} &= -\omega V_g \sin(\omega t) = -\omega v_{\beta g} \\ \frac{dv_{\beta g}}{dt} &= \omega V_g \cos(\omega t) = \omega v_{\alpha g} \end{aligned} \quad (3.16)$$

The real and reactive powers dynamic expressions are presented in (3.17) by substituting (3.10) and (3.16) in (3.13).

$$\begin{aligned} \frac{dp}{dt} &= \frac{3}{2L} (-V_g^2 + u_\alpha v_{\alpha g} + u_\beta v_{\beta g}) - \omega q - p \frac{R}{L} \\ \frac{dq}{dt} &= \frac{3}{2L} (-u_\beta v_{\alpha g} + u_\alpha v_{\beta g}) - \omega p - q \frac{R}{L} \end{aligned} \quad (3.17)$$

where,  $p$  &  $q$  are the dynamic real and reactive powers control outputs and control inputs are  $u_\alpha$  &  $u_\beta$  as expressed in (3.17).

By using voltage modulation technique used in (Gui, Kim, et al., 2018), the dynamic of (3.17) can be simplified as follows:

$$\begin{aligned} u_p &:= u_\alpha v_{\alpha g} + u_\beta v_{\beta g} \\ u_q &:= -u_\beta v_{\alpha g} + u_\alpha v_{\beta g} \end{aligned} \quad (3.18)$$

where,  $u_p$  and  $u_q$  are the new control inputs and since they satisfy (3.19), hence they are changed into DC components.

$$\begin{bmatrix} u_p \\ u_q \end{bmatrix} = V_g \begin{bmatrix} \cos(\omega t) & \sin(\omega t) \\ \sin(\omega t) & -\cos(\omega t) \end{bmatrix} \begin{bmatrix} u_\alpha \\ u_\beta \end{bmatrix} = V_g \begin{bmatrix} u_d \\ -u_q \end{bmatrix} \quad (3.19)$$

where,  $u_d$  and  $u_q$  are the dq axes VSI voltages.

By replacing the control inputs of dynamic real and reactive power in (3.17) with the new control inputs ( $u_p$  and  $u_q$ ), (3.17) can be expressed as (3.20).

$$\begin{aligned} \frac{dp}{dt} &= \frac{3}{2L} (-V_g^2 + u_p) - \omega q - p \frac{R}{L} \\ \frac{dq}{dt} &= \frac{3}{2L} u_q - \omega p - p \frac{R}{L} \end{aligned} \quad (3.20)$$

Due to the similar structure of dynamics in (3.20) and dynamics of dq axes currents of VSI, the real and reactive power can be represented as (3.21) in dq synchronous reference frame.

$$\begin{aligned} p &= \frac{3}{2} v_{dg} i_d \\ q &= \frac{3}{2} v_{dg} i_q \end{aligned} \quad (3.21)$$

where,  $v_{dg}$  is the d-component of instantaneous voltage and given by  $v_{dg} = V_g$  and  $v_{qg} = 0$ .

By multiplying both sides of (3.15) with  $\frac{2}{3V_g}$ , the real and reactive powers dynamics presented in (3.20) could be converted to conventional d-q axis current models as expressed in (3.22). This is the new VSI model without using any PLL system.

$$\begin{aligned} \frac{di_d}{dt} &= \frac{1}{L} (-V_g + u_d) - \omega i_q - i_d \frac{R}{L} \\ \frac{di_q}{dt} &= \frac{1}{L} u_q - \omega i_d - i_q \frac{R}{L} \end{aligned} \quad (3.22)$$

### 3.4.2 PCC Voltage Modulated Theory (PVMT) based PV Inverter Modelling

In this section, DPC modeling of VSI based on PVMT is briefly explained without using PLL system and Park transformation. In Figure 3.5 (a) and (b), the schematics of the proposed PVMT based proportional integral (PI) based DPC (PIDPC) and fuzzy logic based DPC (FLDPC) methods are presented, respectively. For both the control methods (FLDPC and PIDPC), the modeling of the VSI is identical i.e. PVMT based VSIs have been used.

The equations for grid voltages, VSI output voltages, and currents can be expressed in dynamic form as (3.23):

$$\begin{aligned} Ri_{pa} &= -v_{pa} + u_a - L \frac{di_{pa}}{dt} \\ Ri_{pb} &= -v_{bg} + u_b - L \frac{di_{pb}}{dt} \\ Ri_{pc} &= -v_{cg} + u_c - L \frac{di_{pc}}{dt} \end{aligned} \quad (3.23)$$

where,  $v_{pabc}$ ,  $i_{pabc}$ , and  $u_{abc}$  are PCC voltages, VSI output currents and voltages, respectively. R and L are resistance and inductance of filter, respectively.

By using Clark transformation, the stationary reference frame of the dynamic equations expressed in (3.23) can be converted as (3.24).

$$\begin{aligned} Ri_{p\alpha} &= u_{\alpha} - v_{p\alpha} - L \frac{di_{p\alpha}}{dt} \\ Ri_{p\beta} &= u_{\beta} - v_{p\beta} - L \frac{di_{p\beta}}{dt} \end{aligned} \quad (3.24)$$

where, PCC voltages are  $u_{\alpha\beta}$ , and VSI currents & voltages are  $i_{p\alpha\beta}$  &  $v_{p\alpha\beta}$ , respectively in  $\alpha$ - $\beta$  frame.

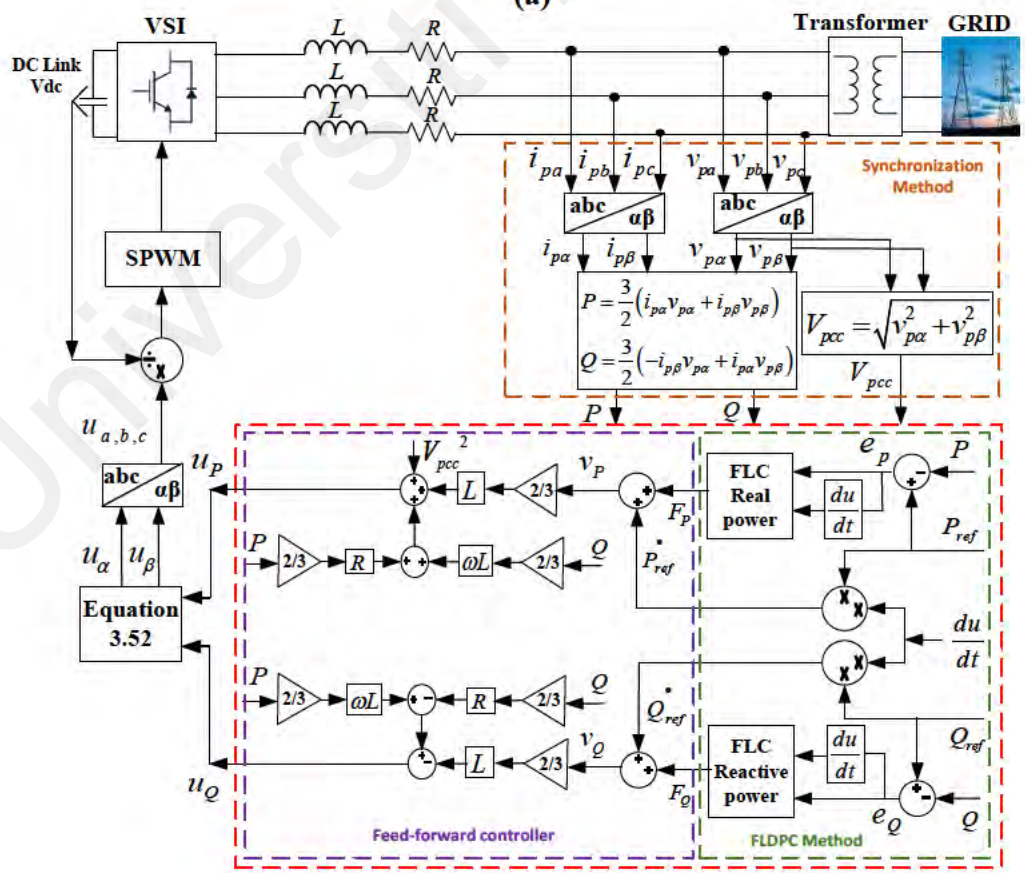
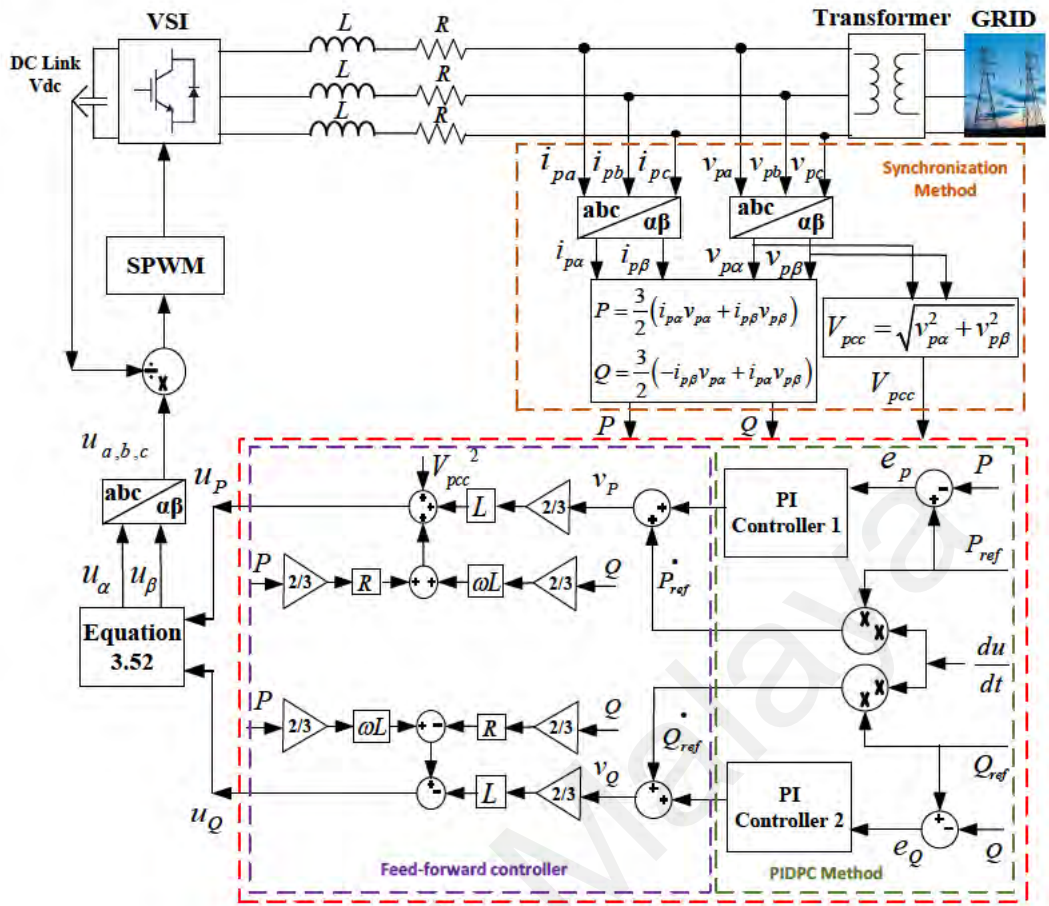


**Figure 3.5: Schematic of grid-connected MG's VSI (a) proposed PVMT based PIDPC, and (b) proposed PVMT based FLDPC without PLL system**

The stationary reference frame representation of instant reactive and real power flow between utility grid and VSI can be presented as (3.25).

$$\begin{aligned} P &= \frac{3}{2} (i_{p\alpha} v_{p\alpha} + i_{p\beta} v_{p\beta}) \\ Q &= \frac{3}{2} (-i_{p\beta} v_{p\alpha} + i_{p\alpha} v_{p\beta}) \end{aligned} \quad (3.25)$$

where, instant real and reactive powers supplied/injected by grid are  $P$  and  $Q$ , respectively.

The dynamic equations of the powers are obtained by differentiating (3.25) which are expressed as (3.26).

$$\begin{aligned} \frac{dP}{dt} &= \frac{3}{2} \left( v_{p\alpha} \frac{di_{p\alpha}}{dt} + i_{p\alpha} \frac{dv_{p\alpha}}{dt} + v_{p\beta} \frac{di_{p\beta}}{dt} + i_{p\beta} \frac{dv_{p\beta}}{dt} \right) \\ \frac{dQ}{dt} &= \frac{3}{2} \left( -v_{p\alpha} \frac{di_{p\beta}}{dt} - i_{p\beta} \frac{dv_{p\alpha}}{dt} + v_{p\beta} \frac{di_{p\alpha}}{dt} + i_{p\alpha} \frac{dv_{p\beta}}{dt} \right) \end{aligned} \quad (3.26)$$

For simplifying the dynamics of  $P$  and  $Q$  in balanced grid condition, the relationship of PCC  $\alpha$ - $\beta$  voltage can be obtained as given in (3.27).

$$\begin{aligned} v_{p\alpha} &= V_{pcc} \cos(\omega t) \\ v_{p\beta} &= V_{pcc} \sin(\omega t) \end{aligned} \quad (3.27)$$

where

$$V_{pcc} = \sqrt{v_{p\alpha}^2 + v_{p\beta}^2} \quad (3.28)$$

where, PCC voltage amplitude is  $V_{pcc}$ , angular frequency is  $\omega$  and grid voltage frequency is  $f$ .

The dynamic equations of PCC voltages are obtained as (3.27) by differentiating (3.29).

$$\begin{aligned} \frac{dv_{p\alpha}}{dt} &= -\omega V_{pcc} \sin(\omega t) = -v_{p\beta} \omega \\ \frac{dv_{p\beta}}{dt} &= \omega V_{pcc} \cos(\omega t) = v_{p\alpha} \omega \end{aligned} \quad (3.29)$$

By substituting (3.23) and (3.29) in (3.26), the dynamic expression of real and reactive powers can be obtained as (3.30).

$$\begin{aligned}\frac{dp}{dt} &= \frac{3}{2L} \left( -V_{pcc}^2 + u_\alpha v_{p\alpha} + u_\beta v_{p\beta} \right) - \omega q - p \frac{R}{L} \\ \frac{dq}{dt} &= \frac{3}{2L} \left( -u_\beta v_{p\alpha} + u_\alpha v_{p\beta} \right) - \omega q - q \frac{R}{L}\end{aligned}\quad (3.30)$$

where, dynamic real and reactive power control inputs and outputs are ( $p$  &  $q$ ) and ( $u_\alpha$  &  $u_\beta$ ), respectively.

Since both the control inputs in (3.30) are coupled in P and Q states, hence by using voltage modulation theory (VMT) (Gui, Kim, et al., 2018), the dynamics of (3.30) can be simplified as (3.31) to define new voltage modulated control inputs.

$$\begin{aligned}u_P &:= u_\alpha v_{p\alpha} + u_\beta v_{p\beta} \\ u_Q &:= u_\beta v_{p\alpha} - u_\alpha v_{p\beta}\end{aligned}\quad (3.31)$$

where, the new control inputs are  $u_P$  and  $u_Q$ , and they are transformed into DC components as they satisfy (3.32).

$$\begin{bmatrix} u_P \\ u_Q \end{bmatrix} = V_{pcc} \begin{bmatrix} \cos(\omega t) & \sin(\omega t) \\ -\sin(\omega t) & \cos(\omega t) \end{bmatrix} \begin{bmatrix} u_\alpha \\ u_\beta \end{bmatrix} = V_{pcc} \begin{bmatrix} u_d \\ u_q \end{bmatrix}\quad (3.32)$$

where  $u_d$  and  $u_q$  are the d-q frame VSI voltages. Though the proposed method has no PLL system, however, the system is still presented in dq axis frame.

The dynamic expression of real and reactive powers presented in (3.30) can be expressed as (3.33) by substituting the control inputs of (3.33) with the new control inputs ( $u_P$  and  $u_Q$ ).

$$\begin{aligned}\frac{dP}{dt} &= \frac{3}{2L} \left( -V_{pcc}^2 + u_P \right) - \omega Q - P \frac{R}{L} \\ \frac{dQ}{dt} &= \frac{3}{2L} u_Q - \omega Q - P \frac{R}{L}\end{aligned}\quad (3.33)$$

### 3.4.3 Voltage Source Inverter Control during AC Microgrid's Grid-connected mode

In this section, three power control methods namely dq axis current based power control and DPC method for grid-connected MG's VSI are modeled.

#### 3.4.3.1 PLL less CCT based Power Control Method

A simple and robust controller containing feedback and feedforward control structure is modeled for the new VSI model presented in (3.22). The schematic of the control system is depicted in Figure 3.4 (b). The controller consists of two control loops. In the outer control loop, the real and reactive power will be controlled and tracked their references using two PI controllers. On the other hand, the dq axes currents will be regulated using two PI controllers in the inner control loop.

The dq axes currents errors  $e_{id}$  and  $e_{iq}$  can be expressed as (3.34).

$$\begin{aligned} e_{i_d} &:= i_{refd} - i_d \\ e_{i_q} &:= i_{refq} - i_q \end{aligned} \quad (3.34)$$

where,  $i_{refd}$  and  $i_{refq}$  are the dq axes reference currents, respectively. These currents can be calculated using (3.35).

$$\begin{aligned} i_{refd} &= e_p K_{p,p} + K_{p,i} \int_0^t e_p(\tau) d\tau \\ i_{refq} &= e_q K_{q,p} + K_{q,i} \int_0^t e_q(\tau) d\tau \end{aligned} \quad (3.35)$$

where,  $K_{p,p}$ ,  $K_{p,i}$ ,  $K_{q,p}$ , and  $K_{q,i}$  are the PI controller gains that are used for obtaining zero steady-state error. The optimal values of the PI controllers' parameters are tabulated in Table 3.4. In addition,  $e_p$  and  $e_q$  are the errors of real and reactive powers, respectively, which can be expressed as (3.36).

$$\begin{aligned} e_p &:= p_{ref} - p \\ e_q &:= q_{ref} - q \end{aligned} \quad (3.36)$$

Feedback and feedforward terms based controller is designed in this study to eliminate the coupling terms of (3.22). The expression for Feedback and feedforward terms are as follows:

$$\begin{aligned}
 u_d &= v_{i_d} + Li_q \omega + V_g \\
 &\quad \downarrow \quad \swarrow \quad \searrow \\
 &\quad \text{Feedback} \quad \text{Feedforward}
 \end{aligned}
 \tag{3.37}$$

$$\begin{aligned}
 u_q &= Li_d \omega + v_{i_q} \\
 &\quad \downarrow \quad \downarrow \\
 &\quad \text{Feedforward} \quad \text{Feedback}
 \end{aligned}$$

where,  $v_{i_d}$  and  $v_{i_q}$  are feedback controller inputs which can be calculated using (3.38),

$$\begin{aligned}
 v_{i_d} &= e_{i_d} K_{i_d,p} + K_{i_d,i} \int_0^t e_{i_d}(\tau) d\tau \\
 v_{i_q} &= e_{i_q} K_{i_q,p} + K_{i_q,i} \int_0^t e_{i_q}(\tau) d\tau
 \end{aligned}
 \tag{3.38}$$

where,  $K_{i_d,p}$ ,  $K_{i_d,i}$ ,  $K_{i_q,p}$ , and  $K_{i_q,i}$  are gains of PI controllers.

The error dynamics of  $e_{i_d}$  and  $e_{i_q}$  can be obtained by substituting (3.37) and (3.38) in (3.22).

$$\begin{aligned}
 \dot{e}_{i_d} &= -e_{i_d} K_{i_d,p} - K_{i_d,i} \int_0^t e_{i_d}(\tau) d\tau \\
 \dot{e}_{i_q} &= -e_{i_q} K_{i_q,p} - K_{i_q,i} \int_0^t e_{i_q}(\tau) d\tau
 \end{aligned}
 \tag{3.39}$$

Finally, by using (3.39) the original control inputs  $u_\alpha$  and  $u_\beta$  are calculated as follows:

$$\begin{aligned}
 u_\alpha &= \frac{u_d v_{\alpha g} + u_q v_{\beta g}}{V_g} \\
 u_\beta &= \frac{u_d v_{\beta g} - u_q v_{\alpha g}}{V_g}
 \end{aligned}
 \tag{3.40}$$

These two control inputs are converted to three phase control signals using  $\alpha\beta$ - $abc$  transformation. These control signals finally are used to generate the switching signals for the BIC switches through a modulation technique called sinusoidal pulse width modulation (SPWM). The reason behind choosing SPWM technique is it provides linear control of the converter output voltage. In addition, it is able to eliminate or reduce the

low order and some higher order harmonics depending on the switching frequency. In SPWM scheme, the switching instants are determined by the intersection between a sinusoidal reference modulating signal (amplitude  $V_r$ ) and a high frequency triangular carrier signal of amplitude  $V_c$ . The pulse width is determined by the time during which the magnitude of the carrier signal is less than that of the modulating signal. Figure 3.6 shows the SPWM waveform where the triangular carrier wave is compared with single phase modulating wave.

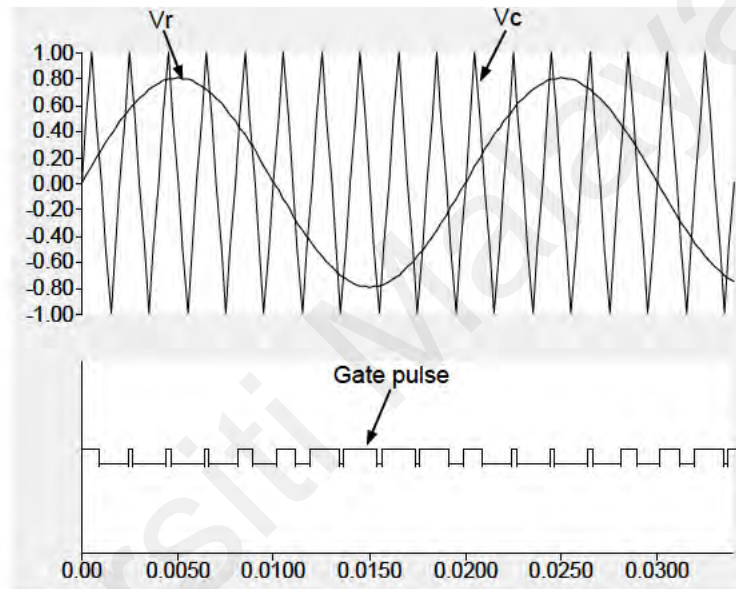


**Figure 3.6: SPWM technique for VSI**

For the proposed PLL less CCT based power control method's PI controllers gain design, substituting from (3.34) to (3.38) into (3.22), a closed-loop system can be obtained, such as

$$\begin{aligned} \frac{di_d}{dt} &= -i_d \frac{R}{L} + K_{p,i_d} (i_{refd} - i_d) + K_{i,i_d} \int (i_{refd} - i_d) dt \\ \frac{di_q}{dt} &= -i_q \frac{R}{L} + K_{p,i_q} (i_{refq} - i_q) + K_{i,i_q} \int (i_{refq} - i_q) dt \end{aligned} \quad (3.41)$$

If differentiate (3.41), it can be changed to a second-order system:

$$\begin{aligned} \frac{d^2 i_d}{dt^2} &= -\frac{R}{L} \frac{di_d}{dt} + K_{p,i_d} \frac{d(i_{refd} - i_d)}{dt} + K_{i,i_d} (i_{refd} - i_d) \\ \frac{d^2 i_q}{dt^2} &= -\frac{R}{L} \frac{di_q}{dt} + K_{p,i_q} \frac{d(i_{refq} - i_q)}{dt} + K_{i,i_q} (i_{refq} - i_q) \end{aligned} \quad (3.42)$$

Applying the Laplace transform to (3.42) yields

$$\begin{aligned} i_d s^2 &= -s i_d \frac{R}{L} + s K_{p,i_d} (i_{refd} - i_d) + K_{i,i_d} (i_{refd} - i_d) \\ i_q s^2 &= -s i_q \frac{R}{L} + s K_{p,i_q} (i_{refq} - i_q) + K_{i,i_q} (i_{refq} - i_q) \end{aligned}$$

or, equivalently,

$$\frac{i_d(s)}{i_{refd}(s)} = \frac{s K_{p,i_d} + K_{i,i_d}}{s^2 + (K_{p,i_d} + \frac{R}{L})s + K_{i,i_d}} \quad (3.43)$$

$$\frac{i_q(s)}{i_{refq}(s)} = \frac{s K_{p,i_q} + K_{i,i_q}}{s^2 + (K_{p,i_q} + \frac{R}{L})s + K_{i,i_q}}$$

The PI controller gains could be selected based on the traditional second-order system as shown in (3.43).

#### (a) *PI Controller Gain Tuning*

By considering the overall system dynamics, the PI controller gains of the proposed PLL less CCT based power control and PVMT based PIDPC method are tuned. The values are calculated using phase margin (PM) and cutoff frequency ( $\omega_{co}$ ) of the VSI. The relationship between cutoff frequency and PM can be expressed as (3.44) (Gui, Wang, Blaabjerg, & Pan, 2019).

$$PM = \Pi/2 - \omega_{co} (1.5T_s) \quad (3.44)$$

where,  $T_s$  is sampling period.

The proportional gain  $K_p$  can be calculated by using the cutoff frequency value obtained from (3.44).

$$K_p \approx \omega_{co} L \quad (3.45)$$

To abate PI regulator's phase contribution at corner frequency, during integral gain  $K_i$  calculation cutoff frequency is set one-tenth (1/10) of  $\omega_{co}$  (Gui et al., 2019). Hence,  $K_i$  can be expressed as:

$$K_i = \frac{\omega_{co}}{10} K_p \quad (3.46)$$

**Table 3.4: Values of PI controllers' coefficients for conventional and proposed CCT based power control methods**

PI Controller Gains	Values
<b>Conventional CCT based Power controller with PLL system (PV VSI)</b>	
$K_{p,p}$	0.18
$K_{i,p}$	3.24
$K_{p,q}$	1.2
$K_{i,q}$	24
$K_{id,p}$	4.04
$K_{id,i}$	262.6
$K_{iq,p}$	2
$K_{iq,i}$	66.6
<b>Proposed CCT based Power controller without PLL system (PV VSI)</b>	
$K_{p,p}$	0.08
$K_{i,p}$	0.0007
$K_{p,q}$	0.0094
$K_{i,q}$	0.032
$K_{id,p}$	10.01
$K_{id,i}$	0.00089
$K_{iq,p}$	0.13
$K_{iq,i}$	3.01
<b>DC link voltage controller (PV VSI)</b>	
$K_{i,dc}$	0.0015
$K_{p,dc}$	105

### 3.4.3.2 Direct Power Control (DPC) method for PV Inverter

Simple and robust controllers containing feedback and feedforward control structures are modeled for the new DPC based VSI model presented in (3.33). In Figure 3.5 (a) and (b), the PIDPC and FLDPC methods' schematics for the PV VSI are depicted. In PIDPC and FLDPC control methods, the real and reactive power references are tracked by controlling their actual values using two PI controllers and two FLC, respectively.

The errors of the real and reactive power for both PIDPC and FLCDC can be expressed as (3.47).

$$\begin{aligned} e_p &:= P_{ref} - P \\ e_q &:= Q_{ref} - Q \end{aligned} \quad (3.47)$$

where active & reactive power references are represented by  $P_{ref}$  &  $Q_{ref}$ , respectively.  $e_p$  and  $e_q$  are the errors of real and reactive powers.

Due to the presence of coupling terms in the new Multiple-Input Multiple-Output (MIMO) system (3.33), a feedback and feedforward based controller is designed in this study to eliminate coupling terms of (3.33) which are applicable for both PIDPC and FLDC methods.

$$\begin{aligned} u_p &= \frac{2}{3}Lv_p + \frac{2}{3}L\omega Q + \frac{2}{3}RP + V_{pcc}^2 \\ u_q &= -\frac{2}{3}Lv_q - \frac{2}{3}RQ + \frac{2}{3}L\omega P \end{aligned} \quad (3.48)$$

where  $v_p$  and  $v_q$  are feedback controller inputs which can be calculated using (3.49) and (3.50) for PIDPC and FLDC methods, respectively.

$$\begin{aligned} v_p &= e_p K_{P,p} + K_{P,i} \int_0^t e_p(\tau) d\tau + \dot{P}_{ref} \\ v_q &= e_q K_{Q,p} + K_{Q,i} \int_0^t e_q(\tau) d\tau + \dot{Q}_{ref} \end{aligned} \quad (3.49)$$

where  $K_{P,p}$ ,  $K_{P,i}$ ,  $K_{Q,p}$ , and  $K_{Q,i}$  are gains of PI controllers which are used for obtaining zero steady-state error. The tuning method of optimal values of the PI controllers' parameters are presented in section 3.4.3.1 (a) and their values are tabulated in Table 3.5.

$$\begin{aligned} v_p &= F_p + \dot{P}_{ref} \\ v_q &= F_q + \dot{Q}_{ref} \end{aligned} \quad (3.50)$$

where,  $F_p$  and  $F_Q$  are defuzzified output of the real and reactive power FLCs. The details of FLC development are presented in the next section.

The error dynamics of  $e_p$  and  $e_Q$  for PIDPC can be obtained by substituting (3.48) and (3.49) in (3.33).

$$\begin{aligned}\dot{e}_p &= -e_p K_{P,p} - K_{P,i} \int_0^t e_p(\tau) d\tau \\ \dot{e}_Q &= -e_Q K_{Q,p} - K_{Q,i} \int_0^t e_Q(\tau) d\tau\end{aligned}\quad (3.51)$$

Finally, by using (3.52) the original control inputs  $u_\alpha$  and  $u_\beta$  are calculated for both PIDPC and FLDPC methods as follows.

$$\begin{aligned}u_\alpha &= \frac{-u_Q v_{p\beta} + u_P v_{p\alpha}}{V_{pcc}^2} \\ u_\beta &= \frac{u_P v_{p\beta} + u_Q v_{p\alpha}}{V_{pcc}^2}\end{aligned}\quad (3.52)$$

These two control inputs by using  $\alpha\beta$ -abc transformation has been converted to 3-ph control signals which are used to generate the pulses for the VSI switches using SPWM.

For the proposed PLL less PVMT based PIDPC method's PI controllers gain design, substituting from (3.47) to (3.49) into (3.33), a closed-loop system can be obtained as,

$$\begin{aligned}\frac{dP}{dt} &= -P \frac{R}{L} + K_{P,p} (P_{ref} - P) + K_{P,i} \int (P_{ref} - P) dt \\ \frac{dQ}{dt} &= -Q \frac{R}{L} + K_{Q,p} (Q_{ref} - Q) + K_{Q,i} \int (Q_{ref} - Q) dt\end{aligned}\quad (3.53)$$

If differentiate (3.53), it can be changed to a second-order system:

$$\begin{aligned}\frac{d^2P}{dt^2} &= -\frac{dP}{dt} \frac{R}{L} + K_{P,p} \frac{d}{dt} (P_{ref} - P) + K_{P,i} (P_{ref} - P) \\ \frac{d^2Q}{dt^2} &= -\frac{dQ}{dt} \frac{R}{L} + K_{Q,p} \frac{d}{dt} (Q_{ref} - Q) + K_{Q,i} (Q_{ref} - Q)\end{aligned}\quad (3.54)$$

Applying the Laplace transform to (3.54) yields

$$\begin{aligned} Ps^2 &= -sP \frac{R}{L} + sK_{p,p} (P_{ref} - P) + K_{p,i} (P_{ref} - P) \\ Qs^2 &= -sQ \frac{R}{L} + sK_{p,p} (Q_{ref} - Q) + K_{p,i} (Q_{ref} - Q) \end{aligned} \quad (3.55)$$

The PI controller gains could be selected based on the traditional second-order system in (3.54) or (3.55). Since, PVMT based DPC method has obtained the same closed loop dynamics as the dq CCT based control method, hence its controller gains have also been determined based on (3.44) to (3.46) presented in section 3.4.3.1 (a).

**Table 3.5: Values of PI controllers' coefficients for proposed PIDPC**

PI controllers' gains	Values
<b>Proposed PVMT based DPC method (PV VSI)</b>	
$K_{p,P}$	1.5
$K_{p,Q}$	45
$K_{i,P}$	0.9
$K_{i,Q}$	16.2
<b>DC link voltage controller (For PIDPC and FLDP methods)</b>	
$K_{i,dc}$	0.015
$K_{p,dc}$	10

### 3.4.3.3 Fuzzy Logic Controller (FLC) for proposed FLDP method

As shown in Figure 3.5, for obtaining zero steady-state error, two error signals ( $e_P$  &  $e_Q$ ) and their rate of change ( $P$ -error\_rate and  $Q$ -error\_rate) are given as inputs to two FLCs. The outputs of FLCs provided the control inputs  $F_P$  and  $F_Q$  for the feed-forward controllers. Due to non-availability of FLC block in RSCAD library, FLC is built in RSCAD software by writing codes using ANSI language in C-builder. Each FLC consists of two inputs and one output which is depicted in Figure 3.5. The two inputs are the error and error-rates of powers for each FLC. The membership functions of inputs and outputs are named identical for both real and reactive power. The variables representing error are NM (negative medium), ZV (zero value), and PM (positive medium). Similarly, error rates variables are NM1 (negative medium 1), ZV1 (zero value 1), and PM1 (positive medium 1). The variables of output are BNE (big negative error), NME (negative medium

error), ZE (zero error) and PME (positive medium error). In Figure 3.7 and 3.8, real and reactive power FLCs' membership functions for error, error-rate and outputs are shown. To ensure smooth control by FLC, triangular based membership functions are considered in this study.

An important part in the design of FLC is choose the scaling factors of input and output membership functions optimally. This can be obtained by implementing optimization techniques to minimize the deviation between inverter output powers and the reference powers. In this study, a black-box optimization technique known as nonlinear Simplex method of Nelder and Mead is adopted for obtaining the optimal scaling factors of input and out membership functions (Filizadeh, Gole, Woodford, & Irwin, 2007). The reason for choosing black-box optimization technique is that it can be easily used in conjunction with time-domain or real-time simulation tools (Hasanien & Matar, 2014). The process of black-box optimization entails the successive evaluation of the objective function for the different sets of parameters for the membership functions. In this process, the real-time simulation program, i.e., RSCAD/RTDS, is used to evaluate the value of the objective function. First, an initial set of parameters is used to initialize the real-time simulation in RTDS and the value of the objective function is numerically evaluated. Then, based on the optimization algorithm and the value of the objective function, a new set of parameters is obtained, and the process is repeated until an optimal set of parameters is determined.

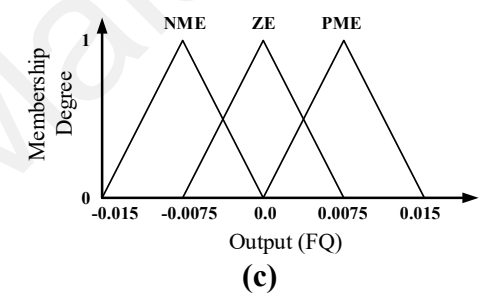
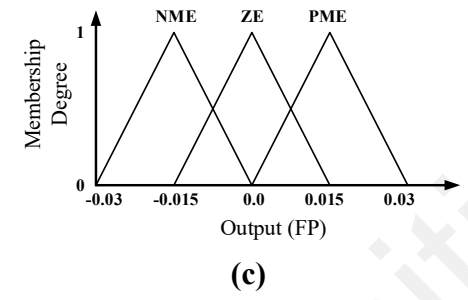
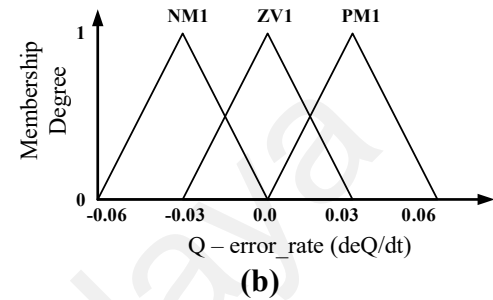
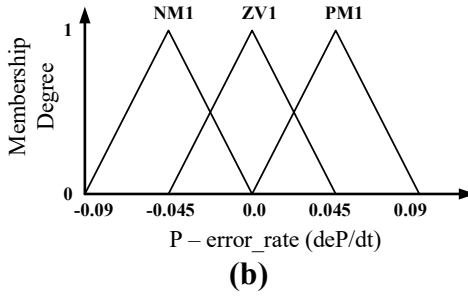
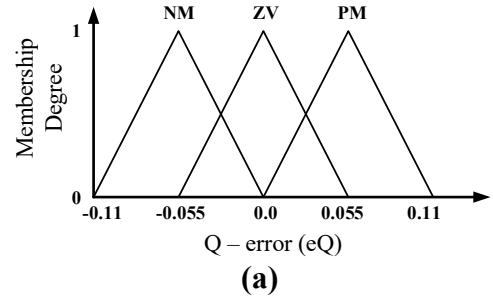
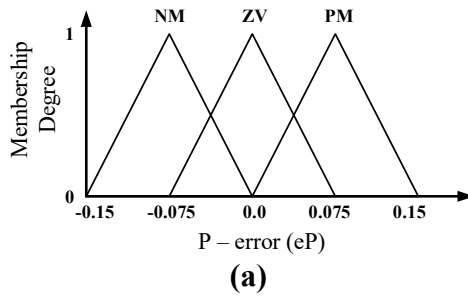


**Figure 3.7: Membership functions of (a) P-error ( $e_P$ ), (b) Error\_rate of P ( $de_P/dt$ ) and (c) Output of FLC ( $F_P$ )**

**Figure 3.8: Membership functions of (a) Q-error ( $e_Q$ ), (b) Error\_rate of Q ( $de_Q/dt$ ) and (c) Output of FLC ( $F_Q$ )**

To assign the input and output control, fuzzy rules are formed based on IF-THEN rules which are summarized in Table 3.6. The rules are decided depending on the cooperation between the estimated error and complexity of FLC. In this paper, defuzzification is carried out by using Sugeno-type weighted average method (Ahmad, Albatsh, Mekhilef, & Mokhlis, 2014) to produce real crisp output  $F_P$  and  $F_Q$ .

**Table 3.6: Rule table for FLCs of real and reactive power**

Membership Functions		ERROR RATE		
		NM1	ZV1	PM1
ERROR	NM	NME	NME	ZE
	ZV	NME	ZE	PME
	PM	ZE	PME	PME

### 3.4.3.4 DC link Voltage Control

The DC link voltage controller is depicted in Figure 3.9. The nominal DC bus voltage  $V_{dc}$  should be larger or identical to the line-line voltage ( $V_{rms.L-L}$ ) to actively control the inverter current.

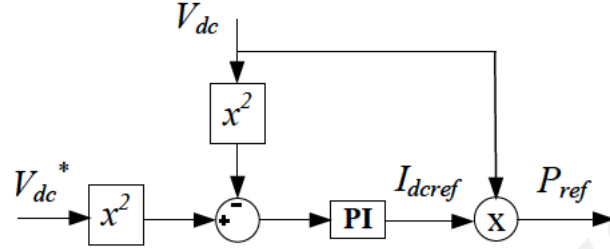


**Figure 3.9: Schematic of DC link voltage controller**

According to the capacity of the system it can be selected as (3.56). By considering the constraint in (3.56), the DC link voltage is calculated using (3.57) as follows:

$$V_{rms.L-L} < V_{dc} \leq 2V_{rms.L-L} \quad (3.56)$$

$$V_{dc} = \frac{V_{rms.L-L}}{0.612 * MI} \quad (3.57)$$

where,  $V_{rms.L-L}$  is inverter line to line output voltage and  $MI$  is the modulation index (MI) of SPWM technique used for control signal generation and  $V_{dc}$  is the DC bus voltage as shown in Figure 3.4 and 3.5.  $MI$  value chosen is 0.8.

The error of DC-link voltage is given by:

$$V_{dc\_error} = (V_{dc}^*)^2 - (V_{dc})^2 \quad (3.58)$$

where,  $V_{dc}^*$  is the reference of  $V_{dc}$ .

This DC-link error is fed to the PI controller to generate the DC current reference  $I_{dc\_ref}$  to ensure DC bus voltage constant value. The expression for DC current reference  $I_{dc\_ref}$  is given by:

$$I_{dc\_ref} = K_{p,dc} \left( (V_{dc}^*)^2 - (V_{dc})^2 \right) + K_{i,dc} \int_0^t \left( (V_{dc}^*)^2 - (V_{dc})^2 \right) dt \quad (3.59)$$

where,  $K_{p,dc}$  and  $K_{i,dc}$  are the controller gains. The values of these gains selected based on trial and error method which are presented in Table 3.4 and 3.5 for PLL less CCT power control method and PIDPC method, respectively.

### 3.4.3.5 Robust Control Design

#### (a) For PLL less CCT based power control method

If  $\dot{\psi}_{i_d} = e_{i_d}$  and  $\dot{\psi}_{i_q} = e_{i_q}$  are defined, then the error dynamics (3.39) can be represented as follows:

$$\begin{bmatrix} \dot{e}_{i_d} \\ \dot{\psi}_{i_d} \\ \dot{e}_{i_q} \\ \dot{\psi}_{i_q} \end{bmatrix} = \begin{bmatrix} -K_{i_d,p} & -K_{i_d,i} & 0 & 0 \\ 1 & 0 & 0 & 0 \\ 0 & 0 & -K_{i_q,p} & -K_{i_q,i} \\ 0 & 0 & 1 & 0 \end{bmatrix} \begin{bmatrix} e_{i_d} \\ \psi_{i_d} \\ e_{i_q} \\ \psi_{i_q} \end{bmatrix} \quad (3.60)$$

In the practical operation, (3.60) could not be affected by the parameter uncertainties, discretization errors, or measurement noises, etc.

#### i Assumption 1

Consider the LTI MIMO system (3.22), suppose that there exist uncertainties  $\delta_{i_d}$ ,  $\delta_{i_q}$

and  $\Delta$  such that

$$\begin{aligned} \dot{x} &= f_a(x, u_{i_d}, u_{i_q}, \delta_{i_d}, \delta_{i_q}) \\ &= \begin{bmatrix} \frac{1}{L}(-V_g + u_d) - \omega x_2 - x_1 \frac{R}{L} + \delta_{i_d} \\ \frac{1}{L}u_q - \omega i_d - i_q \frac{R}{L} + \delta_{i_q} \end{bmatrix} \end{aligned} \quad (3.61)$$

where,  $\delta_{i_d}$ ,  $\delta_{i_q}$  bounded such as

$$0 \leq \left| \delta_{i_d} \right| \leq \Delta, \quad 0 \leq \left| \delta_{i_q} \right| \leq \Delta$$

In VSI systems, a parameter uncertainty depends on the inductance, frequency, or grid voltage. Of course, given an operating point, it is needed to estimate the upper bound of uncertainty  $\Delta$ . It is obvious that the regulation with the control law (3.37) with (3.38) always guarantees the exponential stability of the operating point for the nominal plant. The integral action compensates any DC offset due to model parameter uncertainty. Furthermore, small perturbation from the equilibrium point is ultimately bounded by the exponential stability. Thus, Assumption 1 is reasonable without loss of generality.

*ii Proposition 1*

Consider the new MIMO system (3.22). If a control law such as (3.62) is chosen, then

$$\begin{aligned} \hat{v}_{i_d} &= e_{i_d} K_{i_d,p} + K_{i_d,i} \int_0^t e_{i_d}(\tau) d\tau + K_{i_d} \operatorname{sgn}(e_{i_d}) \\ \hat{v}_{i_q} &= e_{i_q} K_{i_q,p} + K_{i_q,i} \int_0^t e_{i_q}(\tau) d\tau + K_{i_q} \operatorname{sgn}(e_{i_q}) \end{aligned} \quad (3.62)$$

where,  $K_{i_d} > \Delta$  and  $K_{i_q} > \Delta$ , then the closed-loop system is also exponentially stable.

*iii Proof*

When  $\delta_{i_d} = 0$  and  $\delta_{i_q} = 0$ , the closed-loop system is exponentially stable based on (3.60).

When  $\delta_{i_d} \neq 0$  and  $\delta_{i_q} \neq 0$ , for simplicity just consider the terms  $\delta_{i_d}$  and  $\delta_{i_q}$ .

Consider a Lyapunov function candidate such as

$$V = \frac{1}{2} e_{i_d}^2 + \frac{1}{2} e_{i_q}^2 \quad (3.63)$$

The time derivative of (3.58) could be obtained as follows:

$$\dot{V} = e_{i_d} \left( \delta_{i_d} - K_{i_d} \operatorname{sgn}(e_{i_d}) \right) + e_{i_q} \left( \delta_{i_q} - K_{i_q} \operatorname{sgn}(e_{i_q}) \right) \quad (3.64)$$

If the controller gains are taken as  $K_{i_d} > \Delta$  and  $K_{i_q} > \Delta$ , then

$$\dot{V} \leq -K_{\Delta i_d} |e_{i_d}| - K_{\Delta i_q} |e_{i_q}| \quad (3.65)$$

where,  $K_{\Delta i_d} = K_{i_d} - \Delta$  and  $K_{\Delta i_q} = K_{i_q} - \Delta$ .

(b) **For PLL less PIDPC method**

If  $\dot{\psi}_p = e_p$  and  $\dot{\psi}_q = e_q$  are defined, then the error dynamics (3.51) can be represented as follows:

$$\begin{bmatrix} \dot{e}_p \\ \dot{\psi}_p \\ \dot{e}_q \\ \dot{\psi}_q \end{bmatrix} = \begin{bmatrix} -K_{p,p} & -K_{p,i} & 0 & 0 \\ 1 & 0 & 0 & 0 \\ 0 & 0 & -K_{q,p} & -K_{q,i} \\ 0 & 0 & 1 & 0 \end{bmatrix} \begin{bmatrix} e_p \\ \psi_p \\ e_q \\ \psi_q \end{bmatrix} \quad (3.66)$$

$\dot{x} \quad \xleftrightarrow{\quad A \quad} \quad x$

In the practical operation, (3.66) could not be affected by the parameter uncertainties, discretization errors, or measurement noises, etc.

*i Assumption 1*

Consider the LTI MIMO system (3.33), suppose that there exist uncertainties  $\delta_p$ ,  $\delta_q$  and  $\Delta$  such that

$$\begin{aligned} \dot{x} &= f_a(x, u_p, u_q, \delta_p, \delta_q) \\ &= \begin{bmatrix} \frac{3}{2L}(-V_{PCC}^2 + u_p) - \omega x_2 - x_1 \frac{R}{L} + \delta_p \\ \frac{3}{2L}u_q - \omega x_1 - x_2 \frac{R}{L} + \delta_q \end{bmatrix} \end{aligned} \quad (3.67)$$

where,  $\delta_p, \delta_q$  bounded such as  $0 \leq |\delta_p| \leq \Delta, 0 \leq |\delta_q| \leq \Delta$ .

Parameter uncertainty in VSI system depends on the frequency/grid voltage/inductance. It is obvious, for a given operating point, the upper bound of uncertainty  $\Delta$  needs to be estimated. Further, the exponential stability of the VSI system's operating point is always guaranteed by control law (3.48) with (3.49) and any DC offset due to model parameter uncertainty is compensated by integral action. Thus, without loss of generality Assumption 1 is reasonable.

### ii Proposition 1

Consider the new MIMO system (3.33). If a control law such as (3.68) is chosen, then

$$\begin{aligned} \hat{v}_p &= e_p K_{p,p} + K_{p,i} \int_0^t e_p(\tau) d\tau + K_p \operatorname{sgn}(e_p) + \dot{P}_{ref} \\ \hat{v}_q &= e_q K_{q,p} + K_{q,i} \int_0^t e_q(\tau) d\tau + K_q \operatorname{sgn}(e_q) + \dot{Q}_{ref} \end{aligned} \quad (3.68)$$

where,  $K_p > \Delta$  and  $K_q > \Delta$ , then the closed-loop system is also exponentially stable.

### iii Proof

When  $\delta_p = 0$  and  $\delta_q = 0$ , the closed-loop system is exponentially stable based on (3.66).

When  $\delta_p \neq 0$  and  $\delta_q \neq 0$ , for simplicity just consider the terms  $\delta_p$  and  $\delta_q$ .

Consider a Lyapunov function candidate such as

$$V = \frac{1}{2} e_p^2 + \frac{1}{2} e_Q^2 \quad (3.69)$$

The time derivative of (29) could be obtained as follows:

$$\dot{V} = e_Q (\delta_Q - K_Q \operatorname{sgn}(e_Q)) + e_P (\delta_P - K_P \operatorname{sgn}(e_P)) \quad (3.70)$$

If the controller gains are taken as  $K_P > \Delta$  and  $K_Q > \Delta$ , then

$$\dot{V} \leq -K_{\Delta Q} |e_Q| - K_{\Delta P} |e_P| \quad (3.71)$$

where,  $K_{\Delta Q} = K_Q - \Delta$  and  $K_{\Delta P} = K_P - \Delta$ .

#### 3.4.4 Voltage Source Inverter Control during AC Microgrid's Islanded Mode

In this study to control the VSI during MG's Islanded mode of operation, a voltage and frequency (V-f) control strategy is adopted from (Hajilu, Gharehpetian, Hosseinian, Poursistani, & Kohansal, 2015; Mansour, Marei, & Sattar, 2017). In this case, at least one VSI should be operated in V-f control mode to regulate the system voltage and frequency within the acceptable limits. The excellence of this control strategy is that no communication infrastructure is needed, thereby using only local measurements for the MG control in a decentralized method, and plug-and-play operation. The block diagram of a VSI adopted V-f control is shown in Figure 3.10.

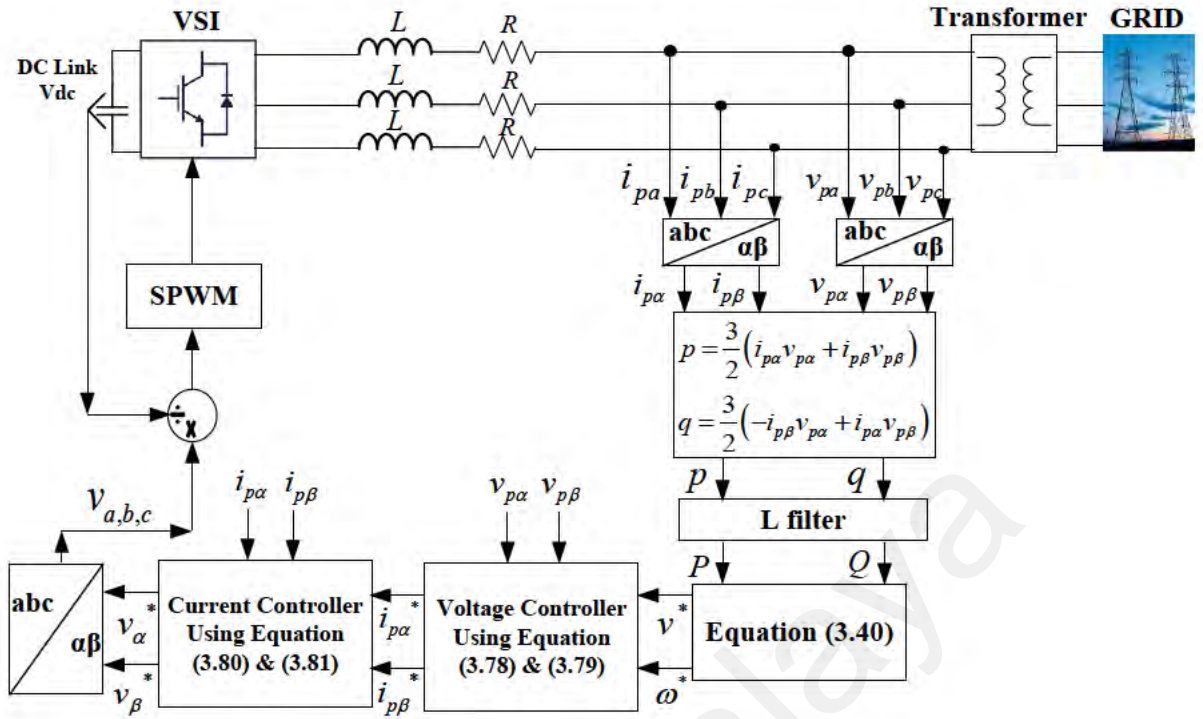


**Figure 3.10: Schematic of V-f control strategy for VSI of islanded microgrid**

As shown in Figure 3.9, the V-f controller consisted of three sections namely droop controller, voltage controller and current controller. The droop controller determines the magnitude and frequency of inverter output voltage according to droop characteristics and active and reactive powers sharing. The voltage and current controllers are designed to reject high frequency disturbances and provide desirable value for the output voltage of a VSI. Instantaneous active and reactive power components in dq frame are calculated by using Equation (3.12).

The power components passed through L-filters are calculated according to (3.72) and (3.73).

$$P = \frac{\omega_c}{s + \omega_c} p \quad (3.72)$$

$$Q = \frac{\omega_c}{s + \omega_c} q \quad (3.73)$$

where,  $\omega_c$  is the cut-off frequency of L-filter.

The active and reactive power share between DGs based on the droop gain as in:

$$\omega^* = \omega_n - m_p P \quad (3.74)$$

$$v^* = v_n - n_q Q \quad (3.75)$$

where,  $\omega^*$  and  $v^*$  are the reference frequency and voltage of the inverters, respectively.  $\omega_n$  and  $v_n$  are the nominal values of frequency and voltage, respectively.  $m_p$  and  $n_q$  are the droop coefficients.

Droop coefficients can be calculated using (3.76) and (3.77) for the given range of frequency and voltage magnitude.

$$m_p = \frac{\omega_{\max} - \omega_{\min}}{P_{\max}} \quad (3.76)$$

$$n_q = \frac{V_{\alpha \max} - V_{\alpha \min}}{Q_{\max}} \quad (3.77)$$

where,  $\omega_{\max}$  and  $\omega_{\min}$  are the upper and lower limits of frequency, respectively.  $V_{\alpha \max}$  and  $V_{\alpha \min}$  are the upper and lower limits of voltage, respectively.  $P_{\max}$  and  $Q_{\max}$  are the maximum power transferred by the DERs.

The output of droop controller is given to the voltage controller. The outputs of voltage controller are given by (3.78) and (3.79).

$$i_{p\alpha}^* = \left( K_{p,v} + \frac{K_{i,v}}{S} \right) (v_{p\alpha}^* - v_{p\alpha}) + f i_{p\alpha} - \omega_n v_{p\beta} \quad (3.78)$$

$$i_{p\beta}^* = \left( K_{p,v} + \frac{K_{i,v}}{S} \right) (v_{p\beta}^* - v_{p\beta}) + f i_{p\beta} + \omega_n v_{p\alpha} \quad (3.79)$$

where,  $(i_{p\alpha}^* \& i_{p\beta}^*)$  and  $(i_{p\alpha} \& i_{p\beta})$  are the reference and actual current values of VSI, respectively.  $K_{p,v}$  and  $K_{i,v}$  are the PI controllers gain values.  $(v_{p\alpha}^* \& v_{p\beta}^*)$  and  $(v_{p\alpha} \& v_{p\beta})$  are the reference and actual voltage amplitudes of VSI.  $f$  is the VSI output voltage frequency.

The output of droop controller is given to the current controller. The outputs of current controller are given by (3.80) and (3.81).

$$v_{\alpha}^* = \left( K_{p,i} + \frac{K_{i,i}}{S} \right) (i_{p\alpha}^* - i_{p\alpha}) - \omega_n L i_{p\beta} \quad (3.80)$$

$$v_{\beta}^* = \left( K_{p,i} + \frac{K_{i,i}}{S} \right) (i_{p\beta}^* - i_{p\beta}) + \omega_n L i_{p\alpha} \quad (3.81)$$

where,  $K_{p,i}$  and  $K_{i,i}$  are the PI controllers gain values.  $L$  is the filter value.  $v_{\alpha}^*$  &  $v_{\beta}^*$  are the original control inputs for V-f control strategy and these signals are compared with carrier signals to generate control signals using SPWM for the VSI switches of DERs of MG in islanded mode. The values of PI controller gains for V-f control strategy is presented in Table 3.7 and these are selected by using trial and error method.

**Table 3.7: Values of PI controllers' coefficients for V-f control strategy**

PI controllers' gains	Values
<b>V-f control strategy (PV VSI)</b>	
$K_{p,v}$	0.08
$K_{i,v}$	0.0094
$K_{p,i}$	0.0007
$K_{i,i}$	0.032
<b>DC link voltage controller (PV VSI)</b>	
$K_{i,dc}$	0.00017
$K_{p,dc}$	20

### 3.4.5 Bidirectional Voltage Source Inverter Control for Hybrid Microgrid

The Bidirectional VSI (BVSI) control strategy applied to control the power transfer between two sub MGs in the hybrid MG is adapted from (Jiao et al., 2019).

#### 3.4.5.1 Droop Characteristics of DC and AC MG

Droop control is adopted for micro sources in AC and DC MG. Typical droop characteristics in DC MG can be expressed by (3.82).

$$P_{dc} = -\frac{1}{k_{dc}}(V_{dc} - V_{dc}^*) + P_{dc}^* \quad (3.82)$$

where,  $k_{dc}$  is active power sag coefficient,  $V_{dc}^*$  and  $P_{dc}^*$  are DC bus rated voltage and reference value of active power, respectively.

In low voltage AC MG, distributed power supply is connected to AC bus through DC/AC converter. Since the equivalent impedance of the line is resistive, it is more appropriate to use P-V and Q- $\delta$  droop characteristics which could be described mathematically by (3.83).

$$\begin{aligned} P_{ac} &= -\frac{1}{k_{ac,p}}(V_{ac} - V_{ac}^*) + P_{ac}^* \\ Q_{ac} &= -\frac{1}{k_{ac,q}}(\delta_{ac} - \delta_{ac}^*) + Q_{ac}^* \end{aligned} \quad (3.83)$$

where,  $k_{ac,p}$  and  $k_{ac,q}$  are the droop coefficients of active power and reactive power, respectively,  $V_{ac}^*$  and  $\delta_{ac}^*$  are the AC bus rated voltage and phase angle reference value, respectively,  $P_{ac}^*$  and  $Q_{ac}^*$  are the reference values of active power and reactive power, respectively.

According to equations (3.82) and (3.83), the bus voltage values of the AC and DC MGs are important indicators reflecting the active fluctuations of the MGs. The change

of load in MGs will cause the change of bus voltage, so BVSI can realize the bidirectional flow of power between MGs by controlling the bus voltage.

### 3.4.5.2 Bidirectional Voltage Source Inverter Control Strategy during Hybrid MG Islanding Operation

Although the AC and DC MGs operate stably through their respective droop control, the bus voltages of the AC and DC subnets have different working ranges, and power flow between AC and DC MG cannot be achieved by the traditional droop methods. Therefore, the key to realizing the bidirectional flow of power between networks is to design a power ring that can effectively integrate the power change information of the subnet and accurately reflect the power difference of the subnet.

The electrical energy stored in the DC capacitor is

$$W_{dc} = \frac{1}{2} C_{dc} V_{dc}^2 \quad (3.84)$$

If the device loss is not considered, the AC and DC output power  $P_{ac} \approx P_{dc}$ . When the power on both sides of the AC and DC is unbalanced, the DC capacitor will charge or discharge, therefore,

$$\frac{d}{dt} W_{dc} = \frac{1}{2} C_{dc} \frac{d}{dt} V_{dc}^2 = P_{dc} - P_{ac} = \Delta P \quad (3.85)$$

According to equations (3.82) to (3.85), the sampling period is set as  $T_s$ , and the relationship between AC side voltage and DC side voltage can be deduced by using forward Euler approximation, as shown in equation (3.86).

$$V_{ac} - V_{ac}^* = k \left[ (V_{dc})^2 - (V_{dc}^*)^2 \right] \quad (3.86)$$

where,  $k = (C_{dc} k_{ac,p}) / (2T_s)$

Through equation (3.86), the DC and the AC voltages can be unified in the same interval. When the voltage on the DC side or the AC side is dropped due to load fluctuation, the power to be exchanged on both sides of the AC and DC can be calculated according to Equation (3.86), which is used as the reference value of the power outer loop of the BVSI controller, as shown in Figure 3.11.

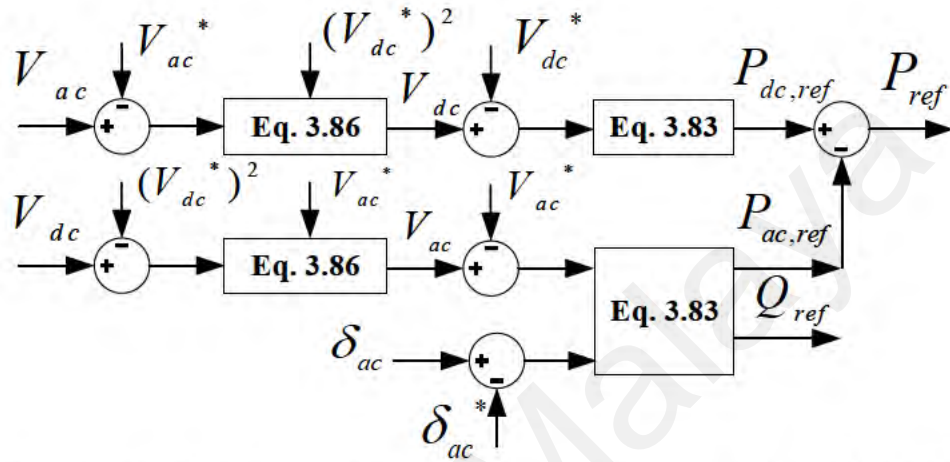


**Figure 3.11: Power transfer control strategy between AC and DC MGs of hybrid MG**

### 3.4.5.3 Power Sharing Strategy of Hybrid MG

Frequency is a global parameter and is the same throughout an AC MG. Any increase in power demand in an AC MG will follow by a decrease in grid frequency,  $f$ . Therefore, the relative amount of frequency deviation with respect to the intended frequency variation range is a good indication of the relative occupied capacity of sources in an AC MG. In this way, the per-unit frequency in the AC MG is defined as

$$f_{pu} = \frac{f - f_{ave}}{\Delta f / 2} \quad (3.87)$$

where,  $\Delta f$  is the intended frequency variation range and  $f_{ave} = f_0 - (\Delta f / 2)$ .

Similarly, the relative amount of voltage deviation with respect to the intended voltage variation range is a good indication of the relative occupied capacity of sources in a DC MG. Therefore, the per-unit DC voltage in the DC-MG is defined as

$$V_{dc,pu} = \frac{V_{dc} - V_{dc,ave}}{(\Delta V_{dc} / 2)} \quad (3.88)$$

where,  $\Delta V_{dc}$  is the intended voltage variation range of DC MG and  $V_{dc,ave} = V_{0dc} - (\Delta V_{dc} / 2)$ .

By setting the per-unit frequency and per-unit DC voltage equal in hybrid MG, the relative occupied capacities of sources on both MGs are equalized.

### 3.5 Proposed Real-time Power Management System for Single Microgrid

Figure 3.12 (a) and (b) show the real-time PMS proposed for the single MG system while operating in grid-connected and islanded modes, respectively. The PMS is developed with the aim to maximize the utilization of PV generation system, BSS and prioritize critical load demands.

#### 3.5.1 Real-time PMS for Single Microgrid's Grid-connected Operation

From Figure 3.12 (a), it is observed that in the grid-connected mode the PMS first checks the PV has more or equal power to fulfill the load demand. If PV power is greater or equal to the load demand, PV will fulfill the total load demand and no power will be drawn from grid, battery and DiG. After fulfilling the load demand if PV has excess power then PMS checks battery required charging or not. If battery requires charging, then the PMS will check excess PV power is sufficient to charge the battery or not. If PV has sufficient extra power to charge the battery, it charges the battery until battery reached its required SOC. If PV power is not sufficient to charge the battery, then the additional PV power will be delivered to utility grid. Similarly, after the battery gets required charging, the PMS will check still PV has excess power than the load demand. If PV has excess power generation then this power will deliver to grid. If PV has less power generation than load demand, during that time first PMS will check battery has sufficient charge to support the load along with PV. If battery has sufficient charge, then the PMS will check whether PV

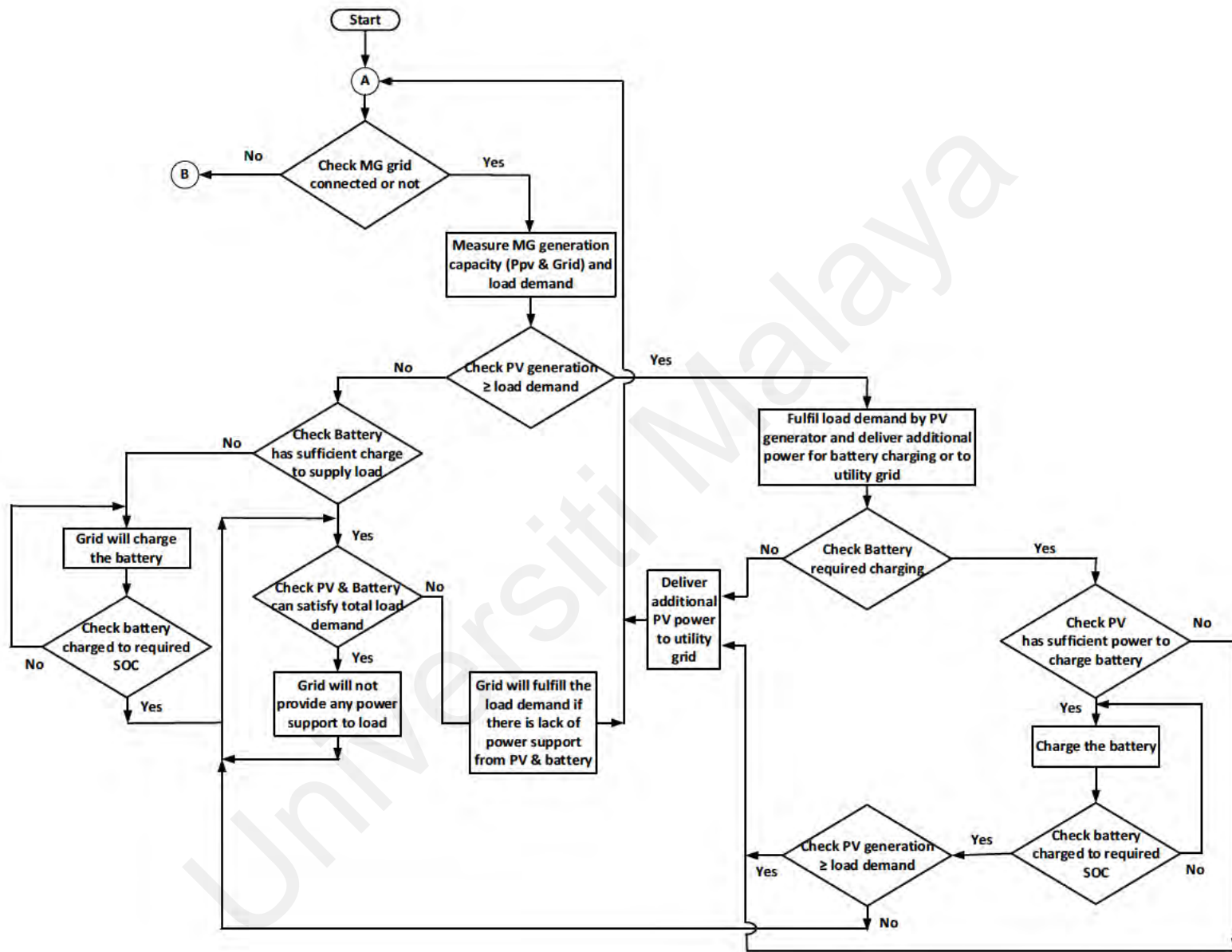
and battery can fulfill the load demand or not. If PV and battery can fulfill the load demand then no power will be drawn from the grid. If there is shortage of power support from PV and battery to the load demand, then the remaining load demand will be fulfilled by the grid. During PV generation less than load demand if battery does not have sufficient charge then grid will charge the battery until battery gets fully charged. At this period, PV and grid will supply power to the load.

### **3.5.2 Real-time PMS for Single Microgrid's Islanded Operation**

During MG's islanded mode of operation like grid-connected mode PMS will check whether PV has more power generation than the load demand as per Figure 3.12 (b). If PV has more power generation, then the load demand will be fulfilled by PV like grid-connected mode. After fulfilling the load demand if PV has excess power then PMS checks battery required charging or not. If battery requires charging, then the PMS will check excess PV power is sufficient to charge the battery or not. If PV has sufficient extra power to charge the battery, it charges the battery until battery reached its required SOC. After the battery gets required charging, the PMS will check still PV has excess power than the load demand. If PV has excess power generation then this power will be dumped since this extra power will create protection issue in the MG operation. Like grid-connected mode operation, if PV has less power generation than load demand, during that time first PMS will check battery has sufficient charge to support the load along with PV. If battery has sufficient charge, then the PMS will check whether PV and battery can fulfill the load demand or not. If PV and battery can fulfill the load demand then no power will draw from the DiG. If there is shortage of power support from PV and battery to the load demand, then PMS will check DiG can provide support or not. If DiG can provide support, then the remaining load demand will be fulfilled by the DiG. If DiG cannot provide support due to technical issues, then some non-critical loads will be shaded by the PMS to balance supply and demand in the MG. Otherwise, this phenomenon will lead

to blackout in the MG. During PV generation less than load demand if battery does not have sufficient charge then DiG will charge the battery until battery gets fully charged. At this period, PV and DiG will fulfill the load demand. At the end of the cycle, the PMS will always check whether the grid is back to normal condition. If the grid backs to normal condition, the PMS will move to grid-connected mode, or else, it will continue MG to operate in islanded mode.

Universiti Malaya



(a)

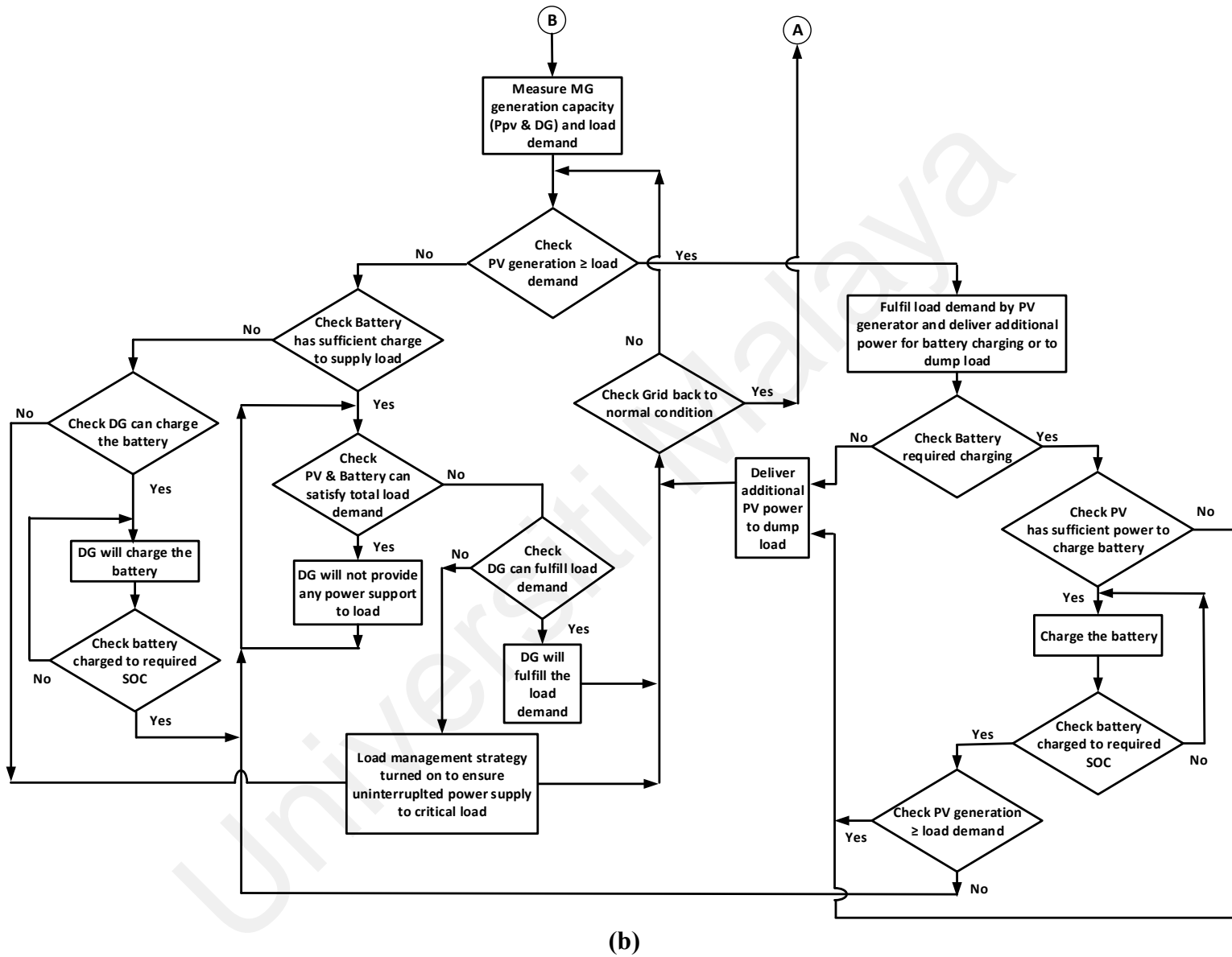
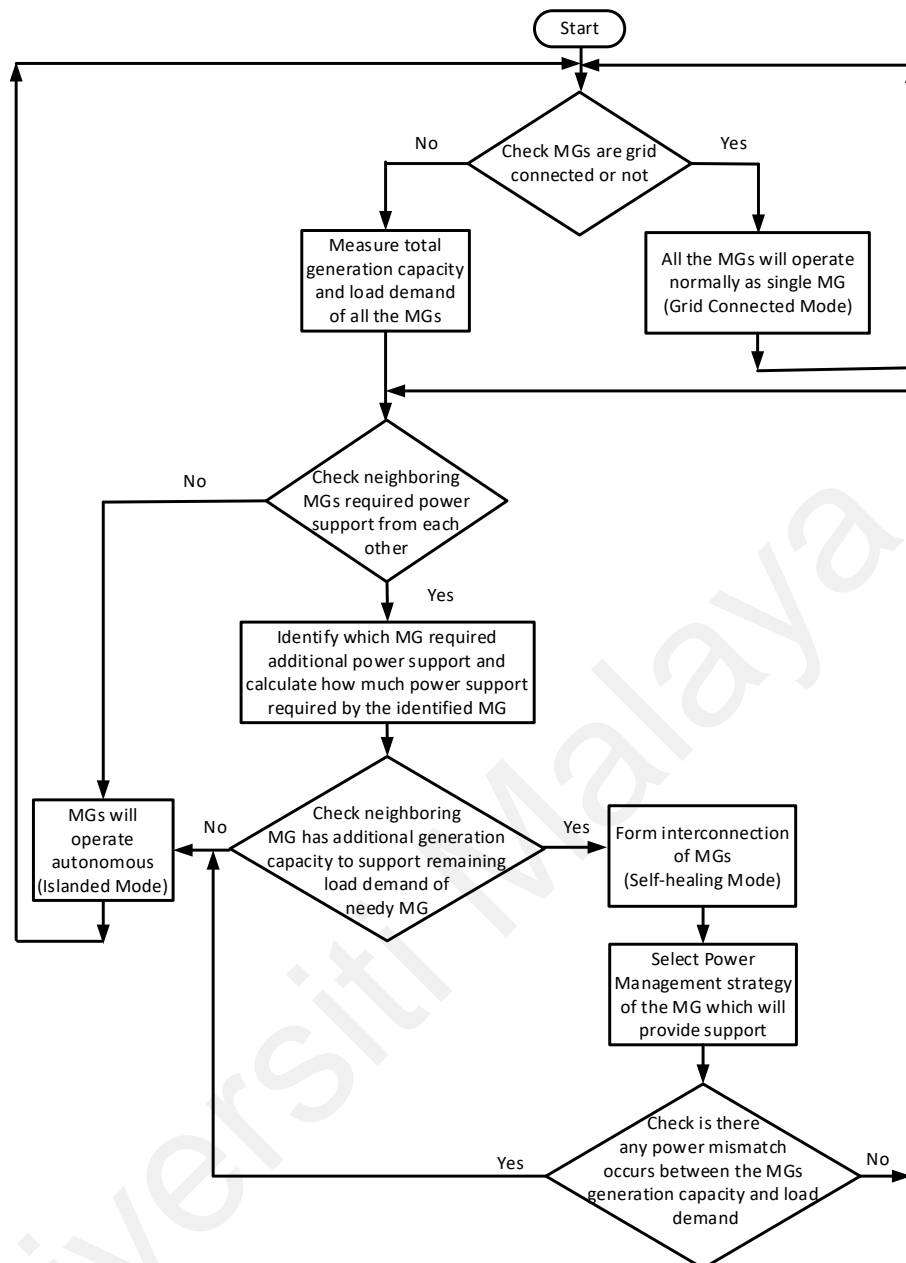


Figure 3.12: Real-time power management systems for single MG during (a) grid-connected and (b) islanded operations

### **3.6 Proposed Intelligent Interconnection Method for Multiple Islanded Microgrids (Self-healing Mode)**

In this section, an algorithm to interconnect multiple islanded MGs during islanded mode of the MGs operation is presented which is named IIM in Figure 3.3. From Figure 3.3, it is seen that the IIM is responsible for the two MGs to be interconnected to overcome the problems of load shedding and dumping power which normally occurred when these two MGs are operated in islanded mode. All the power system parameters measurements from grid, DERs, loads, & ESSs are sent to the IIM and based on that the IIM generates signals to turn on/off the switch BRK2 as shown in Figure 3.3. The flowchart of the operating principle of the proposed IIM is presented in Figure 3.13. The IIM is developed in RSCAD platform by using the C-builder feature where the code is written by ANSI C.

In the beginning, the module checks whether MGs are grid-connected or not. If grid-connected a turn off signal is sent to BRK 2 and all the MGs operate as single MG in grid-connected mode. If the MGs are not grid-connected, then the module first measures all the total generation capacity and load demand of all the MGs. After that it checks whether the neighboring MGs required power support from each other or not. If power support is required, then the IIM identifies the MG which required additional power support and calculates the amount of the power support required. Then IIM checks whether the neighboring MG has enough generation capacity to support the remaining load demand of the other MG which has less generation capacity compared to its load demand. If neighboring MGs can support the load demand of generation scarce MG, then a turn on signal send to the BRK 2 to form the interconnection among the two MGs. Now the MGs are operating in self-healing mode.



**Figure 3.13: Flowchart of the proposed intelligent interconnection algorithm for MGs self-healing mode**

After entering self-healing mode, the module will select the PMS of the MG, which will support the needy MG. The PMSs of the two MGs during self-healing mode are presented in the next section. During self-healing mode, the IIM always checks whether there is any power mismatch that occurs between the two MGs generation capacity and load demand. If there is power mismatched observed, then BRK 2 opens up and the MGs start operating autonomously. On the other hand, after grid disconnected if the neighboring MGs have power scarcity to support the extra load demand needy MGs then a turn off signal sends to the BRK 2 and the MGs operate in islanded mode i.e. no

interconnection among the MMGs do not establish. During both islanded and interconnected modes, the module always checks for whether grid backs to its normal operation or not. If grid returned to normal operating mode, then the MGs get back to grid-connected modes of operation.

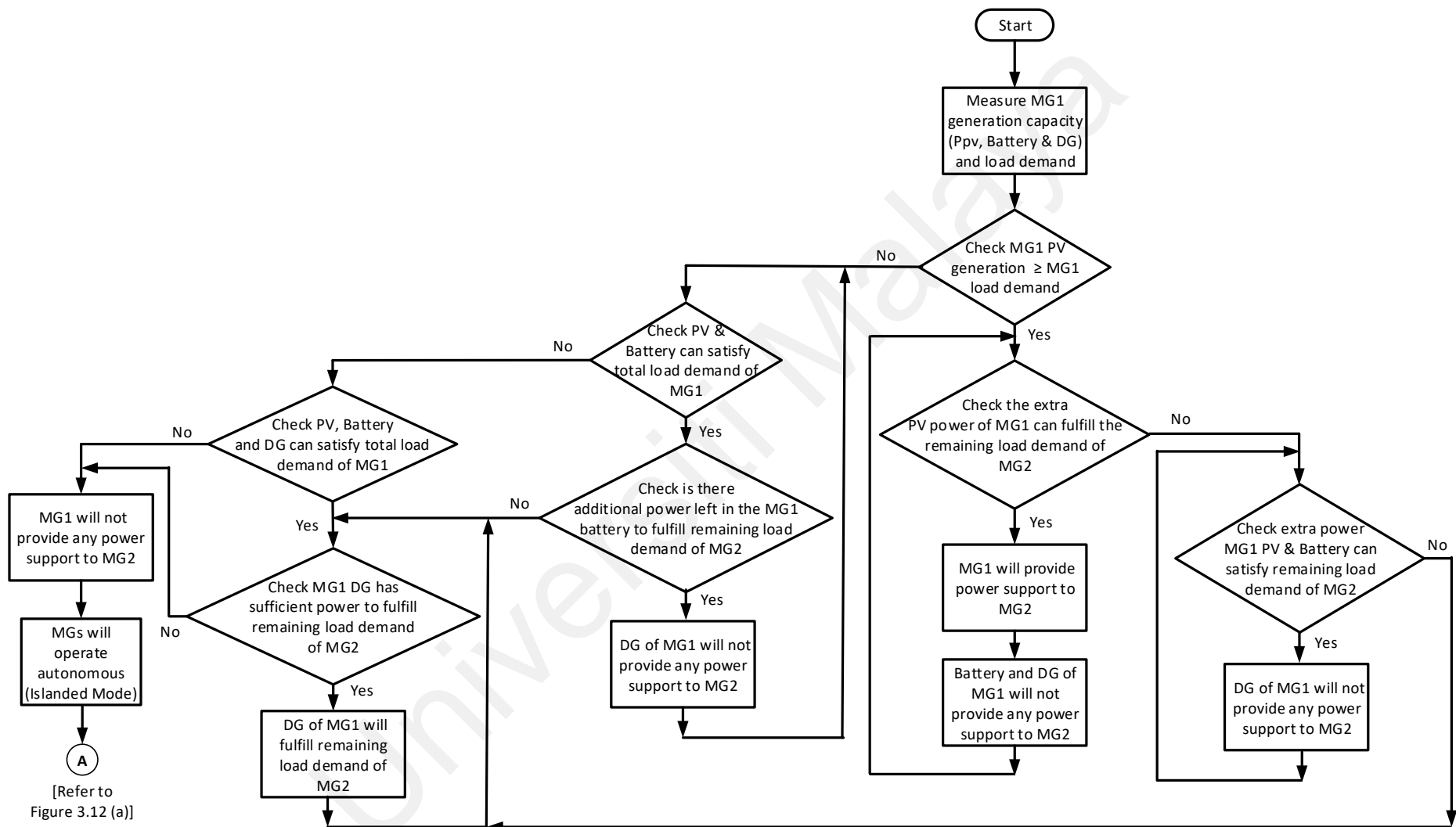
### **3.6.1 Power Management System for MG1 during Self-healing Mode**

In Figure 3.14 (a), the PMS proposed for MG1 during Self-healing Mode is depicted. From the Figure, it is seen that at the beginning, PMS of MG1 will check whether MG1 PV has more power generation than its load demand. If PV has more power than the load demand of MG1 then after fulfilling the load demand of MG1, PMS will check the extra power of MG1 PV is sufficient to fulfill the remaining load demand of MG2. If MG1 extra PV power generation can fulfill the remaining load demand of MG2, then battery and DiG will not provide any power support to MG2. If extra power of MG1 PV is not sufficient to fulfill the remaining load demand of MG2, then PMS will check battery and extra power from PV can satisfy the remaining load demand of MG2. If satisfied then DiG will not operate, otherwise, PMS will check DiG has sufficient power to satisfy the remaining load demand of MG2. If DiG has sufficient power, then MG2 remaining load demand will fulfill by DiG. If DiG cannot fulfill the remaining load demand of MG2, then MG1 will not provide any power support to MG2. The two MGs will operate in islanding mode. Further, if MG1 PV has less power than the load demand of MG1 then the PMS will check PV and battery can fulfill the load demand of MG1. After fulfilling MG1 load demand, PMS will check MG1 battery has sufficient power to satisfy the remaining load demand of MG2. If battery can fulfill the remaining load demand of MG2 then DiG will not operate. Otherwise, PMS will check DiG has sufficient power to satisfy the remaining load demand of MG2. If DiG has sufficient power, then MG2 remaining load demand will fulfill by DiG. If DiG cannot fulfill the remaining load demand of MG2,

then MG1 will not provide any power support to MG2. The two MGs will operate in islanding mode.

### **3.6.2 Power Management System for MG2 during Self-healing Mode**

If MG2 is going to fulfill the remaining load demand of MG1 in self-healing mode then MG2 will operate according to the PMS depicted in Figure 3.14 (b). As like MG1 PMS, the PMS of MG2 will also check at the beginning whether MG2 PV has more power generation than its load demand. If PV has more power than the load demand of MG2 then after fulfilling the load demand of MG2, PMS will check the extra power of MG2 PV is sufficient to fulfill the remaining load demand of MG1. If MG1 extra PV power generation can fulfill the remaining load demand of MG2, then battery will not provide any power support to MG1. If extra power of MG2 PV is not sufficient to fulfill the remaining load demand of MG1, then PMS will check battery and extra power from PV can satisfy the remaining load demand of MG1. If satisfied then MG2 will provide power support to MG1. However, if extra PV power and battery cannot satisfy the load demand of MG1 then MG2 will not provide any power support to MG1. The two MGs will operate in islanding mode. Further, if MG2 PV has less power than the load demand of MG2 then the PMS will check PV and battery can fulfill the load demand of MG2. After fulfilling MG2 load demand, PMS will check MG2 battery has sufficient power to satisfy the remaining load demand of MG1. If battery can fulfill the remaining load demand of MG1 then MG2 will provide power support to MG1. Otherwise, the two MGs will come out from self-healing mode and will start operating in islanded mode.



(a)

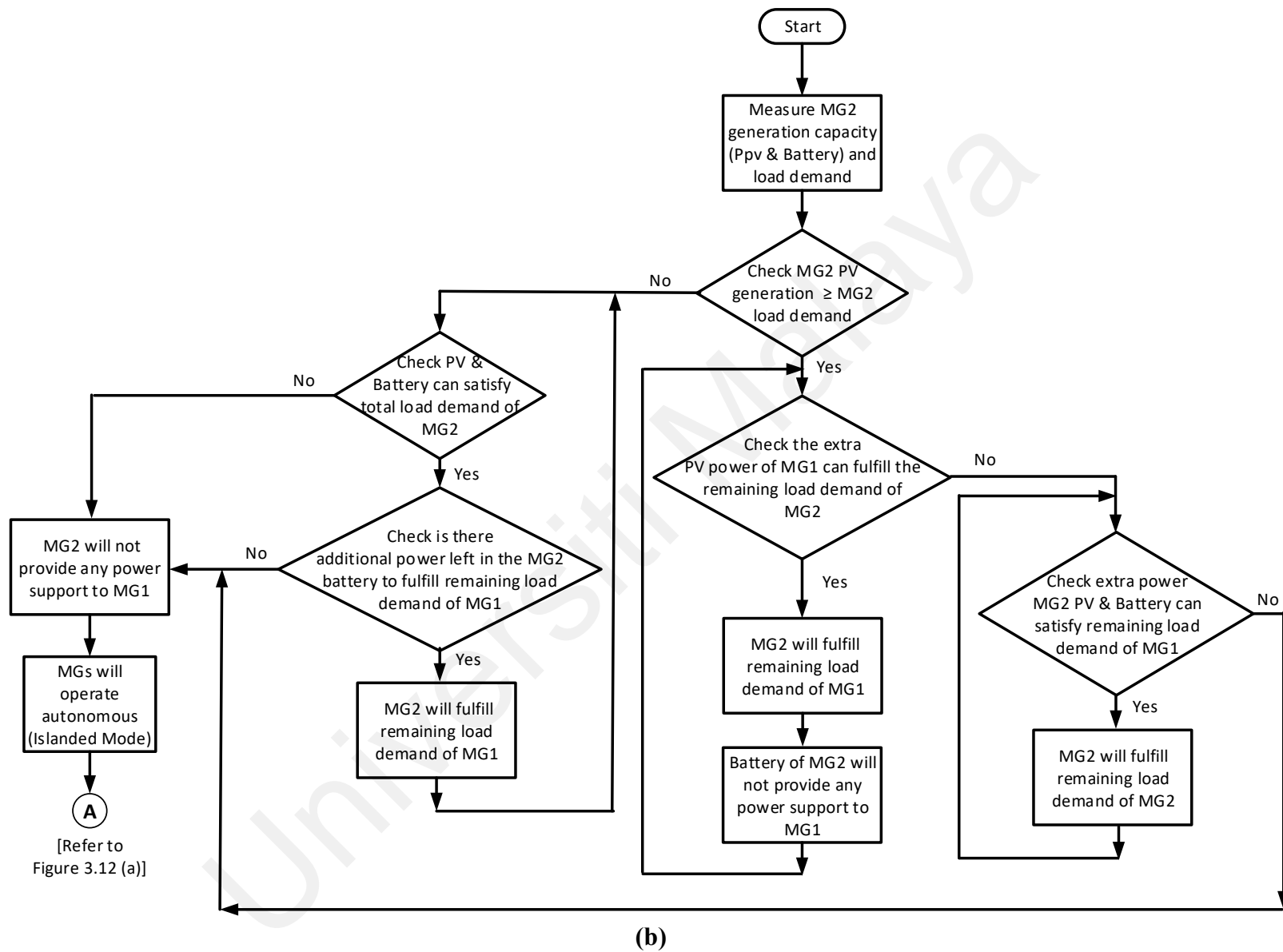


**Figure 3.14: Power management systems for (a) MG1 and (b) MG2 during self-healing mode**

### 3.7 Proposed Intelligent Interconnection Method for Multiple Grid-connected Microgrids (Interconnected Mode)

In this section, an algorithm to interconnect multiple islanded MGs during interconnected mode of the MGs operation which are presented in Figure 3.3. The flowchart of the operating principle of the proposed IIM in interconnected mode is presented in Figure 3.15.

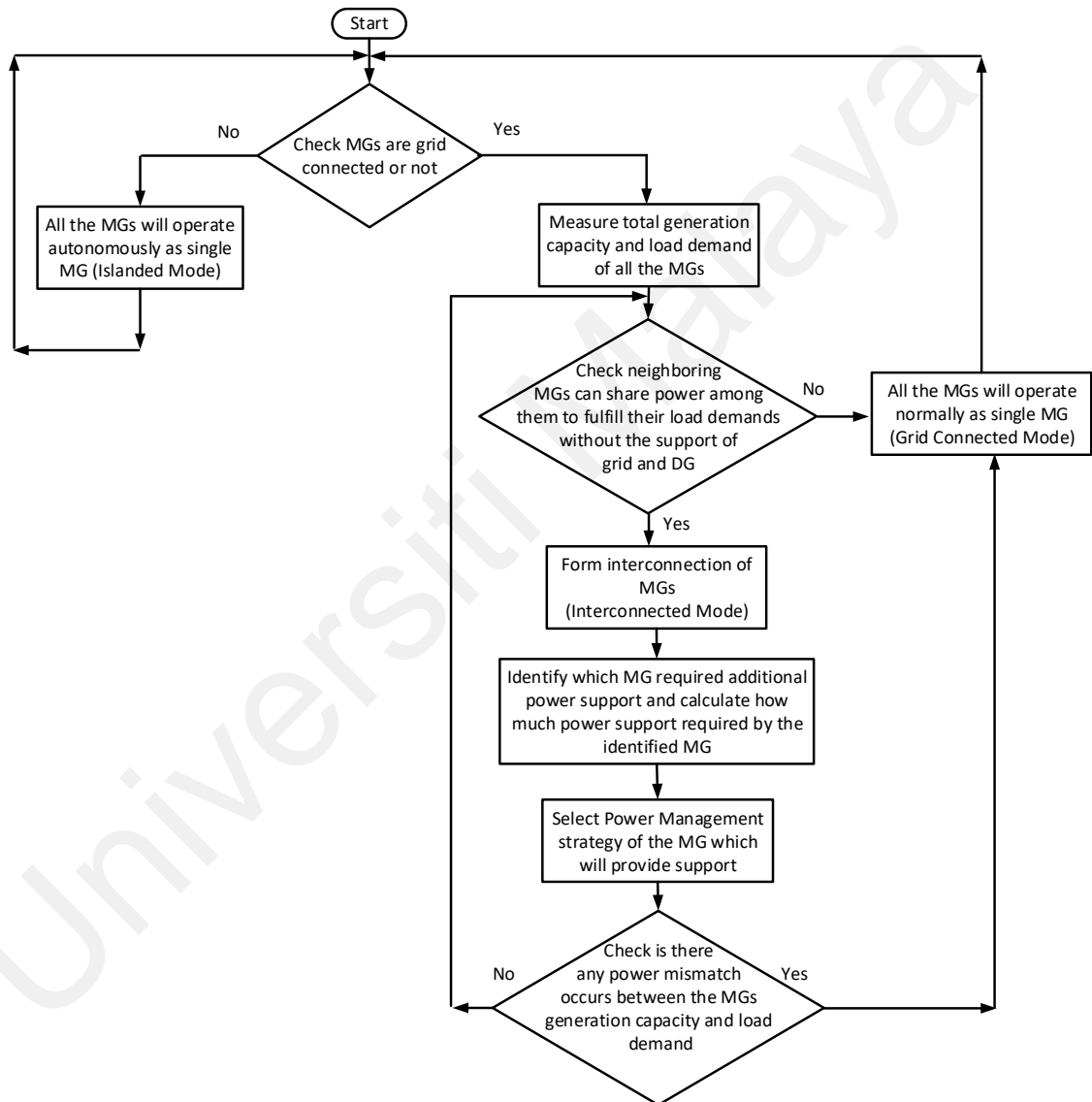


**Figure 3.15: Flowchart of the proposed intelligent interconnection algorithm for MGs' interconnected mode**

In the beginning like self-healing mode, the IIM checks whether MGs are grid-connected or not. If not grid-connected a turn on signal is sent to BRK 2 and all the MGs operate autonomously as single MG in islanded mode. If the MGs are grid-connected,

then the module first measures total PV & battery generation capacity and load demand of all the MGs. If PV and battery of the two MGs have sufficient power to support the load demands of each other then only the two MGs enter interconnected mode, then a turn on signal send to the BRK 2 to form the interconnection among the two MGs. Otherwise, MGs operate individually as single grid-connected MG. In interconnected mode, the MGs do not take any power support from grid and DiG. However, if there is any excessive power generation in any of the MGs after fulfilling their load demands then the excessive power supplies to the grid. Like self-healing mode, in interconnected mode also the MGs operations are regulated by power management strategies which are presented in the next section. During interconnected mode, the IIM continuously checks whether there is any power imbalance occurs between the two MGs' generation capacity and load demand or not. If there is power imbalance observed, then BRK 2 opens up and MGs start operating individually in grid-connected mode.

### **3.7.1 Power Management System for MG1 during Interconnected Mode**

The difference between PMS of self-healing mode and interconnected mode is MG1 will not take any power support from grid and DiG. The PMS for MG1 during MGs interconnected mode is presented in Figure 3.16 (a). Similar to self-healing mode at the beginning, PMS of MG1 will check whether MG1 PV has more power generation than its load demand. If PV has more power than the load demand of MG1 then after fulfilling the load demand of MG1, PMS will check the extra power of MG1 PV is sufficient to fulfill the remaining load demand of MG2. If MG1 extra PV power generation can fulfill the remaining load demand of MG2, then battery and DiG will not provide any power support to MG2. If extra power of MG1 PV is not sufficient to fulfill the remaining load demand of MG2, then PMS will check battery and extra power from PV can satisfy the remaining load demand of MG2. If satisfied then DiG will not operate, otherwise, MG1 will not provide any power support to MG2. The two MGs will operate in grid-connected

mode. After satisfying the remaining load demand of MG2 by MG1 PV system, if it has still extra power then that will be delivered to the grid. Further, if MG1 PV has less power than the load demand of MG1 then the PMS will check PV and battery can fulfill the load demand of MG1. After fulfilling MG1 load demand, PMS will check MG1 battery has sufficient power to satisfy the remaining load demand of MG2. If battery can fulfill the remaining load demand of MG2 then MG1 provides power support to MG2, otherwise, the two MGs will operate in grid-connected mode.

### **3.7.2 Power Management System for MG2 during Interconnected Mode**

From Figure 3.16 (b), it can be seen that PMS of MG2 will operate similarly to PMS of MG1. The only difference is in PMS MG2, there is no additional control circuit required to turn off the DiG because MG2 does not have any DiG. Similar to MG1's PMS, PMS of MG2 initially checks whether MG2 PV has more power generation than its load demand. If PV has more power than the load demand of MG2 then after fulfilling the load demand of MG2, PMS checks the extra power of MG2 PV is sufficient to fulfill the remaining load demand of MG1. If MG2's extra PV power generation can fulfill the remaining load demand of MG1, then battery does not provide any power support to MG1. If extra power of MG2's PV is not sufficient to fulfill the remaining load demand of MG1, then PMS checks battery and extra power from PV can satisfy the remaining load demand of MG1. If satisfied then MG2 will provide power support to MG1 or else vice versa. In addition, if MG2's PV has less power generation than the load demand of MG2 then the PMS checks PV and battery can fulfill the load demand of MG2. After fulfilling MG2's load demand, PMS checks MG2 battery has sufficient power to satisfy the remaining load demand of MG1. If battery can fulfill the remaining load demand of MG1 then MG2 provides power support to MG1, otherwise, the two MGs operate in grid-connected mode.



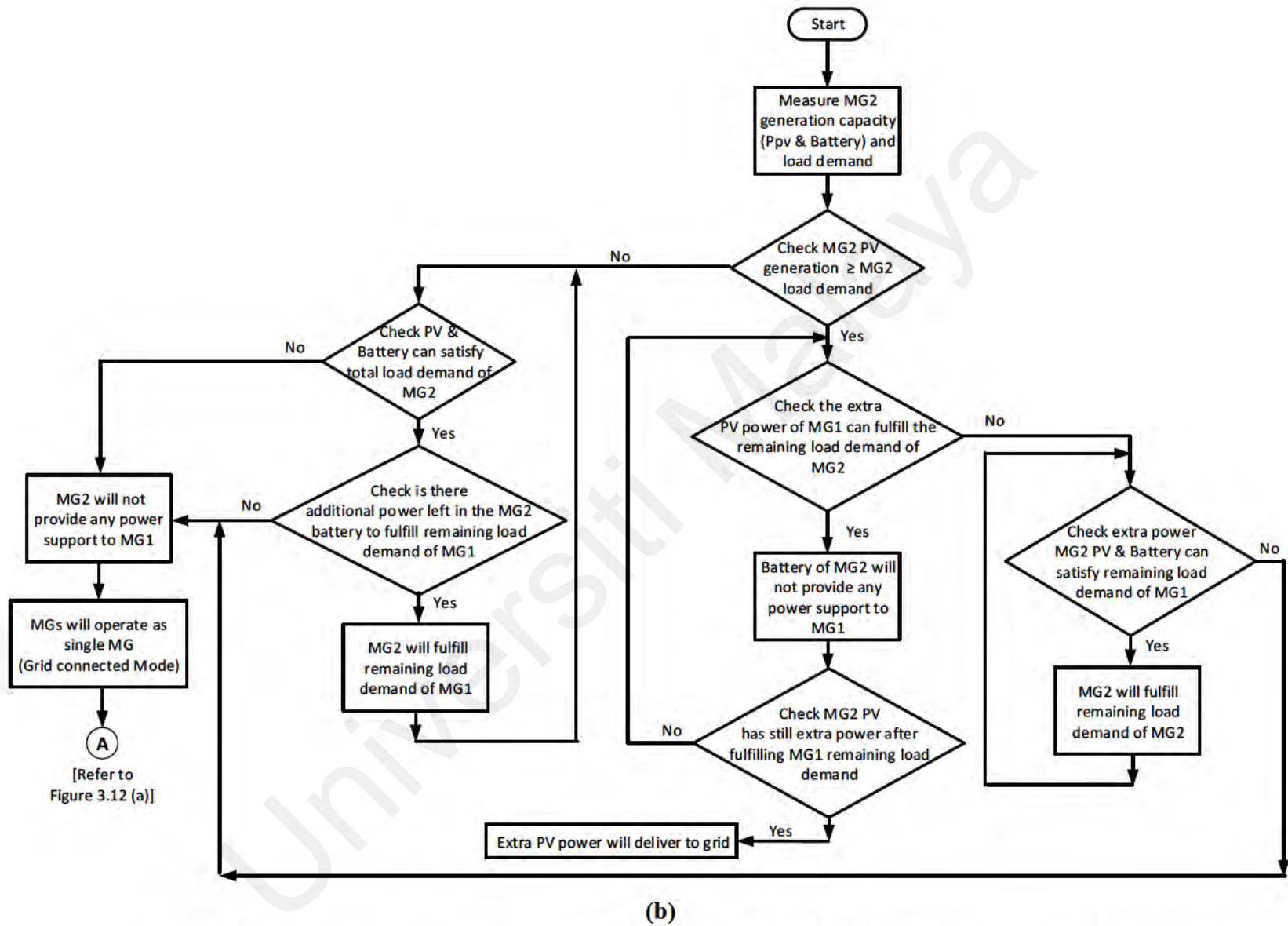
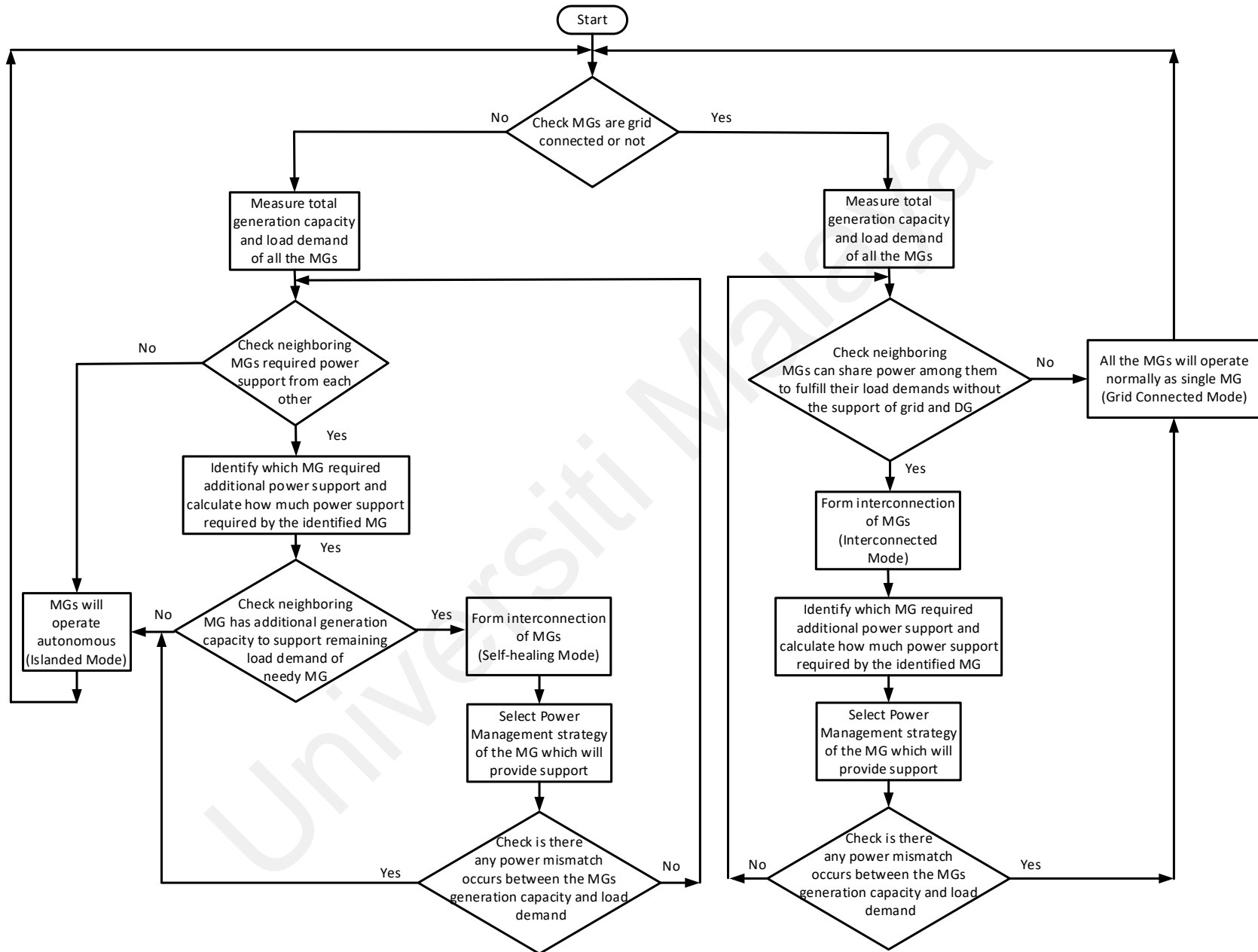


Figure 3.16: Power management systems for (a) MG1 and (b) MG2 during interconnected mode

### **3.8 Proposed Multi-layer Control Strategy for Multiple Interconnected Microgrids**

This section proposes a MLCS for two interconnected MGs to ensure smooth operation of the two interconnected MGs during grid-connected, islanded, interconnected and self-healing modes of operation. In Figure 3.17, the MLCS is presented for multiple interconnected MGs which is developed by combining four power control strategies proposed in sections 3.5, 3.6 and 3.7. From Figure 3.17, it can be seen that through the implementation of the proposed MLCS, the two MGs can be easily transitioned from one operating mode to another operating mode smoothly.

The MLCS initially checks whether the MGs are grid-connected or islanded. If islanded, then MLCS checks whether the neighboring MGs required power support or not. If neighboring MGs required power support and two MGs can fulfill their power demand by sharing power, then they operate in self-healing mode. Otherwise, MGs operate individually in islanded mode. On the other hand, if MGs are in grid-connected mode, first MLCS checks whether the total power generated by PV and battery can fulfill the total load demands of both the MGs or not. If PV and battery power alone can fulfill both the MGs' load demand, then they will operate in interconnected mode. During interconnected mode, MGs do not draw any power from grid and DiG. If MGs have additional power generation, they sell this power to the grid. On contrary, if PV and battery cannot fulfill the total load demands of both the MGs, then MGs operate individually in grid-connected mode.



**Figure 3.17: Multi-layer Control Strategy for Multiple Interconnected Microgrids**

### 3.9 Summary

In this chapter, three different configurations of MGs have been presented along with their components modeling and specifications. Two different power control methods for grid-connected VSI in MG have been modeled without using PLL based synchronization technique. Real-time PMSs for single MG grid-connected and islanded modes of operation are designed. Algorithms for interconnection of two MGs are presented for both self-healing and interconnected modes of operation. PMSs for MG1 and MG2 during self-healing and interconnected modes are proposed. Finally, a multi-layer control strategy is formed to ensure smooth transition of the two interconnected MGs from one operating mode to another one (grid-connected, islanded, interconnected and self-healing modes of operation).

Universiti Malaysia

## CHAPTER 4: RESULTS AND DISCUSSIONS

### 4.1 Introduction

In this chapter, the results obtained to validate the performance of the proposed power control methods for PV VSI of single grid-connected MG, real-time energy management system proposed for grid-connected and islanded modes of operation of single MG are presented at the beginning. Later, the performance of the proposed IIM along with the PMSs during self-healing and interconnected modes of two interconnected MGs are presented. Finally, the performance of the MLCS proposed for smooth transition of multiple interconnected MGs in various operating modes is presented.

### 4.2 Performance Analysis of the Proposed PV VSI Control Methods

This section presents the real-time simulation results obtained from the application of the proposed PLL less CCT based power control method, PVMT based PIDPC and FLDP method for a grid-connected PV VSI. The modeling of MG components like DG sources, VSIs, DC-DC converter and proposed power control algorithm are conducted in RSCAD platform. The real-time simulation is carried out on RTDS which is using a rack mounted PB5 processor card to support the uninterrupted real-time simulation of the grid-tied MG along with the modeling and implementation of the proposed power controller. The laboratory setup of the real-time implementation of the proposed control scheme in RTDS is depicted in Figure 4.1. In this study, the reference power tracking and steady-state performances of the proposed controllers for PV VSI are validated by changing both real and reactive power references and the results are compared with the conventional CCT based power control method with PLL system.



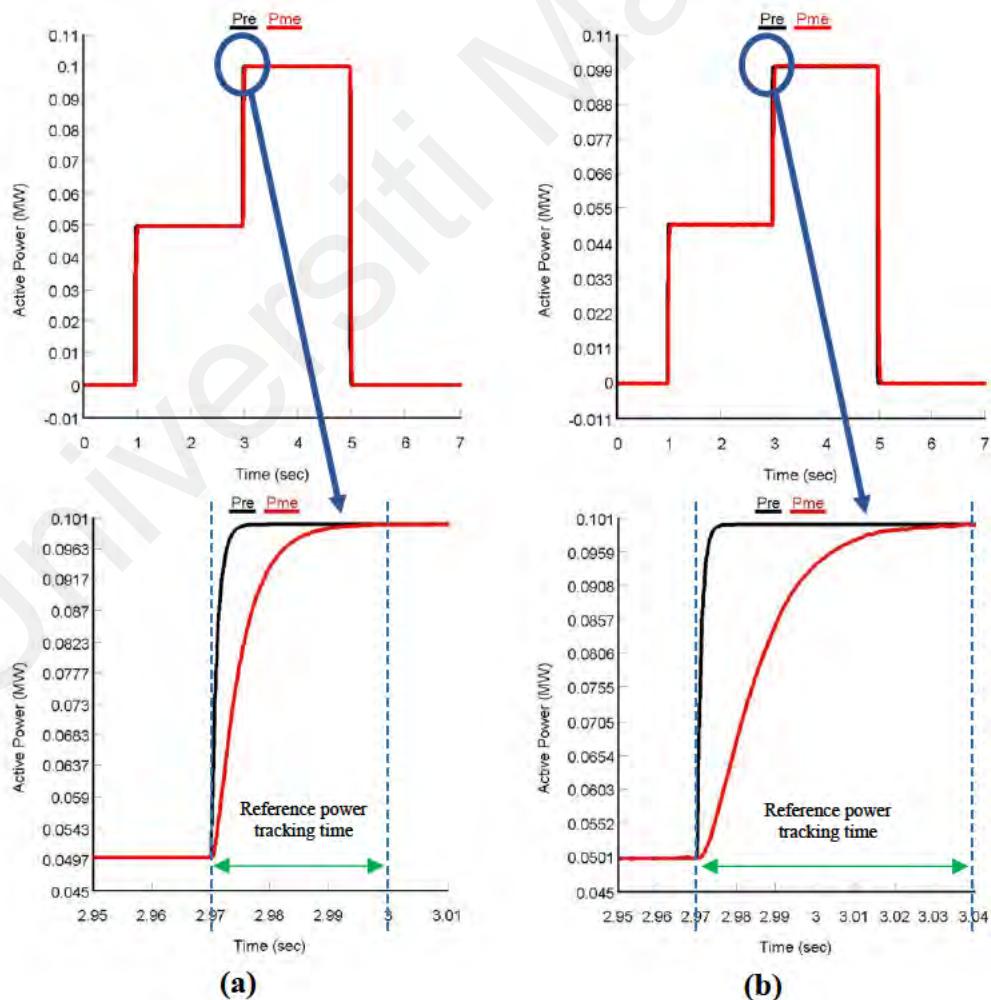
**Figure 4.1: Laboratory setup of the proposed controller for MGs with RTDS**

#### 4.2.1 Reference Power Tracking Performance Analysis

This section presents the results related to the power tracking performances of the proposed PLL less PVMT based FLDP method, PIDPC method and dq axes CCT based power control method for the grid-connected PV VSI for both real and reactive power reference change. Parallely to prove the efficacy of the proposed controllers, their performances are compared with the conventional PLL-PI-integrated dq CCT-based control method (Worku et al., 2019). The results obtained for both the controllers tracking performance analysis are depicted in Figure 4.2 and 4.3. To test the tracking performance of the controllers' real power references are varied in between 0 MW to 0.1 MW (PV output is non-linear) while reactive power references are changed in between 0 MVar to 0.02 MVar, respectively.

From Figure 4.2, it can be seen that real power is stepped up from 0 MW to 0.05 MW in 1s, then at 3 s again it varied from 0.05 MW to 0.1 MW and at 5 s the real power reference decreases from 0.1 MW to 0 MW again. Since PV output power is intermittent and varies with respect to weather conditions, hence, real power references are varied from 0 MW to 0.1 MW. In all the scenarios, it is observed that all the proposed power controllers can track the reference real powers accurately. However, in terms of reference power tracking time and power ripples, there are differences observed in the performances of all the controllers. In this section, only the controllers' performances regarding reference power tracking time are discussed. From Figure 4.2 (a), it is observed that the

proposed FLDPC method takes a tracking time of 0.03 s to reach the steady-state. On the other hand, according to Figure 4.2 (b) and (c), the proposed PIDPC method and PLL less dq CCT based power control method have taken 0.07 s and 0.11 s to track the reference power, respectively, which are 0.04 s and 0.08 s more than proposed FLDPC method. Further, though from Figure 4.2 (d) it is evident that conventional dq CCT based power controller is also tracking the reference powers, however, from zoomed portion it is clear that the tracking speed of proposed PLL less FLDPC method, PIDPC and PLL less CCT based control method are 0.21 s, 0.17 s and 0.13 s, respectively faster than that of conventional PLL-PI integrated dq CCT based power control method whose reference real power tracking speed is 0.24 s.



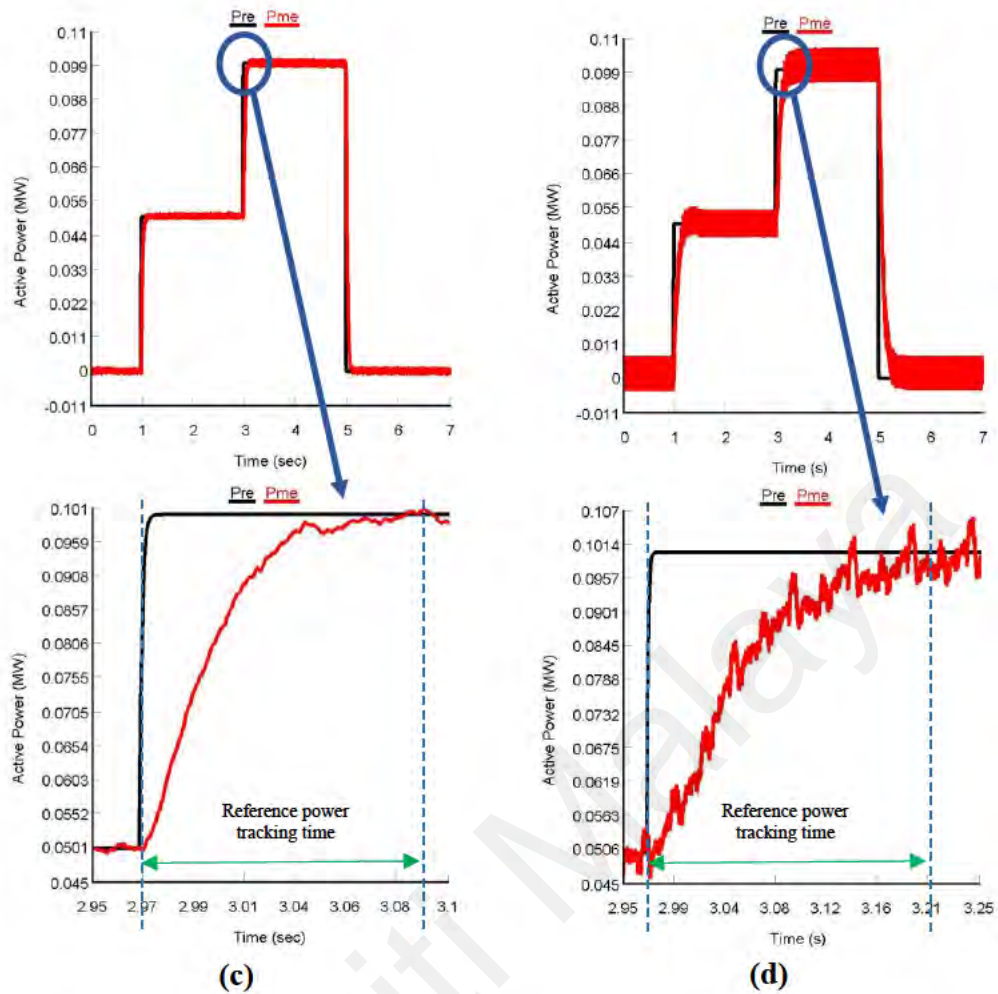
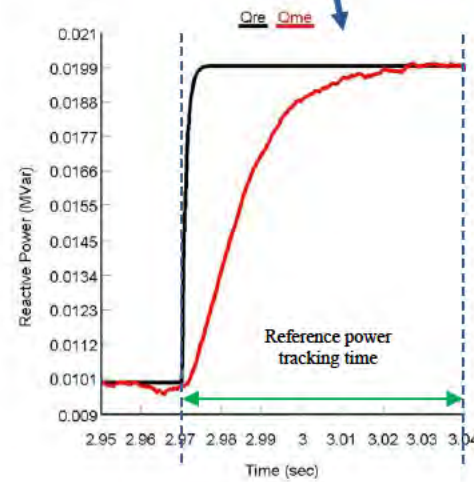
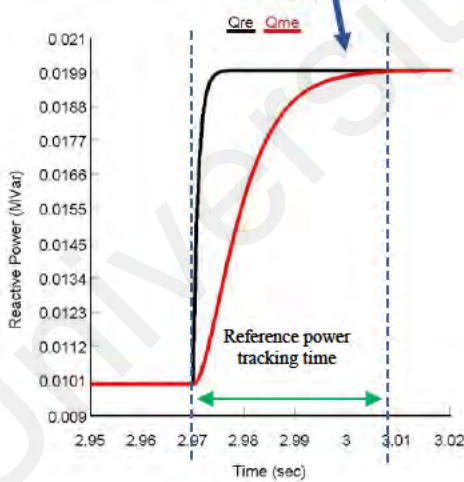
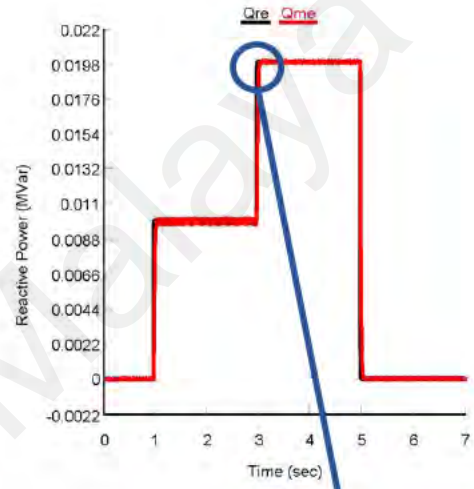
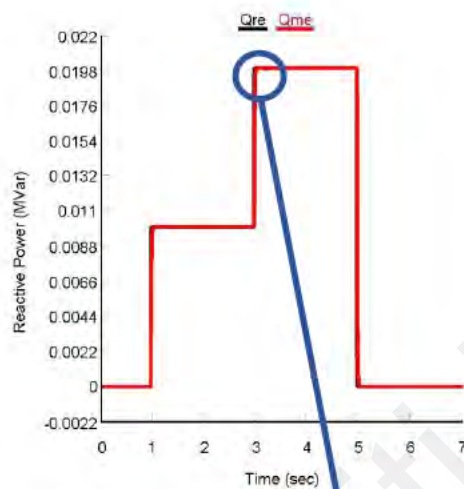


**Figure 4.2: Real power tracking performance of (a) FLDPC method, (b) PIDPC method, (c) PLL less dq CCT and (d) dq CCT based power controller with PLL**

For reactive power also the reference power is kept to 0 MVar initially which is increased to 0.01 MVar and 0.02 MVar at 1 s and 3 s, respectively and finally at 1 s reference reactive power has decreased to 0 MVar. It is observed from Figure 4.3 that the VSI output reactive power controlled by the proposed FLDPC method, PIDPC method and PLL less dq CCT based power control method are following the reference reactive power accurately at different time intervals. However, like real power, the proposed FLDPC has shown better reference power tracking performance than that of PIDPC method and PLL less dq CCT based power control method. As per Figure 4.3 (a), (b) and (c), reference reactive power tracking time for FLDPC is 0.037 s whereas, time taken by PIDPC and PLL less dq CCT based power control method to track the reference reactive power are 0.07 s and 0.11 s, respectively. Nevertheless, all the proposed

controllers tracking speeds have been found faster than conventional PLL-PI integrated dq CCT based power control method. According to the zoomed portion of Fig. 4.3 (a), (b), (c) and (d), the time taken to reach steady-state for reactive power by the proposed FLDPC method, PIDPC method and PLL less dq CCT based power control method are 0.037 s, 0.07 s and 0.11 s, respectively whereas, conventional CCT based power controller tracks it at 0.24 s.



(a)

(b)

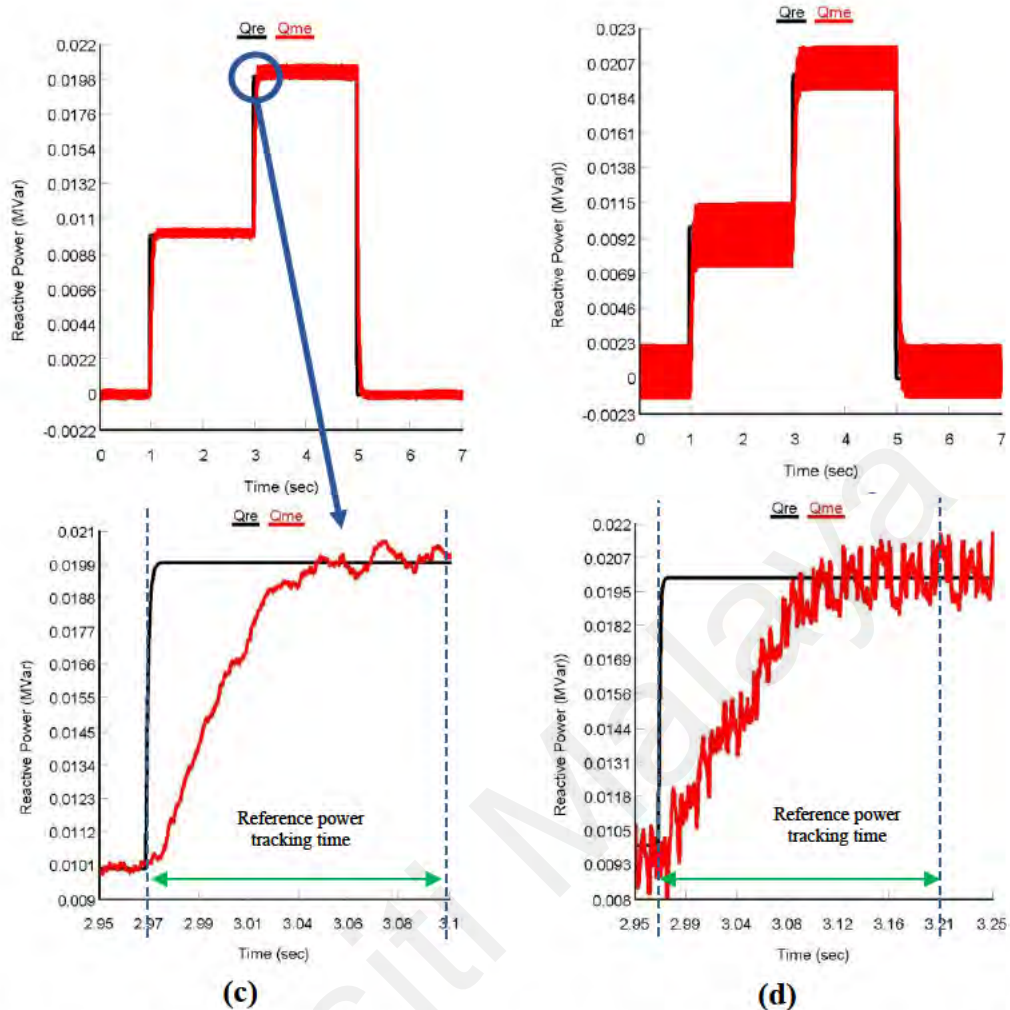


**Figure 4.3: Reactive power tracking performance of (a) FLDPC method, (b) PIDPC method, (c) PLL less dq CCT and (d) dq CCT based power controller with PLL**

#### 4.2.1.1 Steady-state Performance Analysis

The main drawback of the conventional PLL consisted power controller was the existence of power ripple in the steady-state. However, the proposed controller acquires a decoupled LTI error dynamic to resolve this ripple issue in the power. By using the proposed control methods, the power ripple has been significantly reduced both in real and reactive powers compared to the conventional CCT driven PLL based power controller which are presented in Figure 4.4 and 4.5. The time range considered for viewing the ripples of VSI output real and reactive power is 2.88-5 s and also the ripple range for all the controllers are kept to (0.0945-0.107 MW) for real power & (0.0185-0.022 MVar) for reactive power.

From Figure 4.4 (a), (b) and (c), it is observed that there is negligible ripple in the real power for the proposed PLL less FLDP method which is almost 0.1 MW whereas, the PIDPC method and PLL less CCT based power controller have high power ripples than FLDP method which ranges from (0.0995 MW – 0.1006 MW) and (0.0985 MW – 0.1013 MW), respectively. However, compared to all the proposed controllers, according to Figure 4.4 (d), there are very high power ripples are observed in the VSI real power output for the conventional PLL based dq CCT power controller which ranges between 0.0956 MW – 0.1065 MW.

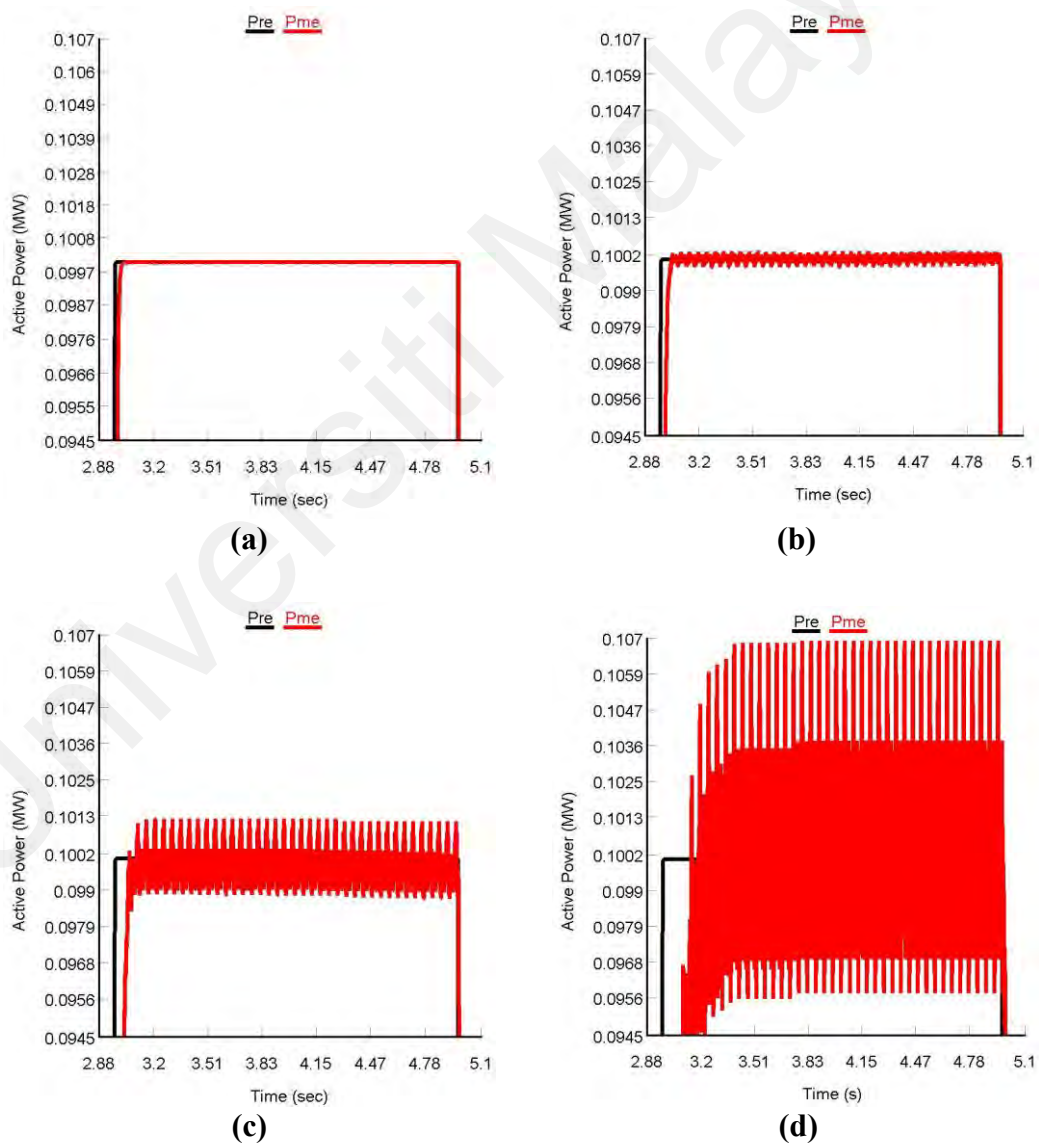


**Figure 4.4: Real power steady-state performance of (a) FLDP method, (b) PIDPC method, (c) PLL less dq CCT and (d) dq CCT based power controller with PLL**

For reactive power also, the ripple is very high for the conventional PLL based dq CCT power controller (0.0189 MVar – 0.022 MVar) which is shown in Figure 4.5 (d). On the other hand, as shown in Figure 4.5 (a), there is almost zero power ripple is observed in the reactive power for the proposed FLDPC method. In addition, for other proposed controllers namely PIDPC and PLL based dq CCT power controllers, there are still undesirable ripples are observed in the reactive power output which are depicted in Figure 4.5 (b) and (c), respectively.

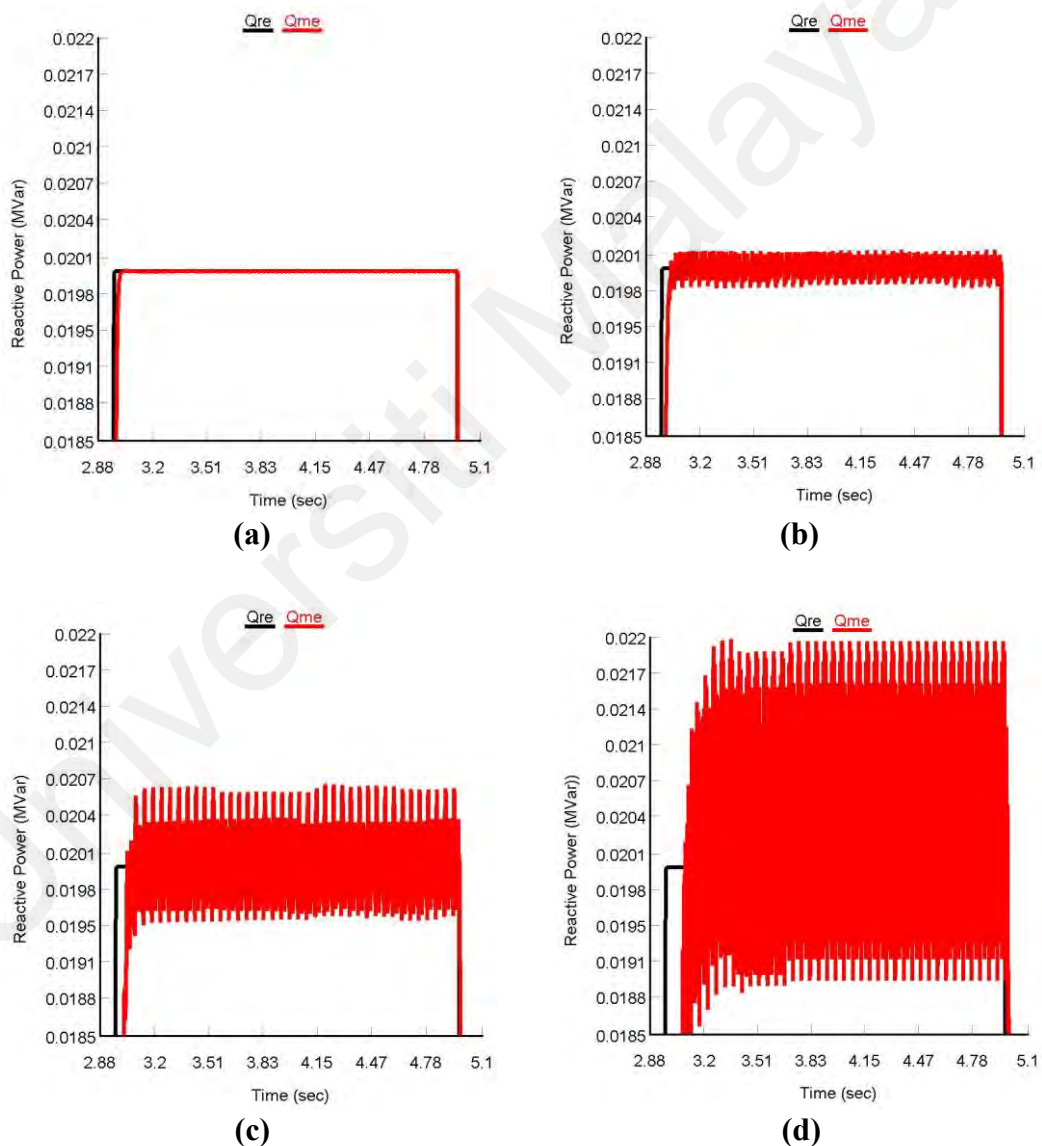
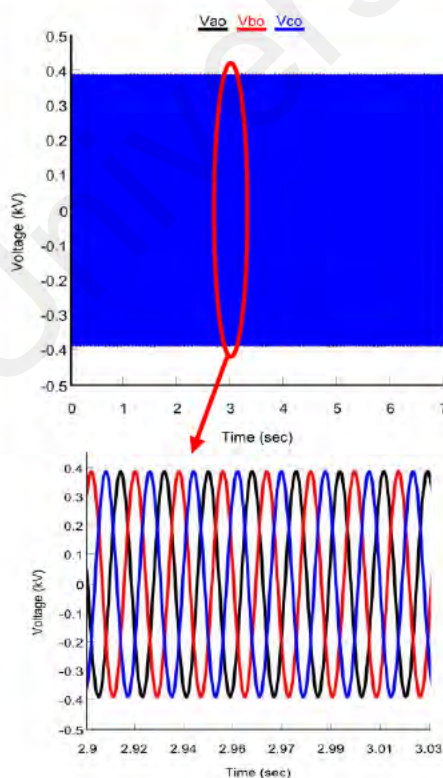
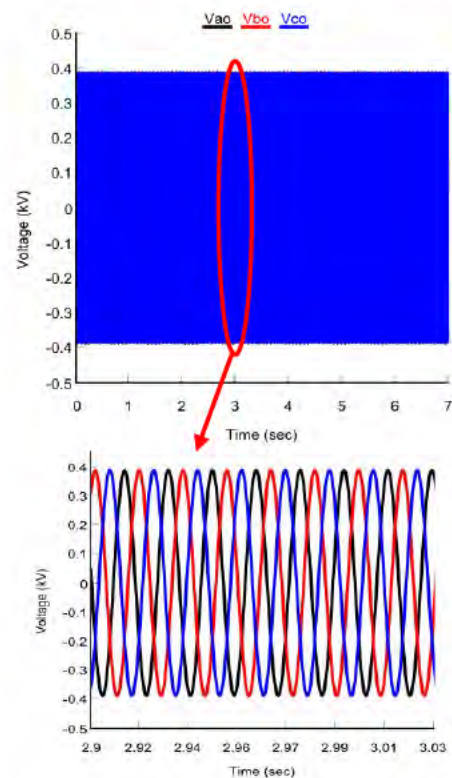


**Figure 4.5: Reactive power steady-state performance of (a) FLDPC method, (b) PIDPC method, (c) PLL less dq CCT and (d) dq CCT based power controller with PLL**

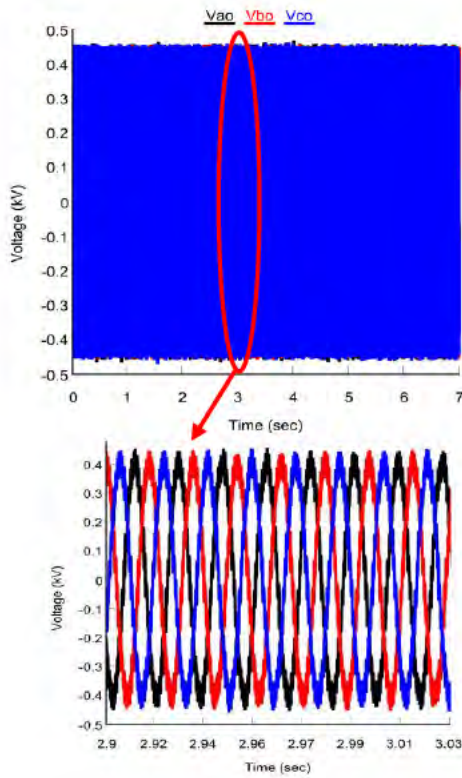
The inverter output current and voltage waveforms for both proposed and conventional controllers are depicted in Figure 4.6 (a) – (d). From the figures, it can be seen that for all the controllers the waveforms of voltage and current are sinusoidal in shape and maintain a frequency of 60 Hz. However, for PLL less proposed FIDPC and PIDPC method, the ripple in inverter output voltage is very less compared which is shown in Figure 4.6 (a) and (b), respectively. On the other hand, with PLL less and PLL based dq CCT based power controller, the output voltages of the VSIs have large distortion which are depicted in Figure 4.6 (c) and (d), respectively. For inverter output current also from Figure 4.7 (a) and (b), same characteristics are observed like the inverter output voltage for both the controllers. For current also from Fig. 4.7 (a), it has been seen that for FLDPC, the PV VSI current is sinusoidal in shape and has negligible noises. Further, even though the PV VSI output current for proposed PIDPC and PLL less CCT based power controllers are sinusoidal in shape, however, still distortions are observed which are shown in Figure 4.7 (b) and (c). However, according to Figure 4.7 (d), there is big distortion observed in VSI output current when it is controlled by PLL based dq CCT based power controller.



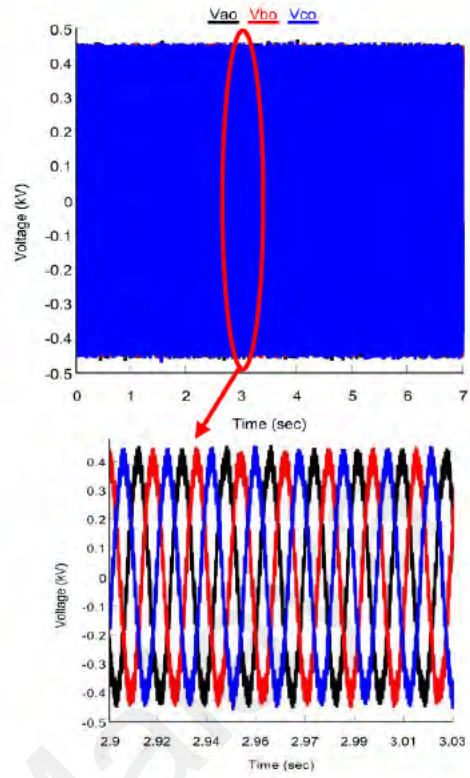
(a)



(b)

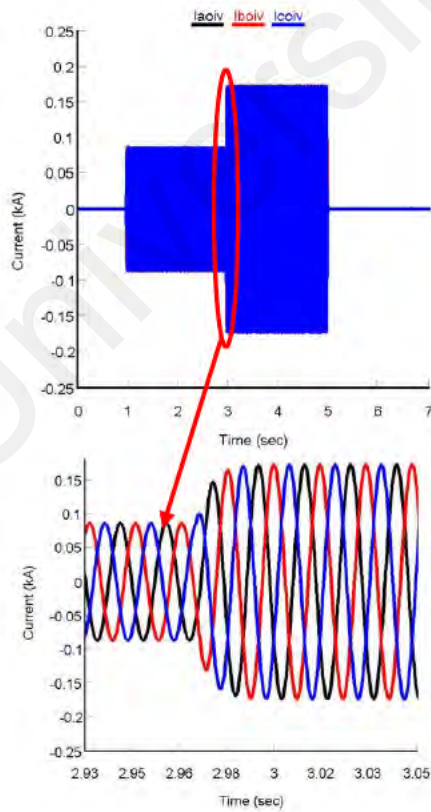


(c)

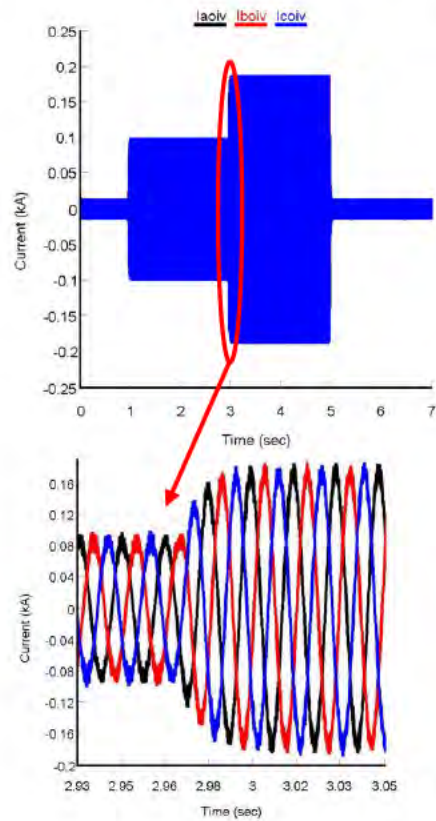


(d)

**Figure 4.6: VSI output voltage for (a) FLNPC method, (b) PIDPC method, (c) PLL less dq CCT and (d) dq CCT based power controller with PLL**



(a)



(b)

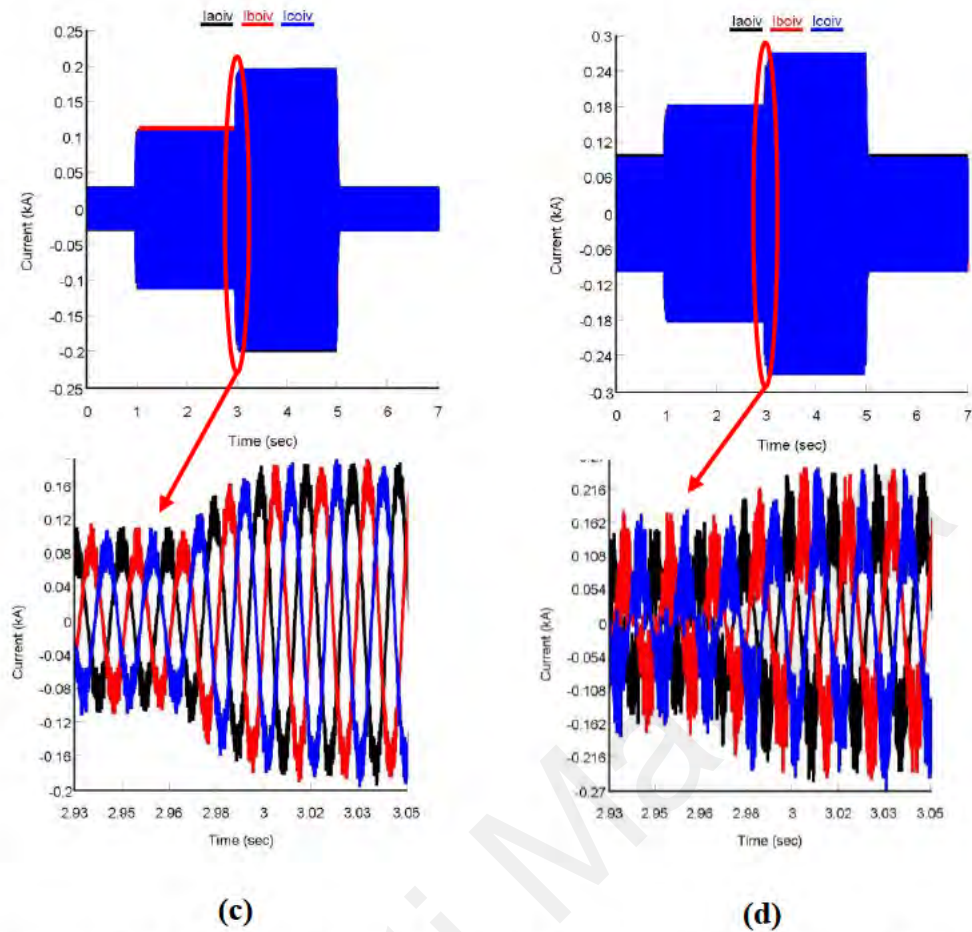


**Figure 4.7: VSI output current for (a) FLDPC method, (b) PIDPC method, (c) PLL less dq CCT and (d) dq CCT based power controller with PLL**

Three cycles of current waveform from 2.98 – 3.03 s are considered to measure the total harmonic distortion (THD) of the VSI output currents for all the controllers and the corresponding current waveforms are depicted in Figure 4.7 (a) - (d). From Figure 4.8, it can be seen that the THD of VSI currents for both all the controllers are less than 5 % according to IEC standard (Photovoltaic, 2004), however, for the proposed FLDPC, PIDPC and PLL less CCT based power controller, current THDs are 1.60 %, 1.91 %, 2.49 % which are much better than that of the current THD (4.967 %) obtained by conventional PLL based dq CCT power control method. Therefore, it can be concluded that the power ripples are low when PLL less DPC methods are implemented to control the VSI output power compared to the conventional PLL based CCT power control method.

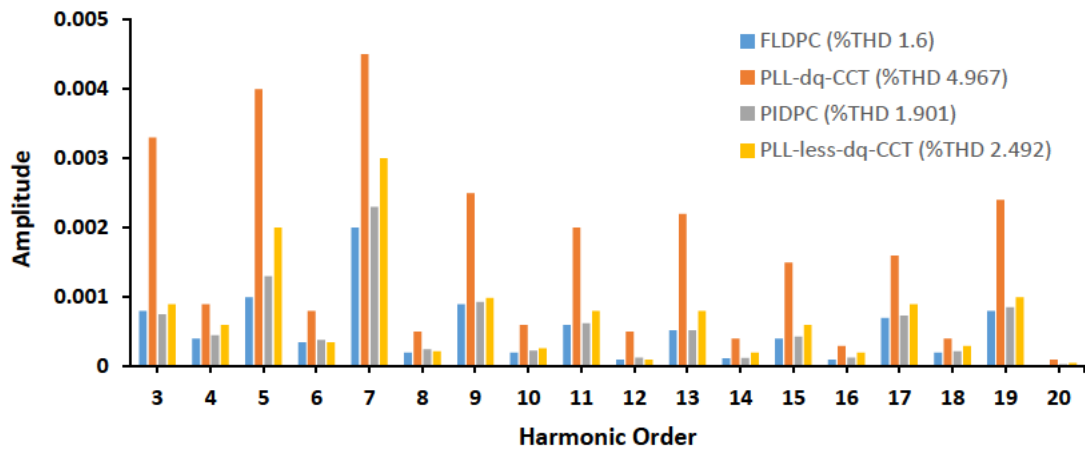


**Figure 4.8: THD of VSI output current for PLL less proposed power controllers along with conventional PLL based dq CCT power controller**

### 4.3 Performance Analysis of the Proposed Real-time Power Management System

In this section, the performance of the proposed real-time PMS along with proposed PVMT based FLDPC is validated on two MG systems namely AC and Hybrid MG.

#### 4.3.1 AC Microgrid

One of the important functions of grid-tied MG power controller is to make sure required power is flowing between MG and utility grid without interrupting power supply to the load. In addition, the MG should also be capable of operating in conditions like varying load, and solar irradiation. To verify these real world features in this section, the performance of the proposed PMS is validated by varying both solar irradiation and load demand. For PV VSI control during MG's grid-tied operation, proposed FLDPC method is implemented and V-f control strategy is implemented for PV VSI control during MG's islanded mode operation. For battery VSI control, conventional dq CCT based control method is adopted in this thesis. The results obtained after implementing the proposed real-time PMS and FLDPC method, the active power flow between different sources and loads are depicted in Figure 4.9 and Table 4.1. For PMS validation only active load has been considered and varied whereas reactive load is considered as zero.

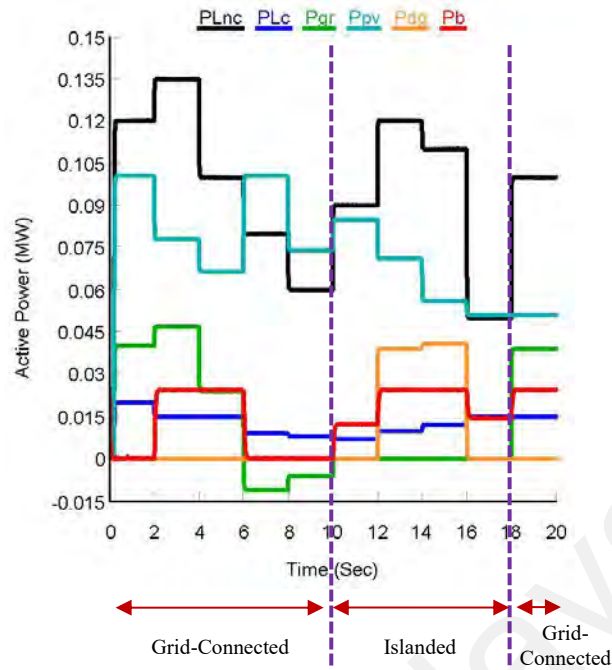


Figure 4.9: Active power flow between different sources and loads in AC microgrid

Table 4.1: Active power flow during both load and solar irradiation changes in AC microgrid

Duration (sec)	Variables		Load Power		Generation				
	Solar Irradiation (W/m <sup>2</sup> )	Load Demand (MW)		Critical load, P <sub>Lc</sub> (MW)	Non-critical load, P <sub>Lnc</sub> (MW)	Grid, P <sub>gr</sub> (MW)	Solar, P <sub>pv</sub> (MW)	Diesel Generator, P <sub>dg</sub> (MW)	Battery, P <sub>b</sub> (MW)
		Critical load (MW)	Non-critical load (MW)						
0-2	1000	0.02	0.12	0.02	0.12	0.04	0.1	0	0
		<b>Total = 0.14</b>		<b>Total = 0.14</b>		<b>Total = 0.14</b>			
2-4	850	0.015	0.135	0.015	0.135	0.047	0.078	0	0.025
		<b>Total = 0.15</b>		<b>Total = 0.15</b>		<b>Total = 0.15</b>			
4-6	700	0.015	0.1	0.015	0.1	0.024	0.066	0	0.025
		<b>Total = 0.115</b>		<b>Total = 0.115</b>		<b>Total = 0.115</b>			
6-8	1000	0.009	0.08	0.009	0.08	-0.011	0.1	0	0
		<b>Total = 0.089</b>		<b>Total = 0.089</b>		<b>Total = 0.089</b>			
8-10	800	0.008	0.06	0.008	0.06	-0.006	0.074	0	0
		<b>Total = 0.068</b>		<b>Total = 0.068</b>		<b>Total = 0.068</b>			
10-12	900	0.007	0.09	0.007	0.09	0	0.085	0	0.012
		<b>Total = 0.097</b>		<b>Total = 0.097</b>		<b>Total = 0.097</b>			
12-14	750	0.01	0.12	0.01	0.12	0	0.071	0.034	0.025
		<b>Total = 0.13</b>		<b>Total = 0.13</b>		<b>Total = 0.13</b>			
14-16	600	0.012	0.11	0.012	0.11	0	0.056	0.041	0.025
		<b>Total = 0.122</b>		<b>Total = 0.122</b>		<b>Total = 0.122</b>			
16-18	550	0.015	0.10	0.015	0.05	0	0.051	0	0.014
		<b>Total = 0.115</b>		<b>Total = 0.065</b>		<b>Total = 0.065</b>			
18-20	550	0.015	0.10	0.015	0.1	0.039	0.051	0	0.025
		<b>Total = 0.115</b>		<b>Total = 0.115</b>		<b>Total = 0.115</b>			

The initial values of solar irradiation and varying load are set to  $1000 \text{ W/m}^2$  and  $0.14 \text{ MW}$  (Critical  $0.02 \text{ MW}$  + Non-critical  $0.12 \text{ MW}$ ), respectively. In between  $0-2 \text{ s}$ , PV is generating full power of  $0.1 \text{ MW}$  which can fulfill  $0.1 \text{ MW}$  of the total load and the remaining  $0.04 \text{ MW}$  demand is supplied by grid. At this period, the power from battery and DiG are nil. The solar irradiation is dropped to  $850 \text{ W/m}^2$  in between  $2-4 \text{ s}$  and contrast load demand is increased to  $0.15 \text{ MW}$ . During this period PV can provide a maximum of  $0.078 \text{ MW}$  power support to the load. Since PV power goes down from the nominal value, hence battery will come in operation. In this case, battery and grid supply  $0.025 \text{ MW}$  and  $0.047 \text{ MW}$  power to the fulfil rest of the load demand. From  $4-6 \text{ s}$ , solar irradiation and load demand reduced to  $700 \text{ W/m}^2$  and  $0.115 \text{ MW}$ , respectively. This situation has compelled the grid to supply power of  $0.024 \text{ MW}$  to the load since PV ( $0.066 \text{ MW}$ ) and battery ( $0.025 \text{ MW}$ ) together can support maximum of  $0.091 \text{ MW}$  power. During  $6-8 \text{ s}$  load demand has decreased ( $0.089 \text{ MW}$ ) and solar irradiation has increased ( $1000 \text{ W/m}^2$ ). Since the total load demand ( $0.089 \text{ MW}$ ) is less than the PV generation ( $0.1 \text{ MW}$ ), hence, the remaining power ( $0.011 \text{ MW}$ ) from MG is delivered towards grid and power from battery becomes zero. At  $8 \text{ s}$ , solar irradiation level reached  $800 \text{ W/m}^2$  and PV system is generated power of  $0.074 \text{ MW}$ . During  $8-10 \text{ s}$ , the load demand is  $0.068 \text{ MW}$  which is supplied by the PV system fully and the remaining power ( $0.006 \text{ MW}$ ) of MG is supplied to the grid. For this period also power obtained from battery is nil and from  $0-10 \text{ s}$  since MG is operating in grid-tied mode, therefore DiG does not provide any power support.

The MG started operating in islanded mode at  $10 \text{ s}$  when grid gets disconnected from the MG. During islanding, according to the power management algorithm, if PV and battery cannot fulfill the load demand then DiG will be activated. From  $10-12 \text{ s}$ , the generation of PV system is  $0.085 \text{ MW}$  while the load demand is higher than PV generation i.e.  $0.097 \text{ MW}$ . As battery has enough power of  $0.012 \text{ MW}$  to fulfill the

remaining load demand, hence DiG remains inactive during this duration. After 12 s, solar irradiation was reduced to  $800 \text{ W/m}^2$  and load demand increased to 0.13 MW. During 12-14 s, the total generation (0.096 MW) from solar and battery (0.071 MW + 0.025 MW) was not sufficient to support the load demand. As a result, diesel generation turned on and supplied 0.034 MW power to fulfill the remaining load demand. Lastly, in between 14-16 s, PV generation was further reduced to 0.056 MW. However, load demand does not reduce much (0.122 MW) which compels DiG to continue power supply as PV and battery cannot fulfill the total load demand. After 16 s, it is assumed that due to some technical issue DiG has turned off. As a result, PMS checks whether PV and battery have sufficient power to fulfill the load demand or not. It is observed that the load demand is 0.115 MW whereas, the total supply from PV and battery is 0.065 MW. As a result, load management strategy has been turned on to ensure that critical load has uninterrupted power supply. It can be seen from Figure 4.10 that in between 16-18 s, the total power supplied to load is 0.065 MW among which 0.015 MW is supplied to critical load and the remaining 0.05 MW is supplied to non-critical load. This indicates that critical load is continuously getting power supply from 0-20 s. On contrary, even though the non-critical load demand is 0.1 MW during 16-18 s, however, it is receiving only 0.05 MW power.

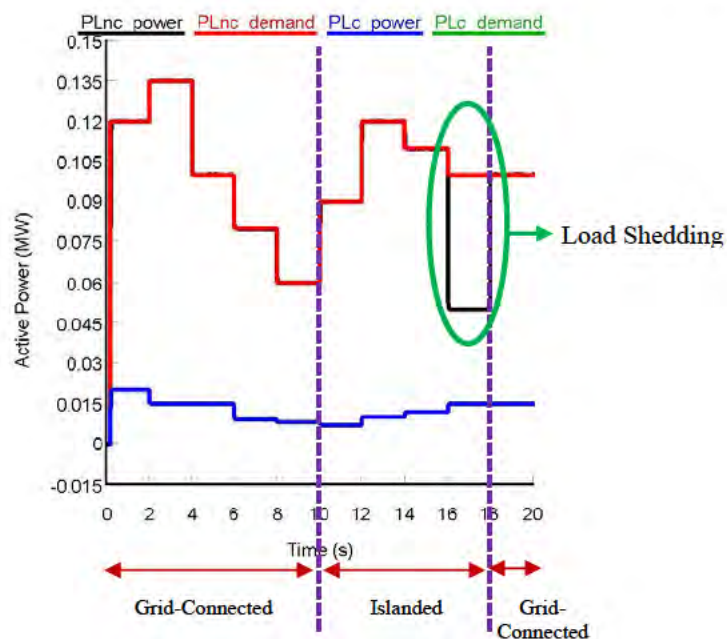
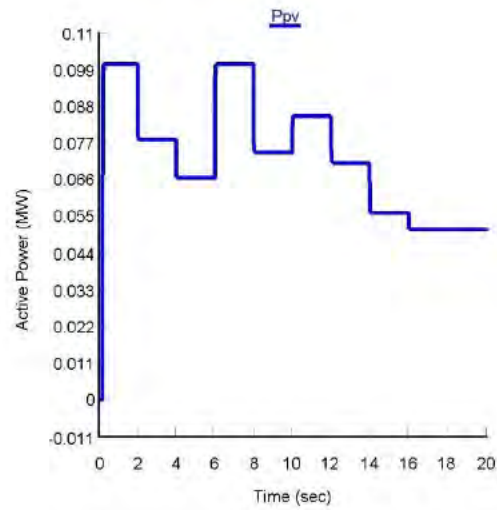


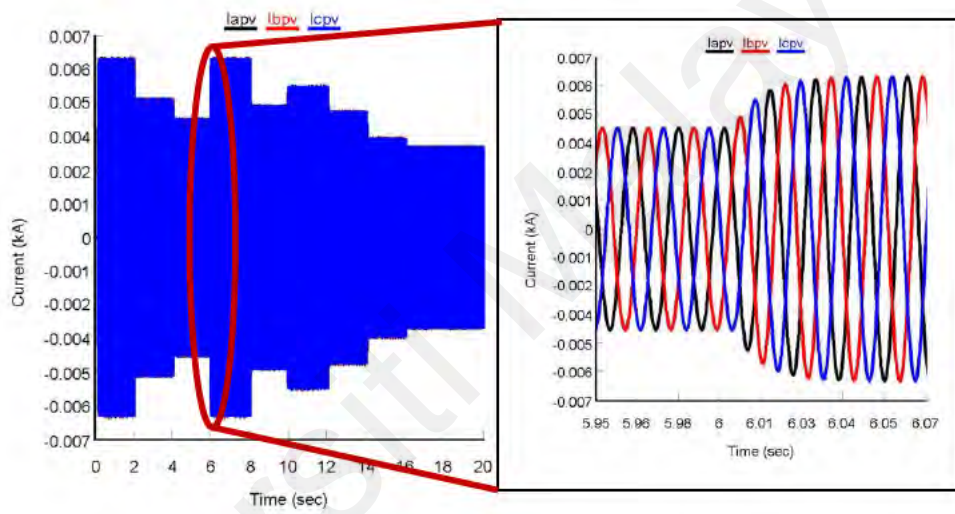
**Figure 4.10: Power supply to critical and non-critical loads in AC MG**

Finally, after 18 s MG again reconnected to the utility grid. During 18-20 s, the load demand and generation of PV remain same 16-18 s which are 0.115 MW and 0.051 MW. Since load demand is 0.064 MW more than PV generation hence battery gives full backup of 0.025 MW while the remaining 0.039 MW is provided by grid.

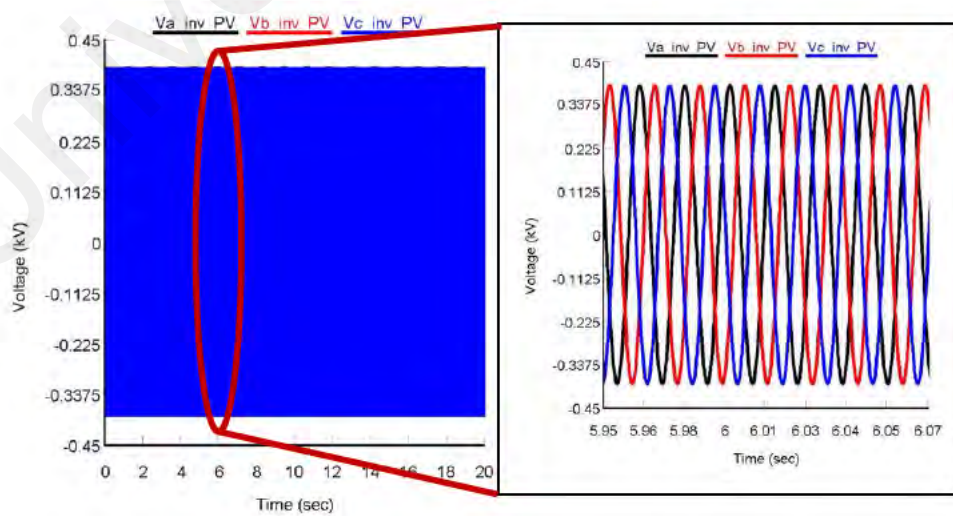
In Figure 4.11 and 4.12, the output power, current and voltages of PV and battery VSIs are presented, respectively. From Figure 4.11 (a), it is seen that the PV inverter is delivering precisely the power supplied by the PV and the ripple is also less. In addition, PV inverter output current also has less distortion which is shown in Figure 4.11 (b) because PVMT based DPC is implemented to control the PV inverter. Similarly, inverter output voltage also has negligible ripple and pure sine wave shape which are shown in Figure 11 (c). On the other hand, due to the use of PLL based CCT controller to control the battery inverter, the output power, current and voltage of battery inverter has high steady-state oscillations and distortions which are presented in Figure 4.12 (a), (b) and (c), respectively. The THD of PV and battery inverter output currents and voltages are depicted in Figure 4.13 (a), (b), (c) and (d), respectively. From the Figures, it is seen that the THD of PV inverter current is only 1.686 %, while battery inverter output current THD is 4.718 % which is higher compared to PV inverter current THD. In case of voltages, also battery voltage THD (2.592 %) is higher than PV voltage THD (1.44 %). The THDs are measured by considering four cycles (1.95 – 2.0167 s) of the currents and voltage waveforms as shown in zoomed portion of Figure 4.11 (b, c) and 4.12 (b, c). Finally, the corresponding grid power, current and voltage are presented in Figure 4.14 (a), (b) and (c), respectively. It can be observed that grid is delivering or absorbing power according to the requirement of MG and has no ripples in the power. Grid current and voltage are also sinusoidal in shape, with very little distortion and a frequency of 60 Hz.



(a)

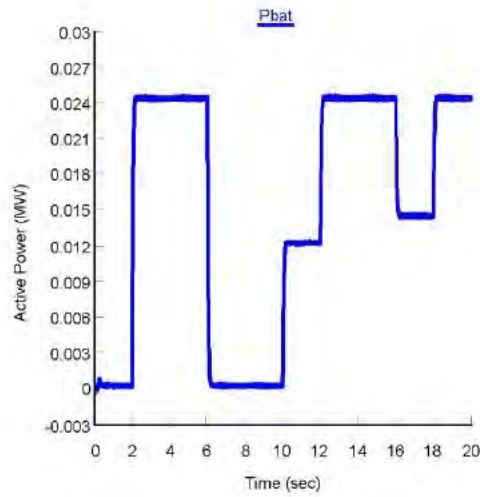


(b)

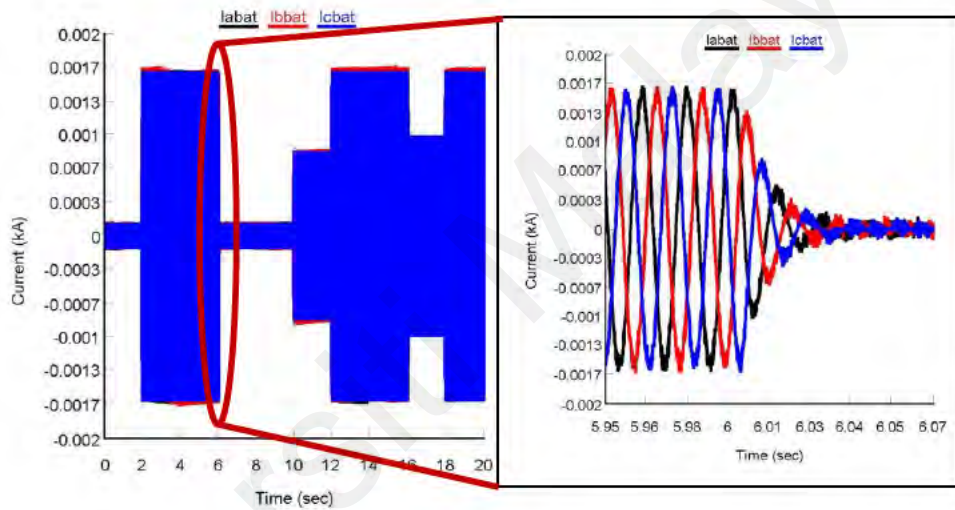


(c)

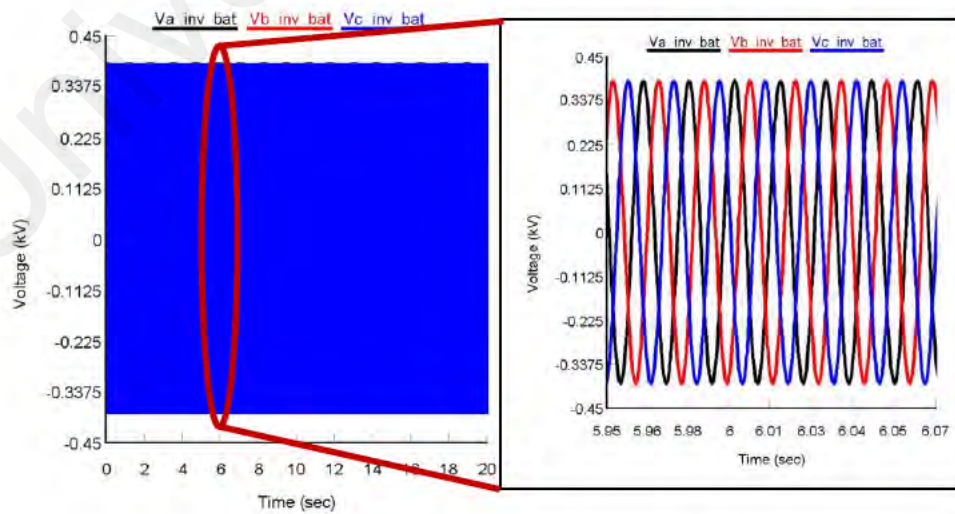
**Figure 4.11: During both load and solar irradiation changes PV inverter output (a) power, (b) current and (c) voltage**



(a)

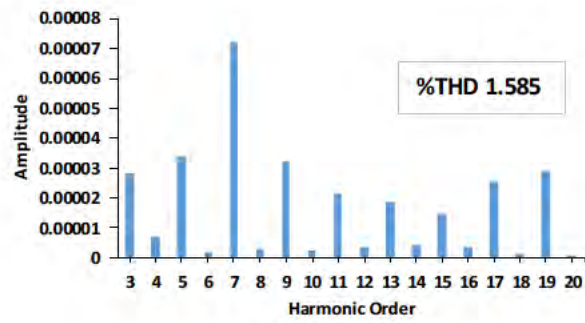


(b)

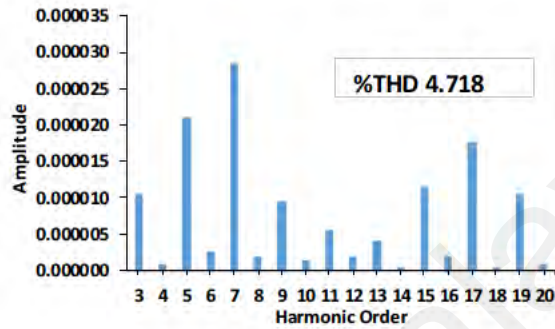


(c)

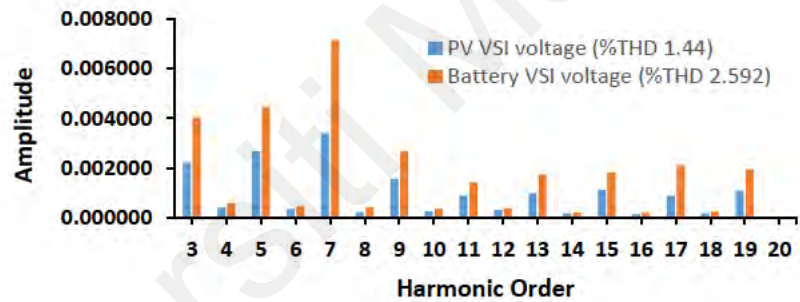
**Figure 4.12: During both load and solar irradiation changes battery inverter output (a) power, (b) current and (c) voltage**



(a)

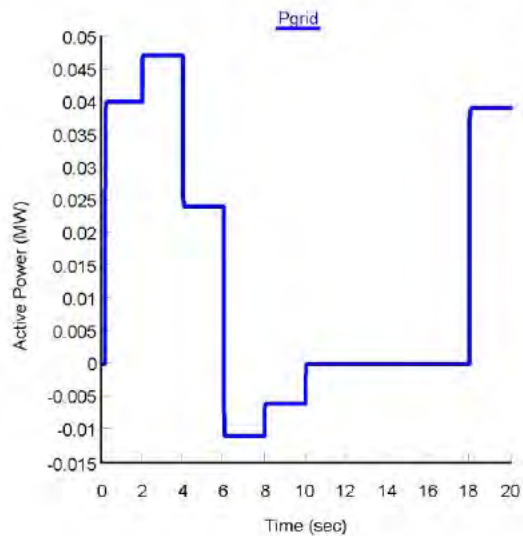


(b)

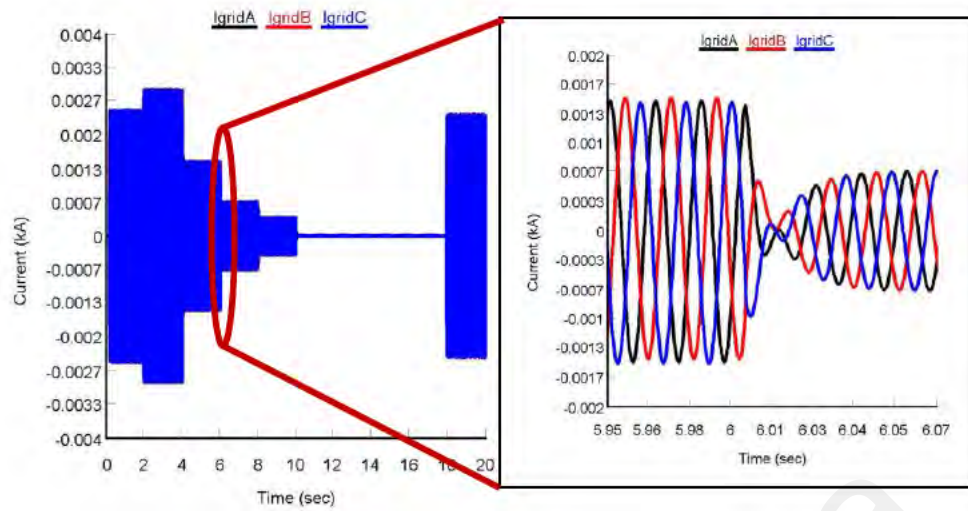


(c)

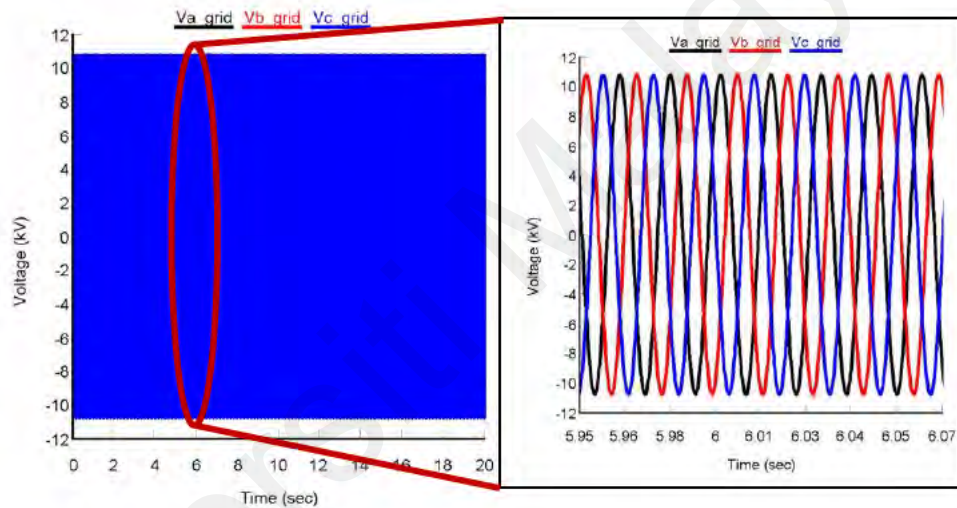
Figure 4.13: THD of (a) PV VSI output current, (b) Battery VSI output current and (c) PV & battery VSIs output voltage



(a)



(b)



(c)

**Figure 4.14: During both load and solar irradiation changes grid (a) power, (b) current and (c) voltage**

### 4.3.2 Hybrid Microgrid

In this section, the performance of the proposed real-time PMS is validated on a hybrid MG which is represented in Figure 3.2 by varying both load and solar irradiance. For hybrid MG, the interlinking VSI is controlled by FLDP method during grid-connected mode. However, droop control strategy explained in Chapter 3 is adapted to control the interlinking VSI during islanded mode. The power flow from different sources to the load in the hybrid MG is presented in Figure 4.15 and Table 4.2.

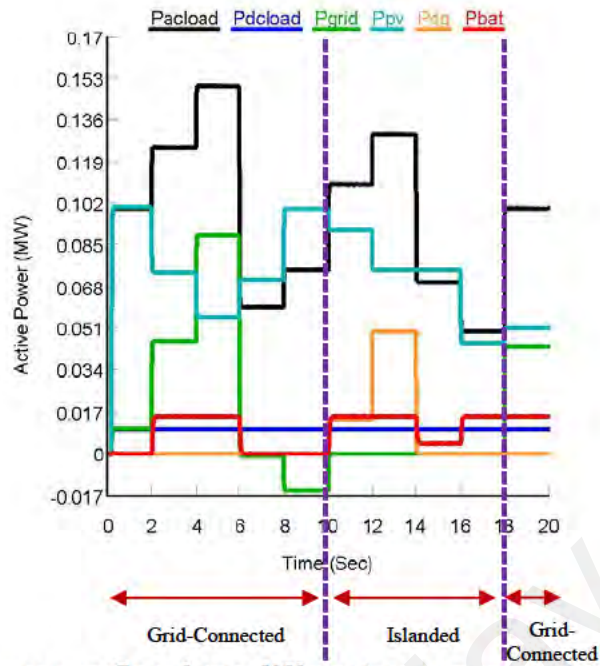


**Figure 4.15: Active power flow from different power sources to loads in hybrid MG**

**Table 4.2: Active power flow during both load and solar irradiation change in hybrid microgrid**

Duration (sec)	Variables		Load Power		Generation				
	Solar Irradiation (W/m <sup>2</sup> )	Load Demand (MW)		Variable AC load, P <sub>acload</sub> (MW)	DC load, P <sub>dcload</sub> (MW)	Solar Power, P <sub>pv</sub> (MW)	Grid Power, P <sub>grid</sub> (MW)	Battery Power, P <sub>bat</sub> (MW)	Diesel Generator Power P <sub>dg</sub> (MW)
		Variable AC load (MW)	DC load (MW)						
0-2	1000 (initial)	0.1	0.01	0.1	0.01	0.1	0.01	0	0
		<b>Total = 0.11</b>		<b>Total = 0.11</b>		<b>Total = 0.11</b>			
2-4	800	0.125	0.01	0.125	0.01	0.074	0.046	0.015	0
		<b>Total = 0.135</b>		<b>Total = 0.135</b>		<b>Total = 0.135</b>			
4-6	600	0.15	0.01	0.15	0.01	0.056	0.089	0.015	0
		<b>Total = 0.16</b>		<b>Total = 0.16</b>		<b>Total = 0.16</b>			
6-8	750	0.06	0.01	0.06	0.01	0.071	-0.001	0	0
		<b>Total = 0.07</b>		<b>Total = 0.07</b>		<b>Total = 0.07</b>			
8-10	1000	0.075	0.01	0.075	0.01	0.1	-0.015	0	0
		<b>Total = 0.085</b>		<b>Total = 0.085</b>		<b>Total = 0.085</b>			
10-12	950	0.11	0.01	0.11	0.01	0.091	0	0.015	0.014
		<b>Total = 0.12</b>		<b>Total = 0.12</b>		<b>Total = 0.12</b>			
12-14	820	0.13	0.01	0.13	0.01	0.075	0	0.015	0.05
		<b>Total = 0.14</b>		<b>Total = 0.14</b>		<b>Total = 0.14</b>			
14-16	820	0.07	0.01	0.07	0.01	0.075	0	0.005	0
		<b>Total = 0.08</b>		<b>Total = 0.08</b>		<b>Total = 0.08</b>			
16-18	500	0.1	0.01	0.05	0.01	0.045	0	0.015	0
		<b>Total = 0.115</b>		<b>Total = 0.06</b>		<b>Total = 0.06</b>			
18-20	550	0.1	0.01	0.1	0.01	0.051	0.044	0.015	0
		<b>Total = 0.11</b>		<b>Total = 0.11</b>		<b>Total = 0.11</b>			

Initially, variable load and solar irradiation are set to 0.1 MW and 1000 W/m<sup>2</sup>, respectively. Until 2 s the total load (variable AC + Fixed DC) demand of 0.11 MW was supplied by both solar and battery. After 2 s, the variable load demand changed from 0.1 MW to 0.125 MW while solar irradiation was also reduced to 800 W/m<sup>2</sup> from 1000 W/m<sup>2</sup>. As a result, PV system was providing power support of 0.074 MW and the remaining load demand is fulfilled by battery and grid. During 4 - 6 s, the load demand further increased (0.16 MW) and solar irradiation decreased (600 W/m<sup>2</sup>) which resulted in less power support from PV system while increasing the power consumption from grid and battery was providing the same power support. After 6 s, solar irradiation increased to 750 W/m<sup>2</sup> and in contrast, total load demand decreased to 0.07 MW. Since the total load demand is lesser than PV generation of 0.071 MW hence it is fully covered by PV system and the remaining 0.001 MW was supplied to grid. During 6 – 8 s, no power is consumed from the grid. Then, PV system has started full power generation as its irradiation level reached 1000 W/m<sup>2</sup> and load demand increased to 0.085 MW during 8-10s. At this period, PV was supporting the whole load demand since its generation reached 0.1 MW. After providing 0.085 MW power support to both the load, still 0.015 MW power is available in PV system, which is delivered to grid. After 10 s, grid goes off and hybrid MG enters islanding mode. As a result, DiG now comes to active mode to provide power back up to the hybrid MG if necessary. During 10-12 s, load demand again increased to 0.12 MW and PV generation decreased to 0.091 MW. Since PV generation is less than the load demand hence battery comes into operation and provides its full power support of 0.015 MW. However, still there is a lack of 0.014 MW power support to the load was observed which was provided by DiG. After 12 s, load increased further to 0.14 MW while PV generation reduced to 0.075 MW. During this period also DiG provided 0.05 MW power to the hybrid MG since PV and battery total power together was not sufficient to fulfill the load demand. After 14 s, the load demand reduced to 0.08 MW and PV generation

remained the same to 0.075 MW. As the load demand is below the power supported by PV and battery sources together, hence no power was drawn from the DiG. Similar to AC MG, in hybrid MG also DiG is assumed to be disconnected due to technical issues. As a result, PMS checks whether PV and battery have sufficient power to fulfill the load demand or not. It is observed that the load demand is 0.11 MW whereas, the total supply available from PV and battery is 0.06 MW. As a result, load management strategy has been turned on to ensure that critical loads have uninterrupted power supply. It can be seen that in between 16-18 s, the total power supplied to load is 0.06 MW among which 0.01 MW is supplied to critical DC load and the remaining 0.05 MW is supplied to AC load. This scenario is presented in Figure 4.16 from where it can be seen that critical DC load is continuously getting power supply from 0-20 s. On contrary, even though the AC load demand is 0.1 MW during 16-18 s, however, it is receiving only 0.05 MW power.

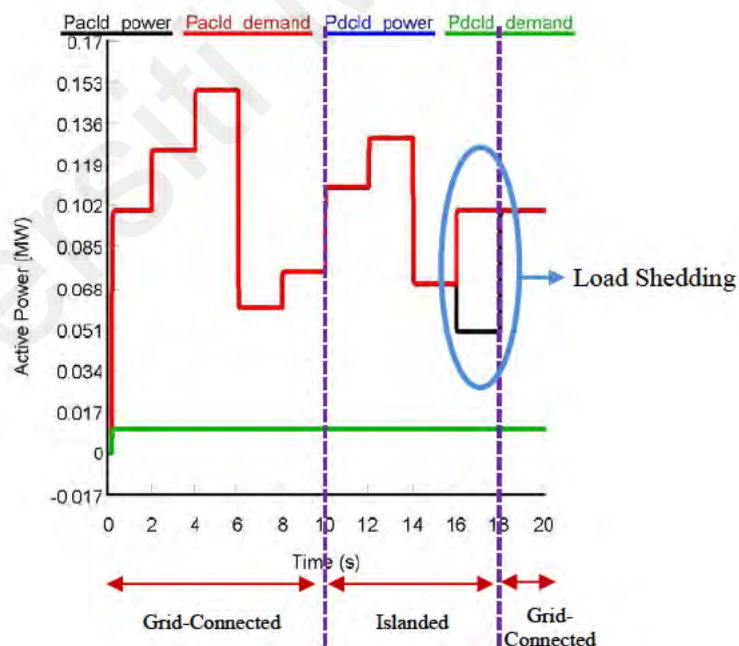
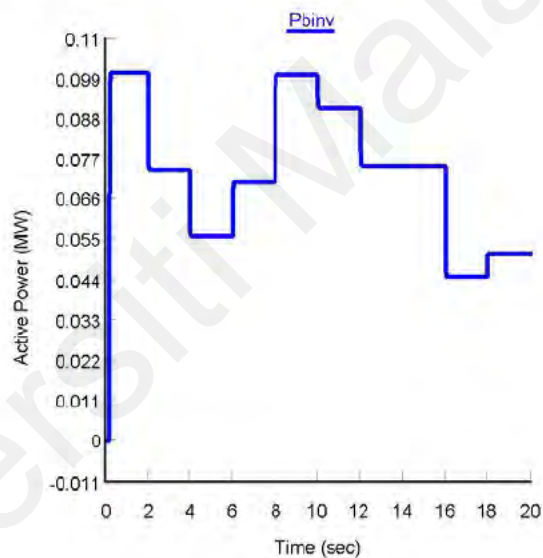


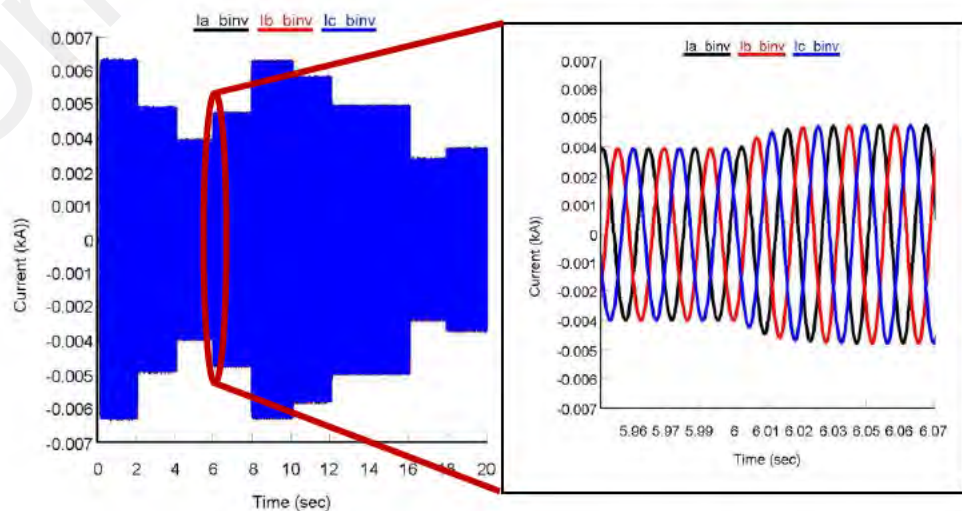
**Figure 4.16: Power supply to critical DC load and variable AC load in hybrid MG**

Finally, after 18 s MG again reconnected to the utility grid. During 18-20 s, the load demand remains the same as 16-18 s which are 0.11 MW whereas and generation of PV is increased to 0.051 MW. Since load demand is 0.059 MW more than PV generation hence battery gives full backup of 0.015 MW while the remaining 0.044 MW is provided by grid.

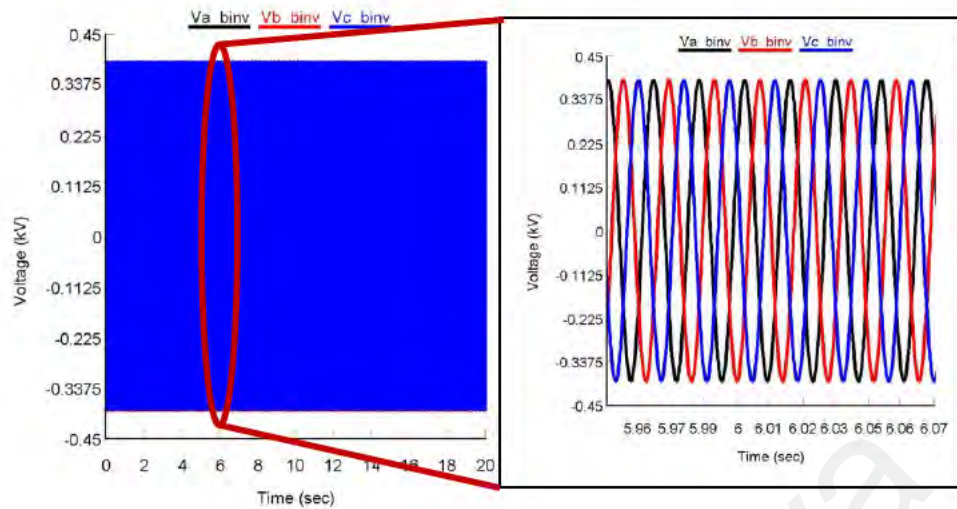
The VSI output power, current and voltage are depicted in Figure 4.17. From Figure 4.17 (a), it is seen that the inverter is delivering exactly the total power supplied by the PV & battery and the ripple is also less. Similarly, inverter output current and voltage also have negligible ripple and pure sine wave which are shown in Figure 4.17 (b) and (c).



(a)



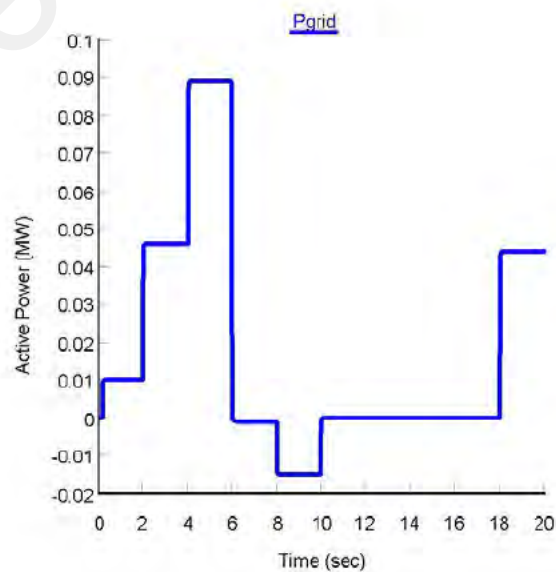
(b)



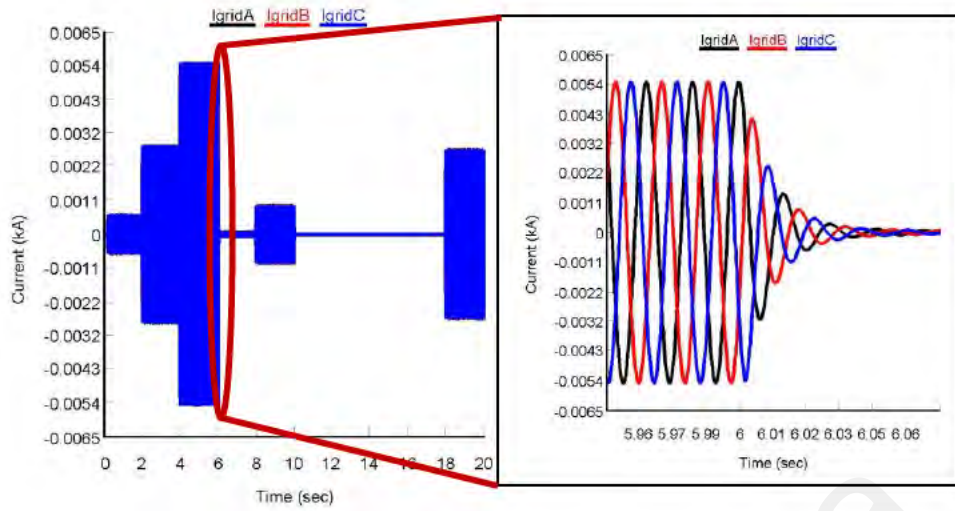
(c)

**Figure 4.17: During both load and solar irradiation changes BVSI output (a) power, (b) current and (c) voltage**

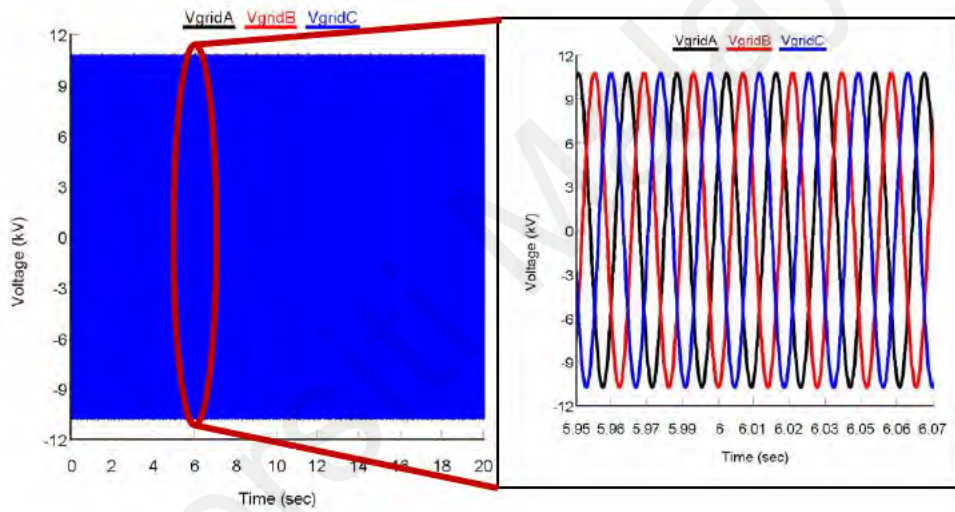
The corresponding grid power, current and voltage are presented in Figure 4.18 (a), (b) and (c), respectively. It can be observed that grid is delivering or absorbing power according to the requirement of MG and has no ripples in the power. Further, grid current and voltage are also sinusoidal in shape, have very small distortion and maintain 60 Hz frequency.



(a)

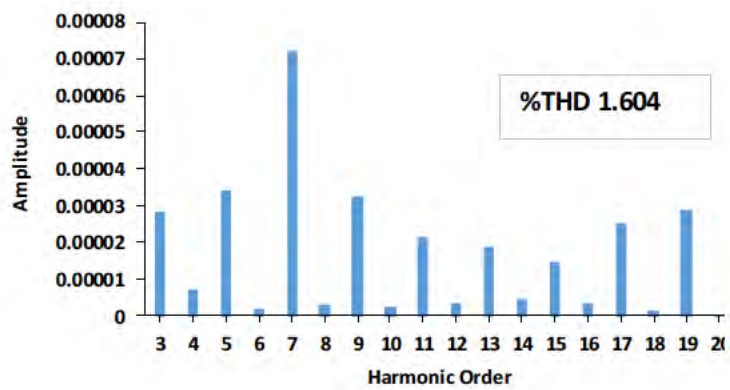


(b)

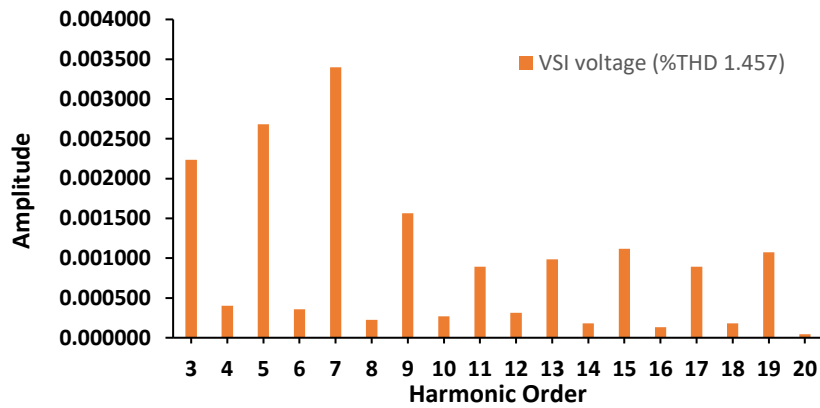


(c)

**Figure 4.18: During both load and solar irradiation change grid (a) power, (b) current and (c) voltage**



(a)

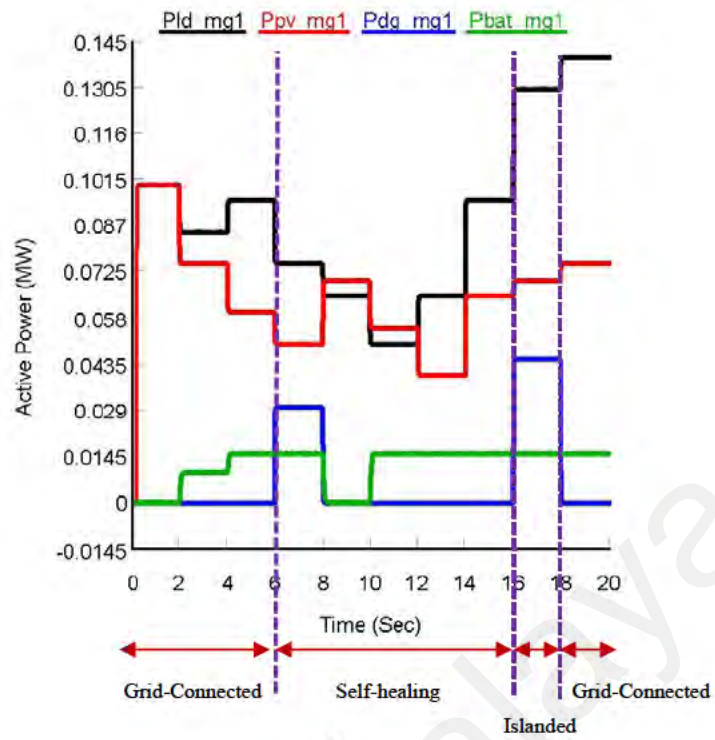


(b)

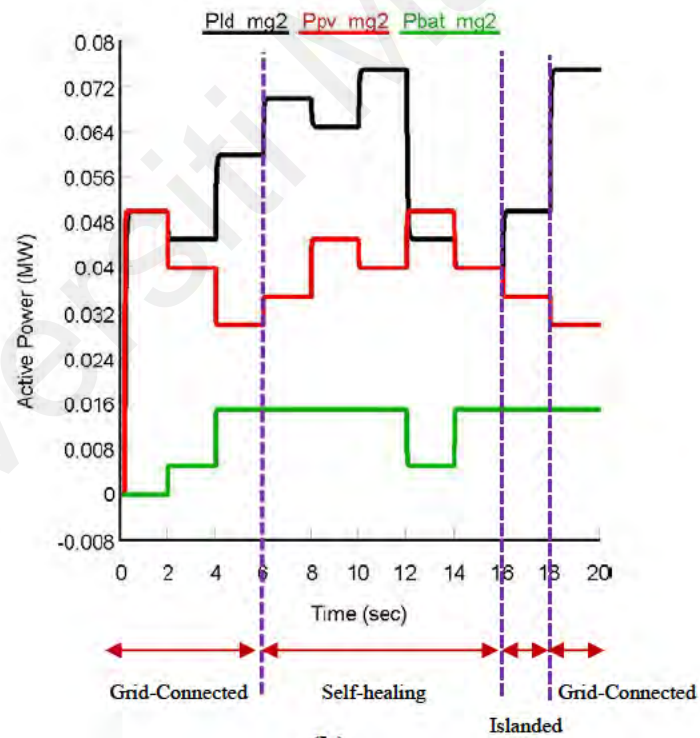
Figure 4.19: THD of BVSI output (a) current and (b) voltage

#### 4.4 Performance Analysis of the Proposed Intelligent Interconnection Method and Power Management Strategy for two MGs in Self-healing mode

In this section, the validation of the proposed IIM along with the PMS proposed for two MGs in self-healing mode is conducted on the testbeds shown in Figure 3.3 through a real-time simulation platform named RTDS. In Figure 4.20 and Table 4.3, the overall power flow between the DERs and loads of both MG1 and MG2 are presented. Initially, both MGs are operating in grid-connected mode as a single MG.



(a)



(b)

Figure 4.20: Power flow between the DERs and load for (a) MG1 and (b) MG2

**Table 4.3: Summary of power flow between the DERs and load for both MG1 and MG2 in self-healing mode**

Time (s)	Operating Mode	Grid (MW)	MG1				MG2				
			Generation			Load		Generation		Load	
			Solar power $P_{pvmg1}$ (MW)	Battery Power $P_{batmg1}$ (MW)	Diesel Generator power $P_{dgm1}$ (MW)	Load demand (MW)	Load power $P_{ldmg1}$ (MW)	Solar power $P_{pvmg2}$ (MW)	Battery power $P_{batmg2}$ (MW)	Load demand (MW)	Load Power $P_{ldmg2}$ (MW)
0-2	Grid-connected	0	0.1	0	0	0.1	0.1	0.05	0	0.05	0.05
			0.1					0.05			
2-4		0	0.075	0.01	0	0.085	0.085	0.04	0.005	0.045	0.045
			0.085					0.045			
4-6		0.035	0.06	0.015	0	0.095	0.095	0.03	0.015	0.06	0.06
			0.075					0.045			
6-8	Self-healing	0	0.05	0.015	0.03	0.075	0.075	0.035	0.015	0.07	0.07
			0.095					-0.02 (absorbed power by MG2)			
8-10		0	0.07	0	0	0.065	0.065	0.045	0.015	0.065	0.065
			0.07					-0.005 (absorbed power by MG2)			
			0.005 (supplied power from MG1)								
10-12		0	0.055	0.015	0	0.05	0.05	0.04	0.015	0.075	0.075
			0.07					-0.02 (absorbed power by MG2)			
			0.02 (supplied power from MG1)								
12-14		0	0.04	0.015	0	0.065	0.065	0.05	0.005	0.045	0.045
			0.055					-0.01 (absorbed power by MG1)			
			0.01 (supplied power from MG2)								
14-16		0	0.065	0.015	0	0.095	0.095	0.04	0.015	0.04	0.04
	0.08			-0.015 (absorbed power by MG1)							
	0.015 (supplied power from MG2)										
16-18	Islanded	0	0.07	0.015	0.045	0.13	0.13	0.035	0.015	0.07	0.05
			0.13					0.05			
18-20	Grid-connected	0.08	0.075	0.015	0	0.14	0.14	0.03	0.015	0.075	0.075
			0.09					0.045			

Figure 4.20, the power of PV, battery, DiG and load of MG1 is denoted by  $P_{pv\_mg1}$ ,  $P_{bat\_mg1}$ ,  $P_{dg\_mg1}$  and  $P_{ld\_mg1}$ , respectively where  $P_{pv\_mg2}$ ,  $P_{bat\_mg2}$  and  $P_{ld\_mg2}$  are used for denoting power of PV, battery and load of MG2, respectively. According to the Figure, during 0-6 s both the MGs are operating in grid-connected mode. During grid-connected mode, it is seen that from 0-2 s the power generated by PV system and load demand of

MG1 is equal which 0.1 MW. As a result, no power is drawn from battery and DiG. For the same period, the PV system of MG2 also generates the same amount of power required by the load which is 0.05 MW and due to that the power drawn from the battery remains null. Both the MGs PV systems generated less power 0.075 MW and 0.04 MW, respectively during 2-4 s due to decrease in solar irradiation. At this period, as the PV power generation reduced, load demands of both MGs also reduced. As a result, according to grid-connected MG PMS, batteries of both MGs come into operation to fulfill the remaining load demand which supply 0.015 MW and 0.005 MW, respectively. During 0-4 s, since PV and battery of both MGs can meet the load demand, hence, no power was drawn from the grid. During 4-6 s, the generation of PV systems of both the MGs further decreased to 0.06 MW and 0.03 MW, respectively. However, load demands increased during this period. To satisfy the load demands of MG1 and MG2 at this period, the battery powers are not enough, since the maximum capacities of both the batteries are 150 kWh. Therefore, the remaining load powers are acquired from grid which is in total 0.035 MW.

At 6 s grid goes off, due to which the operation of IIM is initiated. The IIM is checked for whether any of the MGs required power support from other MG or not, and if required power support whether another MG has extra power generation capacity to support the load demand of the needy MG or not. From Table 4.3, it can be seen that MG2 required power support since its generation (0.05 MW) is less than load demand (0.07 MW). At the same time, it is found that MG1 has extra generation capacity due to the presence of DiG. As a result, IIM sends a turn on signal to the BRK 2 switch and the two MGs by interconnecting enter self-healing mode. During self-healing mode from 6-8 s, the total generated power of MG1 is 0.065 MW (PV+battery) and load demand is 0.075 MW. Therefore, the remaining load demand (0.01 MW) of MG1 is fulfilled by DiG. On the other hand, the total power generated by MG2 is 0.05 MW (PV+battery) and load demand

is 0.07 MW. It is observed that there is a scarcity of 0.02 MW power to the load in MG2 and it has no additional power sources to provide this extra power. However, due to the interconnection, the remaining load demand (0.02 MW) of MG2 is fulfilled by DiG of MG1. Therefore, the total power is supplied by the DiG is observed 0.03 MW which is shown in Figure 4.20. In addition, it is also seen that during 6-8 s, 0.02 MW power is supplied from MG1 to MG2. Further, in between 8-10 s also the self-healing mode of the MGs is continued, and the same scenario is observed like the period of 6-8 s. During this period load demand (0.065 MW) of MG2 is higher with respect to the generation (0.06 MW) due to which 0.005 MW power is delivered from MG1 to MG2. However, at this time the load demand of MG2 is fulfilled by only PV system of MG1, since MG1 PV generation (0.07) is higher than the load demand (0.065). Therefore, no power was drawn from battery and DiG during 8-10 s. In between 10-12 s, again the load demand (0.075 MW) of MG2 is higher than the generation (0.055). On the other hand, MG1 PV generation (0.055 MW) is higher than load demand (0.05 MW). Therefore, the remaining power (0.005 MW) from MG1 PV system and battery power (0.015 MW) is sufficient to fulfill the rest of the load demand (0.02 MW) of MG2. During this period no power is drawn from DiG.

During 12-14 s, power supply of PV & battery MG2 (0.055 MW) has found more than its load demand (0.045). On contrary, MG1 load demand (0.065 MW) has found more than its PV generation (0.04 MW). There is a deficiency of 0.025 MW power is observed in MG1 which can be fulfilled by battery and DiG easily. However, it is found that after getting back up from battery power (0.015 MW), the remaining load demand (0.01 MW) of MG1 can be still fulfilled by the additional power of MG2 (0.01 MW). Therefore, MG2 delivers 0.01 MW power to MG1 and DiG of MG1 does not need to operate. After 14 s, PV generation of MG2 and load demand have become same (0.04 MW). Hence, MG2 does not require any power support. However, in MG1, the load demand (0.095 MW) has

found 0.03 MW more than the PV generation (0.065) and battery can give a maximum backup of 0.015 MW. As a result, there is still 0.015 MW power deficiency is observed in MG1. Therefore, according to the PMS algorithm, before starting the DiG, it checks whether the battery backup power of MG2 can fulfill the remaining load demand of MG1 or not. PMS found that MG2 battery can provide 0.015 MW power support to MG1 which resulted in the transfer of 0.015 MW power from MG2 to MG1 without turning on the DiG of MG1.

At 16 s, it is found that the load demands of both MG1 and MG2 are increased to 0.13 MW and 0.07 MW, respectively. However, MGs' total power generation is not sufficient to support each other during 16-18 s. Because MG2 required additional power support of 0.02 MW whereas MG1 can support only 0.005 MW. As a result, the according to proposed interconnection framework the MGs cannot operate in self-healing mode further and IIM sends a turn off signal to BRK2 switch to open up the interconnection between MG1 and MG2. Further, since grid is not available yet, therefore, the MGs operate autonomously in islanded mode. In this mode, MG1 generation (0.13 MW) can fulfill its total load demand (0.13 MW) because it has a DiG. However, MG2 cannot support its total load demand because its total supply from PV and battery (0.05 MW) cannot fulfill its load demand of 0.07 MW. As a result, the load shedding strategy turned on by ensuring that critical load gets uninterruptible power supply.

Finally, after 18 s grid reconnected again and both the MGs start getting power support from the grid. For MG1, there is a need of 0.05 MW from the grid after fulfilling its load demand from PV and battery (0.09 MW). Similarly, MG2 also absorbs 0.03 MW of power from grid to support its total load demand of 0.075 MW.

The power flow between the two MGs at the point of interconnection (POI) along with the grid power is presented in Figure 4.21. From Figure 4.21, it is seen that during grid-connected mode till 6 s there is no power transfer in between the two MGs. However, after 6 s during self-healing mode, power is shared between MG1 and MG2 till 16 s. From 6-12 s, power is transferred from MG1 to MG2 and from 12-16 s power is transferred from MG2 to MG1. Since MG1 supplied power to MG2 from 6-12 s, hence, the power flow is positive for MG1 while due to absorption of power the power flow of MG2 is shown negative and for 12-14 s, the opposite scenario is observed. The voltage and corresponding current waveforms at POI for both the MGs are presented in Figure 4.22 (a), (b) and (c), respectively. From the zoomed portion of the voltage and current, it is observed that the current of MG1 is in phase with POI voltage while the MG2 current is out of phase. The reason is MG1 is delivering power and MG2 is absorbing power. Further, both MGs currents and POI voltage is sinusoidal in shape and maintain a frequency of 60 Hz.

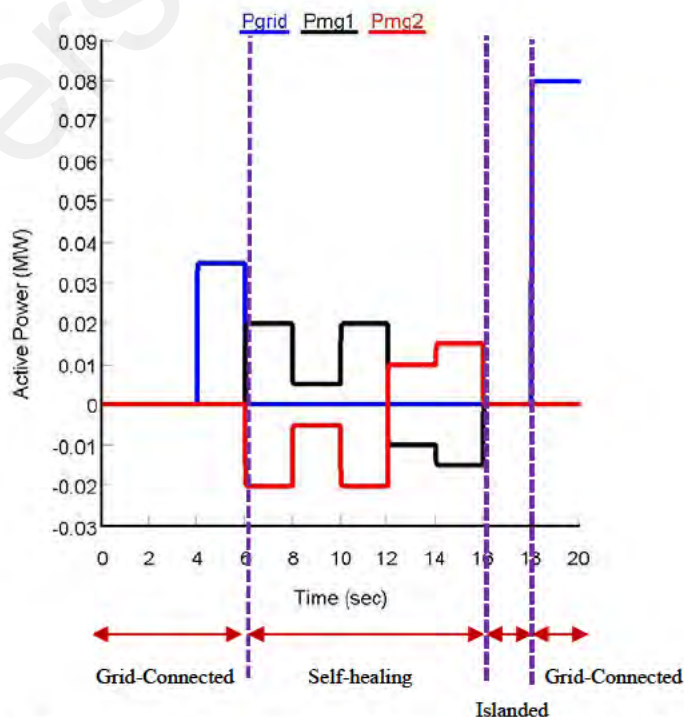
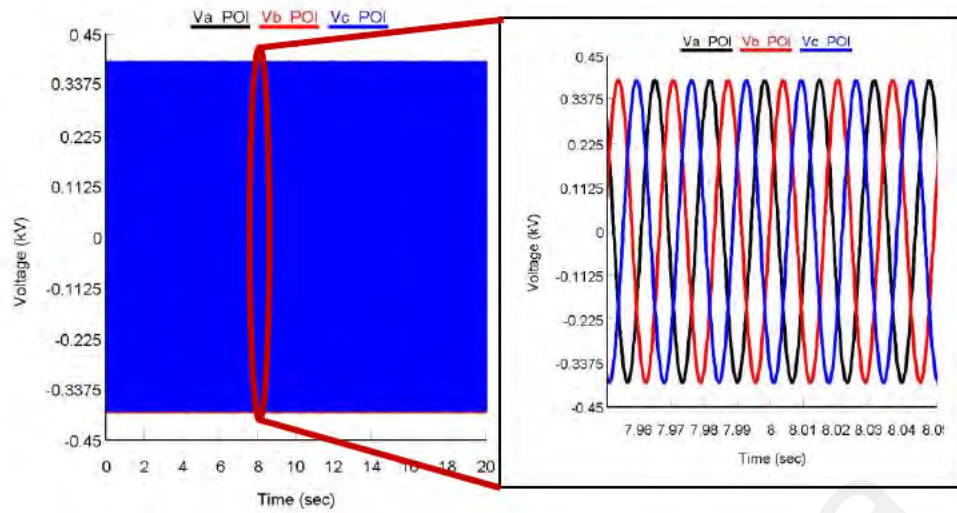
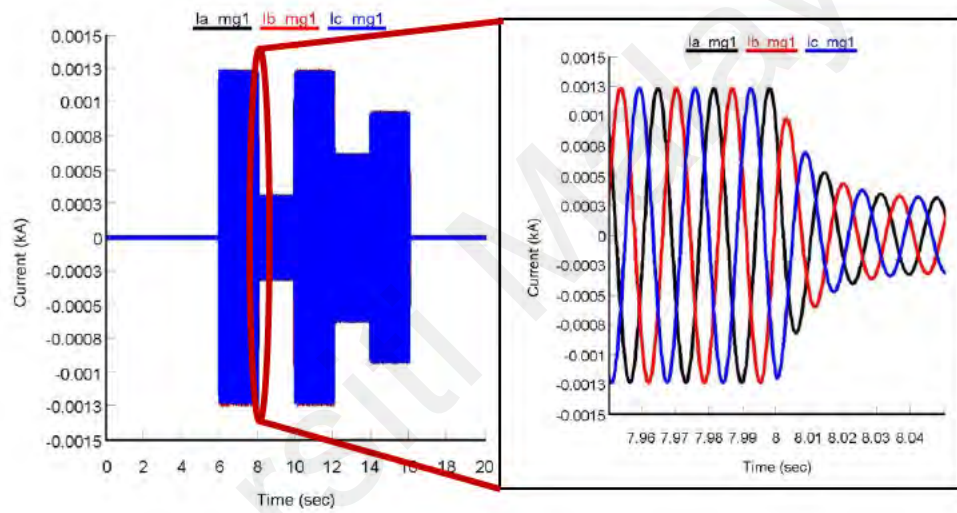


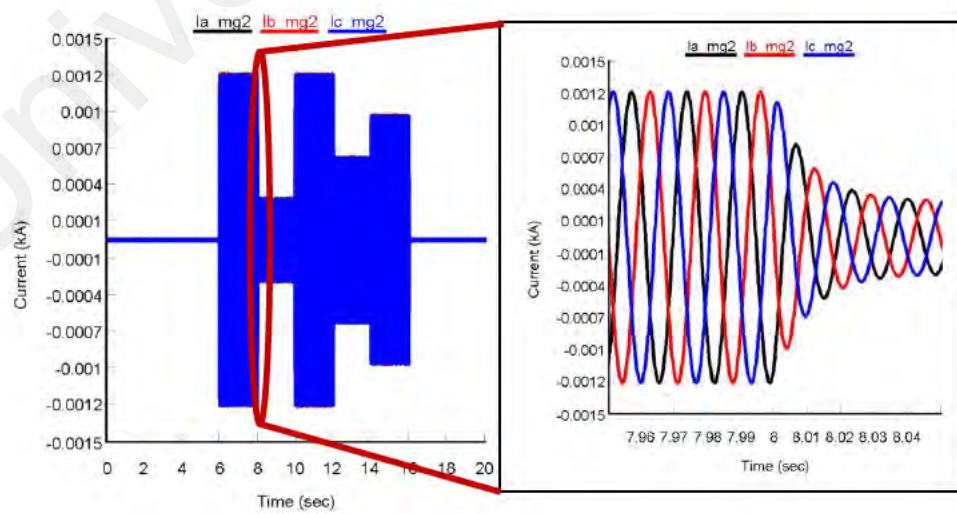
**Figure 4.21: Power flow between MG1 and MG2 at POI**



(a)



(b)

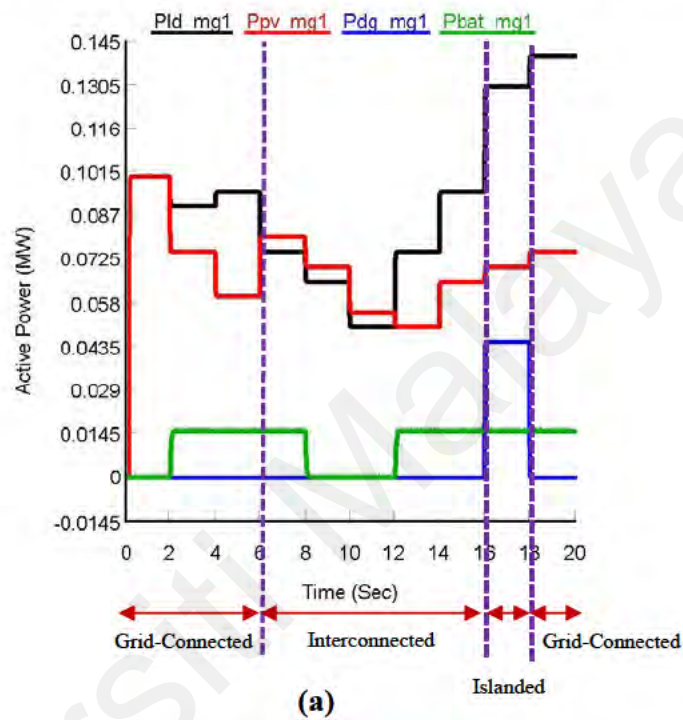


(c)

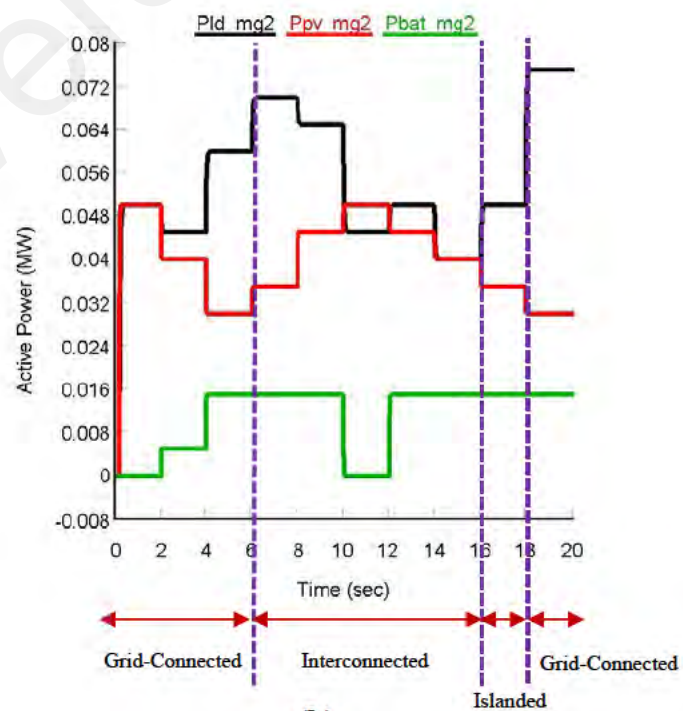
**Figure 4.22: During self-healing mode at POI (a) voltage, (b) MG1 current and (c) MG2 current**

#### 4.5 Performance Analysis of the Proposed Intelligent Interconnection Method and Power Management Strategy for two MGs in Interconnected mode

In this section, the validation of the proposed IIM along with the PMS proposed for two MGs in interconnected mode on the testbed shown in Figure 3.3 through RTDS. In Figure 4.23 and Table 4.4, the overall power flow of both MG1 and MG2 are presented.



(a)



(b)

Figure 4.23: Power flow between the DERs and load for (a) MG1 and (b) MG2

**Table 4.4: Summary of power flow between the DERs and load for both MG1 and MG2 in interconnected mode**

Time (s)	Operating Mode	Grid (MW)	MG1				MG2				
			Generation			Load		Generation		Load	
			Solar power $P_{pvmg1}$ (MW)	Battery Power $P_{batmg1}$ (MW)	Diesel Generator power $P_{dgm1}$ (MW)	Load demand (MW)	Load power $P_{ldmg1}$ (MW)	Solar power $P_{pvmg2}$ (MW)	Battery power $P_{batmg2}$ (MW)	Load demand (MW)	Load Power $P_{ldmg2}$ (MW)
0-2	Grid-connected	0	0.1	0	0	0.1	0.1	0.05	0	0.05	0.05
			0.1					0.05			
2-4		0	0.075	0.015	0	0.09	0.09	0.04	0.005	0.045	0.045
			0.09					0.045			
4-6		0.035	0.06	0.015	0	0.095	0.095	0.03	0.015	0.06	0.06
			0.075					0.045			
6-8	0	0.08	0.015	0	0.075	0.075	0.035	0.015	0.07	0.07	
		0.095					0.05				
			<b>0.02 (supplied power from MG1)</b>				<b>-0.02 (absorbed power by MG2)</b>				
8-10	0	0.07	0	0	0.065	0.065	0.045	0.015	0.065	0.065	
		0.07					0.06				
			<b>0.005 (supplied power from MG1)</b>				<b>-0.005 (absorbed power by MG2)</b>				
10-12	-0.01	0.055	0	0	0.05	0.05	0.05	0	0.045	0.045	
		0.055					0.05				
			<b>0.0 (supplied or absorbed power by MG1)</b>				<b>0.0 (supplied or absorbed power by MG2)</b>				
12-14	0	0.05	0.015	0	0.075	0.075	0.045	0.015	0.05	0.05	
		0.065					0.06				
			<b>-0.01 (absorbed power by MG1)</b>				<b>0.01 (supplied power from MG2)</b>				
14-16	0	0.065	0.015	0	0.095	0.095	0.04	0.015	0.04	0.04	
		0.08					0.055				
			<b>-0.015 (absorbed power by MG1)</b>				<b>0.015 (supplied power from MG2)</b>				
16-18	Islanded	0	0.07	0.015	0.045	0.13	0.13	0.035	0.015	0.07	0.05
			0.13					0.05			
18-20	Grid-connected	0.08	0.075	0.015	0	0.14	0.14	0.03	0.015	0.075	0.075
			0.09					0.045			

Figure 4.23, the power of PV, battery, DiG and load of MG1 is denoted by  $P_{pv\_mg1}$ ,  $P_{bat\_mg1}$ ,  $P_{dg\_mg1}$  and  $P_{ld\_mg1}$ , respectively where  $P_{pv\_mg2}$ ,  $P_{bat\_mg2}$  and  $P_{ld\_mg2}$  are used for denoting power of PV, battery and load of MG2, respectively. According to the Figure, during 0-6 s both the MGs are operating in grid-connected mode. During grid-connected mode, it is seen that from 0-2 s the power generated by PV system and load demand of

MG1 is equal which 0.1 MW. As a result, no power is drawn from battery and DiG. For the same period, the PV system of MG2 also generates the same amount of power required by the load which is 0.05 MW and due to that the power drawn from the battery and grid remain null for MG2. Both the MGs PV systems generated less power 0.075 MW and 0.04 MW, respectively during 2-4 s due to a decrease in solar irradiation. At this period, as the PV power generation is reduced, load demands of both MG 1 and MG2 are also reduced to 0.09 MW and 0.045 MW, respectively. As a result, according to grid-connected MG PMS, batteries of both MGs come into operation to fulfill the remaining load demand which supply 0.015 MW and 0.005 MW, respectively. During 0-4 s, since PV and battery of both MGs are able to meet the load demand no power is drawn from the grid. During 4-6 s, the PV generation of both the MGs further decreased to 0.06 MW and 0.03 MW, respectively. However, load demands have increased during this period. To satisfy the load demands of the MGs at this period, battery powers are not enough, since the maximum capacities of both the batteries are 150 kWh. Therefore, the remaining load powers are fulfilled by grid (0.035 MW).

The operation of IIM is initiated after 6 s, as it is found that two MGs have sufficient power to support each other without taking support from grid. However, during interconnected mode since MGs are still connected to the grid if there is any additional power generation from PVs, then that power will be supplied to grid. From Table 4.4, it can be seen that MG2 required power support from grid since its total supply from PV & battery (0.05 MW) is less than load demand (0.07 MW). At the same time, it is found that MG1 has extra generation capacity as its supply capacity from PV and battery (0.095 MW) is more than its load demand (0.075 MW). As a result, IIM sends a turn on signal to the BRK 2 switch and the two MGs by interconnecting enter interconnected mode. During interconnected mode from 6-8 s, the total generated power of MG1 is 0.095 MW (PV+battery) and load demand is 0.075 MW. On the other hand, the total power generated

by MG2 is 0.05 MW (PV+battery) and load demand is 0.07 MW. It is observed that there is a scarcity of 0.02 MW power to the load in MG2 and it has no additional power sources to provide this extra power. However, due to the interconnection, the remaining load demand (0.02 MW) of MG2 is fulfilled by MG1. Therefore, during 6-8 s, 0.02 MW power is supplied from MG1 to MG2. Further, in between 8-10 s also the interconnected mode of the MGs is continued, and almost the same scenario is observed like the period of 6-8 s. During this period load demand (0.065 MW) of MG2 is higher than the generation (0.06 MW) due to which MG2 requires power support of 0.005 MW. On the other hand, MG1 PV generation (0.07) is found 0.005 MW higher than the load demand (0.065) which is sufficient to support the remaining load demand of MG2. Therefore, 0.005 MW power is supplied from MG1 to MG2 during 8-10 s and now power is drawn from the battery of MG1. In between 10-12 s, the load demands (0.05 MW & 0.045 MW) of MG1 and MG2 are found lesser than their PV generations (0.055 MW & 0.045 MW). As a result, it can be seen that both the MGs do not need any power support from each other, and they have an additional power generation of 0.01 MW. Therefore, this remaining power (0.01 MW) from the MGs is supplied to the grid.

During 12-14 s, power supply of PV & battery of MG2 (0.06 MW) has found more than its load demand (0.05) which means MG2 has 0.01 MW additional power supply capacity. On contrary, MG1 load demand (0.075 MW) has been found less than its PV generation (0.05 MW). There is a deficiency of 0.025 MW power is observed in MG1 which cannot be fulfilled by battery backup. It is found that after getting back up from battery power (0.015 MW), the remaining load demand (0.01 MW) of MG1 can be fulfilled by the additional power of MG2 (0.01 MW). Therefore, MG2 delivers 0.01 MW power to MG1. After 14 s, PV generation of MG2 and load demand have become the same (0.04 MW). Hence, MG2 does not require any power support. However, in MG1, the load demand (0.095 MW) has found 0.03 MW more than the PV generation (0.065

MW) and battery can give a maximum backup of 0.015 MW. As a result, there is still 0.015 MW power deficiency is observed in MG1. Therefore, according to the PMS algorithm, it checks whether the battery power of MG2 can fulfill the remaining load demand of MG1 or not. PMS found that MG2 battery can provide 0.015 MW power support to MG1 which resulted in the transfer of 0.015 MW power from MG2 to MG1.

Similar to self-healing mode, in interconnected mode also at 16 s, the load demands of both MG1 and MG2 are increased to 0.13 MW and 0.07 MW, respectively. However, both the MGs' total power generation is not sufficient to support each other during 16-18 s. Because MG2 required additional power support of 0.02 MW whereas MG1 can support only 0.005 MW. As a result, according to proposed interconnection framework the MGs cannot operate in interconnected mode any longer and IIM sends a turn off signal to BRK2 switch to discontinue the interconnection between MG1 and MG2. However, at the same time, grid also gets disconnected. Therefore, the MGs operate autonomously in islanded mode. In this mode, MG1 generation (0.13 MW) can fulfill its total load demand (0.13 MW) because it has a DiG. However, MG2 cannot support its total load demand because its total supply from PV and battery (0.05 MW) cannot fulfill its load demand of 0.07 MW. As a result, load management strategy turned on by ensuring that critical load gets uninterruptible power supply.

Finally, the grid reconnected back after 18 s and both the MGs start getting power support from the grid. For MG1, there is a need of 0.05 MW from the grid after fulfilling its load demand from PV and battery (0.09 MW). Similarly, MG2 also consumes 0.03 MW of power from the grid to support its total load demand of 0.075 MW.

In Figure 4.24, the power flow between the two MGs at POI along with the grid power is presented. From Figure 4.24, it is seen that during grid-connected mode till 6 s there is no power transfer in between the two MGs. However, after 6 s during interconnected mode, power is transferred from MG1 to MG2 from 6-10 s and from 12-16 s power is transferred from MG2 to MG1. In between 10-12 s, even though the MGs are in interconnected mode, however, since they have surplus PV generation, no power is transferred between them. During 10-12 s, the surplus generation of the MGs is supplied to the grid. Since MG1 supplied power to MG2 from 6-12 s, hence, the power flow is positive for MG1 while due to absorption of power the power flow of MG2 is shown negative and the opposite scenario is observed for 12-16 s. In Figure 4.25, the voltage and corresponding current waveforms for both the MGs are presented. From the zoomed portion of the voltage and current, it is observed that the current of MG1 is in phase with POI voltage while the MG2 current is out of phase. The reason is MG1 is delivering power and MG2 is absorbing power. Further, both MGs currents and POI voltage is sinusoidal in shape and maintain a frequency of 60 Hz.

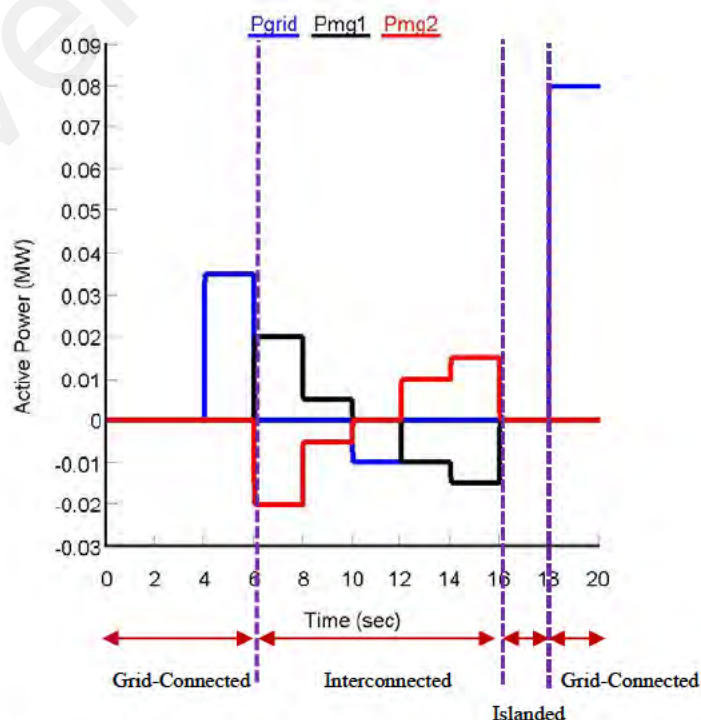
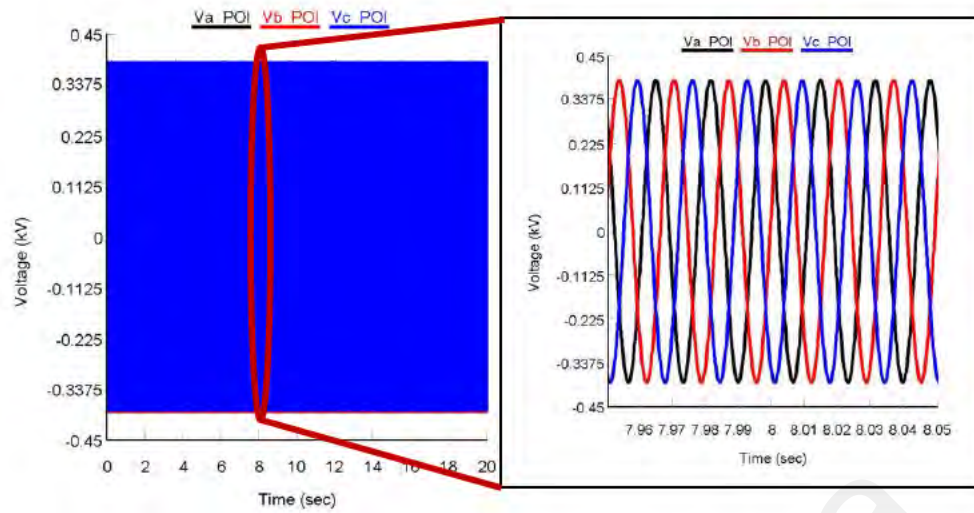
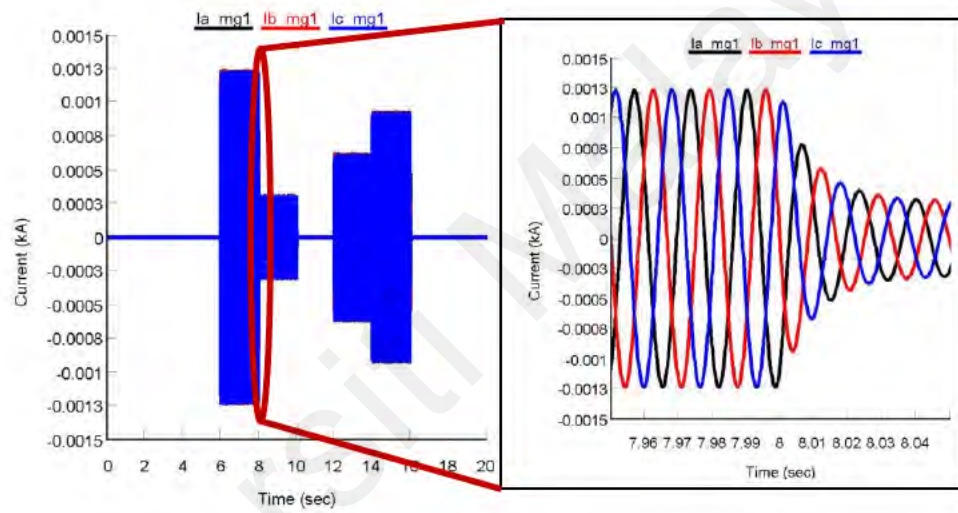


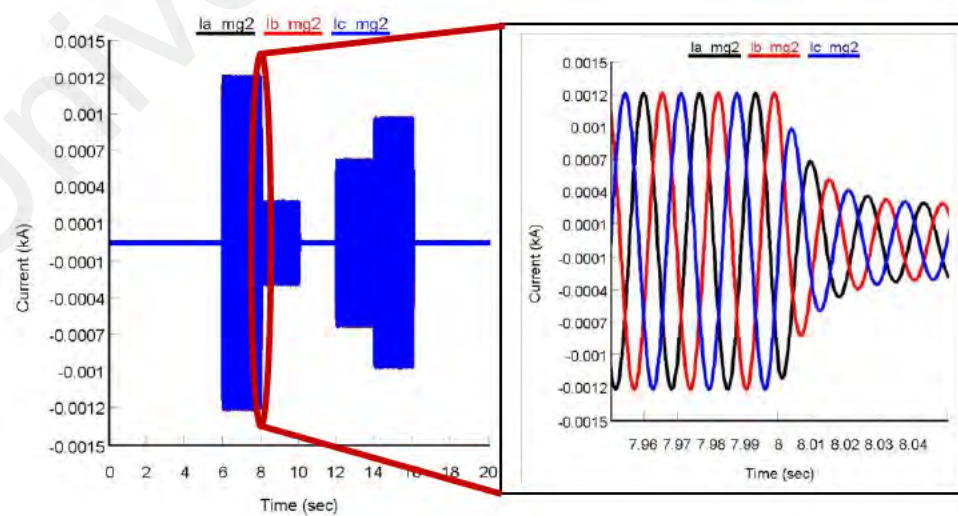
**Figure 4.24: Power flow between MG1 and MG2 at POI**



(a)



(b)

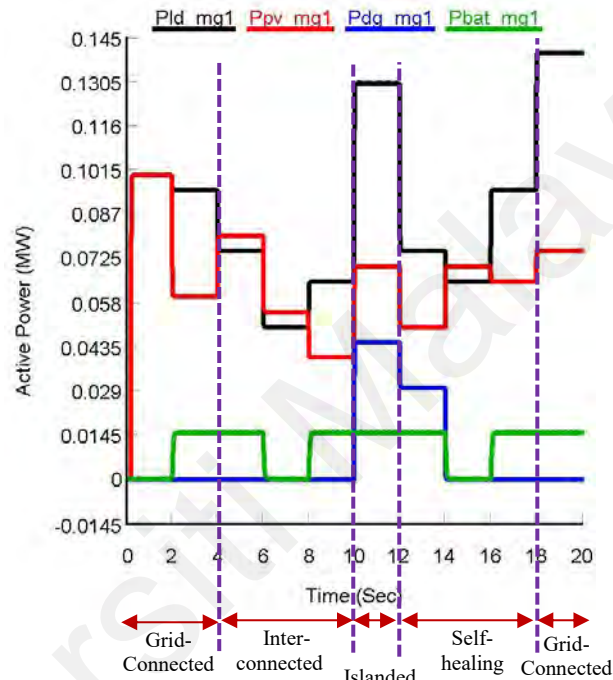


(c)

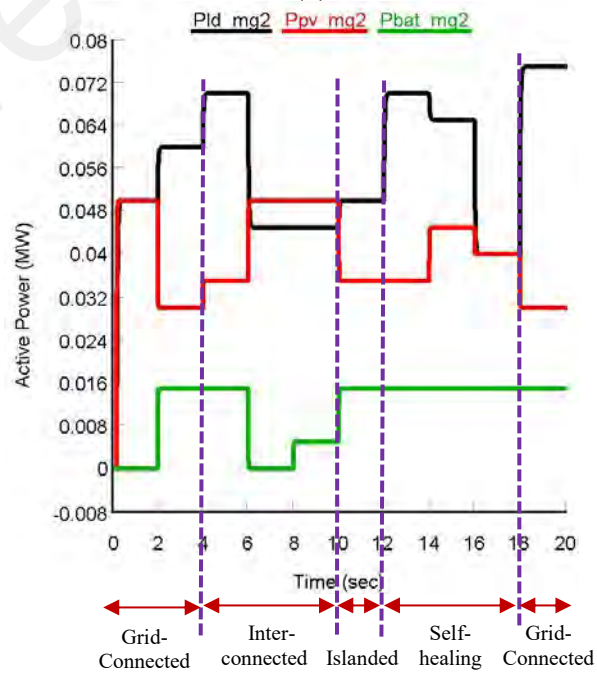
**Figure 4.25: During interconnected mode at POI (a) voltage, (b) MG1 current and (c) MG2 current**

#### 4.6 Performance Analysis of the Proposed Multi-Layer Control Strategy for Two Interconnected MGs

The validation of the proposed MLCS for two interconnected MGs shown in Figure 3.3 is conducted for four different modes of MGs operation (grid-connected, islanded, self-healing and interconnected). After implementing the MLCS, the overall power flow of both MG1 and MG2 are presented in Figure 4.26 and Table 4.5.



(a)



(b)

Figure 4.26: Power flow between the DERs and load for (a) MG1 and (b) MG2

**Table 4.5: Summary of power flow between the DERs and load for both MG1 and MG2 after implementing MLCS**

Time (s)	Operating Mode	Grid (MW)	MG1				MG2				
			Generation			Load		Generation		Load	
			Solar power $P_{pvmg1}$ (MW)	Battery Power $P_{batmg1}$ (MW)	Diesel Generator power $P_{dgm1}$ (MW)	Load demand (MW)	Load power $P_{ldmg1}$ (MW)	Solar power $P_{pvmg2}$ (MW)	Battery power $P_{batmg2}$ (MW)	Load demand (MW)	Load Power $P_{ldmg2}$ (MW)
0-2	Grid-connected	0	0.1	0	0	0.1	0.1	0.05	0	0.05	0.05
			0.1					0.05			
2-4	Grid-connected	0.035	0.06	0.015	0	0.095	0.095	0.03	0.015	0.06	0.06
			0.075					0.045			
4-6	Inter-connected	0	0.08	0.015	0	0.075	0.075	0.035	0.015	0.07	0.07
			0.095					0.05			
			<b>0.02 (supplied power from MG1)</b>				<b>-0.02 (absorbed power by MG2)</b>				
6-8	Inter-connected	-0.01	0.055	0	0	0.05	0.05	0.05	0	0.045	0.045
			0.055					0.05			
			<b>0.0 (supplied or absorbed power by MG1)</b>				<b>0.0 (supplied or absorbed power by MG2)</b>				
8-10	Inter-connected	0	0.04	0.015	0	0.065	0.065	0.05	0.005	0.045	0.045
			0.055					0.055			
			<b>-0.01 (supplied power from MG1)</b>				<b>0.01 (supplied power from MG1)</b>				
10-12	Islanded	0	0.07	0.015	0.045	0.13	0.13	0.035	0.015	0.07	0.05
			0.13					0.05			
12-14	Self-healing	0	0.05	0.015	0.03	0.075	0.075	0.035	0.015	0.07	0.07
			0.095					0.05			
			<b>0.02 (supplied power from MG1)</b>				<b>-0.02 (absorbed power by MG2)</b>				
14-16	Self-healing	0	0.07	0	0	0.065	0.065	0.045	0.015	0.065	0.065
			0.07					0.06			
			<b>0.005 (supplied power from MG1)</b>				<b>-0.005 (absorbed power by MG2)</b>				
16-18	Self-healing	0	0.065	0.015	0	0.095	0.095	0.04	0.015	0.04	0.04
			0.08					0.055			
			<b>-0.015 (supplied power from MG1)</b>				<b>0.015 (supplied power from MG1)</b>				
18-20	Grid-connected	0.08	0.075	0.015	0	0.14	0.14	0.03	0.015	0.075	0.075
			0.09					0.045			

In Figure 4.26, the power of PV, battery, DiG and load of MG1 are denoted by  $P_{pv\_mg1}$ ,  $P_{bat\_mg1}$ ,  $P_{dg\_mg1}$  and  $P_{ld\_mg1}$ , respectively where  $P_{pv\_mg2}$ ,  $P_{bat\_mg2}$  and  $P_{ld\_mg2}$  are used for denoting power of PV, battery and load of MG2, respectively. According to the Figure, during 0-4 s both the MGs are operating in grid-connected mode. During grid-connected

mode, it is seen that from 0-2 s the power generated by PV system and load demand of MG1 is equal which 0.1 MW. As a result, no power is drawn from battery and DiG. For the same period, the PV system of MG2 also generates the same amount of power required by the load which is 0.05 MW and due to that the power drawn from the battery and grid remain null for MG2. Both the MGs PV systems generate less power 0.06 MW and 0.03 MW, respectively during 2-4 s due to decrease in solar irradiation. At this period, load demands of both MG 1 are also reduced to 0.095 MW but MG2's load demand is increased to 0.06 MW. Since PV generations of both MGs are less than total load demand, hence, according to grid-connected MG PMS, batteries of both MGs come into operation to fulfill the remaining load demand which supply 0.015 MW and 0.015 MW, respectively. However, to satisfy the load demands of the MGs at this period, battery powers are not enough, therefore, the remaining load powers are fulfilled by grid (0.035 MW).

After 6 s, according to MLCS, the MGs enter to interconnected mode as it is found that two MGs have sufficient power to support each other without taking support from grid. During interconnected mode from 4-6 s, the total generated power of MG1 is 0.095 MW (PV+battery) and load demand is 0.075 MW. On the other hand, the total power generated by MG2 is 0.05 MW (PV+battery) and load demand is 0.07 MW. It is observed that there is a scarcity of 0.02 MW power to the load in MG2 and it has no additional power sources to provide this extra power. However, due to the interconnection, the remaining load demand (0.02 MW) of MG2 is fulfilled by MG1. Therefore, during 4-6 s, 0.02 MW power is supplied from MG1 to MG2. In between 6-8 s, the load demands (0.05 MW & 0.045 MW) of MG1 and MG2 are found lesser than their PV generations (0.055 MW & 0.045 MW). As a result, it can be seen that both the MGs do not need any power support from each other, and they have an additional power generation of 0.01 MW. Therefore, this remaining power (0.01 MW) from the MGs is supplied to the grid. During

8-10 s, power supply of PV of MG2 (0.05 MW) has found more than its load demand (0.045) which means MG2 has 0.005 MW additional power supply capacity excluding battery backup. On contrary, MG1 load demand (0.065 MW) has found less than its PV generation (0.04 MW). There is a deficiency of 0.025 MW power is observed in MG1 which cannot be fulfilled by battery backup. It is found that after getting back up from battery power (0.015 MW), still 0.01 MW power is required by MG1 to fulfill its load demand. Since, additional PV power and battery backup of MG2 is sufficient to meet the remaining load demand of MG1, hence, MG2 delivers 0.01 MW power to MG1.

At 10 s, grid goes off and the load demands of both MG1 & MG2 are increased to 0.13 MW & 0.07 MW, respectively. However, both the MGs' total power generation is not sufficient to support each other during 10-12 s. Because MG2 required additional power support of 0.02 MW whereas MG1 can support only 0.005 MW. As a result, according to MLCS, the MGs cannot operate either in interconnected mode or in self-healing mode. Therefore, the MGs operation shifted to islanded mode through MLCS. In this mode, MG1 generation (0.13 MW) can fulfill its total load demand (0.13 MW) because it has a DiG. However, MG2 cannot support its total load demand because its total supply from PV and battery (0.05 MW) cannot fulfill its load demand of 0.07 MW. As a result, load management strategy turned on by ensuring that critical load gets uninterruptible power supply.

At 12 s, it is found that the MGs have enough power supply to support the load demands of each other. As a result, MLCS shift the MGs operating mode from islanding to self-healing mode. During self-healing mode from 12-14 s, the total generated power of MG1 is 0.065 MW (PV+battery) and load demand is 0.075 MW. Therefore, the remaining load demand (0.01 MW) of MG1 is fulfilled by DiG. On the other hand, the total power generated by MG2 is 0.05 MW (PV+battery) and load demand is 0.07 MW.

It is observed that there is a scarcity of 0.02 MW power to the load in MG2 and it has no additional power sources to provide this extra power. However, due to the self-healing capability, the remaining load demand (0.02 MW) of MG2 is fulfilled by DiG of MG1. Therefore, the total power is supplied by the DiG is observed 0.03 MW which is shown in Figure 4.26. In addition, it is also seen that during 12-14 s, 0.02 MW power is supplied from MG1 to MG2. Further, during 14-16 s, load demand (0.065 MW) of MG2 is higher than the generation (0.06 MW) due to which 0.005 MW power is delivered from MG1 to MG2. However, at this time the load demand of MG2 is fulfilled by only PV system of MG1, since, MG1 PV generation (0.07) is higher than the load demand (0.065). Therefore, no power was drawn from battery and DiG during 14-16 s. After 16 s, PV generation of MG2 and load demand have become the same (0.04 MW). Hence, MG2 does not require any power support. However, in MG1, the load demand (0.095 MW) has found 0.03 MW more than the PV generation (0.065) and battery can give a maximum backup of 0.015 MW. As a result, there is still 0.015 MW power deficiency is observed in MG1. Therefore, according to the PMS algorithm, before starting the DiG, it checks whether the battery backup power of MG2 can fulfill the remaining load demand of MG1 or not. PMS found that MG2 battery can provide 0.015 MW power support to MG1 which resulted in the transfer of 0.015 MW power from MG2 to MG1 during 16-18 s without turning on the DiG of MG1.

Finally, grid reconnected back after 18 s and both the MGs start getting power support from the grid. For MG1, there is a need of 0.05 MW from the grid after fulfilling its load demand from PV and battery (0.09 MW). Similarly, MG2 also consumes 0.03 MW of power from grid to support its total load demand of 0.075 MW.

In Figure 4.27, the power flow between the two MGs at POI along with the grid power is presented. From Figure 4.27, it is seen that during grid-connected mode till 4 s there is

no power transfer in between the two MGs. However, after 4 s during interconnected mode, power is transferred from MG1 to MG2 from 4-6 s and from 8-10 s power is transferred from MG2 to MG1. In between 6-8 s, even though the MGs are in interconnected mode, however, since they have surplus PV generation, no power is transferred between them. During 6-8 s, the surplus generations of the MGs are supplied to the grid. In between 10-12 s there is no power shared between the MGs because the MGs are operating in islanded mode. Then, after 12 s MGs enter to self-healing mode where MG1 supplied power to MG2 from 12-16 s, and MG2 supplied power to MG1 from 16-18 s. Finally, the MGs enter grid-connected mode after 20 s. In Figure 4.28, the voltage and corresponding current waveforms for both the MGs are presented. From the zoomed portion of the voltage and current, it is observed that the current of MG1 is in phase with POI voltage while the MG2 current is out of phase. The reason is MG1 is delivering power and MG2 is absorbing power. Further, both MGs currents and POI voltage is sinusoidal in shape and maintain a frequency of 60 Hz.

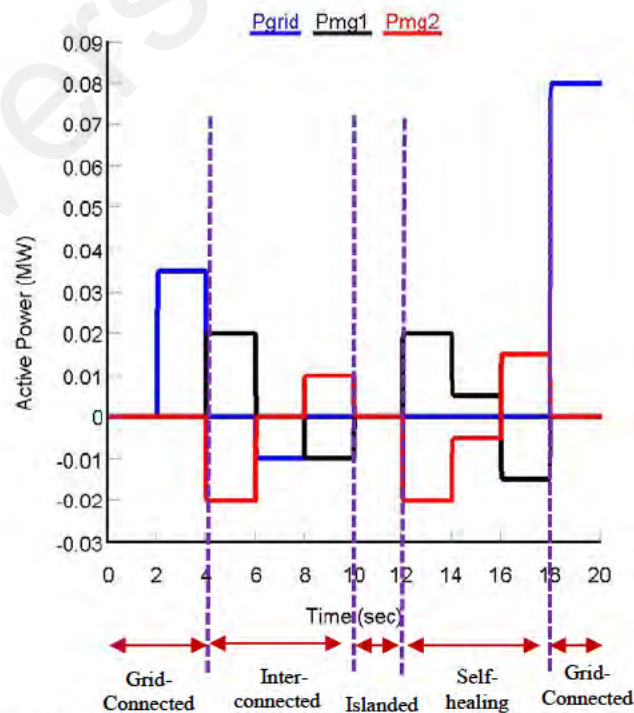
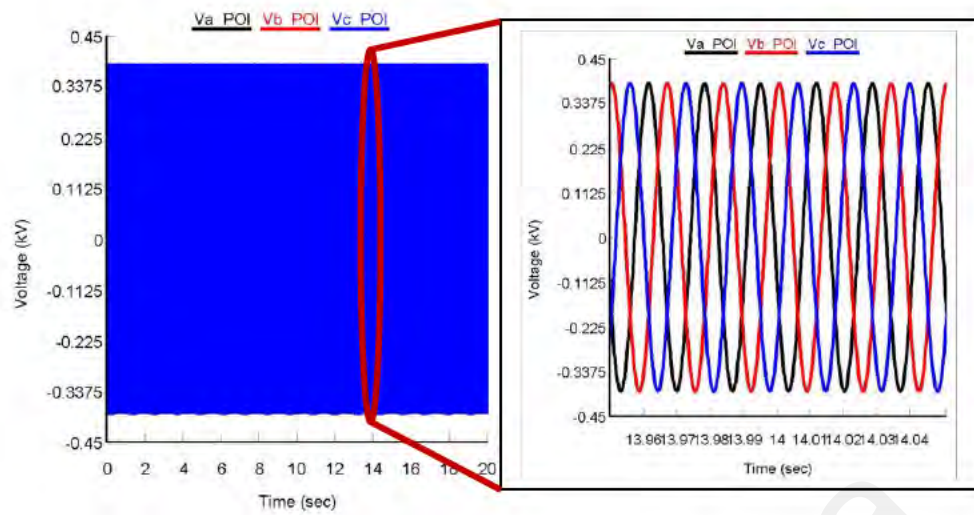
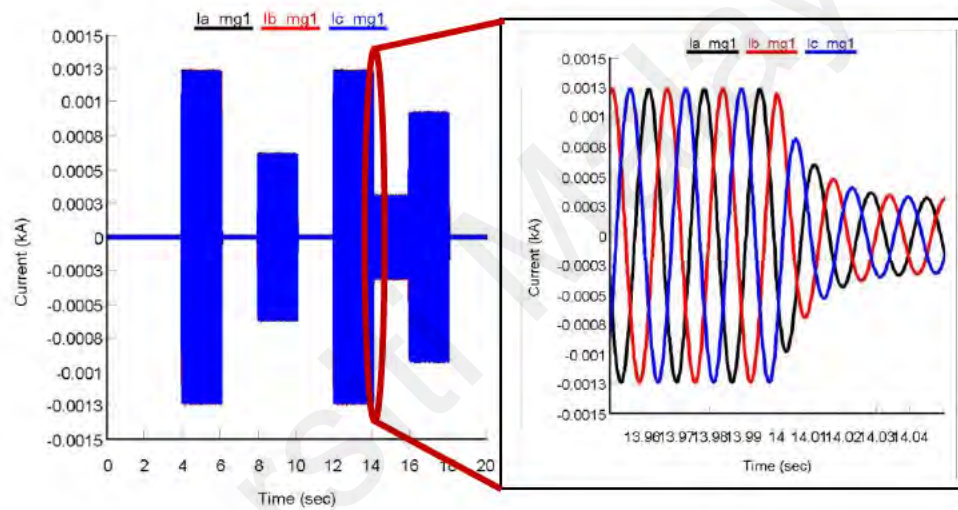


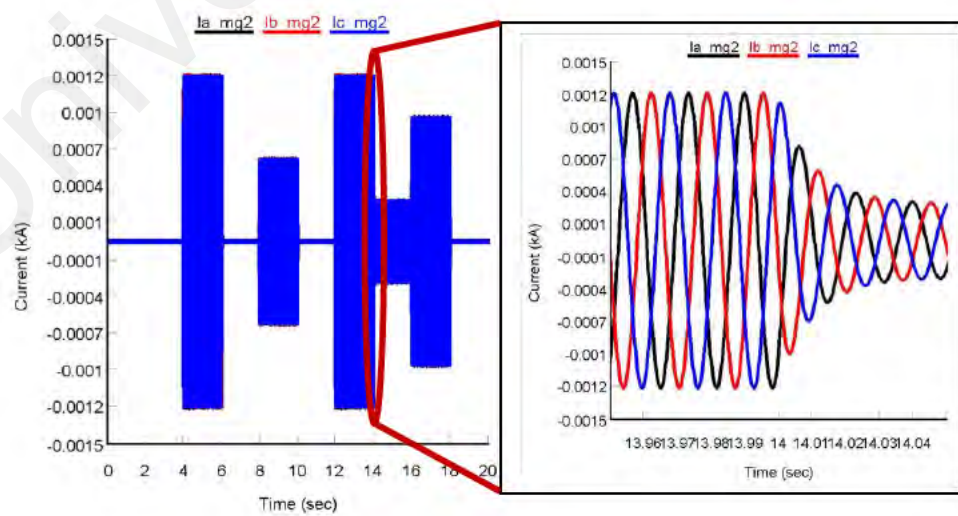
**Figure 4.27: Power flow between MG1 and MG2 at POI**



(a)



(b)



(c)

**Figure 4.28: During MGs different operating modes at POI (a) voltage, (b) MG1 current and (c) MG2 current**

#### **4.7 Comparative Study of Proposed PV VSI Controllers with Conventional PV VSI Controllers used in AC Microgrid**

In this stage, the performance of the proposed power control methods for AC MG's PV VSI is compared with conventional grid-tied MG power control methods from (Guichi et al., 2021; Kaushal & Basak, 2020; Kewat & Singh, 2020; Lou et al., 2020; Mousavi et al., 2018; Safa et al., 2018; Sedaghati & Shakarami, 2019; Worku et al., 2019). All these controllers are implemented for the PV VSI presented in Figure 3.1. Real-time simulations are conducted to obtain the results by implementing the controllers in RTDS. To do a fair comparison, all the parameters of MG have been kept identical for all the controllers. In Table 4.6, the results of the comparative study are presented, which are conducted based on six indicators: synchronization method, number of control loops, reference power tracking time, power ripple, inverter output voltage, and current THD. From the Table, it can be seen that for all the performance analysis indicators, the proposed power control methods for grid-tied MG's PV VSI have outperformed, the other grid-tied MG VSI power controllers. The main reason for the better power performance of the proposed controllers are they do not utilize PLL system to extract voltage angle. Further, for PIDPC and FLDPC, they have used DPC method which reduces the computational burden due to the use of single control loop. All the results are presented for the period of 1-2 s when AC MG is operating in grid-tied mode, as shown in Figure 4.9. For instance, the reference power tracking time of the proposed control methods are found in the range of (0.03-0.11 s) whereas, for the controllers proposed in (Guichi et al., 2021; Kaushal & Basak, 2020; Kewat & Singh, 2020; Lou et al., 2020; Mousavi et al., 2018; Safa et al., 2018; Sedaghati & Shakarami, 2019; Worku et al., 2019), the range is (0.15-0.245 s) which is higher than the proposed control methods. Moreover, the PV VSI output current THD for the proposed controllers are observed in the range of (1.60 - 2.492 %), which is approximately (1.57 % - 3.375 %) lesser than the THD of current obtained

by implementing the controllers in (Guichi et al., 2021; Kaushal & Basak, 2020; Kewat & Singh, 2020; Lou et al., 2020; Mousavi et al., 2018; Safa et al., 2018; Sedaghati & Shakarami, 2019; Worku et al., 2019). Further, the power ripple in the output of PV VSI controller by the proposed controller is found low compared to the ripples that existed in the output powers of PV VSIs regulated by the controllers proposed in (Guichi et al., 2021; Kaushal & Basak, 2020; Kewat & Singh, 2020; Lou et al., 2020; Mousavi et al., 2018; Safa et al., 2018; Sedaghati & Shakarami, 2019; Worku et al., 2019).

**Table 4.6: Results of comparison between proposed and conventional grid-tied MGs power controllers**

#	Control Method	Grid Synchronization	No. of control loops	Active Power Ripples Range	Reference power tracking Time (s)	VSI Output Voltage (%THD)	VSI Output Current (%THD)
1	Proposed PVMT based FLDPCC	Direct power calculation (PLL less)	1	Very small (0.0999-0.10 MW)	0.03	1.445	1.60
2	Proposed PVMT based PIDPC	Direct power calculation (PLL less)	1	Small (0.0995-0.1006 MW)	0.07	1.573	1.901
3	Proposed PLL less dq CCT	Direct power calculation (PLL less)	2	Medium (0.0985-0.1013 MW)	0.11	2.024	2.492
4	Ref (Worku et al., 2019)	PLL based	2	Very Large (0.0956-0.1065 MW)	0.24	3.91	4.975
5	Ref (Sedaghati & Shakarami, 2019)	PLL based	2	Very Large (0.0953-0.1060 MW)	0.237	3.88	4.966
6	Ref (Safa et al., 2018)	PLL based	2	Large (0.0975-0.1041 MW)	0.225	3.85	4.947
7	Ref (Kaushal & Basak, 2020)	PLL based	2	Large (0.0978-0.1040 MW)	0.215	3.83	4.87
8	Ref (Lou et al., 2020)	PLL based	2	Medium (0.0982-0.102 MW)	0.15	2.59	3.95
9	Ref (Mousavi et al., 2018)	PLL based	2	Medium (0.0980-0.1024 MW)	0.17	2.75	4.11
10	Ref (Guichi et al., 2021)	PLL based	2	Large (0.0977-0.1039 MW)	0.22	3.80	4.76
12	Ref (Kewat & Singh, 2020)	FLL based	2	Medium (0.0983-0.1022 MW)	0.15	2.56	3.17

#### **4.8 Comparative Study of Proposed Interconnected Microgrids Performance with previously Developed Interconnected Microgrids**

In Table 4.7, a comparative study among the proposed interconnected microgrids performance with previously developed interconnected microgrids (Bazmohammadi et al., 2019; Gazijahani et al., 2018; Z. Li et al., 2017; Y. Liu et al., 2017; Nikmehr et al., 2017; Ren et al., 2018; Samadi Gazijahani & Salehi, 2017) is presented based on interconnection framework, modes of operation, real-time operation, PMS and MLCS availability. From the Table, it can be seen that the proposed framework and PMS based interconnected MGs are equipped with all types of features to enhance the reliability of the power distribution networks compared to other proposed interconnected MGs. For example, none of the literature proposed a MLCS for interconnected MGs which can enhance their reliability whereas, the proposed interconnected MGs is consisted of a MLCS to operate in different modes based on distribution networks requirement. Then most of the literature did not propose frameworks for interconnection, they just emphasized on PMS or energy management systems of the interconnected MG for power sharing purposes. On the other hand, for the proposed interconnected MG system, an efficient framework is proposed based on power imbalance between MGs' DERs generation capacity and load demand along with PMSs for each MG1 for both self-healing and interconnected modes of operation. Further, previous interconnected MGs performance validated for either interconnected or self-healed conditions. On contrary, the proposed interconnected MGs performance is validated for both interconnected and self-healing modes. Therefore, it can be concluded that the proposed IIMs, PMSs and MLCS have increased the efficiency and reliability of the interconnected MGs better than previously proposed ones.

**Table 4.7: Results of comparison between proposed and existing controllers for interconnected MGs**

#	Ref	Interconnection framework	Self-healing or interconnected mode	Real-time implementation	Availability of PMS/EMS	Availability of Multi-layer control strategy
1	Proposed	Based on power imbalance between MGs' DERs generation capacity and load demand.	Both	Yes possible	Yes	Available
2	(Samadi Gazijahani & Salehi, 2017)	New stochastic multi-objective framework was presented for interconnected MGs under uncertainty from environmental viewpoints.	Interconnected	Not possible	No	Not available
3	(Y. Liu et al., 2017)	By assuming adjacent MGs may have complementary energy production and consumption, which can be utilized to compensate for each other's instant energy deficiency.	Interconnected	Yes possible	Yes	Not available
4	(Nikmehr et al., 2017)	No framework is proposed	Interconnected	Not possible	Yes	Not available
5	(Z. Li et al., 2017)	Through steady communications with the demand side operator, each MG can decide when and how to be networked with participating MGs.	Self-healing	Not possible	No	Not available
6	(Ren et al., 2018)	No framework is proposed	Self-healing	Yes possible	Yes	Not available
7	(Gazijahani et al., 2018)	No framework is proposed	Self-healing	Not possible	Yes	Not available
8	(Bazmohammadi et al., 2019)	No framework is proposed	Interconnected	Not possible	Yes	Not available

## 4.9 Summary

In this chapter, the results obtained by implementing the three MG PV VSI power control methods without PLL system are presented. From the results, it can be seen that both the proposed controllers have outperformed the conventional PLL-PI integrated dq CCT based power control method. In addition, the performances of the proposed real-time PMSs are tested on AC and hybrid MG systems. In both cases, it has been found that proposed real-time PMSs are able to ensure maximum utilization of the RES, BSS and ensure uninterrupted power supply to critical load. Further, the performance of the proposed IIM along with the PMS of MG1 and MG2 is validated on two interconnected MGs during self-healing and interconnected modes of operation. From the results, it can be concluded that the IIM has successfully interconnected the two MGs during self-healing and interconnected mode. Moreover, the PMSs of MGs have shown excellent performance during power flow from MG1 to MG2 and vice versa. Finally, the performance of the proposed MLCS is validated for MGs' different operating modes by varying solar irradiation and load. The results show that through the implementation of the proposed MLCS, the MGs have been able to transit and operate in different operating modes (grid-connected, islanded, self-healing and interconnected) smoothly and flexibly. At the end of the chapter, two comparative studies are conducted to prove the effectiveness of the proposed control methods and PMSs in this thesis. The first comparative study was based on the performances of the proposed and conventional MG VSI power control methods while the second one was based on interconnected MGs control methods. The comparison results show that all the controllers for single and interconnected MGs have outperformed the existing control methods.

## CHAPTER 5: CONCLUSIONS AND FUTURE WORKS

### 5.1 Conclusions

In this study, real-time control and power management of two interconnected MGs are proposed and validated. The work initially started with proposing and modeling of three power control methods for PV VSI for single MG to ensure better power quality, which is followed by the development and implementation of real-time power management strategies to ensure maximum utilization of RES, BSS along with uninterruptible power supply to critical load. After validating the performance of the single MG, in the next stage, to overcome the issues related to single MG, interconnection methods for two MGs are proposed during islanded and grid-connected modes which are termed as self-healing and interconnected modes, respectively are proposed based on the power imbalance between MGs supply and demand. Further, to ensure maximum utilization of RES and BSS during MGs self-healing and interconnected modes of operation different PMSs are developed for MG1 and MG2. Finally, to ensure MGs flexible operation and smooth transition in different operating modes (grid-connected, islanded, self-healed and interconnected), a MLCS is proposed and developed. To validate the performance of the interconnected MGs' real-time control and power management, real-time simulations have been carried out in real-time environment using RTDS.

The first objective of this research work is to model power control methods for grid-connected MG's PV VSI without using PLL and Park transformation. Here, three control methods namely FLDPC, PIDPC and dq CCT based power control methods without using PLL and Park transformation are proposed. FLDPC and PIDPC methods are modeled based on DPC theory where FLC and PI controllers are used in the feedback control loops to minimize the steady-state errors. On the other hand, the third proposed controller is based on the conventional dq CCT based method but without using PLL and Park transformation. The reference power tracking and steady-state performances of the

proposed controllers have been initially validated by changing real and reactive power references for single grid-tied PV VSI. Further, the performances of all the controllers are compared with that of PLL-PI integrated conventional dq CCT based power control method to prove the superiority of the proposed controllers.

Real-time simulation results show that the proposed controllers are able to track both real and reactive power to their reference values accurately and faster. The time required by the proposed FLDPC method to track reference real and reactive power is around 0.03 s while the PIDPC method and PLL less dq CCT based methods took 0.07 s and 0.11 s to track the reference power, respectively. The FLDPC tracks reference power faster than other proposed controllers due to the use of DPC theory and FLC controller. However, compared to all the proposed controllers, conventional PLL-PI integrated dq CCT based power controller has taken 0.24 s which is 0.24 s, 0.17 s and 0.13 s slower than proposed FLDPC, PIDPC and PLL less dq CCT based control method. The proposed FLDPC, PIDPC and PLL less dq CCT based control methods during steady-state also have demonstrated outstanding performance as the ripples in the PV VSI output powers have significantly reduced and THDs of PV VSI output current achieved are 1.60 %, 1.901 %, and 2.492 %, respectively which are well below 5 % set by IEC standard. The proposed PLL less dq CCT based control method implemented PV VSI output current THD higher than the PVMT based FLDPC and PIDPC methods due to the implementation of two control loops in the proposed PLL less CCT based power controller. However, the THD obtained by conventional PLL based dq CCT power controllers has been found very high (4.967 %) compared to the proposed PV VSI power control methods.

The second objective of this research work is to design real-time PMSs for grid-connected and islanded single MG by prioritizing maximum utilization of RES, BSS and critical load. The performance of the proposed PMS is validated in two types of MGs

namely AC and Hybrid MGs in RTDS platform by considering different real world scenarios. For instance, from the simulation results, it has been found that the proposed PMS was able to maintain balance between power supply and demand by ensuring that when PV and battery have enough power to support the demand then no powers have drawn from grid and DiG. After providing support to the load through PV and battery power, if some load still required power support then only grid and DiGs come into operation. Further, it has also been observed that the proposed PMS during islanded mode ensured that the critical loads would get an uninterruptible power supply until battery backup is available.

To overcome the issues related to single MG while operating in islanded and grid-connected modes, in the third objective of the thesis, IIMs are proposed to interconnect two MGs so that the two MGs can share power between them in self-healing (MGs islanded) and interconnected (MGs grid-connected) modes. The proposed IIMs performances are validated by interconnecting two MGs in RTDS platform based on different real world case studies. The results show that proposed IIMs can successfully detect islanding or non-islanding phenomenon, to interconnect two MGs self-healing (MGs islanded) and interconnected (MGs grid-connected) modes, when both the MGs have sufficient power supply to support the load demand of each other without taking support from grid or implementing load shedding or dump load strategy.

In the fourth objective of the thesis, to maintain balance between MGs supply and demand, PMSs are developed by ensuring maximum utilization of RES and BSS for the flexible and reliable operation of the MGs in self-healing (MGs islanded) and interconnected (MGs grid-connected) modes. From the results, it is seen that both MGs PMSs' are optimally controlled the power flow from different sources of MGs to the load when both solar irradiation and load were varying. For instance, in self-healing mode,

when MG2 has surplus of power generation and that can fulfill the remaining load demand of MG1, then no power has drawn from DiG of MG1. Further, in interconnected mode, when MG1 and MG2 have excessive PV generation than load, then the MGs supply that power to the grid. On the other hand, if MGs in self-healing or interconnected modes cannot meet their load demand through generation from PV and BSS then the proposed PMSs compel them to operate in islanded or grid-connected mode as single MG.

In the final objective of the thesis, a MLCS is developed to enhance the resiliency and ensure smooth transition of interconnected MGs among grid-connected, islanded, interconnected and self-healing modes of operation. The validation of the developed MLCS is conducted in RTDS by considering various practical case studies along with solar irradiation and load variations. From the simulation results, it has been seen that the proposed MLCS has successfully detected MGs in different operating scenarios. It has enabled the two MGs to operate flexibly and transit from one operative mode to another based on the case studies smoothly.

Finally, two comparative studies have also been conducted to prove the superiority of the proposed MGs power control methods with respect to other existing MG control methods. It is observed that the proposed FLDPC method has outperformed all the other controllers having PI based feedback controller and PLL based synchronization methods having two control loops for parameters like power ripples, THD and reference power tracking time. Similarly, for interconnected MGs also the proposed IIMs, PMSs and MLCS have increased the reliability of the MG systems better than that of existing control methods of interconnected MG systems.

From the above discussion, it can be concluded that the proposed real-time control and PMSs have been able to ensure the flexible and smooth operation of two interconnected

MGs in different operating modes with better efficiency and power quality. Furthermore, the implementation of this research work will not only improve the reliability of the distribution network but will also ensure continuous power supply to rural communities, which will greatly benefit them, such as residents having access to affordable energy, being better educated, having better health, and becoming more prosperous by raising their living standards. Moreover, the implementation of this research work will contribute to United Nations' Sustainable Development Goals: SDG 7 (Clean and Affordable Energy), and SDG 13 (Climate Action).

## **5.2 Limitations and Challenges of the Study**

1. In this work, only the real-time simulations of the proposed interconnected MGs frameworks are conducted in RTDS platform.
2. Due to the limited number of the processors in the existing RTDS PB5 card, only PV as DG, battery as ESS and single loads are considered. Further, protective devices are not considered due to the unavailability of external control circuits which can be easily interfaced with RTDS.
3. IEC and IEEE standards during grid synchronization and re-synchronization are not taken into consideration in the current research.
4. Detailed techno-economic analysis has not been conducted to prove the financial and environmental viability of the proposed interconnected MGs.
5. For VSI control, conventional FLC has been used where scaling of the membership function is challenging.
6. Only two MGs are considered for interconnected MG operation due to less number of processors in in the existing RTDS PB5 card. If the number of MGs are increased, then complication in operation and power management may also increase.

### 5.3 Future Works

1. In this work, the real-time simulations of interconnected MGs are conducted in RTDS platform. In the future, the work will be further extended through the development of laboratory prototype of the interconnected MGs.
2. In this thesis, only two MGs are considered for the interconnection purpose, and they were located nearby. However, in the future, more MGs will be interconnected which will be located not only in adjacent locations but also in distant locations.
3. In this research work, no economic analysis on the MGs operation is conducted. In future work, a detailed economic analysis will be conducted to prove the viability of the interconnected MGs.
4. In this research work, as a RE source and ESS only PV and battery. However, in future work, different types of RESs along with various ESSs will be considered while developing the MGs. Further, DC MG will also be considered for making the design of interconnected MG system looks more practical.
5. Adaptive neuro fuzzy inference system (ANFIS) or Self-tuned type-2 FL controllers can be used to overcome the problem of membership function scaling in future and to enhance the performance of the VSI control method.
6. More than 2 MGs should be considered to develop more advanced control algorithm for interconnected MGs.
7. IEC and IEEE standards during grid synchronization and re-synchronization should be taken into consideration in future interconnected MG research.

## REFERENCES

- Abadlia, I., Adjabi, M., & Bouzeria, H. (2017). Sliding mode based power control of grid-connected photovoltaic-hydrogen hybrid system. *International Journal of Hydrogen Energy*, 42(47), 28171-28182.
- Adhikari, S., & Li, F. (2014). Coordinated Vf and PQ control of solar photovoltaic generators with MPPT and battery storage in microgrids. *IEEE Transactions on Smart Grid*, 5(3), 1270-1281.
- Adhikari, S., Li, F., & Li, H. (2015). PQ and PV control of photovoltaic generators in distribution systems. *IEEE Transactions on Smart Grid*, 6(6), 2929-2941.
- Ahmad, S., Albatsh, F. M., Mekhilef, S., & Mokhlis, H. (2014). Fuzzy based controller for dynamic Unified Power Flow Controller to enhance power transfer capability. *Energy Conversion and Management*, 79, 652-665.
- Ahmad, S., Rashid, M. T., Ferdowsy, C. S., Islam, S., & Mahmood, A. H. (2015). A technical comparison among different PV-MPPT algorithms to observe the effect of fast changing solar irradiation. Paper presented at the 2015 IEEE International WIE Conference on Electrical and Computer Engineering (WIECON-ECE).
- Ahmadzadeh, M., Mortazavi, S., & Saniei, M. (2018). Investigating the stability of phase-locked loop in network-connected applications affected by microgrid-side and network-side parameters. *International Transactions on Electrical Energy Systems*, 28(4), e2523.
- Akram, U., Khalid, M., & Shafiq, S. (2017). Optimal sizing of a wind/solar/battery hybrid grid-connected microgrid system. *IET Renewable Power Generation*, 12(1), 72-80.
- Al-Saedi, W., Lachowicz, S. W., Habibi, D., & Bass, O. (2013). Power flow control in grid-connected microgrid operation using Particle Swarm Optimization under variable load conditions. *International Journal of Electrical Power & Energy Systems*, 49, 76-85.
- Ali, Z., Christofides, N., Hadjidemetriou, L., Kyriakides, E., Yang, Y., & Blaabjerg, F. (2018). Three-phase phase-locked loop synchronization algorithms for grid-connected renewable energy systems: A review. *Renewable and Sustainable Energy Reviews*, 90, 434-452.
- Arefifar, S. A., Mohamed, Y. A.-R. I., & El-Fouly, T. H. (2013). Comprehensive operational planning framework for self-healing control actions in smart distribution grids. *IEEE Transactions on Power Systems*, 28(4), 4192-4200.
- Arefifar, S. A., Yasser, A.-R. M., & El-Fouly, T. H. (2013). Optimum microgrid design for enhancing reliability and supply-security. *IEEE Transactions on Smart Grid*, 4(3), 1567-1575.

- Bazmohammadi, N., Tahsiri, A., Anvari-Moghaddam, A., & Guerrero, J. M. (2019). Stochastic predictive control of multi-microgrid systems. *IEEE Transactions on Industry Applications*, 55(5), 5311-5319.
- Belmokhtar, K., & Cano, M. H. (2021). Power Flow Management Algorithm for a Remote Microgrid Based on Artificial Intelligence Techniques. *AI and Learning Systems: Industrial Applications and Future Directions*, 175.
- Blaabjerg, F., Teodorescu, R., Liserre, M., & Timbus, A. V. (2006). Overview of control and grid synchronization for distributed power generation systems. *IEEE Transactions on Industrial Electronics*, 53(5), 1398-1409.
- Burmester, D., Rayudu, R., Seah, W., & Akinyele, D. (2017). A review of nanogrid topologies and technologies. *Renewable and Sustainable Energy Reviews*, 67, 760-775.
- Choi, D.-K., & Lee, K.-B. (2014). Dynamic performance improvement of AC/DC converter using model predictive direct power control with finite control set. *IEEE Transactions on Industrial Electronics*, 62(2), 757-767.
- Choudhury, S. (2020). A comprehensive review on issues, investigations, control and protection trends, technical challenges and future directions for Microgrid technology. *International Transactions on Electrical Energy Systems*, 30(9), e12446.
- Ciupageanu, D.-A., Barelli, L., & Lazaroiu, G. (2020). Real-time stochastic power management strategies in hybrid renewable energy systems: A review of key applications and perspectives. *Electric Power Systems Research*, 187, 106497.
- Ciupageanu, D.-A., Barelli, L., Ottaviano, A., Pelosi, D., & Lazaroiu, G. (2019). Innovative power management of hybrid energy storage systems coupled to RES plants: The Simultaneous Perturbation Stochastic Approximation approach. Paper presented at the 2019 IEEE PES Innovative Smart Grid Technologies Europe (ISGT-Europe).
- Dabbaghjamanesh, M., Mehraeen, S., Kavousi-Fard, A., & Ferdowsi, F. (2018). A new efficient stochastic energy management technique for interconnected AC microgrids. Paper presented at the 2018 IEEE Power & Energy Society General Meeting (PESGM).
- Davari, M., & Mohamed, Y. A.-R. I. (2016). Robust vector control of a very weak-grid-connected voltage-source converter considering the phase-locked loop dynamics. *IEEE Transactions on Power Electronics*, 32(2), 977-994.
- DESA, U. (2006). *Multi Dimensional Issues in International Electric Power Grid Interconnections*. New York: United Nations.
- Dou, C.-X., & Liu, B. (2013). Multi-agent based hierarchical hybrid control for smart microgrid. *IEEE Transactions on Smart Grid*, 4(2), 771-778.
- Fang, X., Misra, S., Xue, G., & Yang, D. (2011). Smart grid—The new and improved power grid: A survey. *IEEE communications surveys & tutorials*, 14(4), 944-980.

- Faria, J., Pombo, J., Calado, M. d. R., & Mariano, S. (2019). Power management control strategy based on artificial neural networks for standalone PV applications with a hybrid energy storage system. *Energies*, 12(5), 902.
- Feng, W., Sun, K., Guan, Y., Guerrero, J. M., & Xiao, X. (2016). Active power quality improvement strategy for grid-connected microgrid based on hierarchical control. *IEEE Transactions on Smart Grid*, 9(4), 3486-3495.
- Filizadeh, S., Gole, A. M., Woodford, D. A., & Irwin, G. D. (2007). An optimization-enabled electromagnetic transient simulation-based methodology for HVDC controller design. *IEEE transactions on power delivery*, 22(4), 2559-2566.
- Fusheng, L., Ruisheng, L., & Fengquan, Z. (2016). *Microgrid technology and engineering application*. China Electric Power Press.
- Gao, Y., & Ai, Q. (2018). Distributed cooperative optimal control architecture for AC microgrid with renewable generation and storage. *International Journal of Electrical Power & Energy Systems*, 96, 324-334.
- Gazijahani, F. S., Ravadanegh, S. N., & Salehi, J. (2018). Stochastic multi-objective model for optimal energy exchange optimization of networked microgrids with presence of renewable generation under risk-based strategies. *ISA transactions*, 73, 100-111.
- Go, S.-I., & Choi, J.-H. (2020). Design and dynamic modelling of pv-battery hybrid systems for custom electromagnetic transient simulation. *Electronics*, 9(10), 1651.
- Gu, Y., Xiang, X., Li, W., & He, X. (2013). Mode-adaptive decentralized control for renewable DC microgrid with enhanced reliability and flexibility. *IEEE Transactions on Power Electronics*, 29(9), 5072-5080.
- Guerrero, J. M., Hang, L., & Uceda, J. (2008). Control of distributed uninterruptible power supply systems. *IEEE Transactions on Industrial Electronics*, 55(8), 2845-2859.
- Guerrero, J. M., Vasquez, J. C., Matas, J., De Vicuña, L. G., & Castilla, M. (2010). Hierarchical control of droop-controlled AC and DC microgrids—A general approach toward standardization. *IEEE Transactions on Industrial Electronics*, 58(1), 158-172.
- Gui, Y., Kim, C., & Chung, C. C. (2017). Grid voltage modulated direct power control for grid connected voltage source inverters. Paper presented at the 2017 American Control Conference (ACC).
- Gui, Y., Kim, C., Chung, C. C., Guerrero, J. M., Guan, Y., & Vasquez, J. C. (2018). Improved direct power control for grid-connected voltage source converters. *IEEE Transactions on Industrial Electronics*, 65(10), 8041-8051.
- Gui, Y., Lee, G. H., Kim, C., & Chung, C. C. (2017). Direct power control of grid connected voltage source inverters using port-controlled Hamiltonian system. *International Journal of Control, Automation and Systems*, 15(5), 2053-2062.

- Gui, Y., Wang, X., & Blaabjerg, F. (2018). Vector current control derived from direct power control for grid-connected inverters. *IEEE Transactions on Power Electronics*, 34(9), 9224-9235.
- Gui, Y., Wang, X., Blaabjerg, F., & Pan, D. (2019). Control of grid-connected voltage-source converters: The relationship between direct-power control and vector-current control. *IEEE Industrial Electronics Magazine*, 13(2), 31-40.
- Guichi, A., Mekhilef, S., Berkouk, E., & Talha, A. (2021). Optimal control of grid-connected microgrid PV-based source under partially shaded conditions. *Energy*, 230, 120649.
- Guo, Z., Li, S., & Zheng, Y. (2020). Feedback linearization based distributed model predictive control for secondary control of islanded microgrid. *Asian Journal of Control*, 22(1), 460-473.
- Hajilu, N., Gharehpetian, G., Hosseinian, S., Poursistani, M., & Kohansal, M. (2015). Power control strategy in islanded microgrids based on VF and PQ theory using droop control of inverters. Paper presented at the 2015 International Congress on Electric Industry Automation (ICEIA 2015).
- Hannan, M., Abdolrasol, M., Faisal, M., Ker, P. J., Begum, R., & Hussain, A. (2019). Binary particle swarm optimization for scheduling MG integrated virtual power plant toward energy saving. *IEEE Access*, 7, 107937-107951.
- Hans, C. A., Braun, P., Raisch, J., Grüne, L., & Reincke-Collon, C. (2018). Hierarchical distributed model predictive control of interconnected microgrids. *IEEE Transactions on Sustainable Energy*, 10(1), 407-416.
- Harnefors, L., Wang, X., Yepes, A. G., & Blaabjerg, F. (2015). Passivity-based stability assessment of grid-connected VSCs—An overview. *IEEE Journal of emerging and selected topics in Power Electronics*, 4(1), 116-125.
- Hasanien, H. M., & Matar, M. (2014). A fuzzy logic controller for autonomous operation of a voltage source converter-based distributed generation system. *IEEE Transactions on Smart Grid*, 6(1), 158-165.
- Hatziargyriou, N. (2014). *Microgrids: architectures and control*: John Wiley & Sons.
- Helal, S. A., Hanna, M. O., Najee, R. J., Shaaban, M. F., Osman, A. H., & Hassan, M. S. (2019). Energy management system for smart hybrid AC/DC microgrids in remote communities. *Electric Power Components and Systems*, 47(11-12), 1012-1024.
- Heydari, R., Gheisarnejad, M., Khooban, M. H., Dragicevic, T., & Blaabjerg, F. (2019). Robust and fast voltage-source-converter (VSC) control for naval shipboard microgrids. *IEEE Transactions on Power Electronics*, 34(9), 8299-8303.
- Holtz, J. (1994). Pulsewidth modulation for electronic power conversion. *Proceedings of the IEEE*, 82(8), 1194-1214.

- Hooshmand, A., Asghari, B., & Sharma, R. (2013). A novel cost-aware multi-objective energy management method for microgrids. Paper presented at the 2013 IEEE PES Innovative Smart Grid Technologies Conference (ISGT).
- Huang, Y., Mao, S., & Nelms, R. M. (2014). Adaptive electricity scheduling in microgrids. *IEEE Transactions on Smart Grid*, 5(1), 270-281.
- Hussain, A., Bui, V.-H., & Kim, H.-M. (2016). A resilient and privacy-preserving energy management strategy for networked microgrids. *IEEE Transactions on Smart Grid*, 9(3), 2127-2139.
- Iris, Ç., & Lam, J. S. L. (2021). Optimal energy management and operations planning in seaports with smart grid while harnessing renewable energy under uncertainty. *Omega*, 103, 102445.
- Islam, S. U., Zeb, K., Din, W. U., Khan, I., Ishfaq, M., Hussain, A., . . . Kim, H. J. (2019). Design of robust fuzzy logic controller based on the levenberg marquardt algorithm and fault ride trough strategies for a grid-connected PV system. *Electronics*, 8(4), 429.
- Jamal, S., Tan, N. M., & Pasupuleti, J. (2021). A Review of Energy Management and Power Management Systems for Microgrid and Nanogrid Applications. *Sustainability*, 13(18), 10331.
- Jamma, M., Bennassar, A., Barara, M., & Akherraz, M. (2017). Advanced direct power control for grid-connected distribution generation system based on fuzzy logic and artificial neural networks techniques. *International Journal of Power Electronics and Drive Systems*, 8(3), 979.
- Kaushal, J., & Basak, P. (2020). Power quality control based on voltage sag/swell, unbalancing, frequency, THD and power factor using artificial neural network in PV integrated AC microgrid. *Sustainable Energy, Grids and Networks*, 23, 100365.
- Kazmierkowski, M. P., Krishnan, R., & Blaabjerg, F. (2002). *Control in power electronics* (Vol. 17): Elsevier.
- Kewat, S., & Singh, B. (2020). Grid synchronization of WEC-PV-BES based distributed generation system using robust control strategy. *IEEE Transactions on Industry Applications*, 56(6), 7088-7098.
- Korres, G. N., Hatziargyriou, N. D., & Katsikas, P. J. (2011). State estimation in multi-microgrids. *European transactions on electrical power*, 21(2), 1178-1199.
- Lee, L. A., Liu, C. C., Xu, Y., Schneider, K. P., Tuffner, F. K., Mo, K., & Ton, D. T. (2020). Dynamics and control of microgrids as a resiliency source. *International Transactions on Electrical Energy Systems*, 30(11), e12610.
- Lee, S.-J., Kim, H., Sul, S.-K., & Blaabjerg, F. (2004). A novel control algorithm for static series compensators by use of PQR instantaneous power theory. *IEEE Transactions on Power Electronics*, 19(3), 814-827.

- Li, F., Li, R., & Zhou, F. (2015). *Microgrid technology and engineering application*: Elsevier.
- Li, Z., Shahidehpour, M., Aminifar, F., Alabdulwahab, A., & Al-Turki, Y. (2017). Networked microgrids for enhancing the power system resilience. *Proceedings of the IEEE*, 105(7), 1289-1310.
- Liang, H., Choi, B. J., Zhuang, W., & Shen, X. (2013). Stability enhancement of decentralized inverter control through wireless communications in microgrids. *IEEE Transactions on Smart Grid*, 4(1), 321-331.
- Liu, C.-C., McArthur, S., & Lee, S.-J. (2016). *Smart grid handbook*, 3 volume set (Vol. 1): John Wiley & Sons.
- Liu, Y., Fang, Y., & Li, J. (2017). Interconnecting microgrids via the energy router with smart energy management. *Energies*, 10(9), 1297.
- Logenthiran, T., Srinivasan, D., Khambadkone, A. M., & Aung, H. N. (2012). Multiagent system for real-time operation of a microgrid in real-time digital simulator. *IEEE Transactions on Smart Grid*, 3(2), 925-933.
- Lou, G., Gu, W., Zhu, J., Li, P., & Zhang, X. (2020). A novel control strategy for the seamless transfer of microgrids based on disturbance observer. *International Journal of Electrical Power & Energy Systems*, 118, 105804.
- Lv, T., & Ai, Q. (2016). Interactive energy management of networked microgrids-based active distribution system considering large-scale integration of renewable energy resources. *Applied Energy*, 163, 408-422.
- Ma, W.-J., Wang, J., Gupta, V., & Chen, C. (2016). Distributed energy management for networked microgrids using online ADMM with regret. *IEEE Transactions on Smart Grid*, 9(2), 847-856.
- Madureira, A., Pereira, J., Gil, N., Lopes, J. P., Korres, G., & Hatziargyriou, N. (2011). Advanced control and management functionalities for multi-microgrids. *European transactions on electrical power*, 21(2), 1159-1177.
- Madureira, A. G. (2010). *Coordinated and optimized voltage management of distribution networks with multi-microgrids*. Universidade do Porto (Portugal).
- Mansour, S., Marei, M. I., & Sattar, A. A. (2017). Decentralized secondary control for frequency restoration of microgrids with VF and PQ droop controlled inverters. Paper presented at the 2017 Nineteenth International Middle East Power Systems Conference (MEPCON).
- Marvasti, A. K., Fu, Y., DorMohammadi, S., & Rais-Rohani, M. (2014). Optimal operation of active distribution grids: A system of systems framework. *IEEE Transactions on Smart Grid*, 5(3), 1228-1237.
- Mohan, N., & Undeland, T. M. (2003). *WP robbins. Power Electronics, Converters Applications and Design*, (3rd edition), New York: John Wiley and Sons.

- Mosa, M. A., & Ali, A. (2021). Energy management system of low voltage dc microgrid using mixed-integer nonlinear programming and a global optimization technique. *Electric Power Systems Research*, 192, 106971.
- Mousavi, S. Y. M., Jalilian, A., Savaghebi, M., & Guerrero, J. M. (2018). Coordinated control of multifunctional inverters for voltage support and harmonic compensation in a grid-connected microgrid. *Electric Power Systems Research*, 155, 254-264.
- Nasir, M., Jin, Z., Khan, H. A., Zaffar, N. A., Vasquez, J. C., & Guerrero, J. M. (2018). A decentralized control architecture applied to DC nanogrid clusters for rural electrification in developing regions. *IEEE Transactions on Power Electronics*, 34(2), 1773-1785.
- Nikam, V., & Kalkhambkar, V. (2021). A review on control strategies for microgrids with distributed energy resources, energy storage systems, and electric vehicles. *International Transactions on Electrical Energy Systems*, 31(1), e12607.
- Nikmehr, N., Najafi-Ravadanegh, S., & Khodaei, A. (2017). Probabilistic optimal scheduling of networked microgrids considering time-based demand response programs under uncertainty. *Applied Energy*, 198, 267-279.
- Olatomiwa, L., Mekhilef, S., Ismail, M. S., & Moghavvemi, M. (2016). Energy management strategies in hybrid renewable energy systems: A review. *Renewable and Sustainable Energy Reviews*, 62, 821-835.
- Olivares, D. E., Cañizares, C. A., & Kazerani, M. (2014). A centralized energy management system for isolated microgrids. *IEEE Transactions on Smart Grid*, 5(4), 1864-1875.
- Omar, M., El-Deib, A., El Shafei, A., & Abdallah, M. (2016). Comparative study between PI and fuzzy-logic controllers for three-phase grid-connected photovoltaic systems. Paper presented at the 2016 Eighteenth International Middle East Power Systems Conference (MEPCON).
- Outlook, W. E. (2018). Electricity access database. Retrieved from <https://www.iea.org/topics/world-energy-outlook>
- Parhizi, S., Lotfi, H., Khodaei, A., & Bahramirad, S. (2015). State of the art in research on microgrids: A review. *IEEE Access*, 3, 890-925.
- Pariso, A., Wiezorek, C., Kyntäjä, T., Elo, J., Strunz, K., & Johansson, K. H. (2017). Cooperative MPC-based energy management for networked microgrids. *IEEE Transactions on Smart Grid*, 8(6), 3066-3074.
- Photovoltaic, I. (2004). Systems. Characteristics of the utility interface. *IEC Std*, 61, 727.
- Raju, L., Morais, A. A., Rathnakumar, R., Ponnivalavan, S., & Thavam, L. (2017). Micro-grid grid outage management using multi-agent systems. Paper presented at the 2017 Second International Conference on Recent Trends and Challenges in Computational Models (ICRTCCM).

- Ren, L., Qin, Y., Li, Y., Zhang, P., Wang, B., Luh, P. B., . . . Gong, T. (2018). Enabling resilient distributed power sharing in networked microgrids through software defined networking. *Applied Energy*, 210, 1251-1265.
- Rodríguez, P., Luna, A., Candela, I., Mujal, R., Teodorescu, R., & Blaabjerg, F. (2010). Multiresonant frequency-locked loop for grid synchronization of power converters under distorted grid conditions. *IEEE Transactions on Industrial Electronics*, 58(1), 127-138.
- Safa, A., Berkouk, E. M., Messlem, Y., & Gouichiche, A. (2018). A robust control algorithm for a multifunctional grid tied inverter to enhance the power quality of a microgrid under unbalanced conditions. *International Journal of Electrical Power & Energy Systems*, 100, 253-264.
- Salazar, A., Berzoy, A., Song, W., & Velni, J. M. (2020). Energy management of islanded nanogrids through nonlinear optimization using stochastic dynamic programming. *IEEE Transactions on Industry Applications*, 56(3), 2129-2137.
- Samadi Gazijahani, F., & Salehi, J. (2017). Stochastic multi-objective framework for optimal dynamic planning of interconnected microgrids. *IET Renewable Power Generation*, 11(14), 1749-1759.
- Saveen, G., Raju, P. P., Manikanta, D., & Praveen, M. S. (2018). Design and implementation of energy management system with fuzzy control for multiple microgrid. Paper presented at the 2018 2nd International Conference on Inventive Systems and Control (ICISC).
- Sedaghati, R., & Shakarami, M. R. (2019). A novel control strategy and power management of hybrid PV/FC/SC/battery renewable power system-based grid-connected microgrid. *Sustainable Cities and Society*, 44, 830-843.
- Selakov, A., Bekut, D., & Sarić, A. T. (2016). A novel agent-based microgrid optimal control for grid-connected, planned island and emergency island operations. *International Transactions on Electrical Energy Systems*, 26(9), 1999-2022.
- Sen, S., & Kumar, V. (2018). Microgrid modelling: A comprehensive survey. *Annual Reviews in Control*, 46, 216-250.
- Shadoul, M., Yousef, H., Abri, R. A., & Al-Hinai, A. (2021). Adaptive Fuzzy Approximation Control of PV Grid-Connected Inverters. *Energies*, 14(4), 942.
- Sharma, R. K., & Mishra, S. (2017). Dynamic power management and control of a PV PEM fuel-cell-based standalone ac/dc microgrid using hybrid energy storage. *IEEE Transactions on Industry Applications*, 54(1), 526-538.
- Šimek, P., Škramlík, J., & Valouch, V. (2019). A frequency locked loop strategy for synchronization of inverters used in distributed energy sources. *International Journal of Electrical Power & Energy Systems*, 107, 120-130.
- Singh, P., & Lather, J. (2020). Artificial neural network-based dynamic power management of a DC microgrid: a hardware-in-loop real-time verification. *International Journal of Ambient Energy*, 1-9.

- Smadi, I. A., Albatran, S., & Alyouf, M. A. (2018). Optimal control of a compact converter in an AC microgrid. *Electronics*, 7(7), 102.
- Tabar, V. S., Ghassemzadeh, S., & Tohidi, S. (2019). Energy management in hybrid microgrid with considering multiple power market and real time demand response. *Energy*, 174, 10-23.
- Tahri, G., Foitih, Z. A., & Tahri, A. (2021). Fuzzy logic control of active and reactive power for a grid-connected photovoltaic system using a three-level neutral-point-clamped inverter. *Int J Pow Elec & Dri Syst*, 12(1), 453-462.
- Tan, K. T., Peng, X., So, P. L., Chu, Y. C., & Chen, M. Z. (2012). Centralized control for parallel operation of distributed generation inverters in microgrids. *IEEE Transactions on Smart Grid*, 3(4), 1977-1987.
- Tang, X., Zhang, D., Xiao, D., & Li, M. (2021). Modeling and Stability Analysis of a Novel Voltage-Oriented Power Coordination Controlled Constant-Frequency AC Microgrid System. *Electronics*, 10(16), 1935.
- Teekaraman, Y., Kuppusamy, R., Baghaee, H. R., Vukobratović, M., Balkić, Z., & Nikolovski, S. (2020). Current Compensation in Grid-Connected VSCs using Advanced Fuzzy Logic-based Fluffy-Built SVPWM Switching. *Energies*, 13(5), 1259.
- Thao, N. G. M., & Uchida, K. (2013). Control the active and reactive powers of three-phase grid-connected photovoltaic inverters using feedback linearization and fuzzy logic. Paper presented at the 2013 Australian Control Conference.
- Toro, V., & Mojica-Nava, E. (2016). Droop-free control for networked microgrids. Paper presented at the 2016 IEEE Conference on Control Applications (CCA).
- Trivedi, A., & Saroha, J. (2020). Voltage unbalance and harmonics compensation in AC microgrid using add-on repetitive controller. *International Transactions on Electrical Energy Systems*, 30(4), e12290.
- Valverde, L., Bordons, C., & Rosa, F. (2012). Power management using model predictive control in a hydrogen-based microgrid. Paper presented at the IECON 2012-38th annual conference on IEEE industrial electronics society.
- Vazquez, S., Marquez, A., Aguilera, R., Quevedo, D., Leon, J. I., & Franquelo, L. G. (2014). Predictive optimal switching sequence direct power control for grid-connected power converters. *IEEE Transactions on Industrial Electronics*, 62(4), 2010-2020.
- Wang, T., He, X., & Deng, T. (2019). Neural networks for power management optimal strategy in hybrid microgrid. *Neural Computing and Applications*, 31(7), 2635-2647.
- Wang, X., & Blaabjerg, F. (2018). Harmonic stability in power electronic-based power systems: Concept, modeling, and analysis. *IEEE Transactions on Smart Grid*, 10(3), 2858-2870.

- Wang, X., Harnefors, L., & Blaabjerg, F. (2017). Unified impedance model of grid-connected voltage-source converters. *IEEE Transactions on Power Electronics*, 33(2), 1775-1787.
- Wang, Z., Chen, B., & Wang, J. (2015). Decentralized energy management system for networked microgrids in grid-connected and islanded modes. *IEEE Transactions on Smart Grid*, 7(2), 1097-1105.
- Wang, Z., Chen, B., Wang, J., & Chen, C. (2015). Networked microgrids for self-healing power systems. *IEEE Transactions on Smart Grid*, 7(1), 310-319.
- Wang, Z., & Wang, J. (2015). Self-healing resilient distribution systems based on sectionalization into microgrids. *IEEE Transactions on Power Systems*, 30(6), 3139-3149.
- Wen, B., Dong, D., Boroyevich, D., Burgos, R., Mattavelli, P., & Shen, Z. (2015). Impedance-based analysis of grid-synchronization stability for three-phase paralleled converters. *IEEE Transactions on Power Electronics*, 31(1), 26-38.
- Worku, M. Y., Hassan, M. A., & Abido, M. A. (2019). Real time energy management and control of renewable energy based microgrid in grid connected and island modes. *Energies*, 12(2), 276.
- Yang, X., Zhang, Y., He, H., Ren, S., & Weng, G. (2018). Real-time demand side management for a microgrid considering uncertainties. *IEEE Transactions on Smart Grid*, 10(3), 3401-3414.
- Yu, X., Khambadkone, A. M., Wang, H., & Terence, S. T. S. (2010). Control of parallel-connected power converters for low-voltage microgrid—Part I: A hybrid control architecture. *IEEE Transactions on Power Electronics*, 25(12), 2962-2970.
- Yue, D., Zhang, H., & Dou, C. (2021). Multi-agent Based Hierarchical Hybrid Control for Smart Microgrid Cooperative Optimal Control of Hybrid Energy Systems (pp. 49-66): Springer.
- Yumurtaci, R. (2013). Role of energy management in hybrid renewable energy systems: case study-based analysis considering varying seasonal conditions. *Turkish Journal of Electrical Engineering & Computer Sciences*, 21(4), 1077-1091.
- Zhao, B., Zhang, X., & Chen, J. (2012). Integrated microgrid laboratory system. *IEEE Transactions on Power Systems*, 27(4), 2175-2185.